Measurement of Suspended Sediment Transport Processes off the Holderness Coast - Southern North Sea, England

by

Joanna Catherine Blewett M.Sc., B.Sc. (Hons)

A thesis submitted to the University of Plymouth
in partial fulfilment for the degree of

Doctor of Philosophy

Institute of Marine Studies
Faculty of Science

January 1998

Measurement of Suspended Sediment Transport Processes off the Holderness Coast - Southern North Sea, England

Joanna Catherine Blewett

Abstract

A field campaign was set up as part of the LOIS-RACS coastal program (1994-1996), to identify the near-bed physical processes responsible for suspended sediment movement in shallow water (10-20m depth) off the Holderness coast, NE England. A new benthic tripod system Boundary Layer Intelligent Sensor System (BLISS) has been developed and deployed along a transect at three sites, normal to the coastline at Tunstall. Measurements of current velocity, suspended sediment concentration (SSC), pressure and CTD were recorded at 5 Hz for 17 minutes every hour, on the same data acquisition system. Results are presented for the summer, July 1995 and winter, February, 1996 deployments over two weeks.

Results show that variation in the SSC signal is due to the advection of spatial gradients of SSC by the tidal flows and to the resuspension of sediment from the seabed. Alongshore advection is identified through a strong negative correlation between SSC and salinity, associated with the movement of low salinity, high turbidity water associated with the Humber plume to the south. Resuspension occurs predominantly during storms, when the influence of waves increases the friction velocity at the seabed (determined from measured turbulence spectra) above a threshold value. The threshold friction velocity in February 1996 was found to be approximately $0.023 ms^{-1}$, consistent with a partially consolidated fine sediment seabed. In July 1995, a much lower threshold velocity of $0.008\ ms^{-1}$ was measured and suggests that an unconsolidated layer of fine sediment can be deposited between the mild summer storms. After a winter storm, the decay time of the elevated SSC is consistent with a sediment settling velocity in the range $(1.8\text{-}2.8) \times 10^{-4}\ ms^{-1}$, a value which is associated with fine silt or flocculated clay particles.

Sediment transport during the summer storms in July 1995 was onshore and is due to skewed shoaling waves suspending sediment during the shore-ward phase of the wave, as the wave crest passes. Offshore sediment transport dominated the February 1996 storms, and was due to a steady nearbed offshore flow explained by Stokes theory whereby a net flow in the direction of the wave advance near the surface will be balanced by a net flow in the opposite direction at depth. Sediment flux transport from waves along accounted for ~10% of the total flux transported offshore. The storms are in fact, effective stirring mechanisms which increase the amount of sediment available for transport rather than actual transporters of suspended sediment.

Contents

Acknowledgements

I would first like to express my thanks to my supervisor Professor David Huntley for his excellent guidance and support during the study. I would also like to thank my second supervisor Professor Keith Dyer who was always there to give me encouragement and guidance during the writing up phase. I would also like to acknowledge the following:

Dr Bob Bruce, Nick Bloomer, Colin Barrett (Plymouth Marine Laboratory) and Peter Ganderton (University of Plymouth) for their input into the development of BLISS and continued help and enthusiasm during the field work phase.

The crew of the Janet 'M; Chris Traves, Rob and Dave, for their generosity and much needed help during the field work phase. Rob died in a fishing accident in June 1996. He was a very cheerful and well liked person, who will be sadly missed.

My boyfriend Ian, who I am indebted to for his continual enthusiasm, support and encouragement throughout the project and for putting up with me.

Dr Bablu Sinha (Plymouth Marine Laboratory) for the number of times he has spent solving problems for me.

Dr Paul Russell, Dr Mark Davidson, Dr Philippe Gleizon (University of Plymouth) and Dr Malcolm Christie for their impromptu help at various times.

Andy Salter, for spending time, proof reading my chapters and for being a mate. Darren Stevens for his computer assistance during my writing up period.

My fellow coffee club mates Jo, Tonia, Giovanni, Dr. Mark and the other two Marks for their support and encouragement. We must not forget our ex-coffee club members, Lisa, Paul and Karen, who have been and still are, a great support.

My mum and dad for everything.

Declarations

At no time during the registration for the degree of Doctor of Philosophy has the author been registered for any other University award.

The study was financed with the aid of a studentship from the Natural Environmental Research Council, and was carried out in collaboration with the Plymouth Marine Laboratory.

Relevant scientific seminars and conferences were regularly attended at which, work was presented. Papers were presented for publication.

Presentations and Conferences Attended

Blewett, J.C. and D.A. Huntley. 1997. The Measurement of Suspended Sediment Transport Processes off the Holderness Coast - Southern North Sea, England. Oral presentation. *Plymouth Marine Fund*, Plymouth Marine Laboratory, October, 1997.

Blewett, J.C. and D.A. Huntley. 1997. The Measurement of Suspended Sediment Transport Processes off the Holderness Coast - Southern North Sea, England. Oral presentation. *International Symposium the 1997 Joint Assemblies of the International Association of Meteorology and Atmospheric Sciences and International Association for the Physical Sciences of the Oceans*. Melbourne, Australia, July, 1997. Awarded partial funding from the Plymouth Marine Fund.

Blewett, J.C. and D. A. Huntley. Measurement of Suspended Sediment Transport Processes in the Near-shore Zone off the Holderness Coast. Oral presentation. *U.K. Oceanography, 1996, Bangor*, U.K., September 1996. (Nominated for best talk, Cath Allen Prize).

Blewett, J.C. and D.A. Huntley. 1997. The Movement of Suspended Particulate Matter off the Holderness Coast. Poster Presentation, *LOIS conference, Hull*, March 1997.

Two oral and one poster presentation of current work to Ocean and Fisheries Science Division Research Seminars, Institute of Marine Studies, University of Plymouth, October 1994 to July 1996.

Attended 1st and 2nd Annual LOIS conferences at Plymouth (1996) and Hull (1997).

Attended a workshop LOIS RACS(C) meeting at Burwell's Hall, Bristol, September, 1995.

Publications

Huntley, D. A., **Blewett, J.C.**, Ganderton, P.P., Bruce, R.H., Barrett, C.D. and N.J. Bloomer. 1996. Blissful data acquisition in the North Sea. *LOIS Newsletter*, October, Issue No. 10. P. 1, 6&7.

Blewett, J.C., Huntley, D.A., P.P., Bruce, R.H., Barrett, C.D. and N.J. Bloomer. 1998. Measurement of suspended sediment transport processes in the nearshore zone off the Holderness coast, Southern North Sea, England. 1998. Submitted to *Marine Pollution Bulletin.*

Chen, H., Dyke, P.P.G., **Blewett, J.C.** and D.A. Huntley. 1997. Time series modelling of suspended sediment concentration on the Holderness coast. Submitted to *Journal of Marine Systems.*

Courses Attended

NERC sponsored Summer course at the Graduate School's Programme run by the Engineering and Physical Sciences Research council (EPSRC) in Alcuin College, University of York, July, 1996.

Signed.....

Date.....

Measurement of Suspended Sediment Transport Processes off the Holderness Coast - Southern North Sea, England

by

Joanna Catherine Blewett M.Sc., B.Sc. (Hons)

Glossary of Acronyms

ABS	Acoustic Backscatter Sensor
ADCP	Acoustic Doppler Current Profiler
AVHRR	Advanced Very High Resolution Radiometer
BGS	British Geological Survey
BLISS	Boundary Layer Intelligent Sensor System
CASI	Compact Airborne Spectral Imager
CSD	Cross Spectral Density
CTD	Conductivity Temperature Depth
EMCM	Electromagnetic Current Meter
FFT	Fast Fourier Transform
FTU	Formazin Turbidity Unit
GEOPROBE	Geological Processes Bottom Environmental Station
IDM	Inertial Dissipation Method
IRED	Infra red Emitting Diode
JONSDAP	Joint North Sea Data Acquisition Programme
LISP	Littoral Investigations of Sediment Properties
LDA	Laser Doppler Anemometer
LOIS	Land Ocean Interaction Study
mab	meters above bed
MAFF	Ministry of Agriculture Fisheries and Food
MISO	Multi Input Single Output
NERC	Natural Environmental Research Council
OBS	Optical Backscatter Sensor
ODN	Ordnance Datum
PML	Plymouth Marine Laboratory
PMP	Proudman Monitoring Platforms
POL	Proudman Oceanographic Laboratory
PSD	Power Spectral Density
PSS	Practical Salinity Scale
RACS	River Basins - Atmosphere - Coasts and Estuaries Study
RCM	Rotating Current Meter
RS	Reynolds Stress
RV	Research Vessel
SPM	Suspended Particulate Matter
SSC	Suspended Sediment Concentration
SSS	Side-Scan Sonar
STABLE	Sediment Transport and Boundary Layer Equipment
TKE	Turbulent Kinetic Energy
TSM	Total Suspended Matter
UCNW	University College of North Wales
UHF	Ultra High Frequency

Chapter 1

1. Introduction

1.1 Overview of Research Area

The resuspension, transport and deposition of suspended particulate matter (SPM) play a crucial role in a range of marine processes in continental shelf seas. For example, benthic fluxes, biological productivity, biogeochemical cycling and pollutant dispersal are all in some way influenced by SPM dynamics. The North Sea is an excellent case study for shelf seas since conditions, particularly water depths and tidal current strengths, vary widely. In light of the fact that the North Sea is surrounded by industrialised countries, the North Sea is perceived as being under threat from the increasing pollution burden imposed on it. A major goal over the last decade was to develop accurate transfer models which are capable of predicting the fate of pollutants. To achieve this goal, a better understanding was required of the mechanisms which transfer the pollutants from the rivers and estuaries into and across the North Sea. Hence, a multi-disciplinary approach within the oceanographic community was needed to determine the physical, chemical and biological processes in the North Sea. Recent examples include the North Sea Project (Charnock *et al.*, 1994) which was set up in 1988/89. Results from the study highlighted the need to investigate further the variability of the contemporary fluxes of materials, including water, sediments, nutrients, organics and pollutants, and as a consequence the current Land Ocean Interaction Study 1990-1998 was established. A major aim of the LOIS-RACS (River Atmosphere Coast and Estuary) coastal program is to study and quantify the flux of fine sediments, through the Humber region, both within the estuary and through the adjacent coastline, North and South of the Humber estuary. To the North of the Humber estuary is the Holderness coast which extends from Flamborough Head in the North to Spurn Head at the

mouth of the Humber estuary. It is a region which is subject to much discussion at present, since the Holderness cliffs being composed of 67% material <63μm, have the highest rate of erosion (1.7m a^{-1}) (McCave, 1987) along the North East coast of England and is postulated to be the dominant source of fine material into the North Sea. This thesis concentrates specifically on determining the physical processes which control the movement of the sediment in the nearshore zone off the Holderness coast and on deriving flux estimates. It must be stressed that the Holderness coast was chosen as the study area specifically because its merit lies in the important role of the North Sea sediment budget. Because of the variability of the seabed and the generally unknown nature of the seabed off Holderness (refer to chapter 4), the study area is not ideal to study flow and sediment transport processes. If one wanted to improve sediment transport models from a pure physics perspective, other sites would be more appropriate.

1.2 Specific Aims & Objectives

Sediment transport near to the coastline is thought to increase during storms and is largely intermittent in behaviour. There are however uncertainties in determining what happens to this sediment once it moves offshore. For example what are the relative roles of storms and tidal flows in moving the sediment with distance offshore, and what is the importance of resuspension of bed material relative to advective and other flux contributions? In order to address these questions, three benthic tripod structures called Boundary Layer Intelligent Sensor System (BLISS) were designed and built by Plymouth Marine Laboratory and the University of Plymouth with the overall aim to; investigate the sediment dynamics and flow conditions of the bottom boundary layer within one meter of the seabed. The objectives of the BLISS project are as follows:

1. To deploy the BLISS tripods along a transect normal to the coastline in depths between 5 - 15m for a 1 month period in each season, to measure the cross-shore and alongshore sediment fluxes in storm and calm conditions.

2. To conduct spatial surveys between the tripods over a 13 hour station so that *in situ* water samples can be collected using a modified version of the bottom-landing water sampling system (Bale and Barrett, 1995). The water samples will be used to calibrate the optical instruments. Additional measurements using a self logging

CTD/transmissometer/optical backscatter sensor package will also be deployed to profile the water column at each sampling station.

3. To use the measurements to identify and quantify the important temporal and spatial processes controlling the flux of sediment both along and across the coast. To assess the importance of 1) sediment resuspension 2) storms 3) tidal advection to the overall net sediment flux.

4. From the flux measurements derive sediment flux budgets for the amount of material being eroded from the Holderness cliffs over different time scales. However, due to there being no concurrent measurements of coastal change, it is almost impossible to link the observations to coastal changes except in the most general sense.

5. Relate the SPM measurements and current velocities to models for SPM resuspension and advection.

1.3 Outline of Thesis Content

The introduction and literature review (chapter 1 and 2) are designed to give the reader an insight into the hydrodynamic and physical processes which control and influence the movement of suspended sediment in the Southern North Sea. Chapter 3 describes the instruments on the BLISS tripods and shows schematically the overall BLISS system. The instrument calibration methods and results are also presented. Chapter 4 describes the undertaken field campaign, geophysical survey results and further calibrations. Chapter 5 concentrates on giving a detailed account of the data analysis techniques used to interpret the BLISS data. Particular attention is made to re-orientation of the current meter data. Correct alignment of the velocity data to alongshore and cross-shore flow is critical to a study of this kind especially since sediment flux measurements are directly dependent on the magnitude and direction of the velocity vector. Time series results from two deployments are described and discussed in chapter 6. Bed shear stress estimations from three methods are also given and presented in context to the sediment behaviour. Chapter 7 presents long-term net flux transport estimates for the Holderness coast and gives single point flux measurements in the form of times series, where the relative contributions to the

overall fluxes from the tidal currents and storms are reviewed. The second part of this chapter, concentrates on within burst activity and focuses on determining net sediment transport contributions at different frequencies. Chapter 8 draws together all the observations and analysis in a concise manner focusing primarily on the Holderness coast. The chapter then concludes by making suggestions for future work in this area.

Chapter 2

2. Processes in the North Sea; A Literature Review

2.1 Introduction

Understanding the wide range of processes which operate in shelf seas is considered highly important. Shelf seas not only act to dissipate the energy from the ocean tides and waves, but are also regions of high biological productivity. Economically, for the fishing industry, they are important spawning grounds for many species of fish. Industrially, they are used as throughfares for shipping transport. Increasing population and the growth in industrial activity has lead to an increase in the amount of industrial waste and sewage effluent being dumped into shelf seas. To ensure that shelf seas are managed more efficiently in the future and to combat the increasing pressures, it is necessary to fully understand their processes and to also be able to predict them.

The North Sea is a typical example of a shelf sea being subjected to the environmental threats highlighted above. In 1987, the Natural Environmental Research Council promoted the North Sea Project, which was set up to advance our understanding of the way a shelf sea works and to incorporate that understanding into models which would lay a foundation for the construction of prognostic water quality models (Charnock, *et al.*, 1994). With the aid of these models, the future of the North Sea system may be managed in a more rational and sensible way.

The North Sea had been studied prior to 1987. For example, a physical oceanographic investigation was carried out in 1976, known as the Joint North Sea Data Acquisition Programme, "JONSDAP" (Furnes, 1980), where current velocity recordings were taken at

moorings situated in the southern and northern ends of the North Sea. Data from these moorings were used to discuss residual circulation as well as transport in and out of the North Sea. Early work on sediment transport in the North Sea was documented by McCave (1970, 1973, 1987), who first accounted that the Holderness Cliffs were a dominant source of fine material into the North Sea and that areas such as the Wash were large sinks for suspended material. It was also postulated that sediment in suspension was transported by the residual currents. These findings were further collaborated by the work of Stride (1973) who mapped bedload sediment transport paths around the U.K. by following the direction of sand waves. Eisma (1973, 1981), Eisma and Kalf, (1987) determined the distribution of sediment in the North Sea and attempted to relate the sediment transport paths to marine pollution. Notably, heavy metals and trace metals are adsorbed onto the fine mud particles in estuaries, so understanding the sediment transport paths will help to determine the fate of the pollutants.

What was apparent before the North Sea Project was that the existing data archive of the North Sea was based on random sampling by isolated scientific groups. There was a clear need to obtain integrated data sets which covered long-term changes such as for example, seasonal variability. The North Sea Project aimed at bringing together all aspects of the science community, namely, the physical scientists, chemists, biologists and numerical modellers, to plan an effective interdisciplinary study of the North Sea. They aimed to exploit the capabilities of new *"super computers"* to attempt to model processes involving the chemistry and biology.

All constituents, regardless of their chemical or biological behaviour are acted upon by the same fundamental hydrodynamic processes, i.e by the mean flow, horizontal and vertical dispersion and by turbulence. The key aim of the North Sea Project was therefore to construct and validate a transport model which would adequately describe all aspects of the physics of the North Sea. Incorporated into the model was the consequent requirement for improved understanding of the physical processes which affect the suspension and transport of sediment in the water column and hence the fate of pollutants which are adsorbed onto the sediment surface. The focus of this thesis addresses the latter requirement layed out by the North Sea Project, that is, to determine the physical processes which govern sediment transport in the Southern North Sea. The literature review which follows is split up into three areas. The first part describes the parameters which affect sediment movement, and the ways in which these parameters can be monitored and

quantified. The second part concentrates on findings from actual observational studies of sediment movement under different hydrodynamic conditions in the North Sea. The last section focuses on why there is a need to study the North Sea further in terms of sediment dynamics.

2.2 Factors which Control the Movement of Sediment

2.2.1 The Bottom Boundary Layer

On the continental shelf and in shelf seas, tidal currents are influenced by the effect of friction at the sea bed. As a result of this friction between the flowing water and the seabed boundary, the flow velocity is reduced. This area of flow retardation is called the bottom boundary layer. Reduction is greatest near the sea bed, but gets less further into the body of the flow (Dyer, 1986), so that the velocity increases to a value which equals that at the water surface, if the boundary layer occupies the entire water depth, or to a free stream velocity (u_∞) at the edge of the boundary layer, in water which is deeper than the boundary layer thickness (Soulsby, 1983) (figure 2.1). Surface waves and oscillatory velocities penetrate to the seabed in water depths less than half their wavelength. For example, a 12-s wave, generally in the swell band, will penetrate to the bottom in 112m of water or shallower, whereas a 6-s wave will penetrate in depths of 28m or shallower. Thus, in shelf seas like the North Sea, the bottom boundary layer will not only be affected by the steady currents, but also will be affected by wind waves and swell (Grant and Madsen, 1986). Two distinct bottom boundary-layer regions develop under a combined action of waves and currents. In the immediate vicinity of the bottom, an oscillatory boundary layer exists on the order of 3-5 cm thick in small waves and 10-30 cm in strong waves (Grant and Madsen, 1986). In this thin layer of intense vertical shear, the shear stress is dependent on a non-linear combination of both waves and currents and a roughness associated with the physical bottom roughness (Stapleton, 1996). This wave boundary layer is embedded in a larger boundary layer in which the turbulence is associated with steady or tidal current only.

In the sea, the forces acting in the bottom boundary layer are measured in terms of force per unit area, i.e stress. Two forces dominate in the boundary layer. A real fluid moving past a body will exert a drag force on it. Distortion of the streamlines past the moving body of water will create a pressure differential between the upstream and downstream sides of the

body and each element of the body will have a dynamic pressure directed normal to the surface. The sum over the body of the horizontal component of the dynamic pressures gives the form drag contribution to the total drag. A skin friction will also occur due to the shearing of the fluid past the surface of the seabed, which will depend on the viscosity of the fluid, the roughness of the surface and on the detailed form of the near surface flow. The skin friction is thus the sum of the shear stresses (τ) over the body surface Dyer (1986). Close to the boundary layer, the shear stress and turbulent kinetic energy are due to both waves and currents. Significant amounts of sediment can be put into suspension and transported during storms. On the other hand, the interaction of waves together with the local tidal currents may give rise to a gradual migration of sediment in one preferred direction. The suspended sediment can also modify the density field to cause stratification of the boundary layer, especially if strong sediment-concentration gradients exist.

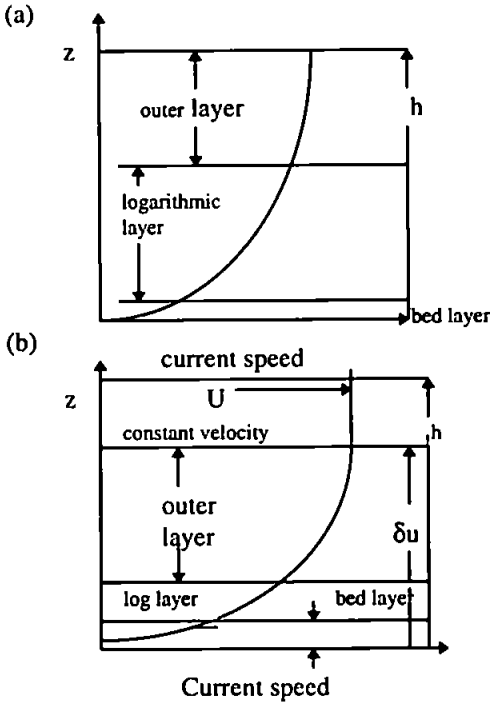

Figure 2.1 Diagrammatic representation of the bottom boundary layer (a) For boundary layer which occupies the entire water depth. (b) for water which is deeper than the boundary-layer thickness.

(From: Soulsby, 1983)

2.2.2 Boundary Layer Thickness

The thickness of the boundary layer (δ) is difficult to measure in the sea, because calculation of the free stream velocity is approached asymptotically. In the laboratory, the thickness is usually defined as the height where the velocity is within 1% of the free stream velocity (Dyer, 1986), or $u(\delta u) = 0.99u_\infty$ (Soulsby, 1983). It is, however, not possible to use such a precise definition in the sea. In a pure oscillatory current, the boundary layer thickness can be defined as $\delta = u_*/f$, where u_* is the friction velocity and f is the angular frequency of the oscillation. If the oscillation frequency is that of the Earth's rotation, the Coriolis parameter is used (Soulsby, 1983; Dyer, 1986,). For semi-diurnal tides in the shelf seas around the British Isles, Soulsby (1983) defined the boundary layer thickness, using modelled current velocity values for mean spring tides (Flather, 1976), and taking the bed drag coefficient value to be constant C_d=0.0025, as:

[2.1]

$$\delta=0.0038\left(\frac{\bar{u}_a\omega - \bar{u}_b f}{\omega^2 - f^2}\right)$$

where $\bar{u}_a$ and $\bar{u}_b$ are the depth mean flows in the direction of the tidal ellipse axes, ω is the angular frequency of oscillation for a semi-diurnal tide given as $1.4 \times 10^{-4} s^{-1}$, and f is the Coriolis parameter. Equation 2.1 is needed when $\omega \sim f$ (for example, tides).

2.2.3 Boundary Layers in Unidirectional Flow

Within the bottom boundary layer, very near to the seabed, is a layer in which either the bed is sufficiently smooth that the effect of molecular viscosity dominates the dynamics, or the presence of roughness elements causes horizontal variations in the profiles of velocity and turbulence around and just above them. This layer is commonly termed the bed layer (Wimbush and Monk, 1970; Soulsby, 1983). In the sea, the bed layer is commonly a few cms thick. In the absence of waves and when molecular viscosity dominates the dynamics, this layer can be split up into two regions. The first consisting of the viscous or laminar sublayer which is a few millimeters thick, and above this viscous layer a transitional or buffer layer. The second region is the fully turbulent logarithmic layer, in which neither the details of the bed nor the nature of the free-stream flow affect the local dynamics. In this layer, the velocity profile is logarithmic with height (figure 2.2 (a)).

In rough turbulent conditions, the sublayer and transitional zones are absent, and the fully turbulent layer extends right down below the tops of the roughness elements (figure 2.2 (b)).

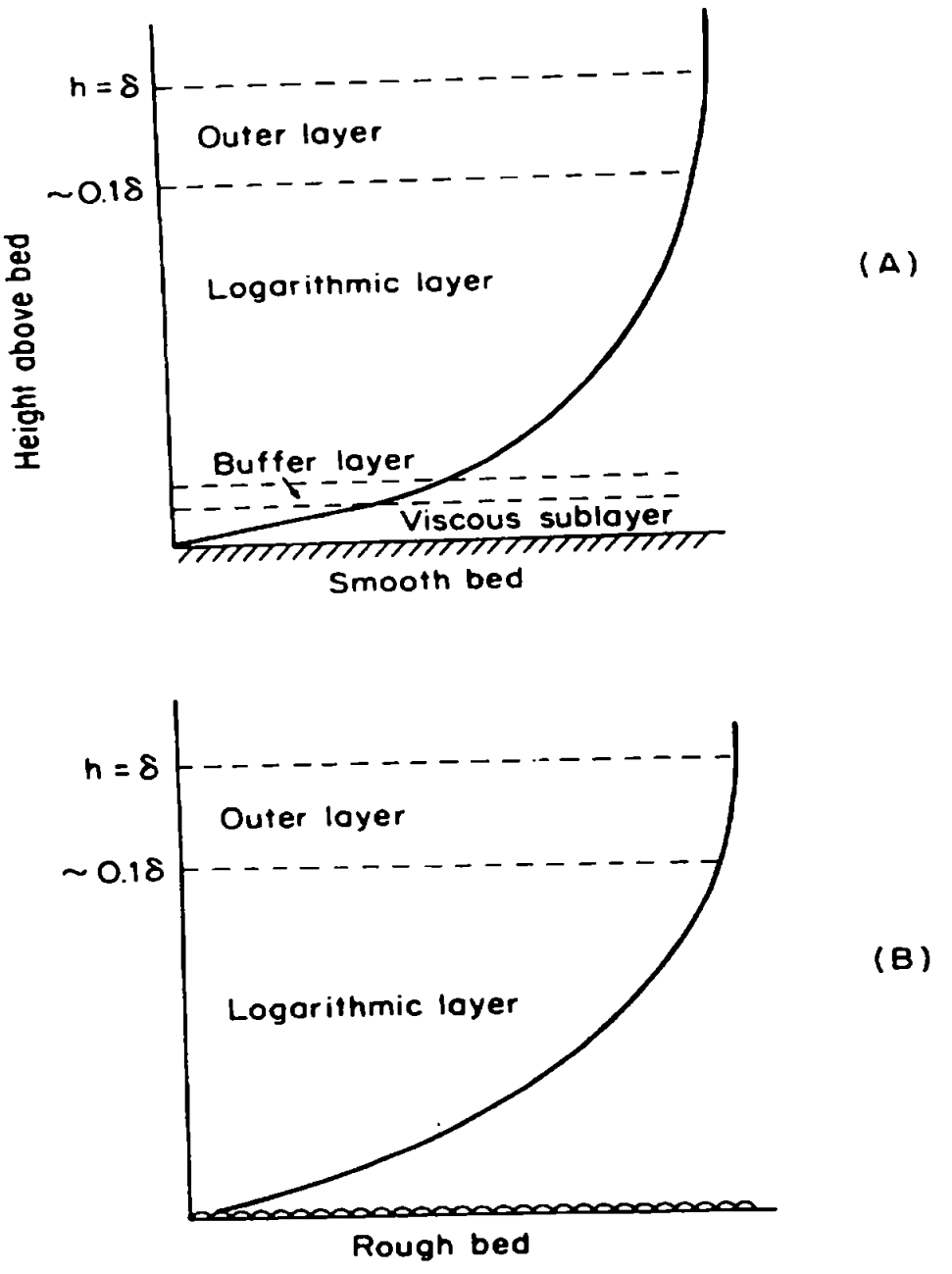

Figure 2.2 Diagramatic representation of the velocity profiles for (a) Smooth turbulent, and (b) rough turbulent flow.

(From: Dyer, 1986)

The velocity profile in this layer is logarithmic, and is given by the von Karman - Prandtl equation:

[2.2]

$$\frac{\bar{u}(z)}{u_*} = \frac{1}{k} \ln \frac{z}{z_0}$$

From measurements of velocity at several heights, a plot of ln z (height) against velocity (u) gives a straight line with a gradient k/u_* and an intercept z_0 which gives a value for the hydrodynamic roughness length. From this value of u_* an estimate of shear stress can be calculated using the relationship $\tau_0 = \rho u_*^2$. The value of the von Karman's constant is taken as 0.4.

Above the logarithmic layer is the outer layer which comprises the remaining 80-90% of the boundary layer. In this layer the flow is independent of viscosity, but depends strongly on the nature of the free stream flow (Soulsby, 1983). In the outer layer, the shear stress and the turbulence energy diminishes towards the top of the boundary layer. The velocity outside the boundary layer is constant, and non turbulent so that the shear stress is zero.

2.2.4 Boundary Layers in Combined Wave and Current Flows

The most important aspect of wave-current boundary layer interaction is the change of current velocity distributions due to the superposition of waves (Nielsen, 1992). Waves alter the current profile by inducing greater mixing in a layer close to the seabed (figure 2.3 (a)) which is given by $z < L$, where L is equal to a layer of thickness close to the bed with direct wave influence on mean current velocity $\bar{u}(z)$. As a result of this wave induced mixing, the current gradients inside this layer will be suppressed. Outside this layer, wave-induced turbulence is weak and the current profile is logarithmic. However, the roughness length z_0 derived from the logarithmic profile, at zero intercept, will be larger, and will be at z_a, corresponding to an apparent increase in the bottom roughness (figure 2.3 (b)).

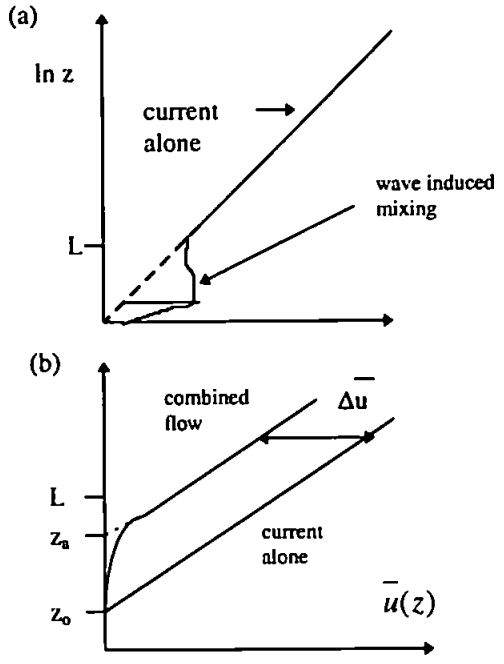

Figure 2.3 Wave-induced changes to current profiles
(From: Nielsen, 1992)

he apparent roughness increase z_a/z_0 and the corresponding velocity reduction $\Delta\bar{u}$ is given as:-

[2.3]

$$\Delta\bar{u} = \frac{u_*}{k} \ln \frac{z_a}{z_0}$$

and can be expected to depend on the relative current strength, the relative roughness, and on the angle between the current and the direction of wave propagation. Kemp and Simons (1983) suggested that, for opposing currents (ϕ = 180°), the apparent increase in roughness is greater than for following currents (ϕ =0 °).

The von Karman-Prandtl logarithmic profile has been used extensively in the sea, and consequently the bed shear stress can be calculated quite easily from the measured velocity profile in the turbulent part of the constant stress layer. However, the shear stress estimated from the slope of the profile may not be the assumed stress for sediment movement at the bed. The reason for this may be slight curvature of the profile which is

not obvious because the effect is hidden by random errors (Dyer, 1986). Since velocity measurements near to the seabed are not normally taken at < 15cm above the seabed, this curvature, if extrapolated to the seabed, will create a steeper slope, and thus a smaller estimated shear stress would result, compared to the shear stress measured from the profile higher up in the flow. Dyer (1986) attributes the disturbance on the velocity profile to a number of factors, one being the acceleration and deceleration of the current. The effect of an accelerating current is to produce a flow profile that is concave upwards, so that the current is smaller than the logarithmic value by an amount that increases with z. Similarly, a decelerating current produces a profile that is convex upwards which produces a steeper velocity profile, and hence, a smaller shear stress value. Typical overall values are ±20 % for u_* and ±60 % for z_0.

A steep velocity profile may also develop when there is stratification due to suspended sediment, resulting from the vertical gradient of sediment concentration giving rise to a vertical gradient of density (Soulsby and Wainwright, 1987). The presence of the density gradient will have an effect on the velocity profile as shown in figure 2.4. The gradient Richardson number given in equation 2.4 is a means of estimating what the vertical concentration gradients need to be to produce the effects highlighted in figure 2.4.

[2.4]

$$Ri = \frac{g/\rho \frac{d\rho}{dz}}{\left(\frac{d\bar{u}}{dz}\right)2}$$

where, the denominator is proportional to the turbulent shear stresses and the upward transfer of momentum is compared with the downward flux of mass due to gravitational forces (Dyer, 1986). The conditions are such that when:

Ri > 0 the stratification is stable,
Ri = 0 stratification is neutral and fluid is stratified between the two depths,
Ri < 0 stratification is unstable

However, most investigators who are faced with the task of obtaining the friction velocity from velocity profiles measured near the seabed have assumed that suspended sediment

effects can be neglected and have used the von Karman-Prandtl equation (Soulsby and Wainwright, 1987).

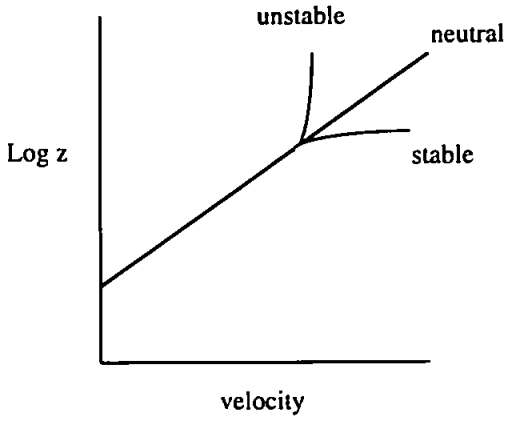

Figure 2.4 Velocity profiles under conditions of varying stratification
(Dyer, 1986)

Presence of ripples on the seabed causes a physical obstruction to the flow and produces a pressure gradient which causes both an additional resistance to the flow as well as an internal boundary layer a few wave heights above the ripple crests. This physical retardation is called the form drag. Although the form drag does not contribute to the drag causing sediment movement, it does reduce the capacity of the flow to transport sediment (Dyer, 1986). If bedforms are large, logarithmic profiles can be used as a measure of skin friction on the bed wave. If bedforms are small, such as ripples, then conventional velocity profiles will only measure the total stress since the profile does not extend close enough to the sea bed to measure the internal boundary layer. Observations by Smith (1977) produced a form drag which was 4.7 times the skin friction in a non-separating flow in the presence of suspended sediment. In a separating flow, the form drag was 3.1 times the skin friction (Dyer, 1986). The von Karman-Prandtl equation cannot be used directly on the BLISS data sets because velocity is only measured at a single height above the seabed. It can however, be used indirectly, if the roughness length is known, or can be assumed.

Understanding the processes which affect the flow is essential to our interpretation of the bed shear stresses. The shear stresses produced under the combined influence of waves and current in the bottom boundary layer will significantly influence the movement of sediment. Measuring this stress *in situ* is almost impossible, because the instruments

available which measure stress directly are too delicate to be used in the natural environment (Stapleton, 1996).

2.2.5 The Relationship between Velocity and Turbulence

The measurement of velocity in the sea can be considered in two ways:

1. An Eulerian measurement, where the speed and direction is recorded through time at a point fixed in relation to external co-ordinates.
2. A Lagrangian measurement, where a particle trajectory is followed, so that the speed and direction at any one time can be reconstructed, but they refer to different positions with respect to external reference.

All velocity measurements taken with regards to this thesis, were taken as Eulerian measurements.

Instantaneous velocity measurements taken near to the seabed are made up of three components, u,v,w. For the BLISS data, the u and v velocity co-ordinates were defined as shore normal or cross-shore (x) and alongshore (y) to the coastline. The w co-ordinate (z), was measured perpendicular to the seabed. The instantaneous velocity components are $\bar{u}+u'$, $\bar{v}+v'$ and $\bar{w}+w'$ in the x, y and z directions, respectively, with u',v' and w' being the wave and turbulent fluctuations about the steady currents $\bar{u}$, $\bar{v}$ and $\bar{w}$. Turbulence in the flow causes random movements of small eddies within the fluid, so that the instantaneous situation is complex and changes quickly. The only way one can observe any variation to the flow in the tidal context, is by considering the time average conditions of typically 10 minutes or more (Soulsby, 1983, Dyer, 1986).

2.2.5.1 *Turbulence*

The point at which flow becomes turbulent was first investigated by Sir Osborne Reynolds (1883). He injected dye into flow of different velocities and watched the stage at which turbulent eddies were produced as the flow passed along a circular pipe. From these studies, Reynolds deduced two modes of flow, laminar and turbulent. He showed that the onset of turbulence occurred at a constant value attained by a dimensionless combination of

the flow velocity u, the diameter of the pipe d and the fluid kinematic viscosity $\nu = \mu / \rho$, namely, the Reynolds Number which is taken as

[2.5]

$$Re = ud/\nu$$

From his experiments, the onset of turbulence arrived at Re. ~2000, but fully turbulent flow did not occur until Re. ~4000. Before Re ~2000, the flow was laminar. In addition to the concept of laminar and turbulent flow, Reynolds in 1894 derived the equations of motion for a turbulent mean flow. This lead onto the introduction of the Reynolds stresses, which are parameters with the same dimensions as stress.

Including water density, the time average of the turbulent fluctuations can be rewritten in terms of Reynolds shear stresses (discussed in section 5.5.2) $-\rho\overline{u'w'}$, $-\rho\overline{v'w'}$, $-\rho\overline{u'v'}$, where the over bar denotes a time average. By far the most important component for sediment transport studies, is that involving a vertical momentum exchange, for at the boundary it is this component of stress that is involved in moving the sediment grains.

It is convenient to express the bed shear stress in the form that has the dimensions of a velocity. This is achieved by defining a friction velocity u_* such that $\tau_o = \rho u_*^2$. Three methods which use the velocity of u, v and w and the turbulent fluctuations u' v' w', to measure bed shear stress, are addressed later in section 5.5.

2.2.6 Sediment Movement

Sediment is generally considered to move either as bedload or in suspension, concentration of the latter will depend on the grain size and on the energy of the flow. Bagnold (1966) defined the demarcation line between these two situations as:-

"the bed-load is that part of the load which is supported wholly by a solid-transmitted stress, and the suspended load is that part which is supported by a fluid-transmitted stress" (Soulsby, 1977).

In this case, the stress is an interaction between particles or fluid and particles. When water flows over a seabed composed of loose sediment, there will be a certain velocity at

which the instantaneous fluid force on a particle is just larger than the instantaneous resisting force related to the submerged particle weight and the friction coefficient (Van Rijn, 1993), so that the sediment is dislodged from its equilibrium position. Hence the driving forces are strongly related to the local near bed velocities and the critical or threshold shear stress (τ_c).

An understanding of velocity threshold is obviously very important to predicting the onset of sediment transport in shelf seas. When the velocity of the current is just above the threshold, the grains will move as bedload in a zone a few grain diameters thick, but at a speed which will be lower than the local water velocity. As velocity increases, the sediment can be suspended up into the water column and will travel at a velocity equal to the local stream velocity. In turbulent flows experienced in shelf seas, the velocities are fluctuating in space and time. Combined with variations in particle size, shape and position, initiation of sediment movement is not merely a deterministic phenomenon but a stochastic process as well (Van Rijn, 1993), so that the threshold is a value that is averaged over the bed and through time. The spatial scales in question are in dm and the time scales are 10's of seconds (Pers. comm., Dyer, 1997).

2.2.7 The Threshold of Sediment Movement

Early work to ascertain the velocity threshold of sediment motion focused on developing empirical relationships taking the form of graphs or equations representative for conditions under uni-directional currents. Hjulstrom, (1935, 1939), Sundborg, (1946), devised such graphs by performing tests in laboratory flumes with parallel sidewalls under conditions of uniform steady flow over an initially flat bed (Miller *et al.*, 1977). They chose non-cohesive sand grains of spherical shape and of a uniform size, not typical of what is found in the marine environment, but in many cases, not too dissimilar either.

The semi-empirical curves of Hjulstrom and Sundborg are difficult to apply in practical conditions because they do not take into consideration the effects of non-uniform grain size and presence of bedforms which, ultimately, will alter the threshold velocity. This has encouraged scientists to investigate the threshold of sediment motion in terms of shear stress exerted on the sea bed, rather than a current at some height above the bed.

2.2.7.1 *Threshold of Sediment Motion in Unidirectional Flow*

A widely accepted parameter for predicting the initiation of sediment motion on a plane bed composed of well-sorted particles is given by the Shields entrainment function θ (Dyer, 1986).

Physical arguments are used to combine the parameters of interest into several non-dimensional relationships. These parameters are the density of the sediment, ρ_s, the grain diameter D, the fluid density ρ, the kinematic fluid viscosity ν and the shear stress of the fluid flow τ, as well as the acceleration due to gravity g (Miller *et al.*, 1977), which are combined by Shields into the dimensionless relationship:

[2.6]

$$\theta = \frac{\tau}{(\rho_s - \rho)gD} = \frac{\rho u_*^2}{(\rho_s - \rho)gD} = f(Re_*) = f(u_* D / \nu)$$

where the combination of u_*D/ν is the dimensionless grain Reynolds number, R_{e*}.

When this parameter represents the threshold condition for sediment motion it is denoted by θ_t and is called the Shields Criterion. It essentially expresses a critical value of the ratio of the entraining force to the stabilising force acting on the sediment grain. The entraining force is related to the shear stress exerted on the bed by the moving fluid, the stabilising force being related to the submerged weight of a sediment grain. When the ratio of the two forces exceeds a critical value, sediment movement is initiated (Larsen, *et al.*, 1981). This criterion is a dimensionless relationship which can be applied for any fluid flow and sediment characteristics as long as the sediment is cohesionless.

A diagram of θ_t versus R_{e*} was presented by Shields (1936) (figure 2.5). The data (Shields data, Dyer, 1986) were represented by a narrow band, below which the bed stress is insufficient to cause motion. Above the band, sediment would be in motion. A full account of unidirectional threshold curves (on flat beds under laboratory conditions) are given in Miller *et al.*, (1977).

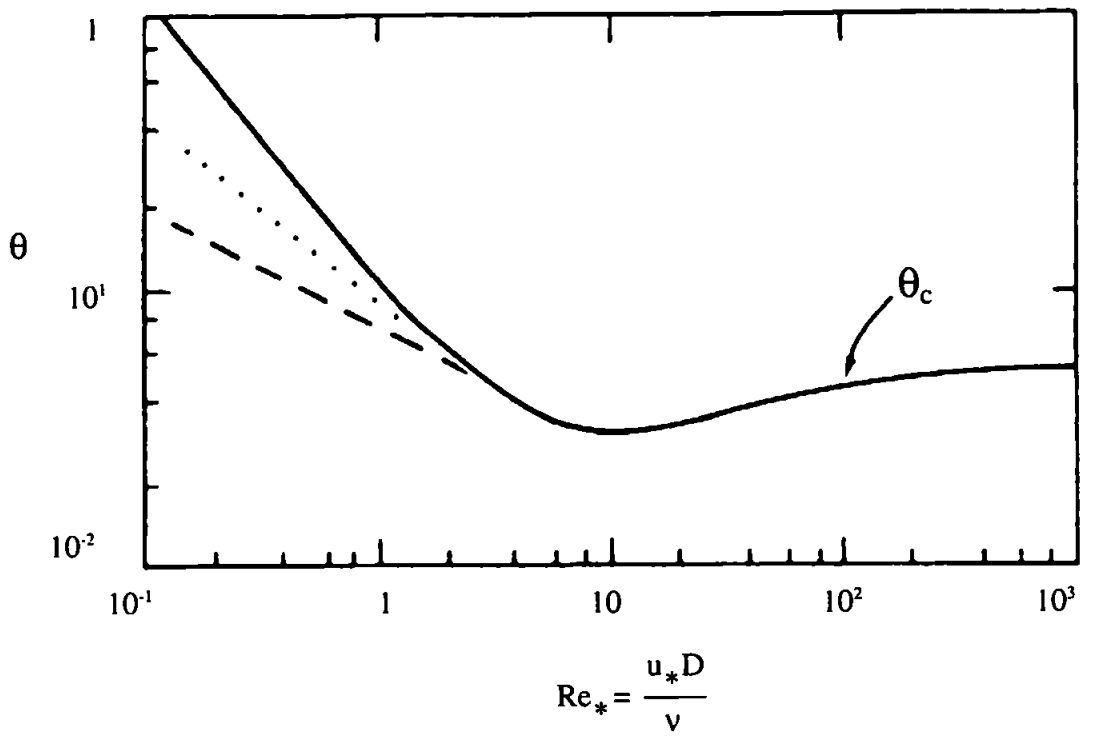

Figure 2.5 Shields threshold curve, solid line.
(From: Dyer, 1986)

2.2.7.2 *Threshold of Sediment Motion Under Waves*

The approach to the threshold of sediment movement under waves has been largely an empirical one (Dyer, 1986). Komar and Miller (1975) evaluated the Shields criterion for oscillatory flow using laboratory data. In applying the criteria they interpreted u* in equation 2.6 as a maximum oscillatory velocity. Their initial conclusions stated that the Shields parameter would lead to considerable error and suggested the following equation to predict the threshold of motion for grain sizes <0.05cm (Larsen *et al.*, 1981).

[2.7]

$$M_{crit} = \frac{\rho U_m^{\,2}}{(\rho_s - \rho) g D} = a'' \left(\frac{d_0}{D}\right)^{1/2}$$

where a" is a dimensionless coefficient, d_o is the orbital diameter of the wave motion, and the other terms are as previously defined.

The value of a" was initially estimated as 0.3 but Larsen *et al.*, (1981), later revised the estimate of a" for the onset of sediment transport under oscillatory flow conditions to:

[2.8]

$$M_{crit} = 0.21 \left(\frac{d_0}{D}\right)^{1/2} \text{ for } D < 0.5\text{mm}$$

(Dyer, 1986, Larsen *et al.*, 1981).

The maximum orbital velocity and the orbital diameter d_0 are related by $U_m = \pi d_0/T$, where T = wave period. Komar and Miller (1975) produced a series of curves of different wave periods which gave a simple way of relating the threshold of orbital velocity to the grain size of quartz particles. The curves give a threshold value of 14 to 22 cms^{-1} under waves of period 5 to 15 seconds respectively for a grain size of 0.2mm. That is, for a given grain size, an increase in wave period will require a higher threshold velocity.

An alternative approach to determining threshold in oscillatory conditions, is to write the threshold conditions in terms of the bed shear stress by using a wave friction factor (f_w) Dyer, (1986), given as:

[2.9]

$$\theta_c = \frac{\tau_{cm}}{(\rho_s - \rho)gD} = \frac{\frac{1}{2} f_w \rho u_m^2}{(\rho_s - \rho g)D}$$

where τ_{cm} is the maximum bottom shear stress, u_m is the maximum oscillatory velocity at the seabed, and f_w is the wave friction factor. The critical value of θ_c for predicting the threshold of grain motion is found to vary depending on the ratio of the thickness of the laminar sublayer to the boundary roughness. This ratio can be expressed in terms of a boundary Reynolds number (Dyer, 1986).

[2.10]

$$Re_* = u_* D/\nu$$

where v is the kinematic viscosity. The Reynolds number dependence is commonly ignored, since in the sea under these conditions a fully turbulent boundary layer is expected. A formula for predicting f_w under rough turbulent conditions was given by Jonsson, (1980) as:

[2.11]

$$f_w = \exp(5.213\,(r/A)0.194 - 5.977) \text{ for } r/A < 0.63$$

where r is the bed roughness and A is the water particle amplitude given as $A = u_m T/2\pi$. Values of f_w are normally in the range 0.01 to 0.07.

Madsen and Grant, (1975) discussed the Shields criterion in respect to threshold of sediment movement under waves. They suggested that the Shields criterion is a valuable tool for predicting the threshold of grain motion under waves if the shear-stress estimate is based on the maximum boundary shear stress due to the oscillatory motion (Larsen *et al.*, 1981) by calculating oscillatory thresholds using equation 2.9. They found that the values of the oscillatory thresholds fitted the Shields threshold curve with about the same degree of scatter as the unidirectional data. Therefore, the standard unidirectional Shields curve is often used for the oscillatory threshold.

2.2.7.3 *Threshold under Combined Wave/Current Flows*

The above considerations for waves exclude the influence of a mean flow component on the estimate of the critical threshold parameter. Tides, wind-driven flows, inertial motions etc., are commonly present in shelf seas. Therefore, the bottom flow will have a low-frequency component (hours to days) and an oscillatory component (5 - 20 seconds), so that the boundary shear stress would be a combination of the two. A mean current is defined as *"a current whose characteristic period is long compared with the response time for sediment suspension"* (Larsen *et al.*, 1981). The response time for resuspension is of the order of 1 sec. Gravity wave currents of the order 10-15 seconds are considered oscillatory currents whereas a current whose period is 15 minutes or longer is a mean current in terms of the response of the sediments to induced stresses (Larsen *et al.*, 1981).

Hence, the difficulty is in defining the shear stress under the combined flows, not the threshold per se (Pers. Comm., Dyer, 1997).

To estimate the total boundary shear stress under the combined action of waves and currents using model formulations was formerly tackled by Grant and Madsen, (1979). They recognised that because of the contrasting time scales of the current and waves, two different boundary layer flows evolve; i.e. the fully developed current boundary layer, assumed to extend over most of the depth of flow in the absence of stratification, and the oscillatory wave boundary layer, confined to a relatively thin region close to the seabed. Thus in the immediate vicinity of the seabed, the shear stresses and turbulent intensities due to the comined effect of both the wave and current, are coupled in a nonlinear fashion. The end result is that the current in the reigon above the wave boundary layer, i.e. the potential flow region for the wave, experiences a shear stress which depends not only on the physical bottom roughness but also on the wave boundary layer characteristics. Grant and Madsen introduced into their model the concept of an apparent roughness which reflects the characterstics of the wave boundary layer, so that the current above the wave boundary layer feels the greater resistance. Larsen *et al.*, (1981) described a model based on the formulations of Grant and Madsen (1979). They used easily measureable variables such as: wave period (T), orbital wave velocity amplitude (u_m), mean velocity u_z at a specified reference height (z), the bed grain diameter (D), the direction angle (ϕ) between the wave and the mean current, and the physical bottom roughness z_0 due to grains and bedforms, to estimate the maximum boundary shear stress of combined flows. The difference between the two models was that in the Larsen *et al.*, (1981) model, a different method was used to calculate the boundary shear stress, whereby fewer variables were involved since the wave friction factor was not used. It must be noted that there are many more methods for estimating the total boundary shear stress, but the focus of this thesis is not on theoretical modelling and so, will not be discussed further.

2.2.7.4 *Summary*

Choosing the threshold of sediment motion is a subjective matter even in controlled laboratory situations. Since the work of Shields in 1936, it has been customary to define the threshold condition as one of weak but reasonably continuous, sediment movement. This problem is magnified in the field, where the choice of threshold is certain to be even

more subjective and imprecise. Drake and Cacchione, (1986) and Larsen *et al.*, (1981), defined a threshold event as a sudden increase in suspended sediment concentration above the background values. In the GEOPROBE study however, Drake and Cacchione (1986) noted two unavoidable problems using this definition. The first was that the suspended matter may have been entrained elsewhere and advected into the GEOPROBE site and secondly, the sampling rate they chose (once per hour or once per two hours) limited the resolution of the timing of threshold events.

The Shields Criterion has been widely accepted as the formula for obtaining the critical bed shear stress in shallow near shore zones, even though it was originally formulated for uni-directional flow on a flat bed. However, flat beds are rare in the sea, where sand is mobile, because the maximum tidal currents are capable of creating ripples which survive over the slack water periods. As a result, the appropriate threshold of motion in the sea is that of grains on an initially rippled bed (Kapdasli and Dyer, 1986). In this situation, the total stress is a combination of the form drag and the skin friction, as discussed earlier in section 2.2.1. Since it is only the skin friction that causes the sediment to move, the threshold of movement on the ripple will occur when the total drag over the bedform produces a skin friction at the crest equal to the Shield's value (Kapdasli and Dyer, 1986). Flume experiments conducted by Kapdasli and Dyer (1986) to establish the threshold of initial motion on a rippled bed, which in theory, should be applicable to sediment transport in the sea suggested that the form drag was between 5 and 12 times the skin friction. It must be noted however, that field conditions will be different from the laboratory flume conditions.

2.2.8 Sediment in Suspension

A reasonable distinction between bedload and suspended load is established in the way through which the weight of the grain is supported (Hanes, 1988). If the immersed weight of the grain is supported by grain to grain interactions (e.g. rolling, sliding and collision) then the grain is said to be part of the bedload. Suspended sediment is therefore described as those grains which are supported by fluid to grain forces. Saltating grains will be a combination of grain to grain and fluid to grain forces, but are usually considered as bedload since movement is in close proximity (only a few grain diameters) to the seabed.

Hence, suspension of sediment occurs when the upward directed components of the turbulent velocity fluctuations w'_{up} exceeds the settling velocity (w_s) of the grains. Thus, $w'_{up} = w_s$.

Bagnold (1966) using the relationship $(w'^2)^{1/2} = 0.8u_*$, (where $(w'^2)^{1/2}$ is the rms vertical velocity fluctuations), deduced that full suspension occurred when $w_s = 1.25u_*$. Substituting this relationship into the Shields Entrainment function gives:

[2.12]

$$\theta_s = 0.4\frac{w_s^2}{gD}$$

According to Bagnold (1966), at high Re_*, $w_s = 4.5\ u_{*c}$, and $\theta_c = 0.06$. This gives $\theta_s = 0.78$. Figure 2.6 shows the curve of equation 2.11 shown together with the Shields threshold curve.

Other values of θ_s have been derived. McCave (1971) devised a value of 0.19 using the nearbed value of $(w'^2)^{1/2} \sim 1.20u_*$.

In the nearshore zone, sediment transported will be a combination of both bedload and suspended load. The quantitative definition of bedload and suspended load has been the subject of considerable discussion. In addition, non-cohesive sediment such as sand and gravel, and cohesive muds move in different ways. In the context of this thesis, attention will focus towards quantifying the suspended sediment flux and determining the processes which control the movement of sediment off the Holderness coast.

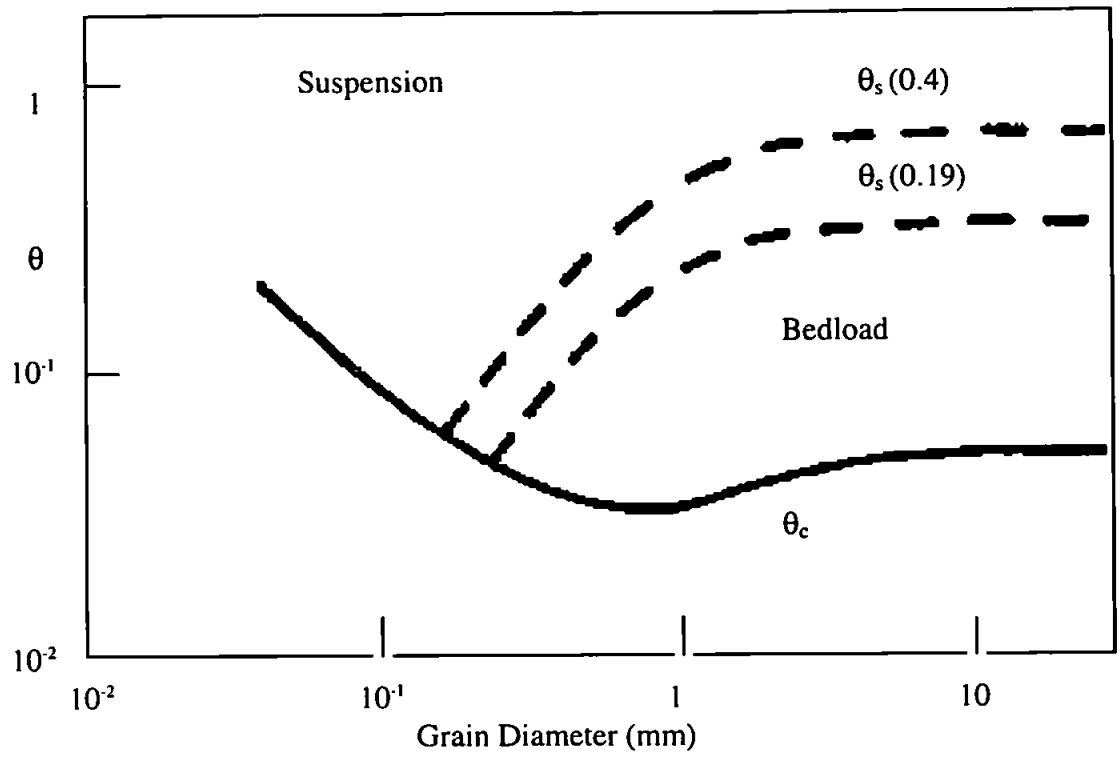

figure 2.6 Shields diagram showing the threshold of suspension according to Bagnold (1956) with a coefficient of 0.4 and McCave (1971) with a coefficient of 0.19.
(From: Dyer, 1986)

2.2.9 The Suspended Sediment Transport Flux

To calculate the suspended load transport flux, it is necessary to be able to predict the profile of concentration throughout the water depth either based on a measurement at a single height above the seabed, or on knowledge of the power of the stream and the bed sediment size (Dyer, 1986). The sediment flux is then calculated by multiplying the current velocity by the suspended sediment concentration and then numerically integrated to obtain the transport flux.

In a turbulent tidal current, the fluxes of suspended sediment will have both mean, wave and turbulent components in the horizontal and vertical axes. Downstream, the mean flux is derived as $\bar{u}\,\bar{c}$ from the product of the mean velocity and mean concentration. In addition to this there is a wave and turbulent component $\overline{u'c'}$. There is also an equivalent mean vertical flux, $\bar{w}\,\bar{c}$ which can either be positive or negative depending on the

secondary flow circulation (Dyer, 1986). The vertical turbulent flux $\overline{w'c'}$ can also be upwards or downwards. Essentially then, the sediment transport flux is the total weight of grains passing through an arbitary section of the water column per unit time, and is the product of the weight of the moving grains present in the water over a unit area, times the velocity at which the grains move (Dyer and Soulsby, 1988). Hence, the relationship between sediment transport flux and the flow is a complex one. Volume flux (Q_s) of sediment transported in the bottom boundary layer transported as bedload or suspended load is related to a power of the friction velocity, u_*. That is $Q_s \propto u_*^n$, where n is ≥ 2 in most formulae (Cacchione and Drake, 1982). At 10cm above the seabed Dyer (1980) found that the suspended sediment transport flux was $Q_s \propto u_*^7$.

2.3 Physical Characteristics of the North Sea

The North Sea is an epicontinental sea lying on the continental shelf off North West Europe (figure 2.7). It is virtually surrounded on three sides by land, being open to the Atlantic Ocean only to the North where it continues into the Norwegian Basin, to the Baltic Sea in the East, and the English Channel to the South through narrow straits. The North Sea has a surface area of approximately 575000 km^2 and a total volume of seawater of ca 54000 Km^3 (Eisma, 1986). Topographically, the North Sea can be divided up into three sections, namely, the Southern Bight (51° - 54°) normally with water depths of <40m; the Central North Sea (54° - 57°) with depths in the region of 40m - 100m (there are exceptions however, for example over the shallower areas of the Dogger Bank) and thirdly, the Northern North Sea (north of 57°) which includes an area of shelf water 100m - 200m deep and the Norwegian Channel with water depth ranging from 200m - 700m, especially in the Skagerrak between Denmark and Norway (Holligan *et al.*, 1989). Several major rivers flow into the North Sea, the largest being the Rhine and the Elbe.

The energetic hydrodynamic mechanisms of the North Sea are generated by several different controlling forces. The most important are the tides. Another major source of energy is the wind, which coupled with atmospheric pressures, is responsible for inducing storm surges. Seasonal forcing of the circulation originates from alternate heating and cooling of the surface layers, which leads to thermal stratification in the Northern North Sea. Freshwater input from the major rivers which flow into the North Sea also cause

density differences (notably the Rhine), resulting in salinity stratification near to river mouth. Away from the rivers, in the shallow areas, the water is well mixed.

2.3.1 Circulation in the North Sea

Circulation of the North Sea is governed by three main branches of inflowing Atlantic water and the outflow of the Norwegian Coastal Current. There is a northward progression of the North Atlantic semi-diurnal Kelvin wave along the shelf edge to the west of Ireland. Energy is transmitted across the shelf edge into the Celtic Sea between Brittany and Southern Ireland. This wave then propagates into the English Channel where some energy leaks into the Southern North Sea and into the Irish Sea and the Bristol Channel. The Atlantic wave continues in a northward direction, taking approximately five hours to travel from the Celtic Sea to the Shetlands (Pugh, 1987).

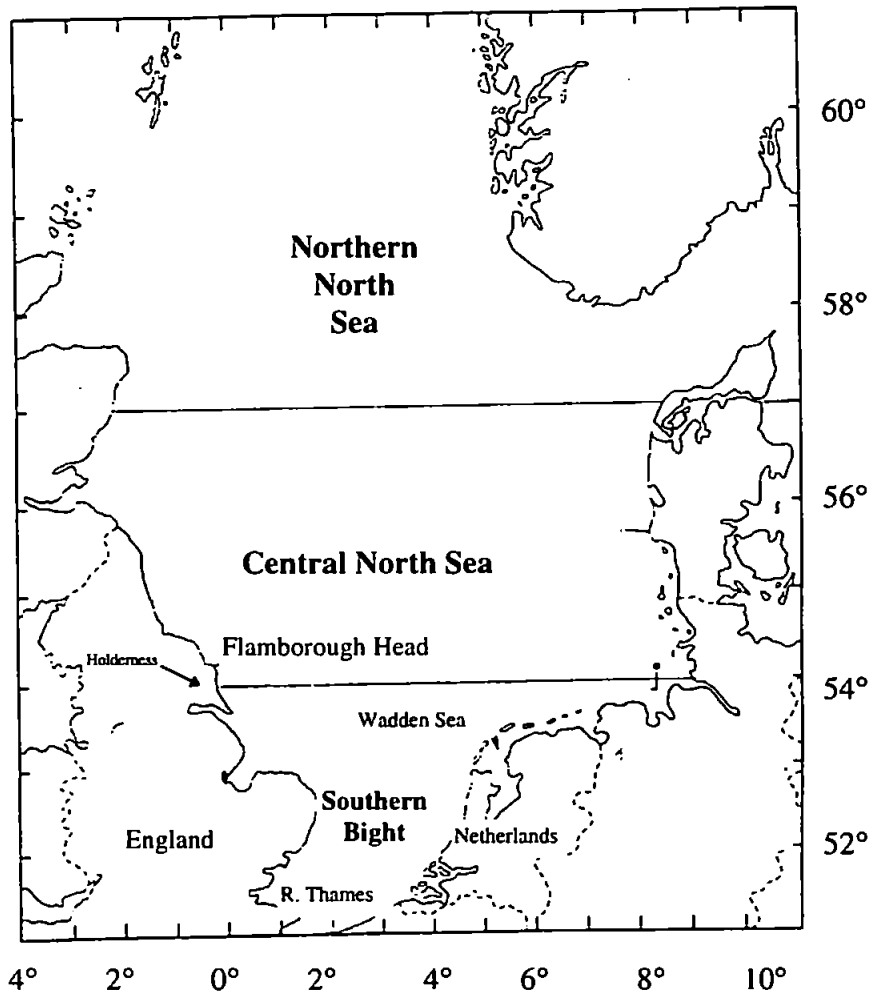

Figure 2.7 The North Sea

(From: Holligan *et al.*, 1989)

On reaching the Shetlands, the semi-diurnal wave is joined by another wave which has flowed through the Celtic and Irish Sea. The joined wave then partly diffracts around the North of Scotland where it turns to the East and to the South, to enter the North Sea through the Fair Isle Channel with a tidal energy of 50 Giga Watts (Charnock *et al.*, 1994). The Kelvin wave then propagates South influenced by geostrophic forces, following the configuration of the east coast of Britain. South of the Dogger Bank, it departs offshore and is guided eastwards by bottom topography (Mork, 1981) to join a second Kelvin-type wave which enters the North Sea through the English Channel and reflects in a North-East direction, continuing to hug the southern and eastern boundaries of the North Sea to its right, but decreasing rapidly in amplitude and becoming negligible off the Norwegian Coast.

A well defined coastal current flows along the Norwegian Coast from Skaggerak towards the Norwegian Sea. This distinct current forms the main transport of water out of the North Sea along the eastern slope of the trench, carrying the surface outflow from the Baltic with the addition of coastal water from the Norwegian fjords (Mork, 1981). Flow is also influenced by deep inflow from the Atlantic as well as by the general circulation of the North Sea, and is estimated to have a mean transport of about 10^6 m^3s^{-1} (Furnes, 1980). The three main inflows together with the effects of the Earth's rotation (Coriolis force), drive the anti clockwise motion of the tides in the North Sea. The semi-diurnal tides in the North Sea are controlled in part by two complete amphidromic systems and a third degenerate system which has its centre in Southern Norway (figure 2.8). The largest amplitudes occur where the south-travelling Kelvin wave moves along the British coast (Pugh, 1987). Co-amplitude lines are parallel to the coast, whereas co-tidal lines are orthogonal. Tidal currents or streams are variable in the North Sea because they are sensitive to changes in depth, and to the influence of the configuration of the coastline eg. headlands and embayments. Mean spring tidal current amplitudes can reach upto 1.2 ms^{-1}, whereas in other regions the tide barely reaches 0.2ms^{-1}. The tide on ebb flows towards the North West, and on flood it flows towards the South East. A good general description of tides in the North Sea can be found in Banner *et al.*, (1980).

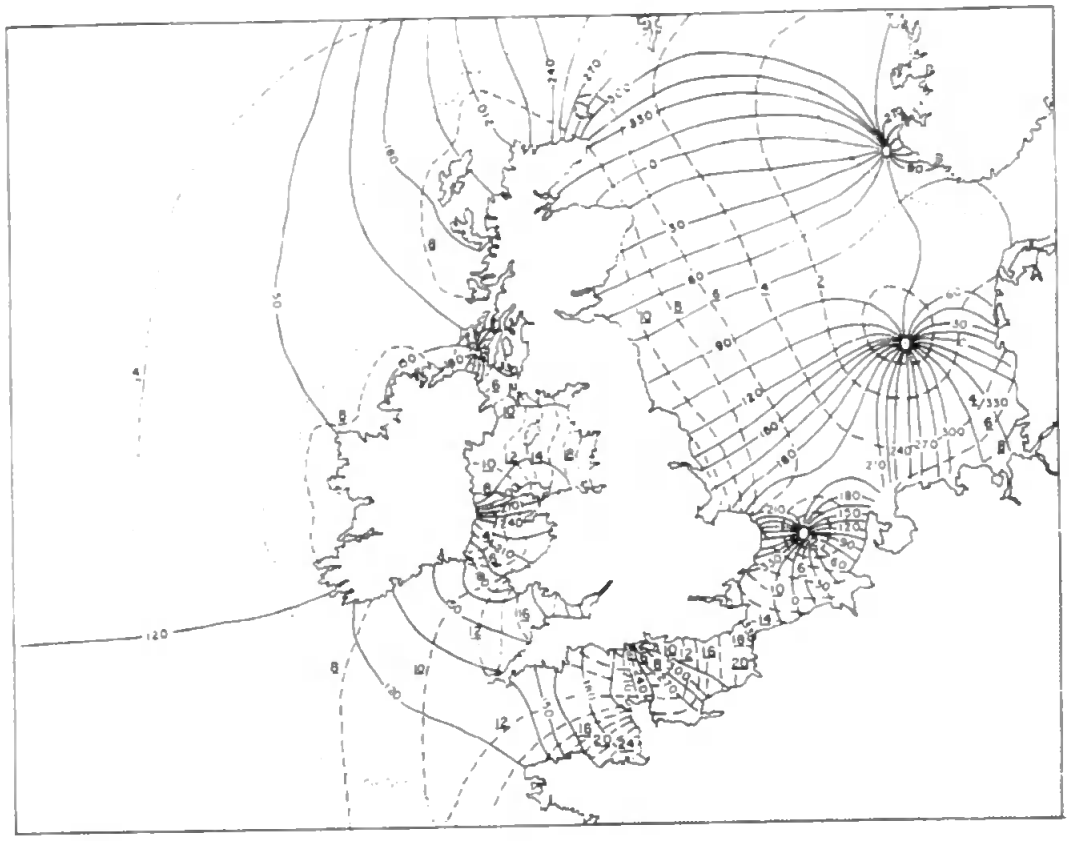

Figure 2.8 Amphidromes in the North Sea
(From: Banner *et al.*, 1980)

2.3.2 Thermal Stratification in the North Sea

The combination of the tidal currents and water depths is such that, in summer, heat input at the surface leads to regions of stratification. Tidal stirring in the Northern North Sea is much weaker than in the Southern Bight, and in the former the water column stratifies, to produce a distinct two layered structure. Between these two regimes is an important frontal region whose position varies little throughout the summer months. These fronts are known as the Flamborough and Frisian Fronts (Howarth, *et al.*, 1994). Tidal mixing fronts are well described by the criterion H/u^3 of Simpson and Hunter (1974), which controls the formation and location of the front, provided that the heat input and the mixing efficiency are constant over the limited time and area of interest. The Flamborough Head front has been modelled using a three-dimensional numerical model developed by James (1989).

The Front bounds a narrow coastal current North of Flamborough Head, where depth changes steeply near the coast. Near to Flamborough Head the front leaves the coast and separates well-mixed water in the southern, shallow North Sea from stratified water in the deeper area to the North (figure, 2.9). Further offshore, the front sometimes separates into a branch going past the banks known as "The Hills" and on to the North of the Dogger Bank and a branch pointing eastwards to the South of the Outer Silver Pit, where depths reach over 80m.

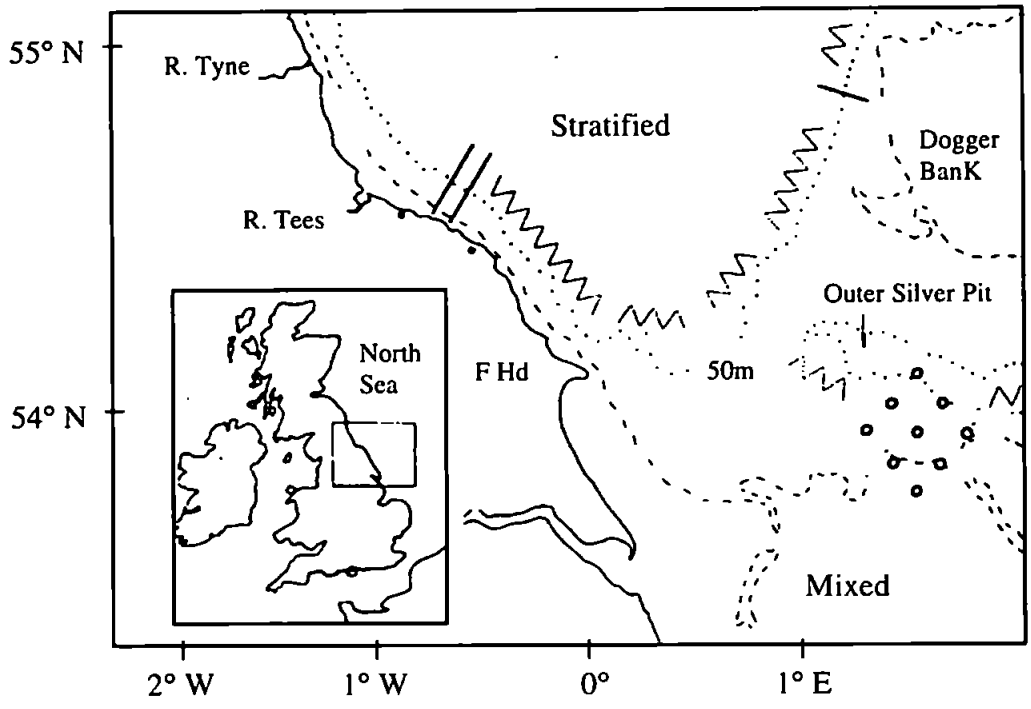

Figure 2.9 The North Sea frontal structure off Flamborough Head (F Hd)
(From: Hill *et al.*, 1994)

2.3.3 Study Region

The focus of the thesis area is concentrated off the East coast of England just inside the top left had corner of the Southern Bight boundary (figure 2.7), South of Flamborough Head (F Hd). This area is called the Holderness coast. In the sections which follow, reference will only be made towards the Southern North Sea as it is our main region of interest.

2.4 Dynamics of Suspended Sediment Concentration in the Southern North Sea - Results from the North Sea Project

Suspended particulate matter (SPM) is a crucial component of the shelf sea system, but in spite of the increasing recognition of its importance, very little was actually known about the distribution and nature of SPM and its variability with time prior to 1990 (Weeks and Simpson, 1991). Very few surveys had been undertaken in the North Sea, to obtain good time series data to define the seasonal and fortnightly cycles in SPM. Both horizontal transport paths and vertical distribution of SPM depend on a number of factors which influence deposition and resuspension or entrainment from the sea bed. These are namely, vertical flux controlled in part by bed shear stress, vertical mixing controlled by turbulent diffusion and settling of particles under the influence of gravity (Jones *et al.*, 1996). These processes are in turn governed by particle size, density and composition of SPM. Particle composition depends on particle provenance and is controlled by sea floor characteristics, water column dynamics and biological production as well as by regional horizontal transport pathways (Jago and Jones, 1993, Jones *et al.*, 1993).

2.4.1 The North Sea Project

The North Sea Project was an interdisciplinary study, set up in 1987 to examine a shelf sea in an extensive way in order to build on the rather basic understanding of the physics which had been achieved in the 1970's. The North Sea is perceived as being under threat from the increasing pollutant burden imposed upon it because it is surrounded by industrialised countries. All constituents, whatever their chemical or biological behaviour are acted upon by the same fundamental processes of movement by the mean flow and dispersion horizontally and vertically by turbulence (Simpson, 1994). Since the aim was to determine the fate of pollutants in the North Sea by means of a transport model, it was crucial that the physical processes which control the sediment, biology and chemistry in the North Sea were determined and included in the model. The models produced may then be used to manage the North Sea system in a rational and sensible way.

Apart from the tides, most processes within the continental shelf seas, for example, advection, mixing, temperature, salinity, turbidity and plankton growth, exhibit strong seasonal cycles ultimately forced by the weather conditions (Howarth *et al.*, 1994). So as to determine the seasonal behaviour of the physics, chemistry and biology in the North Sea,

the research vessel *RV* Challenger was assigned to the North Sea Project for a period of 15 months between August 1988 and October 1989. Cruises lasted 12 days and were repeated every 29 days, during which profile measurements and samples were taken at 120 stations along the survey track. For full survey details and results refer to Charnock *et al.*, (1994). The duration of each cruise and the use of only one ship restricted coverage to the Southern North Sea only. Processes with timescales of less than a month (eg. storms, plankton blooms, onset of stratification) were covered specifically by time series measurements taken at 6 moorings and by process studies which were conducted between each survey study on Challenger.

Cruise survey results will be shown in the next section with regards to the distribution of sediment in the southern North Sea.

2.4.2 The Distribution of Suspended Sediment in the North Sea

The following section gives an account of the distribution, origins, dispersion and budgets of suspended sediment in the North Sea. Previous work shows that sediment is supplied to the North Sea from a variety of sources, and deposition occurs in a number of areas. Eisma and Kalf (1987) and McCave (1987), consider that the major supply comes from the North Atlantic and from the English Channel, both of which contribute to ~ 10 x 10^6 tonnes a^{-1}. Other sources include river discharge 4.8 x 10^6 tonnes and sea floor erosion 6-7.5 x 10^6 tonnes, although this estimate is uncertain (Dyer and Moffat, 1994). Other important sources are from cliff erosion, particularly along the Holderness Coast and East Anglia. These two areas are the dominant British sources of suspended sediment, and supply more than 2 x 10^6 tonnes a^{-1} (McCave, 1973; 1987). The Humber and Thames in contrast, supply sediment to the North Sea in the order of 2 x 10^5 tonnes a^{-1}. This sediment input is balanced by deposition and outflow. The Norwegian Coastal current is estimated to have an outfall of 11.4 x 10^6 tonnes a^{-1}. Depositional areas include the extensive mud areas and sand banks of the Wash and the Wadden Sea which, as estimated by Eisma and Kalf (1987), total 3.5 x 10^6 tonnes a^{-1}. Other depositional areas include estuaries, in which an estimated 2.5 x 10^6 tonnes a^{-1} of sediment is deposited.

Regional distributional studies have shown that sediment concentrations tend to decrease from the Southern Bight towards the North, and towards Skagerrak and the Norwegian

Channel. Eisma and Kalf (1987) produced a 2 mgl^{-1} suspended sediment contour line which coincided with the frontal transition zone described by Pingree and Griffiths (1978) which separates the well mixed water in the Southern Bight and along the English and continental coasts, from the main body of North Sea water, which stratifies in the summer. The highest concentrations of suspended sediment >10mgl^{-1} were seen to occur along the coasts of the Southern Bight and in the German Bight.

The concentration and transport paths of suspended sediment in the Southern North Sea is influenced by seasonal and short term variations in water movements. During periods of storms and generally in winter, concentrations are several times higher than those during the summer and periods of calm conditions (Dyer and Moffat, 1994). One aim of the North Sea Project was to determine the seasonal, spatial and temporal and vertical distribution of suspended particulate matter in the Southern North Sea. In addition to this, depth integrated measurements of SPM were combined with current velocity data to estimate SPM fluxes. From the flux measurements, budget estimates were also made.

Over a period of 15 months, SPM measurements were made continuously underway using a 25 cm path length Sea-Tech beam transmissometer working at 670nm, along survey tracks (Dyer and Moffat, 1992) as well as taking vertical profiles at hydrographic stations. In calm conditions, measurements were made within 1-2 m of the seabed, but during storms, measurements were restricted to ~5 m above the seabed. In order to calibrate the transmissometer in terms of SPM, *in situ* water samples were collected and filtered at each station.

From the North Sea cruise SPM data, Dyer and Moffat (1992) produced a series of contour maps to show SPM distribution over different seasons. From the results, the Southern North Sea was divided into three areas based on turbidity.

1. A region of high SPM off the East Anglia and Lincolnshire coasts.
2. A region of low SPM north of about 54° North.
3. A region of high SPM off the European Coast and German Bight.

High levels of turbidity were seen in all the cruises off the East Anglian and Lincolnshire coasts. These results agree with observations of McCave (1972) who identified a zone of high turbidity off the East Anglian coast with a continuation as a plume across the Southern

Bight and towards the German Bight at a latitude of ~ 53° N. The high turbidity levels observed was associated with the sources of suspended sediment coming from river discharge, coastal erosion and possibly from seabed erosion (Dyer and Moffat, 1992). SPM levels increased from summer to winter to levels >20 mgl^{-1}. The highest concentrations were seen in the Humber-Wash area and off Suffolk and Essex. The plume feature was also observed and extended to the East, North-East away from the East Anglian coast. In November 1988 and January 1989, the plume was seen to stretch across the Southern Bight as far as the German Bight. This high turbidity zone remained well developed until late spring. During summer, concentrations diminished somewhat, until late summer and early autumn of 1989, when the intensification of the plume recommenced (Dyer and Moffat, 1992). The plume feature was also been seen by satellite images taken from the North Sea Colour Atlas (Holligan *et al.*, 1989). The distinct plume is known as the East Anglian plume and is thought to transport significant amounts of suspended sediment away from the coastal zone of Eastern England.

Total flux estimates of the plume were made by integrating across a plume width of 80 Km, and assuming a background level of 2 mgl^{-1} (Dyer and Moffat, 1992, 1994). The maximum monthly flux of 3.3 x 10^6 tonnes occurred during December 1988, with a further peak of 1.4 x 10^6 tonnes occurring in March 1989. The total flux over the 15 month period was estimated to be 7.19 x 10^6 tonnes, of which 71% occurred in two months, December 1988, and March 1989. This is equivalent to a flux of 6.6 x 10^6 tonnes a^{-1}. Errors in these flux estimates will arise due to the nature of the data collected. The measurements used to estimate the fluxes were taken from monthly averages. SPM measurements taken by Jago *et al.*, (1994) revealed that SPM levels can vary tidally by as much as ± 50%, and were significantly enhanced during wave activity. Suspended loads also appeared to be source limited and elevated concentrations persisted for several days after a storm event. Taking SPM variation into account and taking the possibility that the modelled velocities were also in error of ± 50%, it is estimated that the overall errors in the annual flux estimates are ~ 50%. Therefore, the annual transport of suspended sediments in the plume probably lies according to Dyer and Moffat (1994) between 3 - 9 x 10^6 tonnes a^{-1} . Further calculations from Dyer and Moffat (1994) for a figure of total sediment load in the Southern North Sea was ~100 x 10^6 tonnes a^{-1}. However, the input and output box model figures that they used did not balance, and they suggested that 17.5 x 10^6 tonnes a^{-1} of sediment was produced by sources within the box. Dyer and Moffat (1994) note that although resuspension by waves must contribute to the enhanced concentrations observed, the long term presence of the

plume means that the transport of SPM is a sequential process of erosion, transport and deposition. Thus the flux eastward from the British waters within the plume must result from river input, coastal erosion and near coast seabed erosion averaged over periods of possibly years.

Sediment budget estimates of possible sources and sinks of suspended sediment for the East coast of England were formulated by McCave, 1987 and by Hydraulics Research (1992), table 2.1. In the case for Hydraulics Research, only erosion estimates were made.

Table 2.1 Eastern England sediment budget

	Source / Sink	**McCave (1987)**	**Hydraulics Research (1992)**
Supply	E Anglian Rivers	5.6	
	Wash Rivers	~100	
	Humber	~100	225
	Thames		690
	Norfolk Cliffs	665	2950
	Suffolk Cliffs	120	3320
	Holderness	1400	2610
	Total Supply	~2500	9880
Deposition	Wash	790-1600	
	Humber / N Lincs	127	
	N Norfolk Marshes	104	
	E Anglia Estuaries	~100	
	Total deposition	~1100 - 2000	
	Lost from system	~1400 - 500	

Amounts are Kilo tonnes per annum

(From: Dyer and Moffat, 1994)

McCave's estimates show that the Holderness coast (based on his assumption that the coastline is retreating at a rate of ~ 1.7m a^{-1}), is by far the largest fine sediment source into the North Sea, providing an input of 1.4 x 10^6 tonnes a^{-1}, 70% of the total source of cliff erosion. The eroded material then travels consistently southward. Only 3% of the volume of the cliff material goes into maintaining the sand spit of Spurn Head at the mouth of the Humber estuary (Valentin, 1971). The remainder of the material travels across the Humber mouth, towards the Wash on the South coast. The high concentration area of the Wash was formed as a result of inshore circulations which trap sediment from the main source of supply (i.e the Holderness cliffs) (McCave's response to Sundermann, 1993). The most

obvious poorly quantified source is erosion of the nearshore seabed, which McCave (1987) estimates as accounting for an additional supply of ~ 0.16 x 10^6 tonnes a^{-1}. The erosion figures calculated by Hydraulics Research assuming, as was done by McCave (1987), that mud constituted only 67% of the eroded material in Holderness and 44% elsewhere, were considerably higher than those of McCave (1987). They showed that the cliffs of Suffolk and Norfolk supplied more sediment into the North Sea than Holderness although, their calculations for Holderness of 2.61 x 10^6 tonnes a^{-1} was greater than McCave's estimate (McCave, 1987) by 1.21 x 10^6 tonnes a^{-1}. Taking McCave's budget estimates into account, there does not appear to be sufficient material in his sediment budget to support the interpreted plume transport of Dyer and Moffat (1994). Hydraulics Research budget results (assuming that McCave's depositional values are correct) do provide sufficient material to supply the sediment transport within the plume of Dyer and Moffat (1994). It is noted that the transport plume of Dyer and Moffat do not include sediment concentration data from the nearshore waters of the Holderness coast. Since this region is recognised by Hydraulics Research (1992) and McCave, (1987) as an important source of fine material into the North Sea, sediment transport in the plume may be therefore under estimated.

Another poorly defined potential source is the near coastal sub-tidal seabed where the elevational accuracy is poor and where annual bed level erosion of a millimeter or so could produce large sediment inputs. Clearly further measurements which incorporate the nearshore zone are necessary to improve the sediment source budgets. Dyer and Moffat (1994) also remark that the coastal erosion input will vary according to the number of winter storm events. Hence, some averaging of the coast erosion input is likely to occur by temporary accumulation of sediment along the transport path during calmer periods. The cliff material eroded will therefore move along the plume path by a series of suspension episodes, depending on the sequence of storm events. The budgetary figures are averages over several years, whereas the flux measurements of the transport plume are for a single year. There are undoubtedly considerable short term variations in both estimates. However, despite these uncertainties in the estimated fluxes and sediment budgets, it is obvious that the plume which is persistent throughout the year across the Southern Bight, exports the majority of the fine sediment eroded from the coasts of Eastern England (Eisma and Kalf, 1987) and is important in the budget of suspended sediments in the North Sea.

2.4.3 Time Series Results from Mooring Sites during the North Sea Project

The main focus of the project is directed towards analysing time series results of nearbed suspended sediment concentration in response to currents and storms off the Holderness coast on timescales less than a month. In the next section, a review will be given of time series results collected from the mooring sites during the North Sea Project. Emphasis will be placed on the physical processes which are thought to control the movement of sediment in the North Sea and attention will also focus on other mooring sites taken outside the North Sea Project. Three sites were chosen during the North Sea Project to investigate the hydrodynamic and biological controls of suspended particulate matter (SPM) flux (refer to figure 2.10 and table 2.2). Since many factors determine SPM properties and dispersal, it was necessary on a scale of that of the North Sea Project, to plan field experiments which isolated particular phenomena (Jago and Jones, 1993). The sites chosen (figure 2.10; table 2.2) encompassed a whole range of conditions, such as water column structure (stratified and mixed), boundary layer dynamics such as steady current or combined action of waves and currents, and finally seabed properties which included both cohesive and non-cohesive sediments (Jago *et al.*, 1994).

Table 2.2: Summary of site characteristics

Variable	**Site A**	**Site B**	**Site C**
Geographical Location	52° 39' N 03° 40'E	54° 35' N 04° 50'E	54° 59' N 01° 21'W
mean water depth (m)	30	47	24
water column structure	mixed	seasonally stratified	mixed
tidal range (m)	1.2	0.6	3.6
maximum tidal current (ms^{-1})	0.6	0.2	0.3
median grain size (μm)	250	100	100
bedform wavelength (m)	0.15		

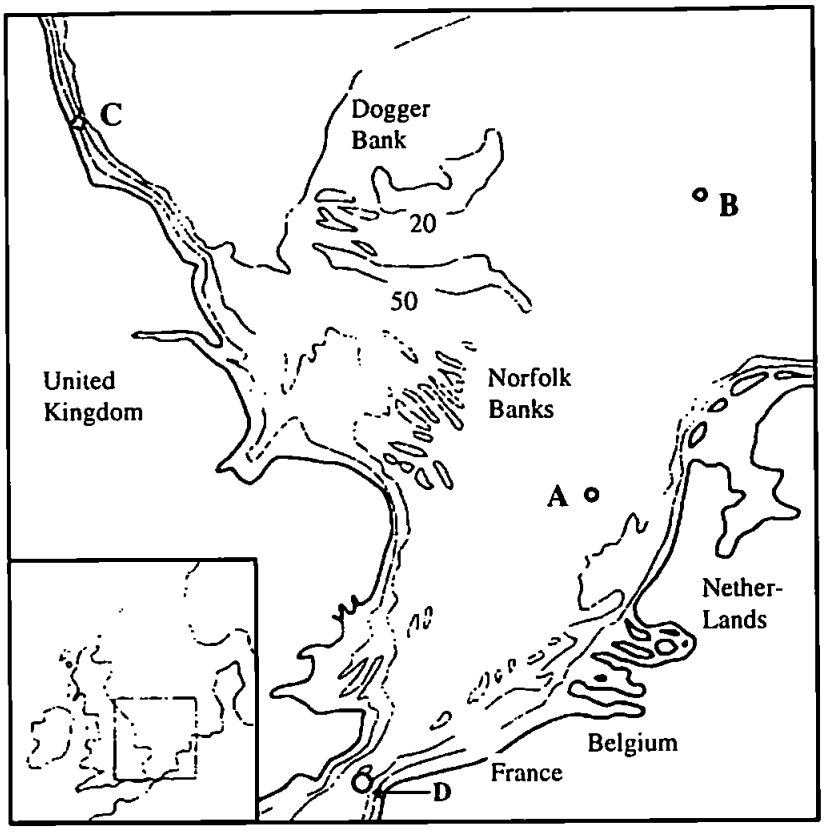

Figure 2.10 Geographical location of study sites A, B and C. Site D Data taken outside the North Sea Project (refer to section 2.4.5)
(From: Jago *et al.*, 1994)

Attention will focus on results obtained from the well mixed regions mentioned above (site A and C), since our study area the Holderness coast, is in essentially a well mixed region of the Southern North Sea. No storms were recorded in the above results, but the response of sediment in suspension to storms will be reviewed from studies taken after the North Sea Project.

2.4.4 Sediment Suspension During Fair Weather Conditions - Time Series Observations Taken from the North Sea Project

The principal aim of these experiments was to determine sediment resuspension in response to the tides and to wave-current interaction. Site A (figure 2.10) was chosen to represent a well mixed water column structure, because the water depth (30m) was such that the combined wave/current flows should episodically stir the sea bed. Observations were made at site A during three cruises (January, May and September, 1989) in order to

encompass seasonal factors governing SPM dynamics. Measurements were taken from both moored and ship deployed instrumentation (Jago and Jones, 1993). Moorings were deployed over 6-11 day periods and ship deployments were made over tidal cycles (13 and 25 hours). Current velocity was measured with Anderaa RCM current meters and suspended particulate matter (SPM) was measured at three heights above the bed (5, 10 and 20 meters) with beam transmissometers designed in-house at the University of North Wales, Bangor (UWB). SPM was also monitored during the May cruise at 1 meter above the seabed (mab) from a beam transmissometer which was attached to the benthic boundary platform STABLE (Humphrey, 1987). Details of the instrumentation on STABLE are given by Humphrey, (1987). *In situ* water samples were used to calibrate the optical instruments. Water samples were also collected and analysed for particle size distribution using a shipboard Mark TAII Coulter Counter (Jago and Jones, 1993) and the determination of settling velocity spectra (Owen, 1976).

Because site A represents a shallow water environment, there should be a strong influence from wave activity during storm events to the flux of SPM. It is essential that measurements are made during storm conditions if sediment dynamics across the whole range of environmental conditions is to be understood (Green *et al.*, 1995). However, most of the results collected from site A pertained to fair weather conditions when the flux of SPM was determined by tidal processes only.

Time series of SPM concentration taken for the deployment period (figure 2.11 A) exhibited both quarter-diurnal and semi-diurnal variation. The explanation for the variability arises from the knowledge that regional (horizontal) SPM concentration gradients are common in shallow shelf seas (Weeks and Simpson, 1991, Jago and Jones, 1993). The double maxima at the M_4 frequency in terms of SPM variations are understood to be due to the local erosion of sediment from the sea bed by tidal currents. From these signals two important factors determining SPM dynamics at this site are revealed. Firstly, under certain conditions, tidal currents resuspend bed material at the site, and secondly, the resuspended material has a settling velocity that is fast enough to re-deposit the sediment between times of maximum flow. An additional M_2 tidal signal indicates advection past the site of a regional horizontal concentration gradient.

To explain more fully the concept of suspension events caused by advection and resuspension, figure 2.11 B shows a gradient of suspended sediment which increases in

concentration away from the mooring site. Taking the assumption that a horizontal gradient of sediment concentration exists, as the tide flows from high water to low water for example, the concentration gradient moves with it. At maximum tidal streaming, the local bed material may be resuspended in the vicintiy of the mooring site. Resuspension should also occur on the next stage of the tide, giving rise to a sediment peak every 6 hours (quarter-diurnal) over the 24 hour period. When the tide has reached its maximum displacement on ebb, at low water, the horizontal sediment gradient is at a maximum concentration in the vicinity of the mooring site, giving rise to a second semi-diurnal sediment peak. From this signal there is an alternation of concentration minima, which suggests that the SPM concentrations were reduced to different values at slack water depending on whether slack water was high or low. Combination of these components give rise to the characteristic 'twin peaks' signature. This 'twin peaks' signal has been observed in the Northern Irish Sea and is documented in Weeks and Simpson, (1991); Weeks *et al.*, (1993). From their observations, it was also noted that the semi-diurnal peaks showed strong spring to neap periodicity.

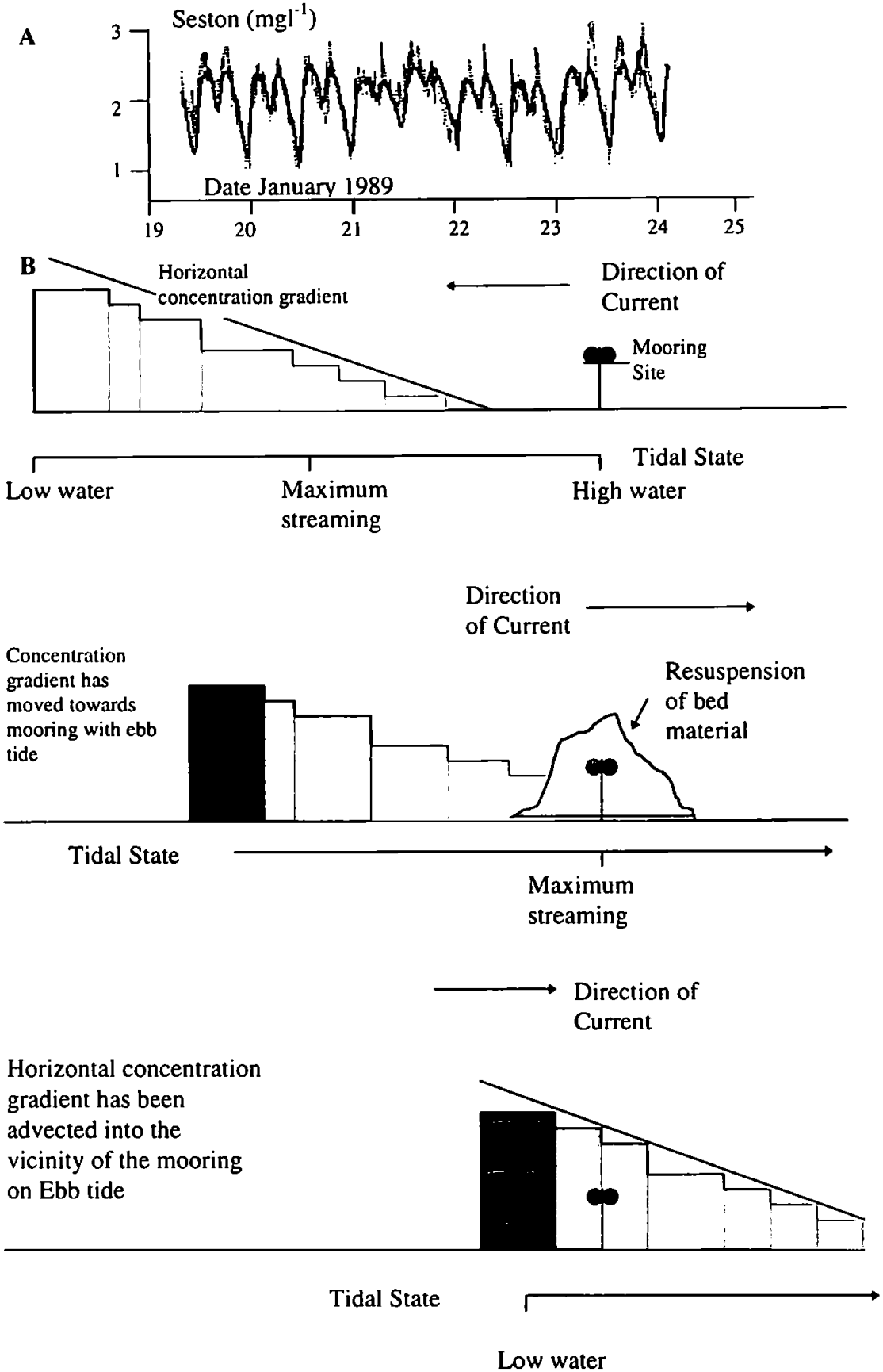

Figure 2.11 A. Combination of advection signal and resuspension signal in the seston concentration time series (Site A). From Jago *et al.*, 1994). B. Cartoon diagram to explain the concept of tidal advection of a horizontal concentration gradient and sediment resuspension.

2.4.5 Suspended Sediment Time Series Results Recorded in the Southern North Sea Outside the North Sea Project

SPM signals of this nature were also observed at 5mab from a study site located 4km off Cap Griz Nez on the Eastern (French) shore of the Dover Strait (Jones, *et al.*, 1994) (see figure 2.10, site D). A combination of current meter, transmissometer and bottom mounted acoustic doppler current profiler (ADCP) was deployed at this site for a period of one month. The time series (figure 2.12) of concentration and current velocity from this study revealed several components of variability.

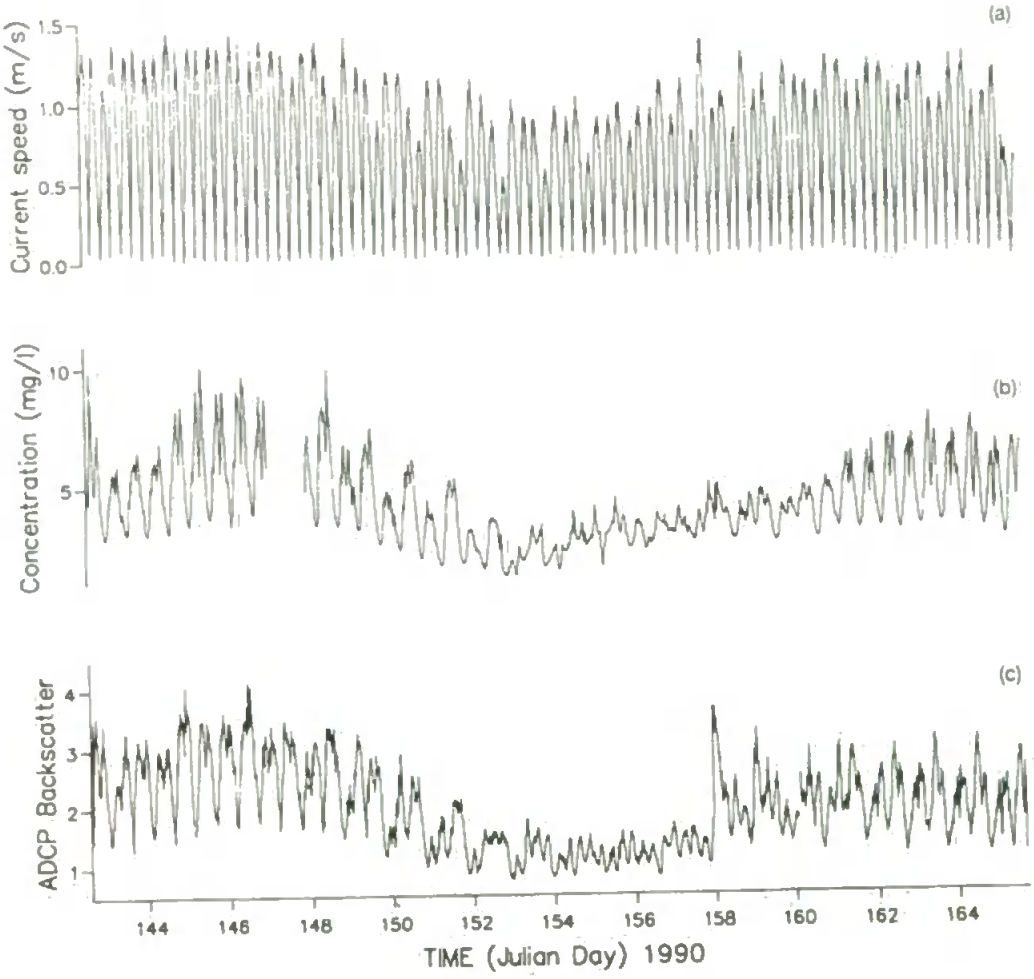

Figure 2.12 Time series of moored observations 5m above the bed a) Current speed b) SPM concentration c) ADCP backscatter strength (arbitrary units) - Data taken from 4Km off Cap Griz Nex on the Eastern shore of the Dover Strait.

(From: Jones *et al.*, 1994)

Jones *et al.*, (1994) attributed the significant spring/neap variation in 'background' concentration to increased levels of regional resuspension during spring tides. The quarter-diurnal concentration signal also varied in strength over the spring/neap cycle. The additional semi-diurnal signal resulting from tidal advection of a horizontal concentration gradient was present only during spring tides. Jones *et al.*, (1994) suggested that this gradient must be due to either spatial heterogeneity in resuspension levels (because of local variability in current speeds or bottom sediments), or to the regional influence of fine sediment sources such as river mouths. Both the transmissometer and the ADCP showed a similar 'twin-peaked' response, but there are times when the ADCP resuspension signal was broader and more closely in-phase with the current speed. This feature is explained by considering the effect of two populations of sediment, that is, a fine population in background suspension which is additionally locally resuspended, producing the record observed by the transmissometer and a coarse population which is tidally resuspended, but not subject to a horizontal concentration gradient, so not shifted in phase, as observed (in addition to the fine population) by the ADCP. The two instruments also showed enhanced SPM concentrations in the upper part of the water column just after slack water ebb. Salinity and temperature profiles for this time indicated that this corresponds to the advection of stratified coastal water, causing a warm, turbid fresh water layer to encroach on the mooring site (Jones *et al.*, 1994).

The important conclusion from the concentration time series studies in the Southern North Sea, is that there were at least two distinct components of SPM present. During high tidal flow, a relatively large diameter, rapidly settling sediment component was observed, indicating that it was undergoing local resuspension and deposition. In addition to this, a finer diameter, more slowly settling background sediment component was present at all times, but its concentration was regionally variable. Bale and Morris (1993), from the same site, noted that background component was relatively rich in organic carbon, which implies that the background component contained a significant biotic contribution. The re-suspension component was less rich in organic carbon, but still significantly greater than the bed sediments. Sea bed photographs taken during this study revealed that in between the sand ripples, there was clearly a distinct debris of organic-rich material laying in the troughs. This meant that the resuspended material was not the true bed sediment material, as was thought earlier, but was fallout of the fine background sediment, which in the present discussion is termed 'fluff' and can be organic as well as inorganic material. Under fair weather conditions, tidal currents resuspended this organic rich 'fluff', but

resuspension ceased once this had been entrained. From the three cruises (January, May and September, 1989), it was noted that the amount of material resuspended was time-variable, with the greatest re-suspension occurring in May. Clearly then there is a seasonal (or episodic variation) in the amount of resuspendable material available. It is postulated, that in May, the aftermath of the spring phytoplankton bloom, generated a high concentration of organic rich 'fluff'. Very little resuspension occurred in September, even though the tidal currents were greater than those which produced a strong resuspension signal experienced in May, and it is thought that there was very little resuspendable material available from the sea bed.

During winter, there was a relatively strong resuspension signal, although very little biological activity would have occurred at this time. It is thought that storm events re-suspended finer organic rich material off the seabed from less sandy sites and this material now in suspension, was advected into the mooring site, while still undergoing tidal re-suspension and deposition on its passage to the mooring location (Jago and Jones, 1993). Wave activity induced resuspension in the region of site A during May, although the SPM dynamics were affected more by the phytoplankton bloom at that time. Production of biological aggregates would have been capable of scavenging fine-grained SPM and therefore altering its hydraulic behaviour. The strong winds, however, coincided with the supression of the reduction of SPM concentration during slack water, which would normally be due to the settlement of the tidal resuspension population. This phenomenon occurred over two consecutive tides, suggesting that enhanced vertical mixing by wave activity was the cause. At this time maximum peak flow conditions in SPM concentrations were unaffected because resuspension was source limited, and wave action only suppressed settlement of resuspended material rather than enhanced resuspension (Jago and Jones, 1993). The results indicated that under even moderate wave conditions, there was a significant impact on the SPM dynamics at the site.

Clearly, a higher shear stress than that achieved by the tides and moderate wave activity is needed to resuspend the sandy bed sediment in this study. The only time this can arise is during a storm which is strong enough to resuspend the bed sediment. The consequence of this would be a much greater effect on the SPM dynamics than is experienced during moderate wave conditions. Unfortunately, the periods of observation which covered the North Sea Project did not coincide with storms, so that resuspension of bed sediment itself was never observed.

2.4.6 The Influence of Storms on Sediment Suspension in the Southern North Sea

The emphasis of this project is on the influence of storm activity on sediment transport in the nearshore zone off the Holderness coast. The nearshore zone is a highly energetic environment and is a site of complex interactions between fluid processes (Hequette and Hill, 1993). It is effectively the shoreward boundary to the larger scale circulations of the middle and outer shelf (Wright *et al.*, 1991). On the shoreface, surface winds and orbital motions of shoaling waves cause a significant turbulent mixing of the relatively shallow water column, especially during storm conditions. As a result, the nearshore zone is a friction dominated environment in which surface and bottom boundary layers overlap and commonly occupy the entire water column (Wright *et al.*, 1991). Consequently, mean flows over the shoreface are little affected by the Coriolis force and internal density field, and are mainly driven by winds, horizontal pressure gradients and tides (Hequette and Hill, 1993). Notably, suspended sediment concentrations in the nearshore zone occur predominantly as a result of a combined action of waves and currents. The waves are the principal cause of the entrainment of the sediment, which are diffused into the flow by turbulent processes, and subsequently transported by the currents.

To quantify the amount of sediment transported during storms, nearbed measurements of suspended sediment concentration, velocity (at different elevations), waves and seabed configuration must be obtained in order to establish the threshold conditions for sediment suspension and subsequent transport. A number of studies have been conducted of storm sediment transport, by attaching instruments to robust tripod structures and deploying them for a period of time with the hope of capturing storm events. This review will concentrate on the results of two studies completed in the Southern North Sea at different depths.

Two storm events were recorded at the EDDA location in the North Sea (56° 28.2' N, 03°0.3' E) in 70m of water over the winter of 1984-1985 (figure 2.13). The first storm E1 lasted for three days and the second storm E2 lasted for about one day. Current velocity was measured at 6 elevations above the seabed using acoustic current meters mounted on a tripod frame. Suspended sediment concentration were measured at two heights from the same tripod and wave activity was monitored using a WAVEC directional buoy. A stereo photo system, from which the seabed configuration was obtained, was also mounted on the tripod (Myrhaug, *et al.*, 1994).

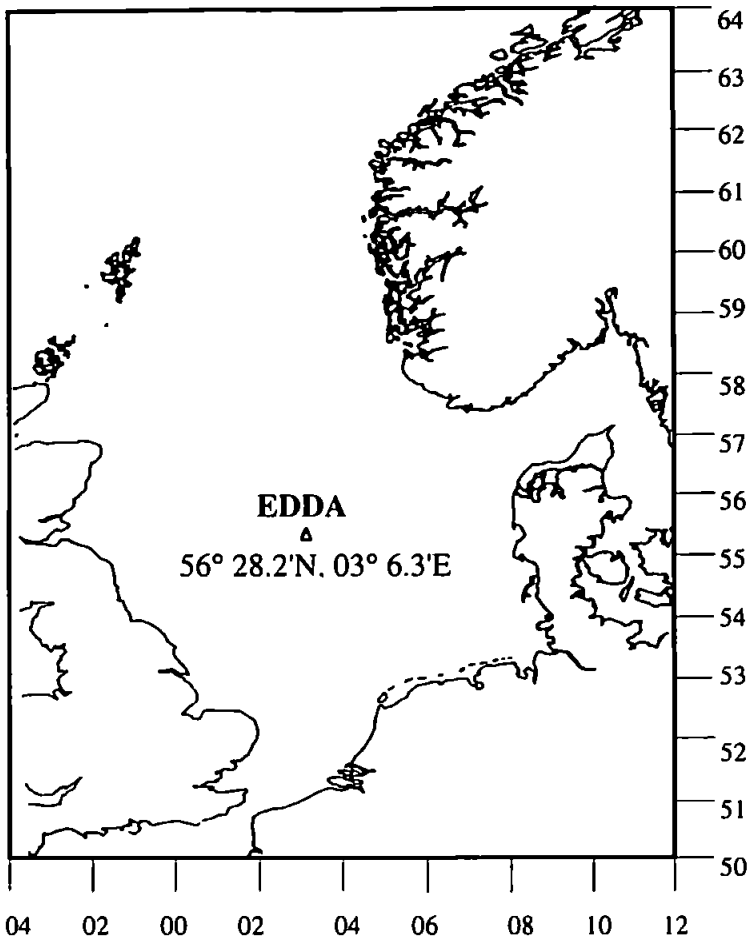

Figure 2.13 EDDA locations in the North Sea
(From: Myrhaug, *et al.*, 1992)

Current velocities during the storms were similar in magnitude, as was wave activity and average wave period, but with larger variance in the E2 storm. Results from the first storm revealed peaks in sediment concentration at 0.25mab with M_2 tidal modulation, with the highest concentration occurring coincident with minimum current.

There was little correlation between wave activity and peaks in sediment suspension, and in fact peaks in sediment concentration occurred after the wave activity peak in the storm. Photos of the seabed showed weak ripple formation before and after the storm, but it was assumed to be flat during the storm because of suspended sediment clouding the view of the seabed. This also suggested that the shear stress was high enough to bring sediment into suspension, which further suggests that there would be significant sediment transport during the storm. Results from the second storm E2, showed no distinct correlation between the concentration peaks and the semi-diurnal tidal signal, but did show that higher concentrations occurred after the wave activity peak in the storm. During the storm, photos again revealed that sediment was in suspension, which suggests that the ripples formed

prior to the storm were washed out. Considering the overall trend of both the storms, the suspended sediment concentration decreased when current was added to the waves, which is opposite to what is normally expected (Myrhaug *et al.*, 1994, Fredsoe and Deigaard, 1992). A possible explanation was that high suspended sediment concentrations were associated with flow reversal such that sediment suspension would occur when the current component in the combined wave-current boundary layer was relatively low. Hence, when the current dominated, there was no flow reversal and the SPM decreased. Flow reversal was seen to occur when $\bar{u}_r / 2\sigma < 1$ (Myrhaug *et al.*, 1994), where $\bar{u}_r$ is the free stream velocity at 5m elevation and 2σ is wave activity, taken as the standard deviation of the flow velocity. For both storms, high concentrations occurred when $\bar{u}_r / 2\sigma < 2$, when flow reversal was present. However, if the current became significantly large, the concentration could increase with the current. Advection of sediments from other areas with other types of bottom sediments was another possibility put forward, but this was unlikely because the site was located in an area which was relatively flat and more importantly with uniform seabed conditions. Another reason for high concentrations occurring with a low current, may be due to stratification of the bottom boundary caused by the high concentrations during the storm, which would affect the shape of the velocity profile, and reduce the bed stresses, such as experienced in the following storm results from Green *et al.*, (1995).

The second study in the North Sea was taken in Marsden Bay off the North East coast of England (54° 59.2' N, 01° 21.0' E) at a mean water depth of ~ 25m (figure 2.14) (Green *et al.*, 1995). Similarly to the BLISS project, near bed current velocities, bed shear stresses, SPM, wave activity and fluxes were obtained from instruments mounted on a tetrapod, during the waxing phase of a severe storm.

Bed sediments at the site were essentially bimodal in distribution. North East winds generated an along-coast mean flow that reinforced the southerly setting flood tidal current. Peak flood current speed increased from 35cms^{-1} before the storm to 60cms^{-1} during the storm. Bed shear stresses were obtained from velocity profiles using the von Karman-Prandtl equation [2.2]. High suspended loads were monitored during the storm. During these conditions, an increase in suspended sediment may cause stratification of the bottom boundary layer, which will affect the shape of the velocity profile, and alter the bed shear stresses.

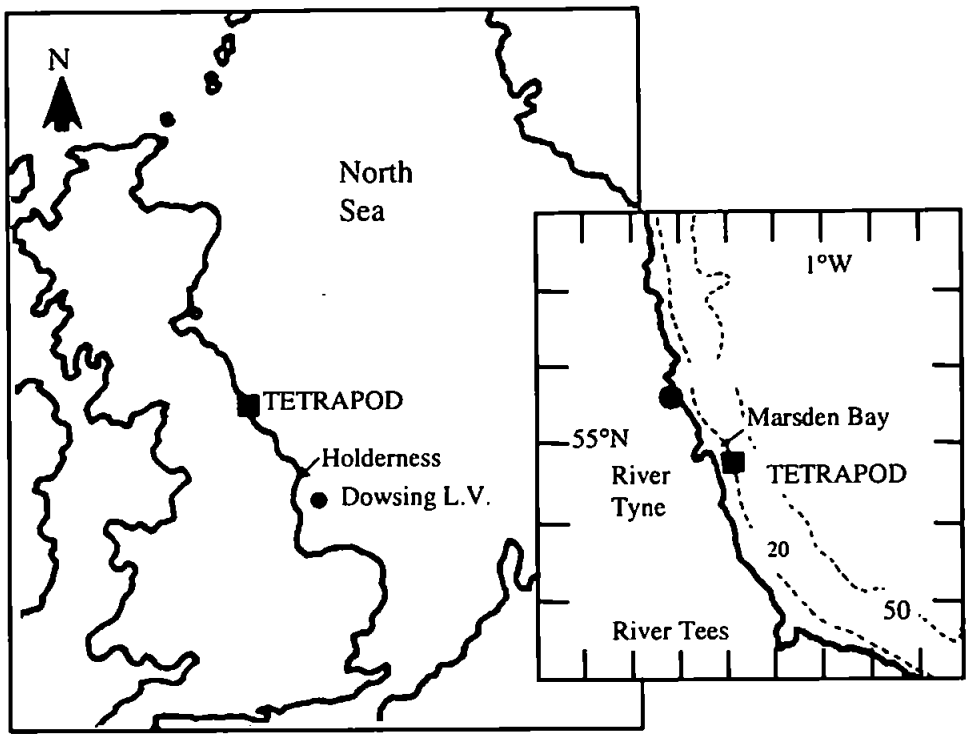

Figure 2.14 Study site: Marsden Bay
(From: Green *et al.*, 1995)

To determine whether stratification occurred or not, Green *et al.*, (1995) applied a stability parameter, defined as:

[2.16]

$$z\backslash L = \frac{zkg(\rho_s / \rho - 1)w_s C_s}{u_*^3}$$

where L is the Monin-Obukhov length, g is acceleration due to gravity, w_s is settling velocity, ρ_s is sediment density, here assumed to be quartz sand where $\rho_s = 2.65$ g cm^{-3}, and thus z/L <0.03 is necessary for near-neutral stability (Soulsby and Wainwright, 1987).

Evidence from this study suggested that conditions were suitable (at times) to stably stratify the bottom boundary layer, with z/L > 0 (10^{-1}). Concentration time-series taken from the study site (figure 2.14) during the storm (figure 2.15), showed wave resuspension of bed sediments combined with advection of suspended sediment by the mean flow. In figure 2.15, concentration fluctuations at about the wave period were seen to be 'pumped' by a wave group starting near 250s, and a large concentration plateau centred at 300s was

suggestive of advection of a dense cloud of sediment past the sediment concentration sensor.

Estimates of the depth-integrated sediment flux (g s^{-1} cm^{-1}) per unit width of seabed is defined as

[2.17]

$$Q_{\delta b\text{-}h} = \rho_s \int_{\delta b}^{h} ucdz$$

where h is water depth, $z = \delta_b$ is the top of the bedload layer and δ_b is the bedload-layer thickness, were obtained from a period of fair-weather conditions immediately preceding the storm, and also during the storm.

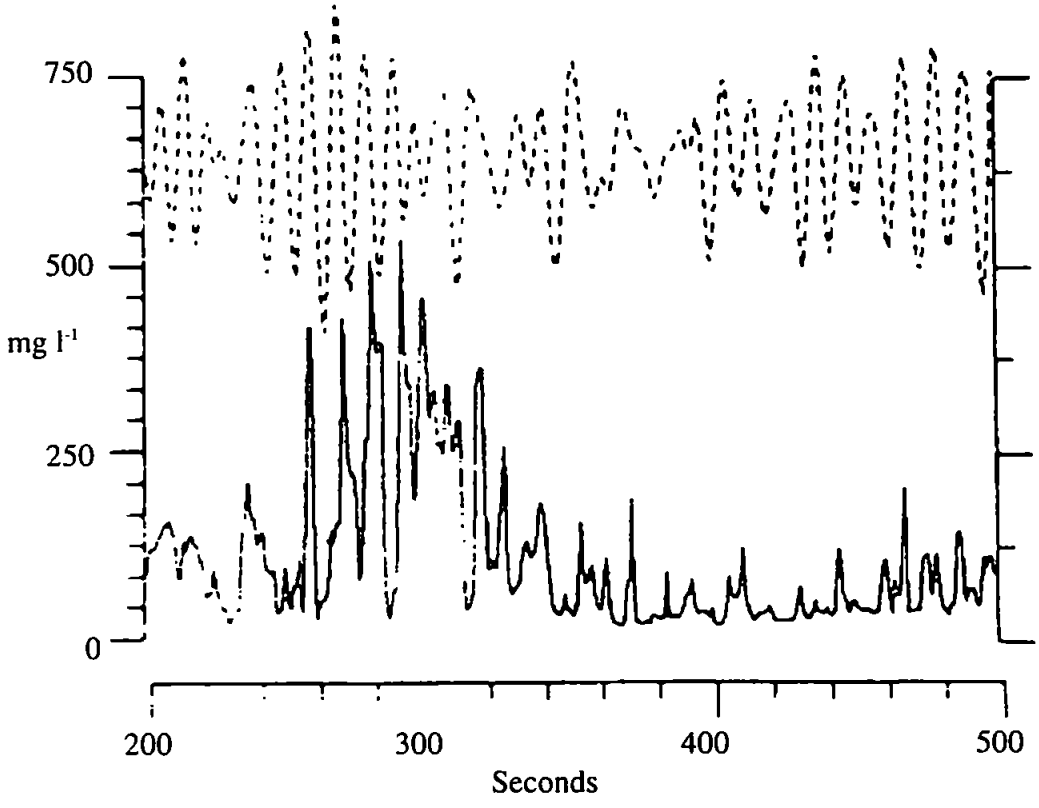

Figure 2.15 Burst time series of suspended-sediment concentration (mgl^{-1}) at 68cm above the bed (solid line) and water depth (dashed line)
(From: Green *et al.*, 1995)

Green *et al.*, (1995) suggest that the only meaningful measure of sediment transport for comparative purposes is the vertically-integrated flux, because entrainment and vertical diffusion of sediment, which together cause a quantity of sediment to be lifted to a specified level, and the advecting velocity at that level, which translates the sediment

horizontally, are not all uniquely related to each other. Sediment transport of this nature conforms broadly to the traditional concept of waves as a sediment entrainer and currents as a transporter of suspended sediment. During the storm, there was a net movement of sediment through the deployment site offshore and towards the South. Peak net flux of sediment was in the order of 10 g cm s^{-1} (3.6 tonnes m^{-1} h^{-1}). Resolving the peak into alongshore and offshore components yielded a shore-normal flux through the deployment site of ~0.5 tonnes m^{-1} h^{-1}, directed offshore. Hence, the depth-integrated transport during the storm was up to two orders of magnitude greater than during the fair-weather period prior to the storm. Suspension was the dominant transport mode, even during fair-weather conditions. During the storm an estimate of an order of magnitude more sediment was being carried in suspension than was being carried as bedload.

2.5 The Land Ocean Interaction Study (1994 - 1997)

From the North Sea Project suspended sediment distribution data (Dyer and Moffat, 1994) and budget estimates (McCave, 1987; Hydraulics Research, 1992), it is clear that the Holderness coast is recognised as a major source region for fine sediment input to the North Sea. From the flux and budget results it became clear that a full study of the processes contributing to the flows and sediment transport in the nearshore coastal region must be conducted if more accurate short-term estimates of source sediment flux from the cliff erosion and seabed resuspension are to be determined. Considerations must also be given to the wash load advective sediment component which may be in long-term suspension and continuously transported by the reversing tidal currents. Sediment transport near to the coastline is expected to be intermittent due to storms and irregular cliff erosion, but the intermittancy may become smoothed as the sediment moves offshore, due to deposition and resuspension.

To address the uncertainties in the flux estimates and the questions proposed above, a large field campaign called LOIS, (Land Ocean Interaction Study) was set up in 1990 by the Natural Environmental Research Council. LOIS was a five year community research project, aimed at bringing together researchers from marine, terrestial, earth and atmospheric sciences. Their primary motivation was to achieve an integrated scientific study of the North Sea, the continental shelf edge, the riverine and coastal environment and the atmosphere, so that the energy and material fluxes affecting these zones could be

identified, quantified and the processes which govern these fluxes established. The Holderness coastline (figure 2.16) is already know to be a region which has a history of severe coastal erosion (Valentin, 1971; Pringle, 1985; McCave, 1987). Situated along the North East coast of England, it extends 61.5 Km from Flamborough Head in the North to Spurn Head in the South. The cliffs (plate 2.1, 2.2) are largely composed of boulder clay, 67% of particles with a diameter of < 63μm (Al Bakri, 1986, McCave, 1987), and are retreating at an approximate rate of ~1.7m year according to the estimates of McCave (1987). The resulting yearly supply of 1 million cubic meters of sediment to the North Sea, defines the Holderness coastline as being one of the largest single coastal source of sediment on the Eastern coast of Britain. It must be stressed again that no concurrent measurements of coastal change were taken during the LOIS project, so it is almost impossible to link the observations to coastal changes, except in the most general sense.

To investigate the processes directly responsible for the transport of sediment away from the Holderness coast in the near-shore zone, and to determine their contribution to the total sediment flux, direct measurements of sediment concentration coupled with measurements of current velocities and wave activity were necessary. In order to address the above questions, LOIS set up the Holderness Experiment (Prandle, 1994), and approved the funding for a number of instrumented tripods to be developed and deployed off the Holderness coast for a period of 3 years, so that the transport of sediment could be compared over seasons. The monitoring program was carried out by the University of Plymouth (see next section), and by Proudman Oceanographic Laboratory who were involved in deploying 8 Proudman Monitoring Platforms (PMPs) on the sea bed along two transects perpendicular to the coast off Tunstall and Withernsea respectively. The PMP is essentially an upward looking system, which measures vertical profiles of current and suspended sediment using an acoustic doppler current profiler (ADCP), together with near-bed monitoring of turbulence and surface wave currents by an S4 electromagnetic current meter. Suspended sediment concentration was measured by an optical transmissometer, as well as water level, temperature and conductivity. The platforms were designed to mount a variety of autonomous instruments with a protective, stable and recoverable housing.

It is important to note from the outset that the Holderness coast is not an ideal location to study flow and sediment transport processes, for a variety of reasons, but particularly because, as we shall see in Chapter 4, the sedimentary nature of the seabed is highly spatially variable. If the primary objective were to improve our generic understanding of

physical processes other simpler sites would be more appropriate. However the importance of Holderness lies in its role in the sediment budge of the North Sea.

The characterstics of the seabed sediment influence the physical processes of sediment advection and resuspension in two ways: through the influence of bed roughness on stress at the seabed and through providing material for resuspension. Even where a careful grab and sidescan sonar survey of the region of sensors deployment is undertaken, as in the present work, the highly variable bed creates considerable difficulties for the first of these processes. The reason is that boundary layers will develop depending on the nature of the sediment and its distribution. If the surface sediment collects in patches and is not uniformally distributed on the seabed, a situation will arise where there will be individual boundary layers developing for each patch of seabed and only specific to those roughness conditions. Hence, to understand precisely the bottom boundary layer conditions and hence the bed stresses in that area will become very complicated indeed. In the present work the bed stress is measured directly close to the seabed, and must be assumed to be representative of the stress which causes the measured resuspension.

The second process, that of providing material for resuspension, is less important since the bed is bimodal, with a variable but coarse fraction overlain by a blanket of finer material. So the key point to emphasise in a study of this type is that although the nature of the seabed off Holderness is variable and is essentially unkown it is not crucial to the BLISS study when determining resuspension events because we are dealing with the suspension of a blanket of fine material and not resuspension of the underlying bed material.

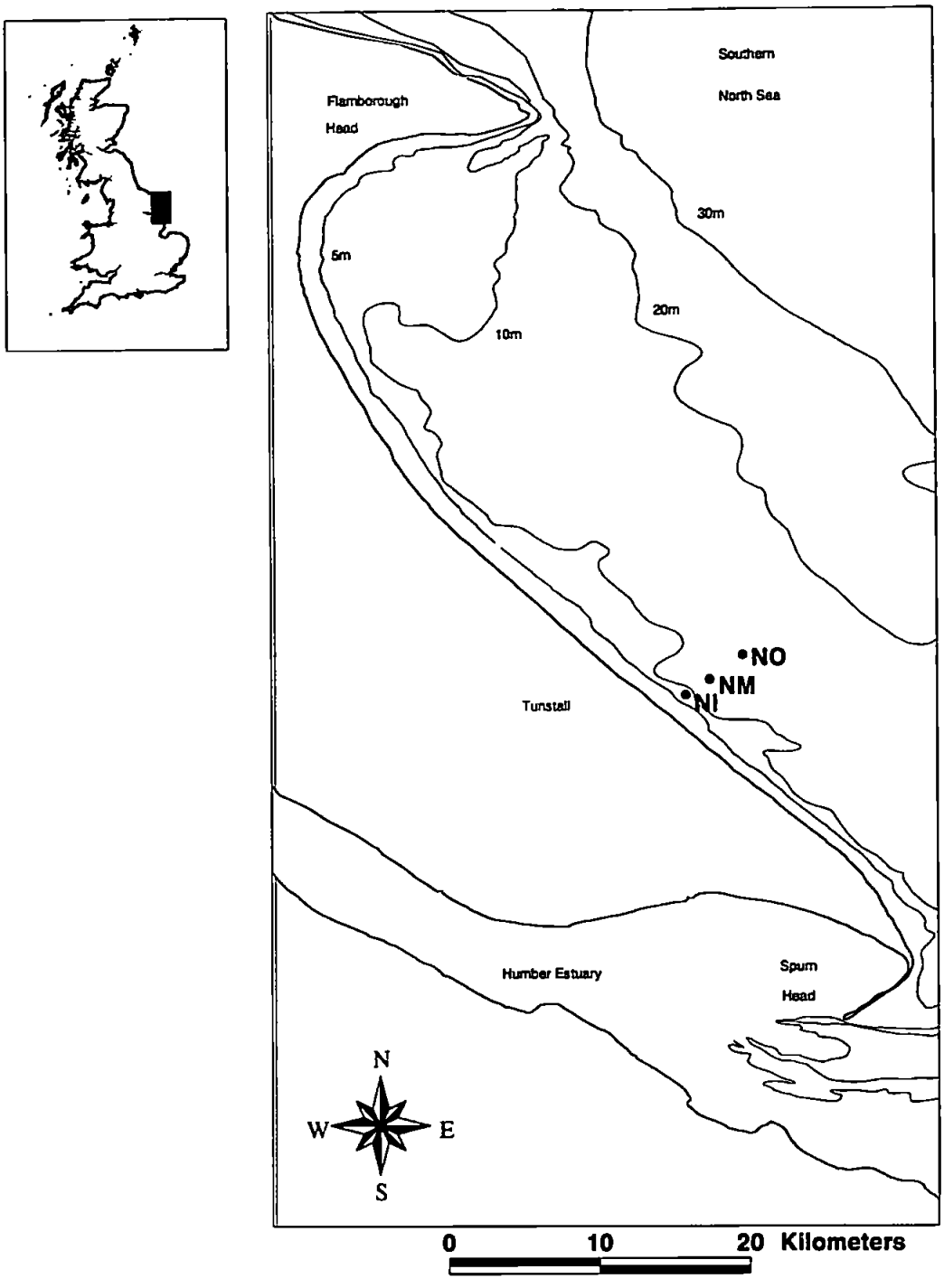

Figure 2.16 Holderness coast - BLISS study region

Plate 2.1 Holderness cliffs

Plate 2.2 Holderness cliffs

2.5.1 Boundary Layer Intelligent Sensor System (BLISS)

A collaborative study (LOIS special topic 351) was set up between the Universtiy of Plymouth and Plymouth Marine Laboratory to develop three benthic tripods which were given the name Boundary Layer Intelligent Sensor System (BLISS). BLISS is a more specialised instrument package when compared to the PMPs, since it is essentially a downward looking bottom boundary layer sensor system (see chapter 3 for sensor details). The aim was to deploy BLISS along the same northern line moorings as the PMPs so that there would be a data overlap between the two instrument systems.

BLISS was an entirely new concept, designed and built specifically for the Holderness Experiment. Further data overlap was planned with CASI (Compact Airborne Spectral Imager) overflights and LOIS Challenger Cruises (118 and 119). The Challenger cruises formed part of the other half of the special topic 351, in which the nature of the suspended sediment distribution would be investigated. However, the Challenger cruises never went as far inshore as the BLISS tripods.

Chapter 3

3. BLISS Instrumentation and Calibration

3.1 Introduction

In oceanic flows, the suspension of non-cohesive sediment is confined to a relatively thin region of the flow immediately above the bed (Downing *et al.*, 1981). It has been noted that breaking waves can play a significant role in suspending the sediment throughout the water column (Brenninkmeyer, 1976), although the largest gradients in sediment concentration and their main influence on flow hydrodynamics, will be observed within a few tens of cms of the bed (Downing *et al.*, 1981). To measure suspended sediment concentration (SSC) in such regions requires instrument sensors to have adequate frequency and spatial responses, over long periods of time so as to ensure meaningful results (Jones *et al.*, 1996). Before 1978, there was a lack of sensors that were capable of measuring sediment suspensions near to the seabed without disturbing the transport process (Downing *et al.*, 1981). Those instruments that were available were unable to survive adverse storm conditions, which are seen to play an important role in uplifting large quantities of sediment into suspension.

In 1981, Downing *et al.* developed the optical backscatter sensor (OBS) (the design of which, is discussed in section 3.2.2). Since its development, many studies have been successfully conducted, using the OBS to measure near bed concentrations (Hanes and Huntley, 1986, Sternberg *et al.*, 1984 Hanes *et al.*, 1988, Kineke and Sternberg, 1992, Green and Boon, 1993, Osborne *et al.*, 1994). In addition to the OBS, acoustic devices such as the acoustic backscatter sensors (ABS) have also been employed to measure

suspended sediment (Hanes *et al.*, 1988, Thorne *et al.*, 1991, Thorne *et al.*, 1993). In some cases, field investigations include both sensors, so that inter-comparisons between the sensors can be made (Osborne *et al.*, 1994, Lynch *et al.*, 1997). Electromagnetic current meters are generally employed to measure flow conditions, since their small size and robustness makes them ideal instruments for long-term deployments. Nevertheless, acoustic travel time and laser doppler anemometry (LDA) devices have been gaining attention recently (Thorne *et al.*, 1993).

It is recognised that in the shallow marine environment, bottom stresses responsible for the transport and suspension of sediment are generated by forcing mechanisms such as the tides, wind driven currents, surface waves and alongshore currents (Cacchione and Drake, 1979) which are variable in space and time. It is also recognised that to monitor these processes, sensors are required to stay in the marine environment for longer and longer periods of time. To overcome the difficulty of taking simultaneous measurements in the bottom boundary layer, free standing platforms in the shape of tripods and tetrapods have been used to deploy the sensors. A number of instrument systems have been built to date; for example; Ternberg *et al.*, (1995); Cacchione and Drake, (1979); Humphrey, (1987); Pearson and Thomas, (1991) to list but a few.

It must be recognised that data sets of this nature have also opened up new avenues for testing 1-D, 2-D and 3-D hydrodynamic and resuspension models, which before such events relied heavily on laboratory results.

Recent investigations of the bottom boundary layer have concentrated on deploying benthic landing tripod and tetrapod structures with instruments attached, at point moorings, for periods in some cases of up to a year. The crucial factor in this type of method is that not only must the tripod structure sit upright on the seabed in a stable position, but that the instruments used should not be obtrusive to the natural flow conditions (Hanes and Huntley, 1986), at the same time as accurately measuring the natural flow parameters and suspended sediment concentration (SSC).

In this chapter, a detailed description of the Boundary Layer Intelligent Sensor System (BLISS) will be given, in terms of instrumentation and calibrations. BLISS was designed specifically so that it could measure independently the nearbed sedimentary and flow processes in the bottom 1 m of the water column in shallow waters (10-25 m). The

purpose was to record data during storm events, so requiring a system that was both robust and which could operate continuously for long periods of time. The shallow water conditions would restrict the type of survey vessel used to a small fishing trawler operating out of Bridlington. Therefore, taking these factors into considerations, before the BLISS tripod was developed a number of essential prerequisites had to be adhered to.

BLISS had to be:

1. Deployable from a small fishing vessel in depths as little as 5m.

2. An instrument system which would cause negligible interference with the flow near the seabed.

3. An instrument system that could obtain rapid response measurements of the nearbed flow and sedimentary conditions so that we could monitor bed shear stresses and capture any resuspension events.

4. A system which has a deployment duration of at least a month to ensure that storm events were recorded.

5. An instrument system that could withstand high energy storm conditions.

6. A system which could operate independently without the need for an external power supply.

7. A system that could store data internally on its own logger as well as transmitting data to a shore station on demand.

In total, four BLISS systems have been developed in a collaboration between Plymouth Marine Laboratory electronics group and the University of Plymouth. For ease of comparison between each system, the tripods were numbered accordingly as BLISS 1, 2, 3 and 4. BLISS 1 was the prototype, BLISS 2 was used in the first deployment, BLISS 2 and 3 used in the second deployment, BLISS 2 used in the third deployment and BLISS 2, 3 and 4 used in the fourth deployment (for further deployment details refer to section 4.3). The following sections will give a general description of the full system, followed by a detailed discussion of each separate component and where applicable the calibration procedure and results.

3.2 Boundary Layer Intelligent Sensor System (BLISS)

Each BLISS instrument system (figure 3:1) consists of a seabed tripod, which carries a suite of sensors, a data logger/controller, and a battery pack (plate 3.1). The logger is connected by an umbilical steel cable, via an anchor clump (half a tonne), to a surface yellow spar buoy (plate 3:2), which carries a UHF[1] (458 MHz) radio transceiver. This allows the transfer of signals and data between the controller on the tripod, to a shore station at Tunstall, Holderness.

Because of the vulnerability of the tripods to storms and fishing activity in the shallow inshore waters, the telemetry link was seen from the outset as an important part of the overall system. It enables data to be transmitted to shore in near real time, so that the system performance can be checked and the data safely recorded. It also gives the potential to alter the logging mode of the rig from the shore, for example, by putting it into standby mode during extended periods of calm weather, to conserve battery and memory capacity. Each BLISS tripod stands 1.6m high, is designed to sit upright on the seabed and is capable of operating up to depths of 60m within 10Km of the shore.

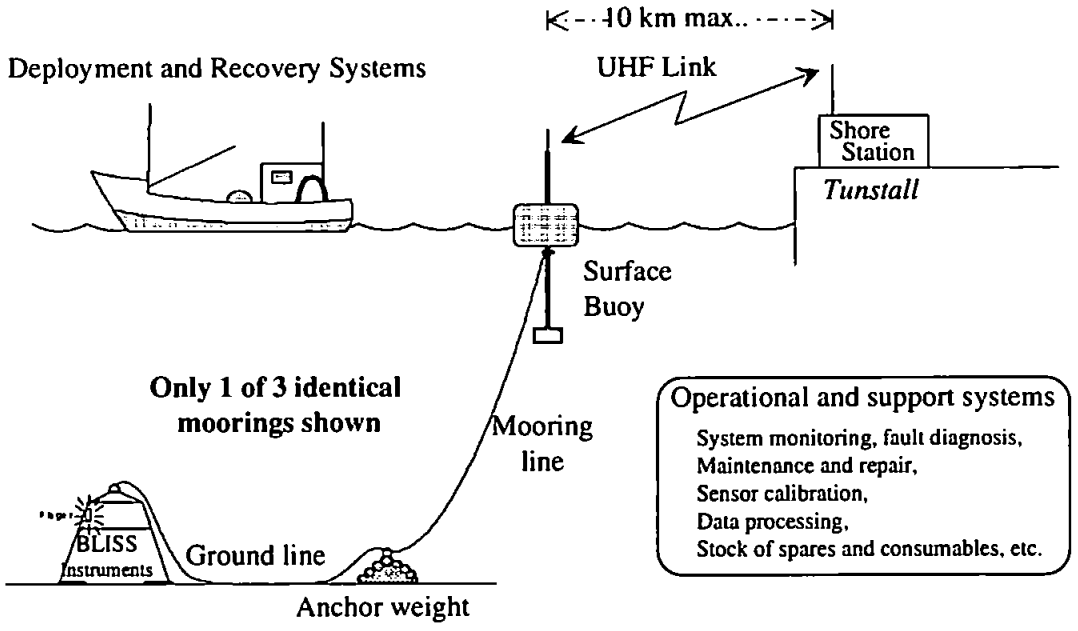

Figure 3.1 Total system, outline only, showing sub-systems and major components

[1] UHF Ultra High Frequency.

Plate 3.1 BLISS tripod

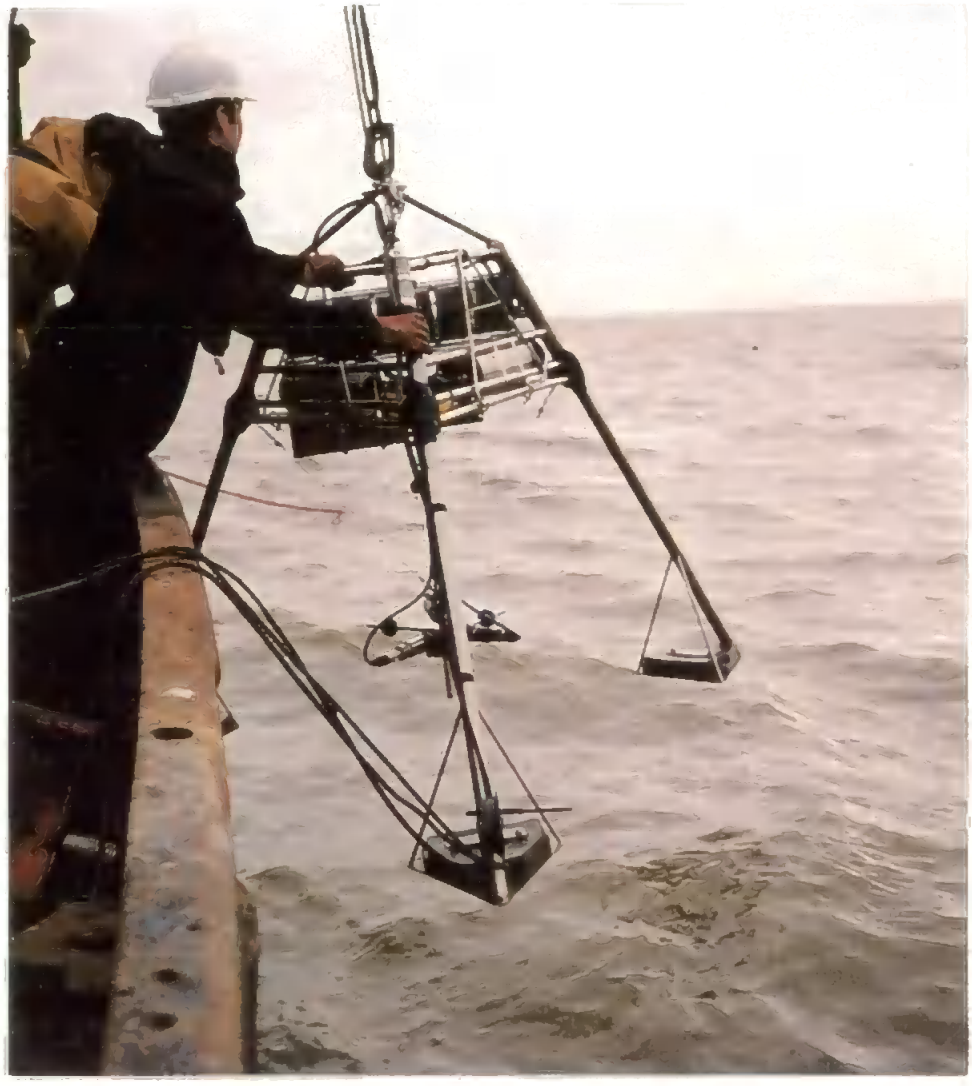

Plate 3.2 Surface buoy - Telemetry link

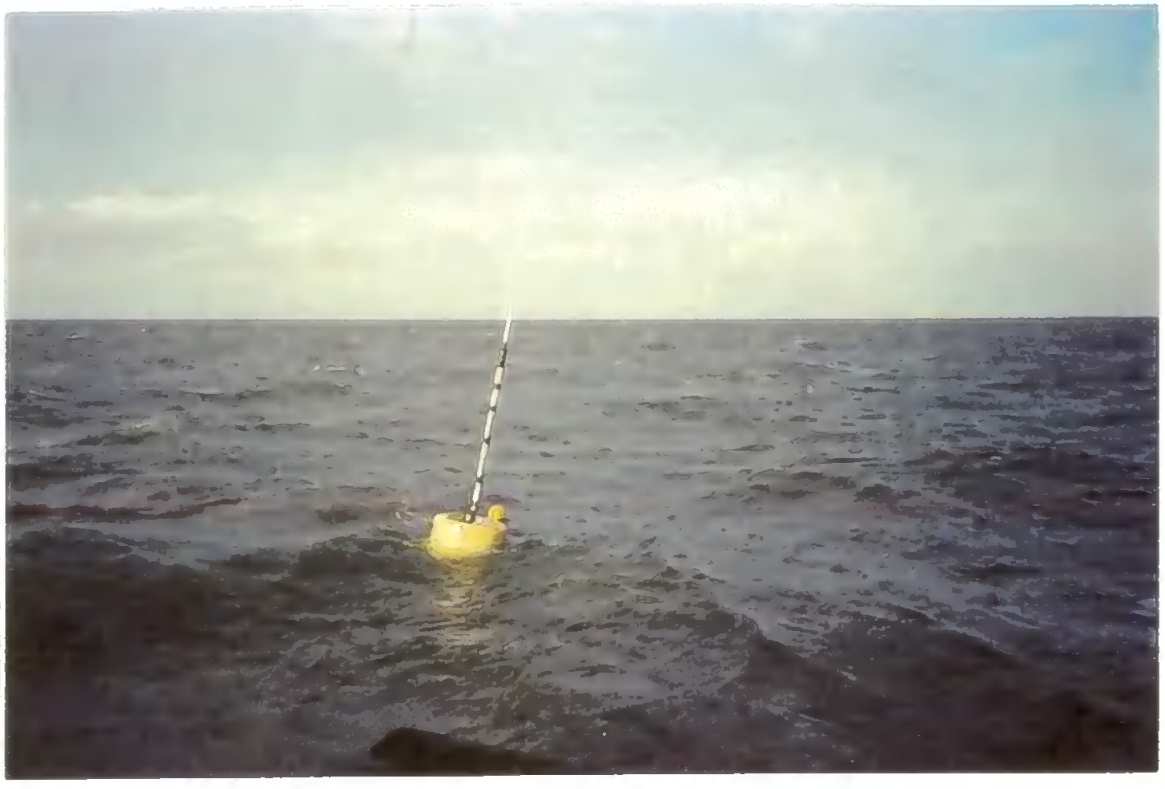

Table 3.1 gives a summary of all the sensors on BLISS as well as their height above the sea bed.

Table 3.1 BLISS data channels

Channel	Sensor	Manufacturer	Maximum input range of channel	Height above seabed (m)	Sampling rate (Hz)
1	**Pressure**	Druck Ltd	0 - 4 bar abs	0.70	5
2	**Temperature**	Lab Facility Ltd	4 - 22°C	0.48	5
3	**Conductivity**	Anderraa Instruments	0 - 55 ms/cm	0.48	5
4	**OBS 1**	D & A Instrument Co	0 - 900 FTU	0.41	5
5	**OBS 2**	D & A Instrument Co	0 - 900 FTU	0.90	5
6	**EMCM 1X**	Valeport Ltd	± 5 ms^{-1}	0.39	5
7	**EMCM 1Z**	Valeport Ltd	± 5 ms^{-1}	0.39	5
8	**EMCM 2Y**	Valeport Ltd	± 5 ms^{-1}	0.41	5
9	**EMCM 2Z**	Valeport Ltd	± 5 ms^{-1}	0.41	5
10	**Compass**	K.V.H. Industries Inc	0 - 360°	NA	0.2
11	**Tilt (pitch)**	Spectron Systems Technology Inc	± 45°	NA	0.2
12	**Tilt (roll)**	Spectron Systems Technology Inc	± 45°	NA	0.2
NA	**Transmissometer**	UoW, Bangor	0 to 100%	0.93	4

The following sections will now consider each of the sensors mounted on the BLISS tripods during the current programme.

3.2.1 Electromagnetic Current Meter

Two bi-axial spherical electromagnetic current meters (EMCM) manufactured by Valeport Marine Scientific Ltd[2] were aligned on the tripod to provide simultaneous measurements of current velocity, in the two perpendicular horizontal directions (x,y) and also in the vertical direction (z) (plate 3.3). Each EMCM is firmly clamped to the centre post (0.41m above bed), to avoid any vibration which would affect the noise level on the measured output and contaminate measurements of the water flow.

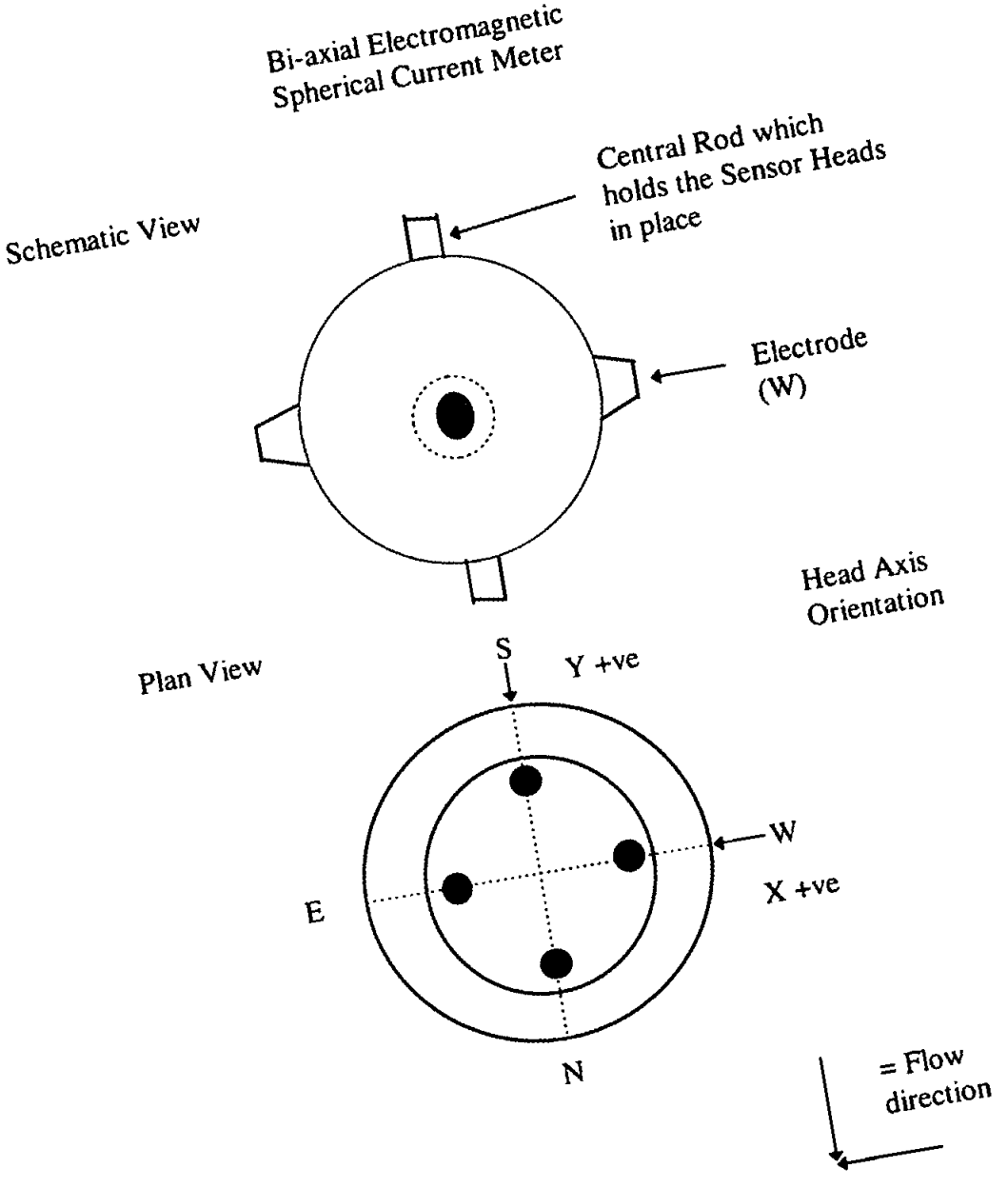

Figure 3.2 Bi-axial electromagnetic current meter

[2] Valeport Marine Scientific Ltd., Unit Townstal Industrial Estate, Dartmouth, Devon.

Plate 3.3 Bi-axial electromagnetic current meters on BLISS

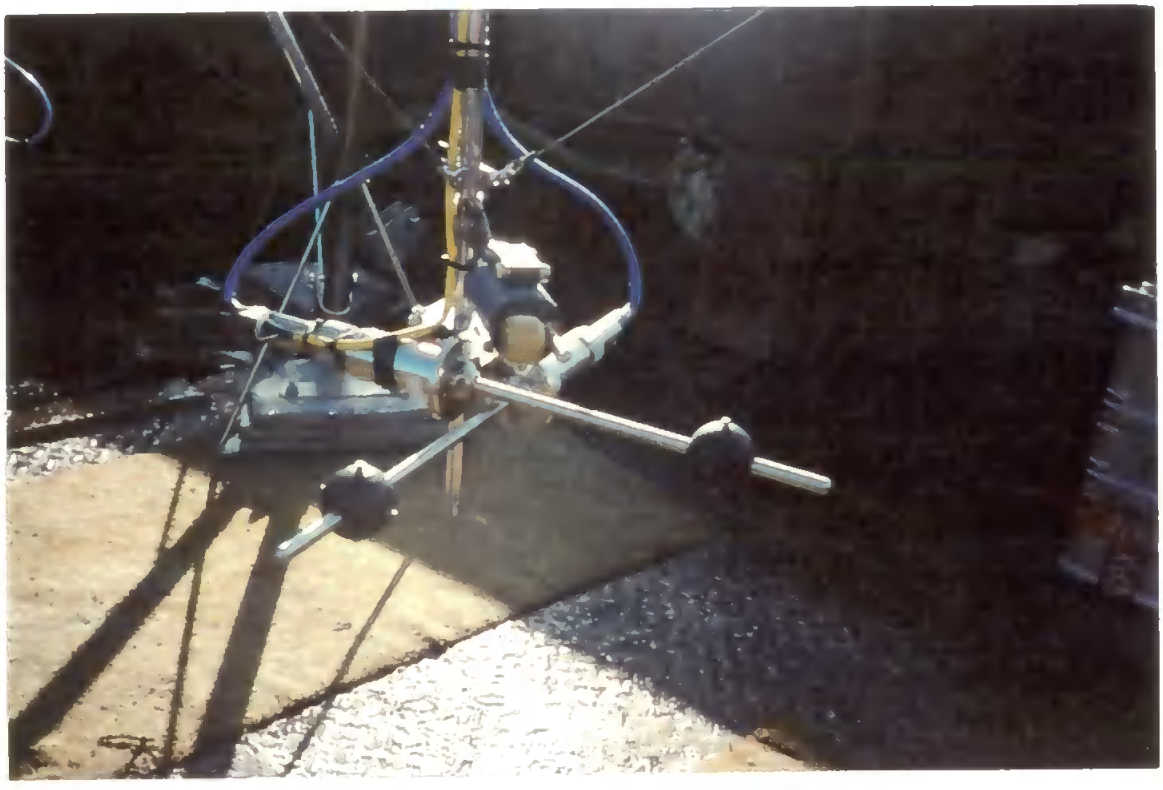

The spherical probe has an electromagnet and two orthogonal pairs of electrodes which extend into the flow field from the sphere. Sensor operation is based on Faraday's Principle of Induction (Aubrey and Trowbridge, 1985), whereby a voltage potential is induced in a conductor (sea water) when it moves relative to the magnetic field. In this case the magnetic field is produced by a coil in the head of the sensor. The voltages are induced across the electrode pairs and are proportional to the vector components of flow velocity through the plane of the electrodes. In other words, water flowing through this field, generates an electrical potential difference which is detected by the electrodes. In this case, two pairs of diametrically opposite electrodes register voltages proportional to the flow components in the horizontal and vertical plane.

Because of the robustness of the EMCM, and the absence of any moving parts, it is an ideal instrument to use during long term deployments under high energy conditions.

Whilst the EMCM sensors measure flow velocity within approximately 1 probe diameter of the probe, the boundary layer and wake structure around the probe are complicated functions of the flow field itself (Guza, 1988) when considering combined steady and oscillating flows, as experienced in the near-shore zone. Because of these complications, it was suggested by Aubrey and Trowbridge, (1985), that one would expect spherical EMCM's to have limitations. Cunningham *et al.*, (1979), noted that in oscillatory flow, the non-linear effects in the probe's boundary layer were likely causes for the observed fluctuations in the gain response of the EMCM. To test the performance of our EMCMs to steady and combined steady and oscillatory flows is beyond the scope of this project, but many investigations have been conducted and documented, notably, Aubrey and Trowbridge, (1985), Guza, (1988), Aubrey, (1989).

Although there are uncertainties in the accuracy of the EMCMs to combined wave/current flows, the high sensitivity of the sensors to flow conditions and the robustness of the instrument in a high energy marine environment, makes the EMCM the ideal choice of instrument for measuring current flow in this particular project, providing there is good calibration.

3.2.1.1 *Calibrating the Electromagnetic Current Meter*

Calibration of the EMCMs was essentially done in two parts. Firstly the sensors were calibrated for gain and offset, by towing the EMCMs in Valeport's open channel tow tank, under controlled speeds. The measured voltage outputs were then related to the different tow speeds chosen, for both the channels. Valeport provided measured calibrations (over the range of 0 to ± 1 ms^{-1}) for each current meter. The offsets of each EM current meter was factory adjusted to zero, that is the zero measured voltage was derived from an immersed sensor with no water flowing past it.

We refer to our results in bits which relate to voltages and ms^{-1} as: $-5ms^{-1}$ = -5 volts =-4096 bits, 0 ms^{-1} = 0 volts = 0 bits, $+5ms^{-1}$ = + 5 volts = +4096 bits.

Non zero offsets were present in the calibration checks preceding the first EM current meter deployment (BLISS 2). It was recognised that there was a problem with the performance of the EMCMs and all were sent back to Valeport for factory correction before the second deployment.

After Valeport corrections, pre and post deployment EMCM checks were performed in a plastic tank (0.66m by 0.54m). Water depth was 0.39m. The EMCM sensors were mounted vertically with the spheres at mid-depth. One EMC sensor was 0.08m from the end wall, the other (the one being checked) was placed at the centre of the tank 0.25m away from the first. Checks were limited to:

a) Confirming that large offsets, if any, were independent of whether or not the conductivity / temperature sensor and the other EMC sensor were in the water.

b) To take spot measurements of the offsets in still water for each sensor in turn at the centre of the tank.

c) Confirmation of substantial response to vigorous swishing to and fro on both axes.

d) Logging the monitor data (30 scans at 1s intervals) so that the confirmation could be made as to whether the noise on the EMC signals was consistent with Valeport's specified 10mV noise in still water ($0.01 ms^{-1} \equiv 10mV \equiv 8$ bits).

Results from the pre-deployment 2 calibrations can be found in appendix A1.

For both axes of all the sensors, there was a significant difference between pre (separated) and post (on rig, uncleaned) offsets. In all cases, the post offset varied between ~ 25 bits (0.03V, BLISS 2) and ~ 400 bits (0.49V, BLISS 3) deployment 2.

The sensor heads were then cleaned, by scrubbing gently with dilute detergent and a soft brush, followed by rinsing with tap water from a hose. Any slight sediment or superficial rust deposits came off very readily. The rigs were repositioned as before with the sensors centred by eye in the tank. In every case, cleaning had an appreciable effect, to bring the offsets closer to the pre deployment values. The main effect was largely to reduce the

offset by amounts varying between ~ 5 bits (0.006V, BLISS 2) and ~ 290 bits (0.35V, BLISS 3). The offsets were then calculated by taking the averages of the data runs (i.e. mean of 30 monitor scans for each entry) in still water. Data from the current meters were calibrated by using the following equation:

[3.1]

$$\text{current } (ms^{-1}) = \text{slope} \times (\text{bits output} - \text{Offset}).$$

Because we did not have a tow tank to calibrate the current meters, we could not perform any linear regression analysis. Instead, we used Valeport specifications for the slope coefficient i.e. 0.0012209. Table 3.2 gives all the offsets derived before and after the deployments. The offsets used as input into equation 3.1 to calibrate the EMCMs for each BLISS rig at each deployment are the highlighted values in table 3.2.

3.2.2 The Optical Backscatter Sensor

The optical sensor used on the BLISS systems to monitor suspended sediment concentration was the Optical Backscatter Sensor (OBS) (plate, 3.4) developed by Downing *et al.*, (1981). The OBS has proved an excellent tool for suspended sediment studies due to its high frequency response, relative insensitivity to bubbles, approximately linear response to concentration, and small size, causing minimal disruption to the transporting flow and allowing measurements within a few cms of the seabed (Kineke and Sternberg, 1992). Each sensor consists of a high intensity infra red emitting diode (IRED), a detector and a linear, solid state temperature transducer (figure 3.3, figure 3.4). Each IRED produces a beam with half power points at 50° in the axial plane and 30° in the radial plane. The detector integrates infra red radiation backscattered from the suspended sediment between 140° and 165°.

Output of the detector is then amplified and low pass filtered (-3 dB point: 20 Hz, roll off: 20 dB per decade) to achieve a voltage which reflects the amount of sediment in suspension. An infra-red emitter is used in the OBS sensor because infra-red (IR) radiation is strongly attenuated by sea water.

Table 3.2 Calibration offsets derived for all the pre/post deployments for the Electromagnetic Current Meters on BLISS

Deployment	Slope	BLISS 2 Offsets				BLISS 3 Offsets				BLISS 4 Offsets			
		EMC1		EMC2		EMC1		EMC2		EMC1		EMC2	
		x	y	x	y	x	y	x	y	x	y	x	y
1	0.001221	0	0	0	0	0	0	0	0	0	0	0	0
Pre 2	0.0012209	-20 -0.024ms^{-1}	9 0.011ms^{-1}	-5 -0.002ms^{-1}	61 0.074ms^{-1}	88 0.11 ms^{-1}	-854 -1.04 ms^{-1}	-31 -0.038ms^{-1}	-64 -0.078ms^{-1}	-360 -0.44ms^{-1}	-300 -0.37ms^{-1}	387 0.47ms^{-1}	525 0.641ms^{-1}
Post 2[1]	0.0012209	-37 ± 3 -0.045ms^{-1}	-67 ± 3 -0.082ms^{-1}	-23 ± 3 -0.028ms^{-1}	-35 ± 3 -0.043ms^{-1}	70 0.085ms^{-1}	-800 -0.98ms^{-1}	-50 -0.061ms^{-1}	-80 -0.098ms^{-1}	EMC sent back to Valeport			
Offset used (deploy 2)	**0.0012209**	**-40 -0.049ms^{-1}**	**-67 -0.082ms^{-1}**	**-5 -0.002ms^{-1}**	**-35 -0.043ms^{-1}**	**70 0.085ms^{-1}**	**-800 -0.98ms^{-1}**	**-50 -0.061ms^{-1}**	**-80 -0.098ms^{-1}**	-	-	-	-
Pre 3	0.0012209	-16 ± 4 -0.02ms^{-1}	-60 ± 5 -0.073ms^{-1}	-20 ± 2 -0.024ms^{-1}	-35 ± 2 -0.043ms^{-1}	-40 -0.049ms^{-1}	0 0ms^{-1}	-210 -0.26ms^{-1}	180 0.22ms^{-1}	40 0.049ms^{-1}	-10 -0.012ms^{-1}	-30 -0.037ms^{-1}	-80 -0.098ms^{-1}
Pre 4	0.0012209	23 ± 3 0.028ms^{-1}	102 ± 5 0.13ms^{-1}	-50 ± 5 -0.061ms^{-1}	140 ± 5 0.171ms^{-1}	67 ± 3 0.082ms^{-1}	220 ± 4 0.27ms^{-1}	39 ± 2 0.048ms^{-1}	104 ± 3 0.13ms^{-1}	27 ± 3 0.033ms^{-1}	60 ± 4 0.073ms^{-1}	-20 ± 4 -0.024ms^{-1}	60 ± 4 0.073ms^{-1}
Post 4	0.0012209	15 ± 5 0.018ms^{-1}	23 ± 5 0.028ms^{-1}	0 ± 5 0ms^{-1}	35 ± 5 0.043ms^{-1}	No offsets due to damaged sensors on recovery				8 ± 5 0.009ms^{-1}	37 ± 5 0.045ms^{-1}	-13 ± 5 -0.016ms^{-1}	37 ± 5 0.045ms^{-1}
Offset used deploy 4	**0.0012209**	**15 0.018ms^{-1}**	**23 0.028ms^{-1}**	**0 0ms^{-1}**	**35 0.043ms^{-1}**	**64 0.078ms^{-1}**	**216 0.264ms^{-1}**	**37 0.045ms^{-1}**	**101 0.123ms^{-1}**	**17 0.021ms^{-1}**	**49 0.059ms^{-1}**	**-17 -0.021ms^{-1}**	**49 0.059ms^{-1}**

[1] Slope = -0.0012209 for y-axis of EMC1, BLISS 3. (Y-axis reversed in this sensor head).

This poses an inherent advantage over previous instruments because the IR attenuation minimises interference between closely spaced sensors and secondly, when operating in shallow water, the compliment of low sub surface IR irradiance and the low-pass optical filter of the OBS, will suppress the level of ambient solar radiation which would otherwise swamp the detector.

The intensity of backscattered IR is a function primarily of the concentration and size of suspended particles in front of the sensor. The response to a given mass concentration is affected also by the composition, refractive indices and the distribution of sizes of the particles present (Osborne *et al.*, 1994). Measurements by D & A Instruments (1989), have shown that the OBS sensor is more sensitive to fine sediments such as mud than to sand. For high sediment concentrations, particularly in suspensions with high clay and silt contents, the infra-red radiation from the emitter can be partially blocked, so that the backscatter decreases with increasing sediment concentration above a critical level (D & A Instruments, 1989), Kineke and Sternberg, (1992). The maximum level on the response curve in this case is at $5000mgl^{-1}$. Consequently, the output voltage can represent two concentrations and, an ambiguity in the results occur. However, this limit is unlikely to be reached except in very energetic situations.

Before deploying the OBS sensor, it is important to set the gain to match the type of sediments being measured. For example, if the gain is too high, then data will be lost because the sensor output is limited by the supply voltage and will saturate before peaks in sediment concentration are detected. If the gain is too low, the full resolution of the data logger will not be utilised.

Sensor performance and offset for the OBS sensors on BLISS prior to and after a deployment was determined using known standards of Formazin solution so that the output measurements during each deployment were in Formazin Turbidity Units (FTU's). Turbidity is the cloudiness in water produced by light scattered from suspended particles, colloidal material and other impurities. It is an apparent optical property that depends on the characteristics of the scattering particles, external lighting conditions and the instrument used to measure it.

Plate 3.4 Optical backscatter sensors on BLISS

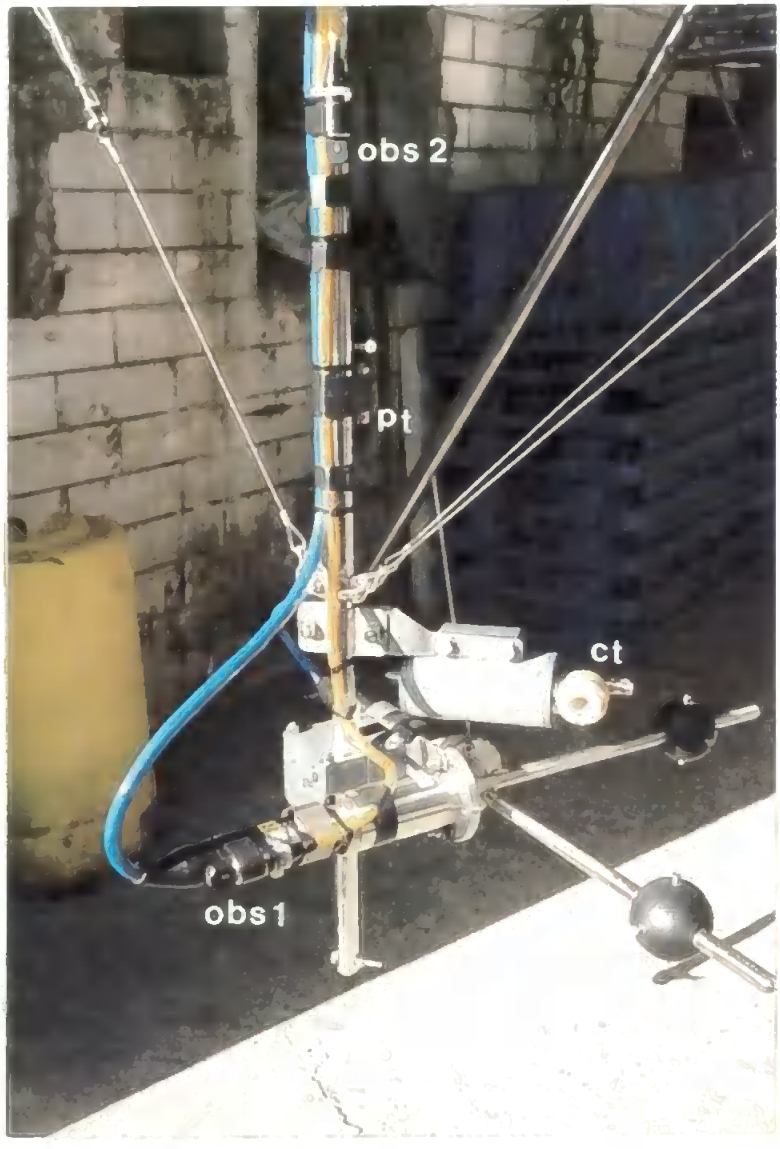

Plate 3.5 Beam Transmissometer

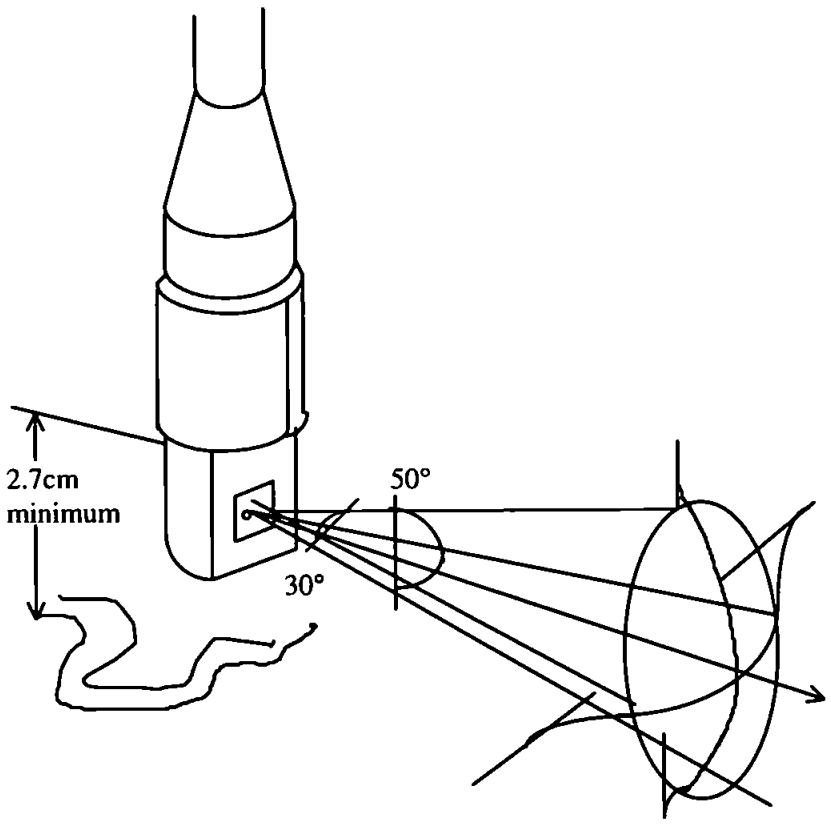

Figure 3.3 Optical backscatter sensor - Beam pattern

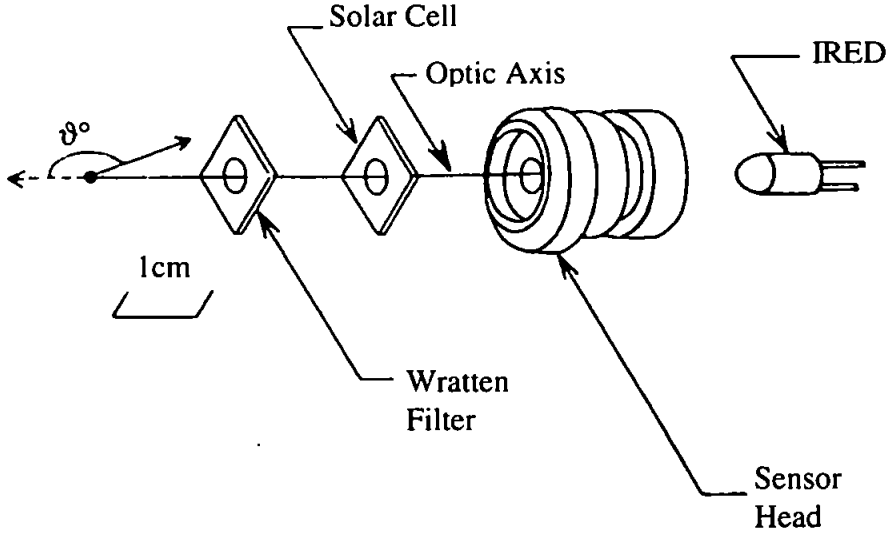

Figure 3.4 Exploded view of the OBS sensor.

(From: Downing *et al.*, 1981)

3.2.2.1 *Calibrations to Determine OBS Sensor Performance and Offset using Formazin Solution*

For calibration procedure in each deployment refer to appendix A.2.1.

There were significant differences in the OBS sensor performance before and after the sensor deployments. As a result, the most appropriate performance and offsets from the Formazin calibrations were difficult to determine.

The optical backscatter sensors' FTU data was calibrated using:

[3.2]

$$FTU = Bits \times (Slope + offset)$$

The relationship between bits and FTU's determined to full resolution was FTU = 0 to 2000, bits = 0 to 4096. 1 FTU = 2.048 bits. FTU calibration results for the remaining deployments were broadly the same, although there were small changes between pre- and post-deployment calibrations. The changes varied in magnitude and sign between different sensors, but not in any obvious systematic manner. The pre-and post-deployment calibrations were performed in exactly the same way and should have had equal reliability. With no further explanations to this, we could only assume the changes as being due to sensor ageing, more than the manufacturers specification of 3.5% in 2000 hours.

Post deployment two calibrations were used as the pre-deployment calibrations for deployment three and four. Full calibrations were then conducted after deployment 4. Table 3.3 summarises the FTU calibrations used to optimise the OBS sensor's performance and offsets in each deployment.

Sediment concentration measured in FTU will qualitatively give a good indication as to what processes are occurring. However, for quantitative flux measurements, the FTU values must be converted to units of mgl^{-1}. *In situ* water samples were collected during the deployments very close to the optical sensors on BLISS. Their filtered dry weights were then compared with time corresponding to OBS FTU outputs (at the time the samples were taken). The results were then regressed to produce a calibration coefficient which was used to convert the FTU values into mgl^{-1} (refer to section 4.5).

Table 3.3 Slope and offsets used to calibrate the optical backscatter sensors in FTU - all BLISS deployments

Deployment	BLISS 2				BLISS 3				BLISS 4			
	OBS 1 (FTU)		OBS2 (FTU)		OBS1 (FTU)		OBS2 (FTU)		OBS1 (FTU)		OBS2 (FTU)	
	slope	offset	slope	offset	slope	offset	slope	offset	slope	offset	slope	offset
1	0.4884	0.00	0.4884	0.00	0.4884	0.00	0.4884	0.00	0.4884	0.00	0.4884	0.00
2	0.34454	-13.37	0.19109	-28.071	0.2156	-10.758	0.2033	-0.51678	-	-	-	-
3	0.34454	-13.37	0.23242	-7.7374	-	-	-	-	-	-	-	-
4	0.33376	-14.683	-	-	0.2225	-1.0754	0.2395	-10.219	0.1925	-9.14	0.2564	-15.171

3.2.3 Beam Transmissometer

The beam transmissometer (Plate 3:5) borrowed from University College of North Wales (UCNW) operates by directing a beam of light from Eo to Et (figure 3.5). The amount of suspended sediment in this region is then measured by calculating the amount of light which reaches Et after absorption and scattering has occurred. If clear water dominated, the ratio of ET/Eo would be 1.0, as 100% of light had reached the far end. Attenuation is then equal to 1.0 - Et/Eo, and it is this inherent optical property which relates to the amount of sediment in suspension.

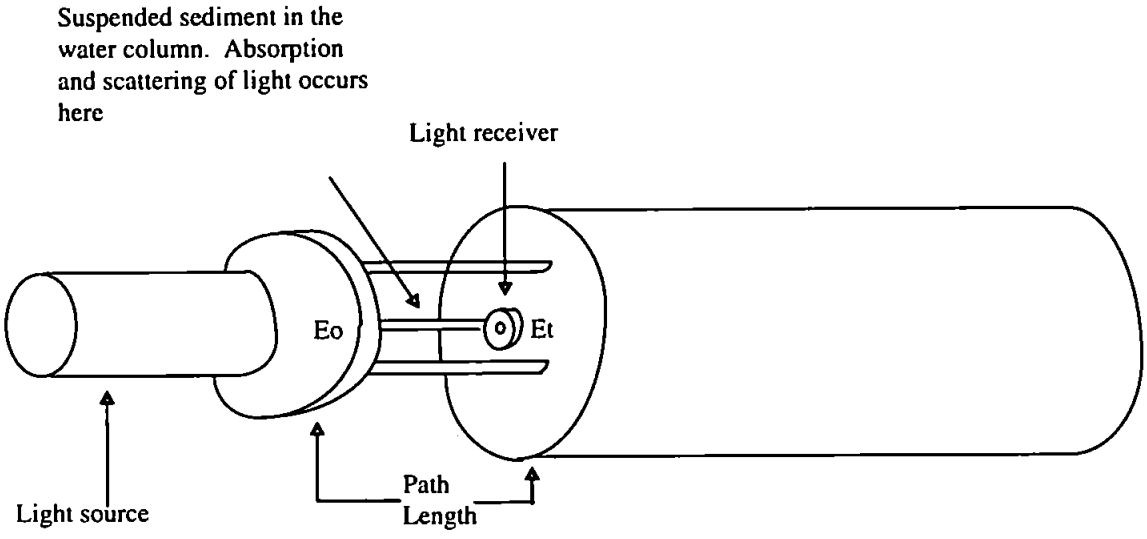

Figure 3.5 Beam transmissometer - Operation

It is readily accepted that transmissometers are more sensitive at low concentrations of suspended sediment than the OBS sensor. Above about 10 FTU and 50 mgl^{-1}, large changes in turbidity produce disproportionately small changes in transmissometer output. The upper limit of linear response of transmissometers can be extended by shortening the path length (L). Hence the optimum situation in any suspended sediment research is to use both types of optical sensors concurrently. Unfortunately, the transmissometers on BLISS were fixed at a path length of 25 cm, and were only operational during the February 1996 deployment phase. Due to the nature of the water column being very turbid, the transmissometers saturated to full scale, showing no variation in sediment concentration. Because of this, we have no transmissometer data that can be compared to the outputs from the optical backscatter sensors.

3.2.4 Pressure Transducer

Water depth and surface elevation was measured on BLISS by a Druck Ltd. PDCR 940, 7 bar absolute pressure sensor (plate 3.4, pt). Pressure sensors have been used for many years to monitor wave activity and water depth, and are noted for their reliability, robustness and ease of installation. The Druck pressure sensor is 25mm in diameter and has a titanium external body which fully seals the internal components. Because of this, it is recommended for salt-water applications. It has an operating temperature range from -20° to +80°C. It weighs 100 gm and has a continuous resolution. Sensor operation is based on a high technology silicon diaphragm which functions under absolute pressure such that the reference side of the diaphragm is sealed under vacuum. Hence, sensor output at zero applied pressure (i.e. vacuum) is equal to 0 voltage nominal.

Output of the sensor is proportional to the total applied pressure (i.e. atmospheric pressure + hydrostatic pressure of the water column above the sensor). The voltages recorded in BLISS's pressure channel are therefore proportional to sensor output and hence to total pressure with a small offset.

i.e. atmospheric pressure + hydrostatic pressure = (slope x bits) + offset

or equivalently,

hydrostatic pressure + barometric correction = (slope x bits) + offset - reference atmosphere.

[3.3]

i.e $\rho(S,t).g(\varphi).z + (P-Po) = (\text{slope x bits}) + \text{intercept}$

where:

$\rho(S,t) = \rho(S,t,0) =$ density of water column in kgm^{-3} at Practical Salinity S, temperature t°C and zero pressure. This can be derived with sufficient accuracy for BLISS purposes from the table on p.23[3], or with maximum accuracy from the algorithm given on p. 20-21. The dependence of ρ on pressure is negligible for BLISS depths.

[3] Fofonoff, N. P. and Millard, R.C. 1983. Algorithms for computation of fundamental properties of sea water. *UNESCO Technical Papers in Marine Science*. No 44 .

$g(\varphi)$ = acceleration of gravity in ms^{-2} at sea level at latitude $\varphi°$.

z = height of water column (i.e. depth) in m.

$P-P_o$ = barometric correction, where P = barometric pressure in Pascals at time of measurement (1 bar = 10^5 Pa, i.e. 1mb = 100Pa ≅ 0.01m depth), and P_o = reference atmosphere (chosen arbitrarily for arithmetic convenience as 1 bar = 1000mb; this is absorbed in "Intercept"). Maximum likely range of P is ~ 980 to 1035 mb, equivalent to an apparent depth change of ~0.55m.

3.2.4.1 *Calibration Procedure*

1. Record bits as a function of z in m using tap water (S=0).
2. Note temperature t°C of water, barometric pressure P in Pascals (1mb = 100 Pa), and latitude $\varphi°$ of calibration site.
3. Calculate f = applied pressure - reference pressure.
   = hydrostatic pressure + barometric correction
   = $\rho(0,t).g(\varphi).z + (P-10^5)$.
4. Plot f against bits to show spread in calibration data, and regress f against BITS to derive Slope and Intercept.

To use the calibration:

rearrange equation (3.3) =

[3.4]

$$z = \frac{\text{SlopexBits} + \text{Intercept} - (P - P_o)}{\rho(S,t).g(\varphi)}$$

Insert the relevant field values of P_o, $\rho(S,t)$ and $g(\varphi)$ in equation 3.4 to calculate depth (z) in m of seawater. P_o and $\rho(S,t)$ may vary with time during a deployment. Work to 5 significant figures to ensure calculation is more accurate than ± 0.01m in depth. The calibration coefficients (slope and intercept) used to calculate depth from the pressure sensor are summarised in table 3.4 and are given by using the formula:

[3.5]

$$\text{depth (m)} = \text{slope x bits} + \text{intercept}$$

Table 3.4 Calibration coefficients used to calculate water depth from the pressure sensors on BLISS - all deployments

Deployment	BLISS 2		BLISS 3		BLISS 4	
	slope	intercept	slope	intercept	slope	intercept
1	0.008352	-9.87	-	-	-	-
2	0.008764	-10.235	0.008671	-9.955342	0.008567	-9.645175
3	spot checks	-	-	-	spot checks	-
4	0.008758	-10.228	0.008758	-10.228	0.008758	-10.228

3.2.5 Temperature Sensor

The temperature sensor used on BLISS was built in-house at Plymouth Marine Laboratory (plate 3.4, ct). It is made up of a Comark Platinum resistance thermometer. Calibration is relatively straight forward. The sensor is placed in water of known temperature and the bits output read off and regressed against temperature. The thermometer was also checked along side the National Physics Laboratory calibrated mercury thermometers. The calibration coefficients used to convert bits output to temperature in °C were derived by inverting the regression equations from pre and post deployment calibrations.

The resultant calibrations used in each deployment are given in table 3.5. Temperature is derived using the same formula: Temp (°C) = slope x bits + intercept.

Table 3.5 Calibration coefficients used to calculate temperature - all deployments

Deployment	BLISS 2		BLISS 3		BLISS 4	
	slope	intercept	slope	intercept	slope	intercept
1	0.002005	12.99	-	-	-	-
2	0.002005	12.99	0.001991	13.763	0.002013	13.196
3	-	-	-	-	-	-
4	0.002494	13.298	-	-	-	-

3.2.6 Conductivity Sensor

The conductivity sensor on BLISS is made by Anderraa Instruments (plate 3.4, ct). Calibration is achieved by immersing the sensor prior to and after deployment in water of known salinity (a sample having been measured on a bench salinometer). The water temperature is measured with a platinum resistance thermometer, and the sensor output response in BITS (voltages) is recorded. The temperature and / or the salinity of the water is then changed, ensuring that the water is well mixed, and that the sensor is in thermal equilibrium with it, ensuring no bubbles. The measurements are then repeated to cover the full range of conductivity.

The Conductivity Ratio of the water at each step is calculated using the UNESCO algorithms[4]. The Conductivity Ratio is then regressed against conductivity BITS to obtain the coefficients in **Cond. Ratio = slope x bits + Intercept**. Expressed in terms of Conductivity Ratio (by dividing by conductivity C(35,15,0) = 42.914 mmho/cm)

[4] Fofonoff, N.P. & Millard, R.C. 1983. Algorithms for computation of fundamental properties of seawater. UNESCO technical papers. *Marine Science*, No. 44.
JPOTS panel. 1991. ***Processing of Ocean Station Data***. UNESCO.

[3.6]

$$\text{Conductivity Ratio} = \frac{C(S,t,p)}{C(35,15,0)} = \text{slope x bits + intercept}$$

In deployment 1 there was no calibration data, so we used nominal values based on component specifications, with the calibration expressed in conductivity units. Hence:

[3.7]

Conductivity (in mmho/cm) = 0.012558 x bits - 0.63

The slope and intercept calculated and used in the remaining deployments are given in table 3.6.

Table 3.6 Calibration coefficients used to calculate conductivity ratio deployments 2, 3 and 4

Deployment	BLISS 2		BLISS 3		BLISS 4	
	slope	intercept	slope	intercept	slope	intercept
2	-	-	0.000283	-0.011173	-	-
3	0.0002826	-0.011173	-	-	-	-
4	0.0002826	-0.011173	-	-	0.0002826	-0.011173

3.2.7 Salinity Calculation

Salinity is obtained by calculation through the Practical Salinity Scale (PSS-78)and the International Equation of State of Seawater (UNESCO, 1991). The Practical Salinity scale expresses salinity as a function of electrical conductivity ratio R, temperature t and pressure p. R is the ratio of the conductivity of the sample, at *in situ* temperature and pressure, to the conductivity of Standard Seawater of salinity 35, temperature 15°C and atmospheric

pressure. The algorithm for converting conductivity ratio to salinity is constructed in terms of the conductivity ratio R defined as:

[3.8]

$$R = C(S,t,p)/C(35,15,0)$$

The ratio is factored into the functions

[3.9]

$$R = r_t(t) \,.\, R_t(S,t).R_p(R,t,p)$$

where

$$r_t(t) = C(35,t,0)/C(35,15,0)$$
$$R_t(S,t) = C(S,t,0)/C(35,t,0)$$
$$R_p(R,t,p) = C(S,t,p)/C(S,t,0)$$

Salinity is given by the function

[3.10]

$$S = \sum_{n=0}^{5}[a_n + \frac{\Delta t}{1+k\Delta t}b_n].R_t^{n/2}$$

Given a measurement of R, t and p, salinity is computed by solving equation 3.9 for R_t; $R_t = R/(r_t R_p)$ and evaluating S from equation 3.10, using the coefficients outlined in PSS-78 (UNESCO, 1991). For easy computation, a Matlab program was devised which could run continuously in a loop, and at the end of each data run, save the data under a separate heading (appendix B, program 6).

3.2.8 The Compass, Pitch and Roll

The compass on BLISS was manufactured by K.V.H. Industries Inc., and the pitch and roll sensors manufactured by Spectron Systems Technology Inc. Data from these attitude sensors were recorded in bits (voltages) during the background data sampling period.

3.2.8.1 *Calibration Procedure*

Pre- and post-calibrations for compass orientation were achieved by taking a hand compass bearing from the leading bow leg. The BLISS frame was then moved into different positions and the voltages relating to each bearing, noted. The pitch and roll were tested by

lifting one leg up at a time and noting the change in the bit readings from horizontal. The bit values were then plotted against the compass, pitch and roll respectively, and the data regressed. The regression equations were then inverted and the resultant coefficients were used to convert bits to angles. Full calibration was conducted on BLISS rigs 2 and 3 after the July deployment. The system on rig 4 did not work at all. Because the compass, pitch and roll settings are unlikely to alter, the calibration coefficients derived after deployment 2 were used to convert the bit values to angles for the remaining deployments. Since the pitch and roll data were within 1° of horizontal, it was assumed, that the BLISS tripods were sitting horizontal on the sea bed.

Compass Calibration

BLISS Rig 2 Heading of bow leg (°M) = 90 -16.7546 + 0.236349 x bit (less 360° if answer >360°)

BLISS Rig 3 Heading of bow leg (°M) = (Bits -155.53)/3.8341 + 90 = 0.26082 x Bits - 40.565 + 90 = **0.26082 x Bits + 49.435** ((less 360° if answer >360°)

Knowing the nominal positions and angles of the sensors on the tripod before deployment, one can deduce exactly how the tripod is lying with respect to North by calculating the angle of the leading bow leg. Once this angle is known, the angle required to rotate the current meters so that they align to alongshore and across-shore flow can then be deduced. Further discussion regarding the orientation of the current meters follows in chapter 5.

3.2.9 Data Logging and Data Storage

BLISS is designed to measure on the same data acquisition system, the x,y,z components of flow, waves and turbulence, suspended sediment, salinity, temperature and pressure within 1m of the seabed. A miniature, low power, single board computer, manufactured by Triangle Digital Systems Ltd, forms the brain of BLISS. It is programmed in the high level language FORTH (Pers. Comm., Barrett, 1996) to control the operation of the logger and communications, and to allow user-selection of logging parameters. Data is recorded in burst mode, which operates at 5Hz (0.2 seconds) for 1024 seconds (17 minutes) every hour. In addition, the system also records data in slow background mode, which samples at 5

minute intervals. It is within this mode that the compass, pitch and roll data is recorded as well as the battery levels.

Measured data is logged *in situ* on a miniature 40 Mbyte hard disc and is stored as a compressed Hex file, as well as being transmitted to a shore station at Tunstall at three hour intervals. Shore telemetry is achieved via an aerial attached to a surface buoy using the 458 MHz telemetry band. By employing this procedure, real time data bursts can be down-loaded after transmission at Tunstall and processed on another computer to reveal any anomalies which may exist in the sensor outputs. After each deployment, the Hex data is decompressed and down-loaded in blocks onto computer in ASCII format by using an in-house computer program developed by Colin Barrett (PML). The data is stored in block format, and each block contains header information, such as Rig Identifier, Run number, and Start Date/Time, background data, or transmissometer data. The sensor data for each run is stored in rows and columns (5120 by 10) respectively. The background data is much less dense (2 readings every hour), but contains valuable information on compass, pitch and roll of the tripod. In each block of data, there are three runs (data bursts), 2 background data sets and 3 transmissometer corresponding runs saved into one file. Before the data can be calibrated, the blocks must be split up and then each run saved separately as an individual file. Matlab programs were designed for this process (see programmes 1-5, appendix B).

Matlab is a commercially available mathematical package which can deal most efficiently with large data sets. Matlab operates using a language which is closely related to C. All the programs used to process the raw data, and for data interpretation, have been written using Matlab.

Chapter 4

4. Site Selection and Fieldwork

4.1 Introduction

This chapter gives an account of the fieldwork completed off Holderness and the data collected. The next section describes a geophysical site survey which was completed prior to the first deployment of BLISS off the Holderness coast. The aim of the site survey was to determine the nature of the seabed. These results were then compared with other site surveys taken in the same region.

4.2 Geophysical Site Survey off the Holderness Coast

Previous sea bed records in the study region described a sea bed composed of gravel and sand (British Geological Survey (BGS)). Video recordings of a survey taken by MAFF also revealed small stones mixed with sand and gravel overlaying boulder clay. To maximise the value of data collected by BLISS, it was important that the three BLISS tripods were deployed over level ground to ensure that orientation of the EMCM's were actually measuring horizontal and vertical velocity within 1° of vertical, and that the ground was largely composed of sand and silt, so as to monitor resuspension events, if any, in the vicinity of the BLISS tripod. Areas with large pebbles or boulders should therefore be avoided. It is anticipated that, locally, sea bed configuration can change quite considerably after a severe storm, and as a result geological records of sea bed sediments published by the BGS should not be taken as an exact representation of the current conditions. Therefore, it was necessary to conduct our own site survey of the seabed off Tunstall, in order to ascertain locations for deploying the BLISS tripods. To achieve this

objective, a side-scan sonar was towed along predetermined transect lines (figure 4.1) representing the area of interest, and the results of the side-scan sonar validated by grab samples. At all times, location points would be recorded using GPS to achieve the accuracy required.

4.2.1 Survey Tools

4.2.1.1 *Side-Scan Sonar*

The side scan sonar is a sideways-scanning acoustic survey tool (plate 4.1). With the side-scan, the floor to both port and starboard of the survey vessel is insonified by beams of high-frequency sound (30-110 KHz), transmitted in this case by a tow-fish with piezoelectric transducers running along its side (Abbot, 1992). The towing cable also acts as the data transmission line. The fish is a streamlined, hydrodynamically balanced unit about 1m in length which has adjustable fins to maintain its position relative to the sea bottom when being towed behind the boat. The high frequency transmission beam is slightly depressed, with the main lobe being projected 10° below horizontal, achieving a very narrow horizontal width, 1.2°. This design ensures a reasonable resolution even at maximum range (300m). However, in our case, the range was limited to 75m so that good resolution could be achieved when towing in relatively shallow water (25m maximum). Principally, the SSS measures the two way time lag between the transmitted to received signal, which can then be converted to distances, assuming a constant velocity. The recorder was set to the same speed as the vessel (in our case 3.5 and 4 knots) to get a quasi true scale record. Sea bed features facing towards the survey vessel, such as rock outcrops or sedimentary bedforms, reflect acoustic energy back towards the transducers whilst in the case of features facing away from the vessel, or a featureless sea floor, the acoustic energy is reflected away from the transducers. The record of the resulting pattern of returned acoustic energy is known as a sonograph. In order to interpret the sonographs in terms of seabed materials, it was essential that sediment grab samples were collected and that other information, for example morphological maps and local knowledge, were taken into account.

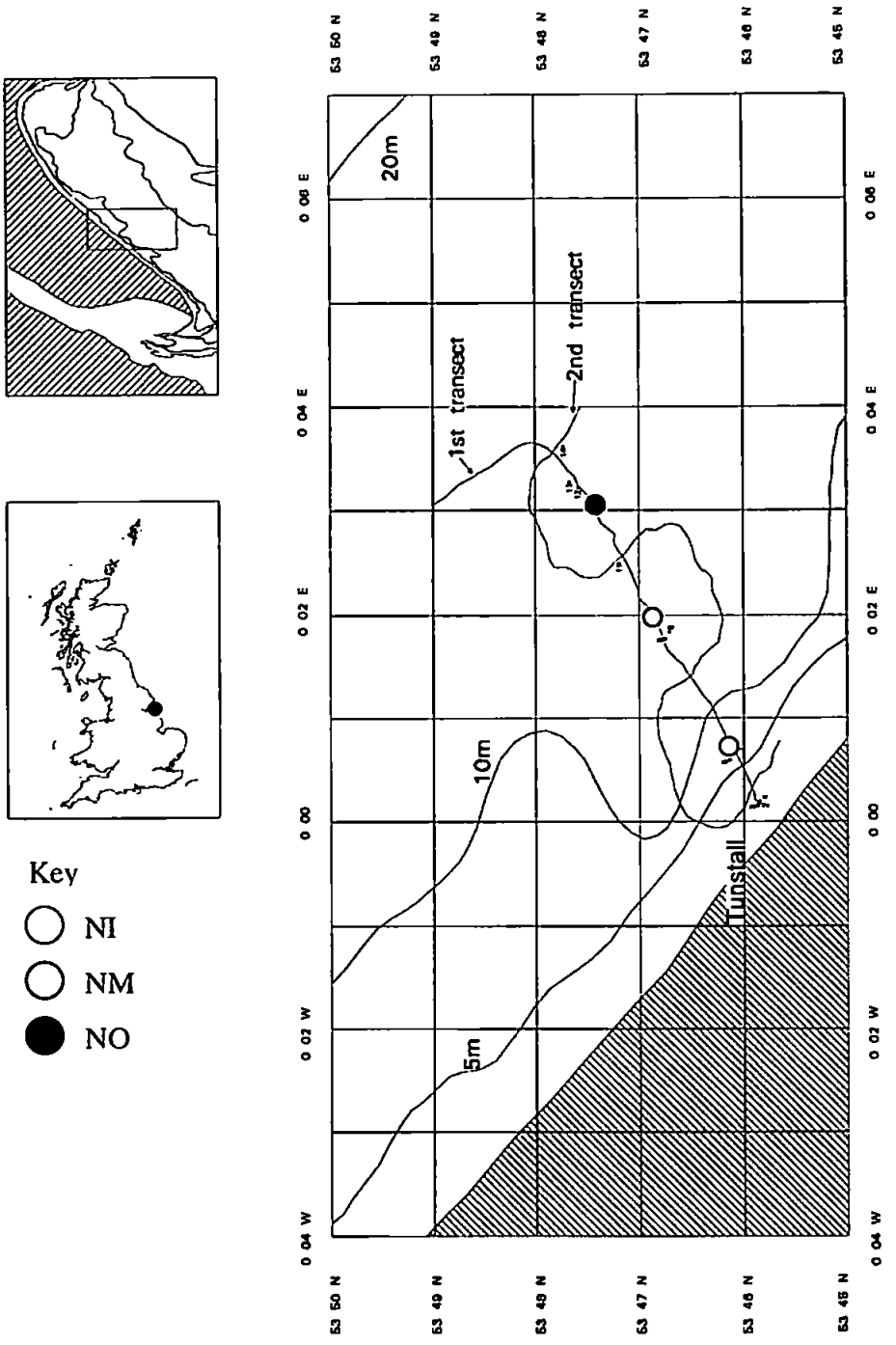

Figure 4.1 Survey area off the Holderness coast, showing transect lines of side-scan sonar and positions of grab samples. The mooring sites are also shown.

Plate 4.1 Side-scan sonar

4.2.1.2 *The Shipek Grab Sampler*

The Shipek grab sampler was designed to obtain samples of sediments. The sampler operates by spring-driven rotation of a bucket upon contact with the bottom, encircling the sediment to about 10cm depth. The sampler is lowered at a moderate speed with the bucket in its inverted position. On contact with the sea bed, an internal weight triggers a release mechanism. The bucket is then forced to rotate on its axes at high speed, encapsulating the sediment in a 180° rotation. Once rotated, the bucket is held in an upwards, closed-concave position.

4.2.2 Types of Sediment and Seabed Found off Tunstall

The following information (table 4.1) has been gathered from a report undertaken in 1988 by Halcrow and Partners on coastal protection (Anglian Water, 1988). This information, although old, has proved useful for comparison with the data collected from our own site survey.

As part of the Holderness Experiment, MAFF conducted a similar site survey, to ascertain the best locations for laying the MINIPOD tripod systems off the Holderness coast along a northern and southern transect. Using a low light TV camera, MAFF located stones (ranging in size from 2-3cm up to 30-40 cm) and areas of sand and gravel. Operating a side-scan sonar, it was discovered that there were bands of stones and boulders running North, not actually parallel to the coast, and not in line with the tidal ellipse (Pers. Comm., MAFF, 1994). These bands of stones and boulders were interspersed with ribbons of sand waves. From visual sitings using a video camera, Dead Man's Fingers (*Alcyonium Digitatum*) 10/20 cm high were present on the boulders, accompanied by sea urchins, which suggested a stable bed. MAFF suggested that the boulders and stones may be a relic feature from either glacial moraine or a past shoreline. When Halcrow and Partners undertook their survey with a side-scan sonar, records revealed a common occurrence of wave-like bedforms. Grab samples showed epifauna-encrusted cobbles and coarse gravels. They revealed that this type of bed extended inshore of the break of slope into depths of -10 to -12m ODN (table 4.1). Between these depths and -6 to -8m ODN, side scan sonar indicated a swathe of exposed clay some 100m in width. Localised patches of sand occurred within this clay zone, and formed a more continuous cover inshore of -6 to -8m.

Table 4.1 Description of sediment and seabed found off Tunstall

400m OFFSHORE	**(-12m ODN)**
400m	~ 3cm sand overlying soft silt. Thin sand overlying soft silt. Occasional boulder protruding through sand. Boulders, cobbles and thin sand on clay.
300m	Sand. Thin sand overlying soft silt. Sand >25cm thick. 1cm of sand over clay, occasional patches of bare clay. Sand with protruding cobbles. Bare clay, pock-marked.
200m	1cm sand over clay. Bare clay, 2-3cm diam. pock-marks. Sandy gravel and boulders. Clay immediately below. Small boulder 'reefs'. Sand and pebbles. Sand, pebbles and cobbles.
100m	Sand. Sand and pebbles. Sand. Mega-rippled sand, stones exposed in troughs.
50m	Sand >0.5m deep.
0m INSHORE	**(-8m ODN)**

Source: Anglian Water (1988)

4.2.3 Results From the Site Survey

A description of the grab samples taken are given in table 4.2. The sonar tracks followed are shown in figure 4.1 as well as the locations for the sediment samples. From analysing the side-scan transect recordings, taken on 28th January 1995, it is clear that the sea bed offshore of Tunstall is very variable. It must be stressed however, that the seabed description which follows, only considers a swath 75m wide on each side of the transect lines. Description of the sea bed moves from inshore to offshore.

Inshore of the 10m contour line (figure 4.1) the sonograph revealed a sandy seabed which was littered with boulders (some quite large), with the underlying bed rock being exposed in places. Where the two transects converged, inside the 5m contour line, the exposed bed rock was covered in places with patches of loose sand. This type of situation may arise when sediment is quickly deposited out of suspension, at slack water for example, and at any time could be resuspended. Where transect line 2 crossed transect 1 at 53° 46.529'N, 00° 01.397'E, the sonograph revealed uneven terrain with an overlying covering composed largely of coarse material (sand and shingle). In places, isolated boulders were seen to occur. In the middle section, where transect 2 crosses transect 1 twice, level ground dominated. The sea bed surface was a mixture of coarse material, interspersed with numerous patches of sand and fine material. The sonograph also picked up a number of isolated boulders. Between grab positions 11 and 14, the sonographs revealed large areas of sand waves overlying a boulder surface, which ran in a NW / SE direction. There was also an abundance of large stones and numerous sand patches covering the turning area of transect 2 offshore. As the transect line straightened out (outer section), the nature of the bed changed. Much coarser material was evident. The ground became very uneven, with pebbles and boulders dominating the terrain. There was still a considerable amount of sand, but this was located in patches between the areas of exposed bed rock.

During the course of 1995, further grab studies revealed that the nature of the surface layer is subject to change depending on the weather conditions. In January 1995 during the site survey, the seabed inshore of the 10m contour line was essentially sandy in nature and littered with boulders. In January 1996, grab sampling in the same area showed that there were virtually no sand deposits on the sea floor, and that all the sand appeared to be in suspension as a result of prolonged stormy conditions.

Table 4.2: Description of the grab samples taken during BLISS Project site survey - January 1995

Position no	Sample reference	Depth (m)	Location	Description of sample
2	A	5.5	53° 45.844'N, 00° 00.194'E	Fine silt and Sand
3	B	5.5	53° 45.858'N, 00° 00.167'E	Empty
4	C	5.5	53° 45.844'N, 00° 00.181'E	Sand
5	D	12.8	53° 46.128'N, 00° 00.651'E	Sand, shingle and very small stones
6	E	12.4	53° 46.136'N, 00° 00.598'E	Sand, shingle and small pebbles <5cm
7	F	12.4	53° 40.080'N, 00° 00.663'E	Empty (may signify exposed bedrock)
8	H	12.1	53° 46.708'N, 00° 01.840'E	Coarse sand and shingle. Large pebbles D >10cm.
9	I	12.1	53° 46.752'N, 00° 01.775'E	Very small sample of shells
10	J	12.1	53° 46.850'N, 00° 01.928'E	Coarse sand, small pebbles D <5cm (only a small sample may indicate the presence of large stones which prevented the grab from shutting properly.
11	K	15	53° 47.190'N, 00° 02.497'E	Large sample. Small and large pebbles, presence of finer sand and ground shell shingle and gravel.
12	L	16.6	53° 47.793'N, 00° 03.222'E	Coarse sand, small pebbles, sand, gravel, shingle, shale mixture.
13	M	14.3	53° 47.666'N, 00° 03.275'E	Fine sand, gravel, shingle and coarse sand
14	N	15.5	53° 47.725'N, 00°03.617'E	Large pebbles, fine and coarse sand/gravel, shell fragments and whole shells D = <4cm

In July 1995, the same area had quite a thick covering of fine to sandy material deposited on the sea bed. These results illustrate that the seabed surface topography is constantly

changing from season to season. What is common to all the survey results over the last two years, offshore of the 10m contour line, is that the seabed surface material is much coarser, largely consisting of shingle, coarse sand and boulders.

The location of level ground largely dictated the BLISS mooring sites, although reference was also made to the geographical positions chosen by POL and MAFF for their instrument deployments, as it was planned to deploy the BLISS tripods at the POL northern moorings so that concurrent field data could be collected. Unfortunately, no concurrent data was obtained. The BLISS mooring sites are shown in figure 4.1. NI refers to the innermost site along the transect, NM to the middle site and NO to the outer site. It must be stressed at this point that

4.3 BLISS Deployments

In total there have been four BLISS deployments off the Holderness Coast (Table 4.3) in the near shore zone from a small chartered trawler (Janet 'M') working out of Bridlington.

Table 4.3 BLISS deployments

No	Date	Deployment	Location	Depth (m)
1	22-28 February 1995	BLISS 2 (NM)	53° 46.593'N 0° 02.480'E	13.9m
2	29 June - 15 July 1995	BLISS 2 (NM) BLISS3 (NI)	53° 46.738'N 0° 01.882'E 53° 46.068'E 0° 0.787'E	14.8m 10.9m
3	3 Dec - 17 Dec 1995	BLISS 2 (NI)	53° 46.054'N 0° 0.990'E	12.6m
4	4 Feb - 19 Feb 1996 4 Feb - 23 Feb 1996 15 Feb - 29 Feb 1996	BLISS 4 (NI) BLISS 3 (NM) BLISS 2 (NO)	53° 46.059,N 0° 0.988'E 53° 46.615'N 0° 01.844'E 53° 47.506'N 0° 03.022'E	09.4m 12.4m 16.8m

Originally, the first deployment of the BLISS tripods were scheduled for October/November 1994, to coincide with the POL / PMP deployment phase. As a result of the development phase being plagued by electronic problems, it was not until February 1995 that one system, BLISS 2, was fully operational and ready for deployment. This set back in development not only prevented data collaboration with the PMP recordings, but also prevented any liaison with the LOIS-RACS pre-scheduled RV Challenger cruise 118 which started on 15 January 1995.

BLISS 2 was deployed from RV Janet 'M' on 22 February 1995 at position 53° 46.593'N, 00° 02.480'E, at the middle station (NM) (figure 4.1) in 13.9m of water. The

sea floor at this point was largely composed of gravel and sand. Unfortunately, the tripod was lowered onto its side as a result of a miss-timed deployment procedure. Six days of usable data were collected, but posed the problem of knowing the orientation of the tripod with respect to North or the heights of the sensors relative to the seabed. When considering alongshore and cross-shore flux, knowing these parameters are important. To rectify the problem, divers from the University of Plymouth located the tripod and recorded its orientation relative to North and also measured the height of the optical sensors off the seabed as well as taking some water samples next to the OBS sensors.

The second deployment in June/July 1995 was scheduled to coincide with the third leg of the LOIS 119 Challenger cruise. Three tripods were deployed (refer to figure 4.1 for mooring sites) one at the inner station (NI), one at the middle station (NM) and one at the outer station (NO). The outer station tripod failed to operate as a result of faulty current meters. During this period, a 13 hour tidal station was conducted at the BLISS tripods, which overlapped with a 25 hour anchor station on Challenger offshore of the BLISS moorings (Investigator: Chris Bull, UCNW). CASI (Compact Airborne Spectral Imager) overflights were also conducted at this time.

The next BLISS deployment, scheduled for 20th November 1995, was unsuccessful because the current meters again failed to function properly. This problem did not become apparent until after the tripods had been deployed. It was possible to retrieve the middle and outer station BLISS rigs, but bad weather prevented us from retrieving the tripod at the inner station which had been deployed at a later date (22nd November 1995).

At the inner station (NI, figure 4.1) in the November 1995 deployment, water column profiles of CTD and suspended solids were taken using an internal self logging CTD-Transmissometer profiler borrowed from UCNW, along with surface water samples to aid in the calibration of the optical instrument. The profiling also overlapped with CASI overflights. The inner station tripod was not retrieved until 19th December 1995, when it was noted that BLISS 2 had started to record data during its deployment. These included measurements of current velocity, suspended solids from the transmissometer, pressure and orientation. The optical backscatter sensors, however, failed to operate. Unfortunately, the sensors were not recording information during the *in situ* sampling phase or during the CASI overflights.

The last deployment phase was scheduled for February 1996. This time, the deployments were much more successful. Tripods were deployed at each of the three stations (figure 4.1). The inner and middle station tripods were deployed on the 4th February 1996 but the outer station tripod was deployed later, on 13th February 1996, because of electronic problems with the BLISS 2 system. A number of grab sample attempts at each of the sites were unsuccessful at collecting sediment, which may indicate that the surface sediment was already in suspension. During the February 1996 deployment phase, a 13 hour station was conducted, (which will be discussed in the next section).

A serious hindrance to the BLISS deployments was interference from fishing activity in the region. In the November deployment, the surface buoy was snagged by a trawler and set adrift. Retrieval of the BLISS tripod at the inner station was successful by pinpointing the tripod's pinger signal and then grappling for the free cable end. In the February 1996 deployment, the tripod at the middle station was dragged onto its side after 51 hours of operation, and for a period the logger turned off, only to reboot itself halfway through the deployment. The surface buoy was also set adrift by the trawler, only to be located some time later at the foot of the Holderness cliffs. The middle station tripod was retrieved in the same way as in the November 1995 deployment. Table 4.4 summarises the data collected during each deployment and which sensors worked each time.

Table 4.4 Summary of the amount of data collected during all the BLISS deployments from all sensors

Deployment Number	Working Sensors	Sensor Height above the seabed (m)	Total duration of record (h)	Burst Interval (Hz)
No 1 (middle) 22-28 February 1995	Pressure (Druck)	-	125	5
	Temperature	-	125	5
	Conductivity	-	125	5
	OBS1(D & A)	0.47	125	5
	OBS2 instruments)	0.19	125	5
	EM1 (Valeport)	0.65	125	5
	EM2 (Valeport)	0.42	125	5
No 2 (middle) 29 June - 15 July 1995	Pressure	0.7	360	5
	Temperature	0.48	360	5
	OBS1	0.41	not working	-
	OBS2	0.9	54	5
	EM1	0.39	360	5
	EM2	0.41	360	5
	Compass	-		2 readings every hour
	Pitch	-		
	Roll	-		
No 2 (inner) 29 June - 15 July 1995	Pressure	0.7	273	5
	Temperature	0.48	273	5
	Conductivity	0.48	273	5
	OBS1	0.41	273	5
	OBS2	0.9	273	5

	EM1	0.39	273	5
	EM2	0.41	273	5
	Compass	-		2 readings
	Pitch	-		every hour
	Roll	-		
No3 (inner)	Pressure	0.7	6-341(total)	5
3 - 17 December	Temperature	0.48	6-320	5
1995	Conductivity	0.48	6-341	5
	OBS1	0.41	worked at random	5
	OBS2	0.9	worked at random	5
	EM1	0.39	6-314	5
	EM2	0.41	6-320	5
	Compass	-		2 readings
	Pitch	-		every hour
	Roll	-		
	Transmissometer	0.927	1 min before trans	4
No4 (inner)	Pressure	0.7	357	5
4 - 19 February 1996	Temperature	0.48	357	5
	Conductivity	0.48	357	5
	OBS1	0.41	357	5
	OBS2	0.9	357	5
	EM1	0.39	357	5
	EM2	0.41	357	5
	Compass	-		2 readings
	Pitch	-		every hour
	Roll	-		
	Transmissometer	0.927	1 min before trans	4
No4 (middle)	Pressure	0.7	469	5
4 - 23 February 1996	Temperature	0.48	469	5
	Conductivity	0.48	469	5
	OBS1	0.41	469	5
	OBS2	0.9	469	5
	EM1	0.39	469	5
	EM2	0.41	469	5
	Compass	-		2 readings
	Pitch	-		every hour
	Roll	-		
	Transmissometer	0.927	1 min before trans	4
No4 (Outer)	Pressure	0.7	357	5
15 February -	Temperature	0.48	357	5
1st March 1996	Conductivity	0.48	357	5
	OBS1	0.41	357	5
	OBS2	0.9	357	5
	EM1	0.39	357	5
	EM2	0.41	357	5
	Compass	-		2 readings
	Pitch	-		every hour
	Roll	-		
	Transmissometer	0.927	1min before trans	4

4.4 13 Hour Station

The purpose of a 13 hour station was to take nearbed *in situ* water samples over a complete tidal cycle as close to the BLISS moorings as possible, in order to provide, after filtering, direct measurements of sediment concentration (dry weight) for calibrating the optical instruments. In addition to the water samples, bottom and water column profiles of

conductivity, temperature, depth and suspended solids were collected using either the simple T/S Bridge (in July, 1995) or later the more sophisticated instrumentation of the internal logging CTD/Transmissometer/OBS profiler (in November, 1995 and February 1996).

4.4.1 Bottom Landing Water Sampling System

In situ water samples were collected using a modified version of the bottom-landing water sampling system (plate 4.2) developed by Bale and Barrett (1995). It is unique in that it can obtain vertical profiles of water samples in the bottom boundary layer at known heights above the sediment surface, without disturbing the sediment on the seabed. Bottle 2 on the sampling frame was the same height off the bed as the upper OBS (0.9mab) and the Beam Transmissometer on BLISS, and bottle 4 was the same height as the lower OBS (0.41mab). The sampling system is also well designed in that it takes a water sample which is representative of the conditions at that point in time, rather than being contaminated by water or sediment that has accumulated in the intake prior to, or subsequent to, sampling. In addition, it collects the sample with minimum disturbance to particle aggregates.

Each bottle consists of a 4L cast acrylic tube. The tube could be substituted for other materials depending on the type of sampling required (plate 4.3). Prior to deployment each bottle was cocked by latching the seal in the open position (as shown in plate 4.3). The bottle frame was then lowered to the seabed using an off centre lifting point, at a 40 degree angle, which was necessary to prevent the bottles from firing during the lowering phase, since closure of the bottles is controlled by a set of mercury tilt switches. Assuming that the frame was sitting on the seabed within 5° of vertical, after 1 minute the bottles closed. This time delay ensured that the material which may have been suspended as a result of the frame being lowered had been washed away from the vicinity by the currents. The bottle sampling frame was used in both the July (07.07.95) and February (15.02.96) 13 hour stations. Water samples collected (filling time 3 seconds) during the 13 hour stations were filtered and weighed to obtain total sediment concentration in mgl^{-1}. The procedure for filtering is outlined in appendix A3. The results of both the filtered samples (mgl^{-1}) and the OBS output (FTU at time of sample), were regressed one against the other, to achieve a calibration coefficient which could be used in all the deployments to convert the FTU values into mgl^{-1}. This method is not a new one, and is normally used as standard procedure.

Plate 4.2 Water sampling system

Plate 4.3 Water sampling bottle

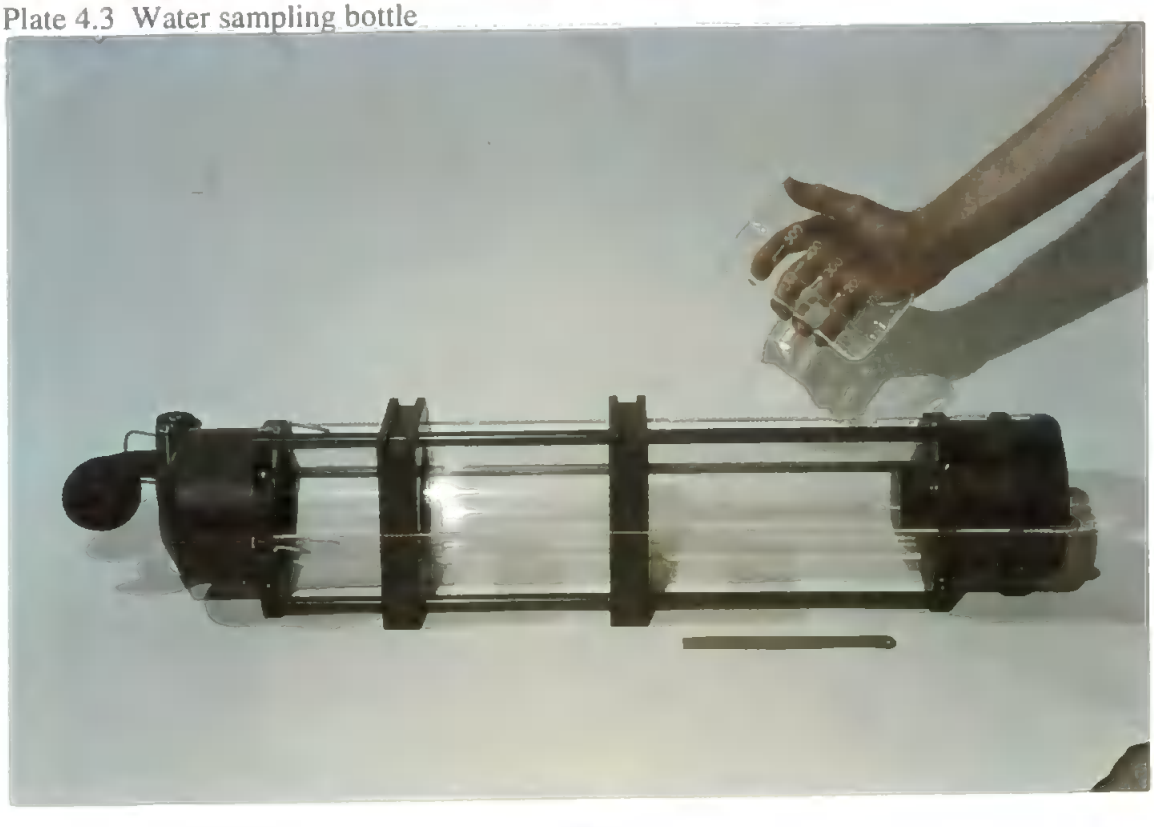

4.4.2 Water Column Profiling

Profile measurements of conductivity, temperature, depth (CTD) and suspended solids were obtained using an internal self logging profiler, the first borrowed from UCNW (plate 4.4) and the second system designed by UoP (Plate 4.5). In both cases, the profiler was operated by turning on the system before deployment via a computer link. The instrument was then lowered via a rope (no cable necessary), continuously recording internally the CTD and suspended sediment concentration. After sampling, the data stored on the profiler was down-loaded onto a computer hard drive via a serial communications box. The UCNW profiler had on it a transmissometer which operated successfully in the November 1995 deployment.

The UoP profiler used in February 1996 as part of the 13 hour station (15.02.96) was attached to an adapted BLISS frame (top portion) with short legs added. The adapted BLISS frame acted as a platform of known heights above the seabed on which the sensors were secured. The measurements of an OBS and 2 transmissometers each operating at different wavelengths were at known distances off the seabed. Details of the instruments used in the February 1996 13 hour station are given in Table 4.5.

Table 4.5 CTD/Transmissometer/OBS profiler - Sensor details

Sensor	Maximum input range
SBE 19 Seacat Profiler includes:	
Strain Gauge Pressure sensor	0-100m.
Temperature (thermistor)	-5 - 35°C, accuracy 0.01°C, resolution 0.001°C.
Conductivity (pyrex cell)	0-7 S/m, accuracy 0.001 S/m.
Memory	1024K byte CMOS static RAM.
Batteries	9 alkaline 'D' cells.
OBS 3 (Optical Backscatter Sensor)	0-2000 FTU.
Chelsea Instruments Transmissometer	Alphatracka 565nm green.
Sea Tech Transmissometer	660 nm wavelength

Plate 4.4 UCNW - CTD-Transmissometer profiler

Plate 4.5 CTD / Suspended solids internal logger (University of Plymouth)

4.5 Calibration of the OBS

It is very difficult to calibrate optical sensors to the rapidly changing responses of the suspended sediment to tide and waves as experienced off the Holderness coast. The optical backscatter sensors used on BLISS are reviewed in section 3.2.2. The OBS output (in volts) can then be calibrated in two ways, either to use *in situ* sediment from the study area to obtain a value in mgl^{-1}, which is the most desirable, or secondly, as was the case for the BLISS experiment, to use standard Formazin solutions, which produce a value of sediment concentration in the form of Formazin Turbidity Units (FTU).

However, the amount of light backscattered and registered by the OBS is strongly dependent on particle size, and so the apparent sensitivity of the instrument may vary from suspension to suspension. In the coastal waters off Holderness, there are two distinct sediment sizes present in the water column, namely a fine sediment fraction, from cliff material and a sand fraction, from seabed resuspension. The mass concentration of these two particle sizes in the water column will largely depend on the tidal and storm conditions. It is already known that optical backscatter sensors have superior linearity in turbid waters dominated by fine material (D & A Instruments, 1989), but are not so accurate in low concentration conditions dominated by coarse material. It has been recognised that above 10 FTU and 50 mgl^{-1}, large changes in turbidity produce disproportionately small changes in transmissometer output. The OBS sensor can also, in very high concentrations of mud, saturate and even show a reduction in signal (Kineke and Sternberg, 1992). Calibrating the OBS sensors on BLISS from FTU to mgl^{-1} is therefore very difficult without knowing the exact sediment size distribution in the water column each time a measurement is taken. Two calibrations may be necessary to calibrate the OBS output, one for coarse material and one for the fine material, as was found for data collected off the Wash (Pers Comm., Chris Bull, 1997).

Two independent calibrations were conducted, to determine the most suitable conversion from FTU to mgl^{-1}. The first involves using results obtained from the BLISS optical backscatter sensors and the filtered results from the *in situ* water samples (for filtering procedure refer to appendix A.3. The second calibration involves using *in situ* water samples and data collected from a beam transmissometer near to the BLISS middle station during the LOIS 119 Challenger cruises.

4.5.1 OBS Calibration Using Filtered Results

Data from the February 1996 deployment was used because the values of both the optical backscatter output and the filtered results were high. In the June/July 1995 deployment, the optical backscatter sensors were operating very close to their lower limit because of the lack of sediment in suspension, which was verified by the low concentration in mgl^{-1} extracted from the water samples. Table 4.6 shows the results of filtered water samples (samples taken over a period of 3 seconds) taken during the February 1996 13 hour station. The values in bold type were the samples used to calibrate the FTU output to mgl^{-1}.

One minute of OBS data (~300 data points) was taken from the burst data corresponding to the same time the water sample was taken, and averaged (table 4.7). Bottle 4 corresponded to a similar height off the sea bed as the lower OBS (0.41mab), and the height of bottle 2 corresponded to the relative height of the upper OBS (0.9mab) on the BLISS tripods.

Table 4.6 Suspended sediment concentration in mgl^{-1} of the filtered water samples collected during a 10 hour field survey on February 15th, 1996 - Water samples were taken over three seconds at the GMT time specified. The highlighted numbers were the values used to calibrate the OBS sensor

Feb	1996	Filtered	Bottle	Water	Samples	in mgl^{-1}
	Height above bed in meters	1.09 (mid point)	**0.83 (mid point)**	0.6 (mid point)	**0.34 (mid point)**	0.08 (mid point)
Sample Station Inner	Time (GMT)	Bottle 1	**Bottle 2**	Bottle 3	**Bottle 4**	Bottle 5
1	12.41	143.03	**152.9**		**142.81**	136.69
2	14.49	149.14	**137.2**	136.42	**139.67**	143.48
3	16.42	94.15	**130.88**	134.68	**124.09**	152.48
4	18.45	154.9	**146.35**	142.45	**141.51**	132.25
Middle						
1	10.49	106.6	**91.68**	100.83	**101.52**	119.25
2	14.08	50.55	**50.69**	48.3	**50.8**	82.09
3	16.11	48.66	**49.25**	43.34	**52.48**	52.51
4	18.13	40.34	**82.94**	35.32	**84.65**	43.41
Outer						
1	9.41	30.6	**37.4**	46.03	**34.4**	38.81
2	13.31	32.99	**28.07**	30.04	**27.32**	26.85
3	15.35	21.04	**25.56**	43.71	**27.33**	26.69
4	17.32	35.9	**31.67**	31.86	**35.43**	33.07

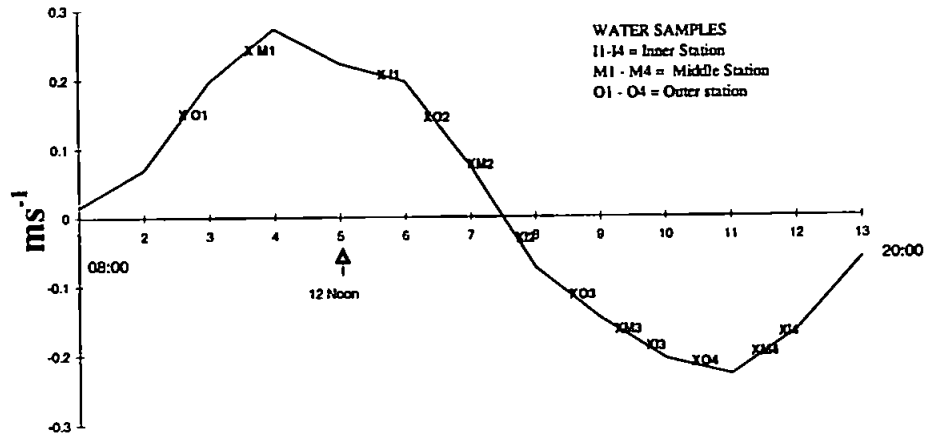

Figure 4.2 Plot to show where the water samples were taken in the corresponding tidal cycle (15 February 1996)

Table 4.7 *In situ* filtered water samples used to convert the optical backscatter sensor output from FTU to mgl^{-1}

Data	collected	on 15th Feb	1996	
Inner Station	FTU		mgl^{-1}	
	obs1	obs2	Water	Samples
Time GMT			Bottle 4	Bottle 2
12.41	115.6308	151.83836	142.81	152.9
14.49	156.2408	188.013954	139.67	137.2
16:42	229.2117	242.8650762	124.09	130.88
18.45	121.4672	154.15112	141.51	146.35
Middle Station	FTU		mgl^{-1}	
Time (GMT)	obs1	obs2	bottle 4	bottle 2
10.49	117.8441	118.3394564	101.52	91.68
14.08	70.51323	69.28462167	50.8	50.69
16.11	95.81816	98.89161167	52.48	49.25
18.13	115.3967	115.8553967	84.65	82.94
Outer Station	FTU		mgl^{-1}	
Time(GMT)	obs1	obs2 broken	bottle 4	
9.41	45.7164		34.4	
13.31	28.71635		27.32	
15.35	27.92287		27.33	
17.32	31.58903		35.43	

To obtain realistic estimates of fluxes, it is essential that the calibration used to convert the FTU values to mgl^{-1} are representative of the sediment type. It may be expected that the type of sediment in suspension will vary according to the current velocities being experienced. For example, at maximum tidal streaming, it may be expected that the

increased velocities will induce local resuspension of a more coarse material, but when velocities are at a minimum, only the finest sediment will stay in suspension. That is, it may be possible to extract two calibrations for the OBS data based on the mean current speed. It must be noted that the following calibration (figure 4.3) is based on measurements taken during a neap tide just leading into springs during moderate wave conditions. The 13 hour station had to be cut short by three hours as a result of the deteriorating weather and increasing storm conditions. It would not be possible to take water samples during large storm events because the fieldwork operation would simply be too dangerous.

One way of determining if there is a correlation between the magnitude of the current and the suspended sediment in the water column off Holderness, is to extract the appropriate burst data in FTU which corresponded to the water samples taken during the 13 hour stations and regress the ratio of mgl^{-1} / FTU against current speed u^2+v^2. If a good correlation resulted from this regression then two separate calibration coefficients would be derived, one for coarse material and one for fine material. The data from all three stations were combined and the ratio of mgl^{-1} / FTU was regressed against u^2+v^2 (figure 4.3).

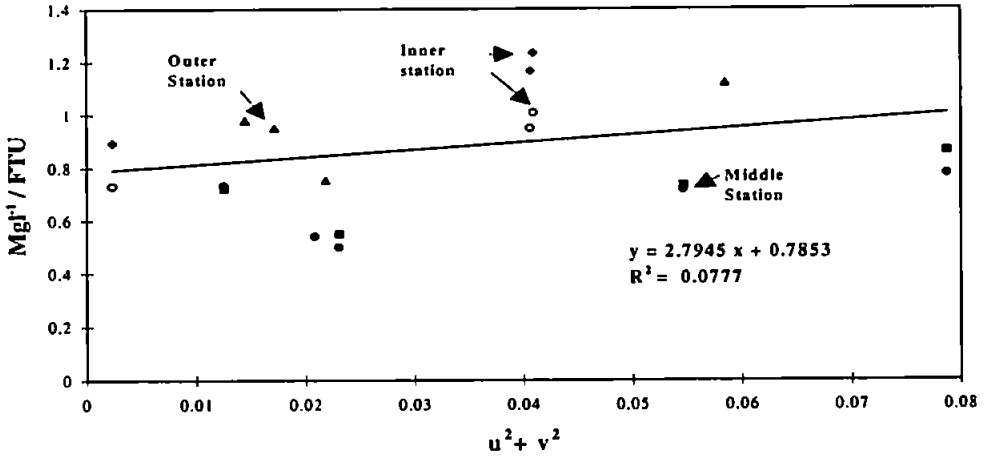

Figure 4.3 Ratio of mgl^{-1} / FTU for all the samples taken on 15 February 1996 against the corresponding u^2+v^2

From figure 4.3, it is clear that there was no correlation between current velocity and the calibration ratio. Thus, within the scatter of the data, it may be assumed that the sediment in suspension off the Holderness coast is generally well mixed (fine and coarse) throughout

a tidal cycle. If the percentage of the mix between the two sediment sizes does change over the tidal cycle, it does not alter significantly enough to affect the OBS output response.

This is further highlighted after drawing two boundary lines by eye on the resultant plot of mgl^{-1} against FTU (figure 4.4). These lines are taken to typify the difference between coarse and fine material. The slope of the two lines differ by a factor of 2. Results taken from Downing and Associates OBS manual to establish OBS sensitivity to Amazon mud and beach sand, showed that there was a factor of 12 difference in the sensitivity of the OBS output between the two sediment types. In comparison with these results, the range of slopes of OBS response off the Holderness coast is relatively small. As a result of these findings it was therefore possible to produce a single calibration coefficient by linear regression, one that could be used on all the OBS data sets to convert FTU to mgl^{-1} (figure 4.5). An R^2 value of 0.6364 indicates that the data is well correlated.

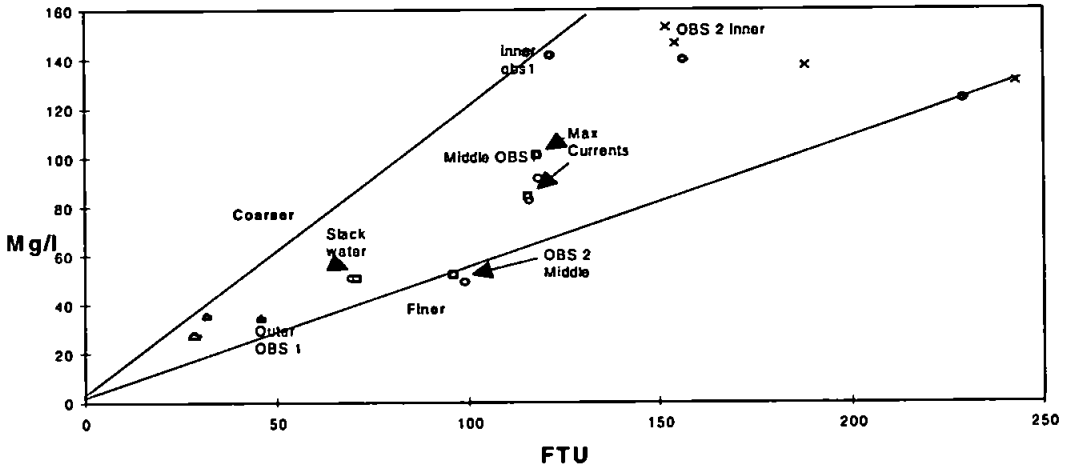

Figure 4.4 Best fit lines to separate coarse from fine material 15 February 1996 - All stations (FTU v mgl^{-1})

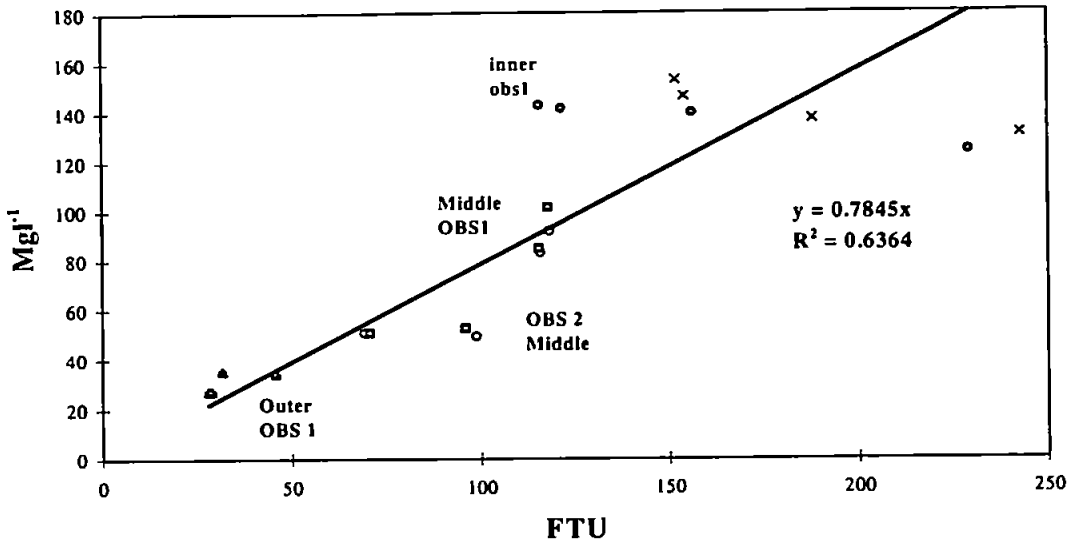

Figure 4.5 FTU values regressed against filtered samples for all stations 15 February 1996 deployment to produce a calibration coefficient

The calibration line was forced through zero to eliminate the addition of an offset, because it was felt that the offset had been properly accounted for in calibrations from volts to FTU. The resultant calibration coefficient is therefore:

$$mgl^{-1} = 0.7845 * FTU$$

4.5.2 Beam Transmissometer Calibration

To validate the procedure of calibrating the OBS sensors based on the assumption that sediment in the water column off Holderness can be treated as exhibiting unimodal behaviour rather than showing bimodal distribution, a comparison is made to data collected within 1 nautical mile to the BLISS outer station over a 13 hour station on 22/23 April 1995, from RV Challenger cruise 118B. Data collection and processing was carried out by Chris Bull from University of North Wales, Bangor. A beam transmissometer was deployed to take near bed and mid depth measurements of suspended sediment concentration, whilst seven water samples were collected to calibrate the beam transmissometer output (table 4.8). Over the sampling period, particle size distribution of the nearbed suspended sediment concentrations (figure 4.6) were also determined using a Galai Cis-100 particle size analyser.

Table 4.8 Data collected on 22/23 April 1995 from the RV Challenger Cruise 118B

Date	Time	Location	Sample No	Water Depth	Sample Depth	SPM Load (mgl^{-1})	Beam Attenuance
23.4.95	02.14	53.789 N 0.021 E	176	15	13.2	55.4133	6.071083
22.4.95	22.26	53.787 N 0.026 E	166	16	5	24.685	5.258128
22.4.95	22.24	53.787 N 0.026 E	165	16	13.4	43.86	5.360698
23.5.95	02.14	53.789 N 0.021 E	177	15	5	31.3133	5.538783
23.4.95	09.04	53.784 N 0.022 E	199	15	5	19.39	4.488343
23.4.95	09.02	53.784 N 0.022 E	198	15	12.3	38.26	5.129179
23.4.95	05.46	53.787 N 0.028 E	187	14	11.1	37.1867	5.459697

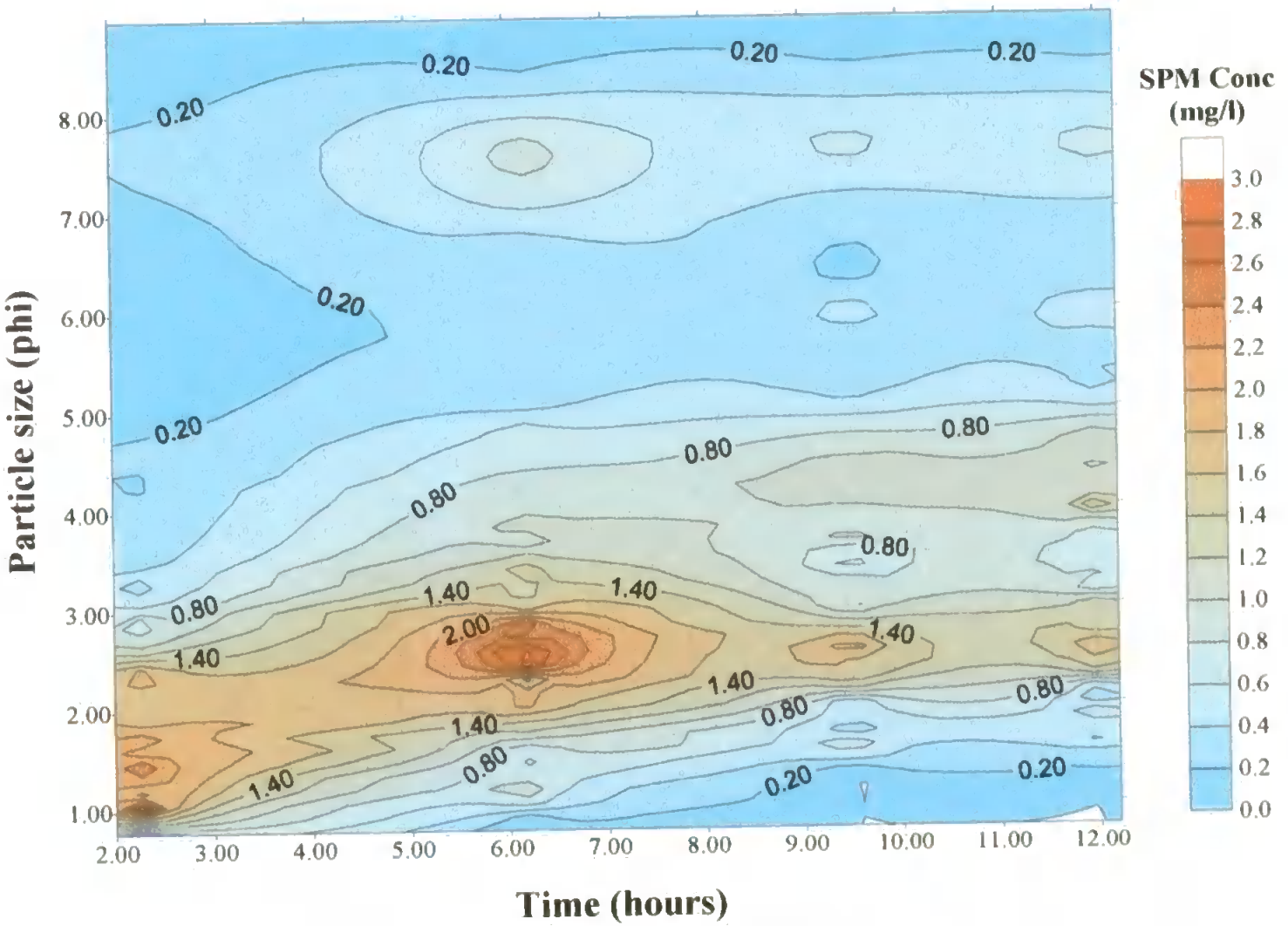

Figure 4.6 Bottom particle size distribution by mass in class size over time on 22/23 April 1995 (Data from: C. Bull, 1997)

Figure 4.6 shows bottom particle size distribution by mass on 22/23 April 1995. Particle size is plotted on a phi scale and ranges from 1 to 8 (coarse sand to very fine silt) which corresponds to a sediment size class distribution of 500 μm (1 phi) to 4 μm (8 phi). From the contour plot, it is clear that suspended sediment concentration is not related to a specific particle size, but exhibits a distribution across a number of particle sizes. There was no distinct separation in particle size distribution relative to SPM concentration over the 10 hour tidal period due to resuspension of the coarse material. SPM concentration was largely determined by particles ranging in size between 250 μm and 60 μm. In that case, it is acceptable to produce by linear regression, a single calibration for converting the OBS output to mgl^{-1}, from using *in situ* water samples. A linear regression was performed on the beam transmissometer data and the *in situ* water samples, given in table 4.8, to obtain a comparative calibration coefficient (figure 4.7). An R^2 value of 0.6667 was obtained, which was slightly higher than the R^2 obtained from the OBS calibration of 0.6364. From the results given, it is apparent that two very similar calibrations were produced from two independent data sources off the Holderness coast. A decision was made to use the calibration coefficient obtained for the BLISS data based on the assumption that the sediment distribution off Holderness changed with concentration in a systematic manner.

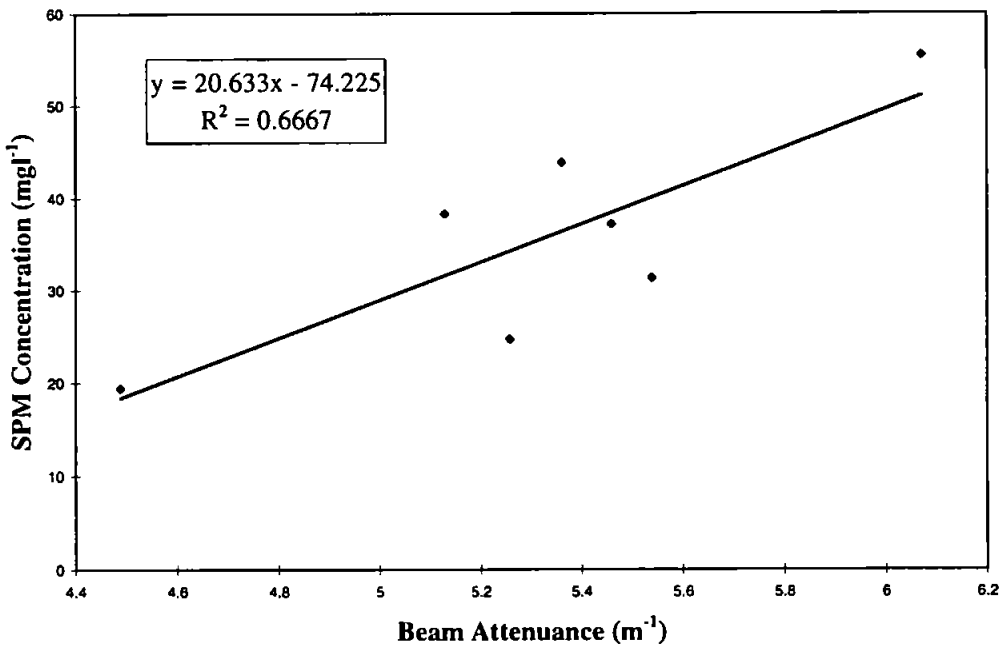

Figure 4.7 Calibration of the transmissometer data at BLISS middle station 22/23 April 1995

Source: C. Bull, (1997)

Chapter 5

5. Data Analysis Methods

5.1 Introduction

A number of statistical and mathematical techniques have been applied to the BLISS data sets to describe and extract information from the data, both for qualitative and quantitative purposes. The traditional way of observing signals is to view them in the time domain. The time domain is a record of the changing values of a particular parameter, and the resulting plot of parameter versus time is called a time series (Hardisty, 1993). Viewing the data in the time domain offers the possibility of obtaining an overall picture of the physical processes in operation off the Holderness coast. Statistical variables such as the mean, standard deviation and variance have been calculated every hour for all the parameters measured on BLISS. The resultant time series are then hourly representatives of the data in each deployment. The descriptors used have been chosen because most random variables are nearly Guassian in their distribution.

For a time-series, however, the order in which the values occur is also important, that is, there is information in the correlation between neighbouring values in the time series. This correlation can be described by presenting the time series in the frequency domain. Over 100 years ago, it was shown by Baron Jean Baptiste Fourier, that any time series which exists in the real world can be generated by adding up sinusoids (Hardisty, 1993). Fourier's work shows that any time series can be constructed by the addition of a number of sinusoids, each with a given frequency, amplitude and phase relationship. The decomposition of a time series into its constituent sinusoids is called a Fourier transform, and the result, when squared and appropriately scaled, is called a spectrum. Spectral

analysis has been used to describe, test and calculate a number of oceanographic parameters all of which will be described in the following sections.

5.2 Calculating the Mean, Variance and Standard Deviation

Both the burst average and variance data have been calculated for all the working sensors for every run in each deployment. Before computing the average and variance, the burst data (17 minutes, every 0.2 seconds) is detrended. Such a procedure helps to exclude the probability of any distortion effecting the data, by creating a quasi-stationary time series. Detrending the data is particularly important in calculating the variance of the burst, since the variance is interpreted in terms of waves and turbulence. A Matlab program (appendix B, No. 10) was devised to detrend and calculate the mean and standard deviation for all the runs in each deployment, and place the results in a matrix.

5.3 Fourier Analysis

Fourier analysis is a mathematical technique which identifies important periodic signals in a series of measurements. For example, current velocity and pressure records. Taking a time series of known length, Fourier analysis breaks down the observations into a series of sine waves, using the finite Fourier series:

[5.1]

$$X(t) = X_o + \sum (a_n \cos(W_n t) + b_n \sin(W_n t))$$

where: X(t) is the observed data set as a function of time.

Xo is a the mean value of X

The bracketed expression is a summation of Fourier harmonics

In Fourier analysis, the first harmonic is taken to be the fundamental frequency of the signal X(t). It corresponds to a period equal to the length of the data record, T, so that $W_1 = 2\pi/T$. The function X(t) is thus composed of a sum of sine and cosine functions whose frequencies are multiples or harmonics of the fundamental frequency. The highest frequency that can be resolved, or the cut off frequency, is called the Nyquist Frequency, which is $Nf = 1/2\Delta t$, where Δt is the time step. The number of harmonics is therefore equal

to one-half the number of points in the data. In the case for our burst averaged data, the dimensions of frequency are cycles per hour. The coefficients, a and b, namely the Fourier coefficients, are calculated from the data using the expressions:

[5.2]

$$a_n = (2/N) \sum (X(t).\cos(W_n t))$$

[5.3]

$$b_n = (2/N) \sum (X(t).\sin(W_n t))$$

The most efficient way of calculating these coefficients is to use Fast Fourier Transformation. Fast Fourier Transform (FFT) is an efficient algorithm designed to compute the Discrete Fourier Transform with minimum execution time. Both the magnitude and phase are computed by the FFT (using Matlab) at each harmonic frequency.

5.4 Spectral Analysis

The amplitude squared of each harmonic is equal to $(a^2 + b^2)$. A graph of harmonic amplitude squared, normalised to unit frequency bandwidth, versus harmonic frequency is called a power spectrum. When the result is not normalised, the output is called a periodogram or variance spectrum. In Matlab, it is possible using the function *"Spectrum"*, to compute the power spectral density (PSD) of signals, and also estimate the cross spectral density between two signals of equal length. The PSD is determined using Welch's periodogram method, which computes the FFT and takes the magnitude squared of the result. The problem with the periodogram estimate is that its variance is large and does not decrease as the number of samples increases. The variance of the PSD is therefore reduced by breaking the signal into non-overlapping sections and averaging periodograms of these sections. The more sections that are averaged, the lower the variance of the result. However, the signal length limits the number of sections possible, so that decreasing segment length gives a decreasing data resolution. To obtain more sections, the signal is broken up into overlapping sections. One more way to improve the periodogram estimate, is to apply a non-rectangular data window to the sections prior to computing the periodogram. This acts to reduce the effect of section dependence due to overlap, because the window is tapered to zero at the edges. Also a non-rectangular window diminishes the side-lobe interference or *"spectral-leakage"*, while increasing the width of the spectral peaks. The window used in our case is a Hanning Window, which achieves an overlap rate

of half the section length and reduces the variance of the estimate significantly. Typical record lengths within the burst for the BLISS data were 5120 data points each point representing 0.2 seconds (5 Hz). The time series was then split up into 10 non overlapping sections. This was achieved by dividing by the total number by 512. The signal was then overlapped using an overlapping segment size of 256, so that 19 segments in all were used in the spectral estimates.

5.4.1 The Cross Spectrum

Cross-spectral analysis of pairs of time series enables a study of correlation between signals at frequencies where peaks are shown to be statistically significant. The CSD function in Matlab forms the periodogram as the product of the FFT of x (e.g., elevation) and the complex conjugate of the FFT of y (e.g., velocity). The CSD is a complex function in which the result has both a real and an imaginary value. The real part is the co-spectrum and the imaginary part is the quadrature spectrum of the two signals.

5.4.2 Calculating the Magnitude and Phase Between Two Variables

To estimate the magnitude and phase between the two signals, x and y, the PSD of x is related to the CSD of x and y by:

[5.4]

$$Pxy(\Phi) = H(\Phi)Pxx(\Phi)$$

whereby, $H(\Phi)$ is the transfer function between x and y and is given by:

[5.5]

$$\hat{H}(\Phi) = \frac{\hat{P}xy}{\hat{P}xx}$$

Hence, the transfer function estimates both the magnitude and phase information.

5.4.3 Calculation of the Coherence Between Two Signals

Correlation, that is the amount of agreement between two signals, is determined by taking the magnitude-squared coherence, namely:

[5.6]

$$Cxy(\Phi) = \frac{|Pxy|^2}{PxxPyy}$$

This quotient is a real number between 0 and 1 that measures the correlation between x and y at that frequency Φ.

5.5 Bed Shear Stress Calculations

An essential precursor to accurate prediction of marine sediment transport is the detailed understanding of wave-current (w-c) interaction and bed shear stress distribution in the bottom boundary layer (section 2.2). The estimation of bed shear stress in wave-current flows is far from simple, due to the complex flow processes in the near-bed region (Hannay *et al.*, 1994). Four different methods are available for calculating bed shear stress, from measurements of flow in the bottom boundary layer.

5.5.1 The Logarithmic Profile Method

The first is the logarithmic profile method (Soulsby, 1983), whereby in the lower part of a simple turbulent boundary layer the mean flow is expected to vary logarithmically with height above the seabed, according to the equation:

[5.7]

$$u_z = (u_*/k) \ln(z/z_o)$$

where u_z is the mean current speed at elevation z above the seabed, $u_* = \sqrt{\frac{\tau}{\rho}}$, is the friction velocity, where τ is the bed shear stress and ρ is the fluid density, k is von Karman's constant and z_o is an appropriate bottom roughness length (Green *et al.*, 1990). This

method requires a vertical array of current meters measuring at a sufficient number of heights above the seabed. u_* and z_o can then be estimated from the slope and intercept respectively of a plot of u against lnz (Soulsby, 1983). This method also requires a number of sensors to be placed in the logarithmic boundary layer, and the mean flow must be measured with sufficient accuracy at each level to provide a reliable estimate of the velocity difference between sensors at different heights above the seabed. In wave-current conditions, the success of this method depends on the flow-meters being able to respond accurately to rapidly changing wave flows, and any non-linearities or zero-drift in the sensors can cause errors in the mean flow estimates (Huntley, 1988).

Accurate measurements of the mean flow current close to the seabed (<1m) are also difficult due to the large ratio of fluctuating turbulent velocities to the mean flow, the influence of form drag on the current and the low overall speeds which are often near the resolution of the current meter (Dewey and Crawford, 1988).

This procedure of calculating shear stress could not be used on the BLISS field data, because current velocity measurements were only taken from a single height above the seabed (0.41mab). Bed shear stress was therefore calculated by employing the next three methods. It is good practice to use more than one technique, because it is notoriously difficult to measure bed shear stress accurately (Soulsby and Humphrey, 1989).

5.5.2 Eddy Correlation Method - Reynolds Stress

The Reynolds stress or eddy correlation method (Soulsby, 1983) is based on direct observations of u and v (horizontal) and w (vertical) velocities over as long a period as is practical (Heathershaw and Simpson, 1978). This method can be used on the BLISS data because the current meters were set to monitor at 5Hz. This high frequency monitoring ensures that any turbulence present in the flow is captured.

The resultant Reynolds stress τ_r, is then given by

[5.8]

$$\tau_r = \rho \left(\overline{u' w'}^2 + \overline{v' w'}^2 \right)^{0.5}$$

Direction of the resultant Reynolds stress is then computed using the relationship:

[5.9]

$$\Psi_{stress} = \tan^{-1} \overline{v'w'}/\overline{u'w'}$$

Soulsby and Humphrey, (1989).

The Reynolds stress method assumes a constant stress layer, and measures the turbulent momentum flux, and hence the stress, at the instrument height (Huntley, 1988). In combined wave and mean flow conditions, it is not necessary to separate out the effect of the waves using this method, because the vertical-wave induced velocity is both small and in quadrature with the horizontal component, so giving zero contribution to $\overline{u'w'}$ and $\overline{v'w'}$. However, the presence of large horizontal oscillatory motion close to the seabed makes estimation of shear stress by the eddy correlation method extremely sensitive to sensor orientation. Error introduced by misalignment of the EMCM relative to the main streamline is typically 8% per degree for a pure current flow, and is as large as 156% per degree for wave-current flows (Soulsby and Humphrey, 1989). An approximate calculation suggests that alignment accuracy of the order of 1/10° or less may be necessary to provide an accurate estimate of the Reynolds stress. The EMCM sensors on BLISS were rotated in the horizontal to obtain alongshore and cross-shore flows. Realignment in the vertical was not performed before calculating Reynolds stress, because the pitch and roll information suggested that for all the deployments, the tripods were lying within 1° of vertical. However, Reynolds stress calculated for the outer station did suggest that realignment in the vertical should be conducted prior to calculation. This was due to the fact that the tripod shifted its position in response to a storm during the deployment. The Matlab programs written in-house to calculate the Reynolds stress and the resultant friction velocity are given in appendix B.

5.5.3 The Turbulent Kinetic Energy Method

All horizontal velocity spectra, obtained using a fast Fourier transformation routine, comprise a characteristic turbulence spectrum and a superimposed wave spectrum, with a peak at the dominant wave frequency (figure 5.1). A method was developed by Soulsby and Humphrey (1989) whereby the turbulent kinetic energy (TKE) was extracted from the horizontal velocity spectrum and used in the estimation of bed shear stress.

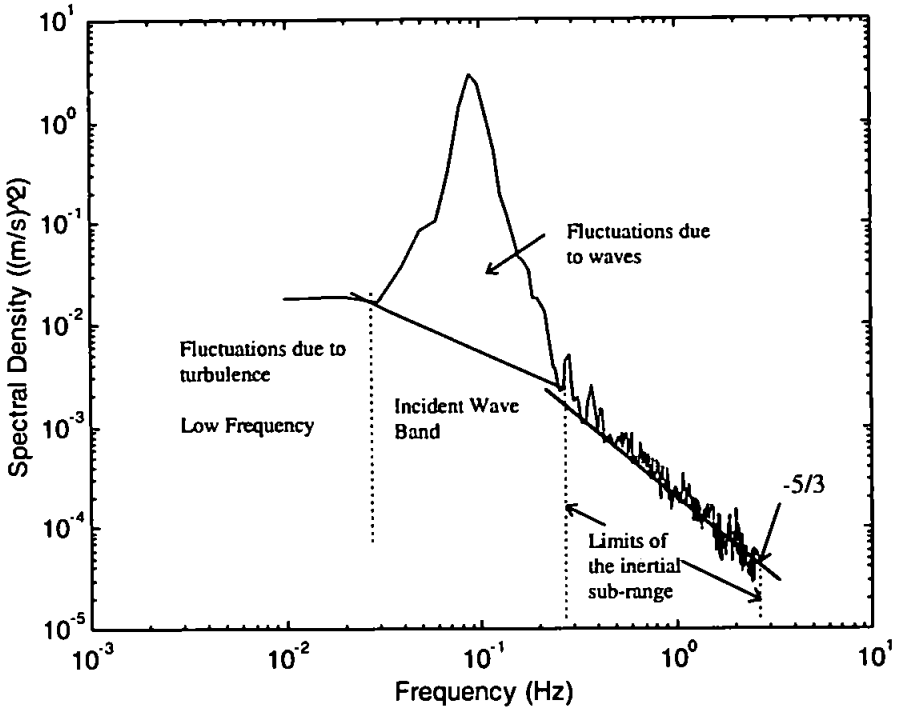

Figure 5.1 Spectrum of cross-shore velocity time series showing areas of variance due to waves and due to turbulence

The area under the energy spectrum is equal to the total variance $\overline{u^2}$. By plotting the velocity spectrum on a log-log axis, the turbulent part of the spectrum exhibits a characteristic $f^{-5/3}$ power law behaviour in the inertial sub-range. Superimposed on this, is the wave velocity spectrum, which exhibits a characteristic -5 power law relationship above the peak frequency. The wave peak typically occurs between 0.04 and 0.17 Hz, but spectral estimates in this range will also contain turbulent variance. This suggests that the wave and turbulent contributions of the spectrum should be separated by interpolating the spectrum across the base of the wave peak (figure 5.1). In this way, the wave variance ($\overline{u'_w{}^2}$) will be given by the area above the line in figure 5.1, and the turbulent variance $\left(\overline{u'_t{}^2}\right)$ will be given by the area under the line and the rest of the spectrum. These variances were computed by using the Trapezium rule:

[5.10]

$$\mathrm{Tr} = \left[\frac{1}{2}(A_1 + A_n) + \sum_{i=2}^{n-1} Ai\right] * \text{ frequency step}$$

This splitting technique was applied to the intra-burst velocity data collected by BLISS. The turbulent kinetic energy, E was then calculated using the relationship

[5.11]

$$E = \tfrac{1}{2}(\overline{u'^2_t} + \overline{v'^2_t} + \overline{w'^2_t})$$

where $\overline{w'^2_t}$ is the total energy beneath the vertical velocity spectrum. Using the constant of proportionality quoted by Soulsby (1983) in a wide variety of flows, the bed shear stress τ_0 was derived using the similarity argument that τ_0 is proportional to E in the region near the bed where energy production equals dissipation. The Bed shear stress is given by:

[5.12]

$$\tau_0 = 0.19\,\rho\,E$$

Matlab programs used to calculate TKE are given in appendix B for each of the BLISS deployments, aided by a program developed by Stapleton and Huntley, (1995).

5.5.4 Inertial Dissipation Method

The third technique for estimating turbulent stress involves the use of spectra of the turbulent fluctuations, and is called the Inertial Dissipation method (IDM), (Huntley, 1988). It is based on the relationship between turbulent kinetic energy density and wave number in the inertial sub-range, where the flux of energy from low to high wave numbers must by equal to the dissipation rate, assuming that there are no local sources or sinks for the energy (Huntley, 1988, Xu *et al.*, 1994).

Field measurements in the boundary layer provide estimates of the one dimensional spectra, which are functions of the wave number components in the direction of the mean flow. Hence, the turbulent kinetic energy spectrum in the inertial sub-range takes the form:

[5.13]

$$\phi = \alpha_i\,\varepsilon^{2/3}\,k^{-5/3}$$

where K is the one dimensional wave number, α_i is the one dimensional Kolmogorov constant which depends on what axis is being used (horizontal or vertical) for the turbulent fluctuations, ε is the energy dissipation rate and the subscript (i) represents a given direction (Huntley, 1988). This equation is usually called Kolmogorov's $k^{-5/3}$ Law (Kundu,

1990). Two assumptions must be made in order to relate equation 5.13 to the bottom stress (Huntley, 1988) as follows:

1. There is a local balance between the production and dissipation of turbulent energy. The production of turbulent energy is given by $(\tau / \rho)\, du/dz$, and in the logarithmic boundary layer, the "law of the wall" is described by $du/dz = u_* / kz$ where the local stress is equal to the bottom stress $\tau = \rho u_*^2$. k is Von Karman's constant and is taken as 0.4. ρ is density of sea water (1025 kgm^{-3}). u_* is friction velocity and z is height of measurement above the seabed.

2. It is essential that measurements are made within the constant stress part of the log layer. If this is true, then the energy dissipation rate can be written as:-

[5.14]

$$\varepsilon = \text{production} = u_*^3/kz$$

Substituting equation 5.14 into equation 5.13, gives:

[5.15]

$$u^* = \phi_{ii}(k)^{5/3} / \alpha_i)^{1/2} (kz)^{1/3}$$

where k is now used to denote the along-flow wave number component k_i. $_i$ represents a given direction.

To summarise this method of estimating bottom stress, it involves:

1. Calculation of a one-dimensional wave number spectrum of turbulent velocity.
2. Finding the range of wave numbers over which the energy density falls as $k^{-5/3}$.
3. Use the level of the spectrum in this range to estimate u_*.

The major attraction of this method is that it is relatively insensitive to errors in axis alignment, since the expected ratio of longitudinal to vertical spectral amplitude in the inertial sub-range is 4:3 (Huntley, 1988). With this ratio, errors in stress values from gross misalignment of the axes should not exceed 33%. There are however, complications to using this method, in that turbulent measurements are usually in the form of time series, so that they provide spectra as functions of frequency and not wave number. To convert to a wave number spectrum, the Taylor concept of "frozen turbulence" is invoked. Hence:

[5.16]

$$\phi_{ii}(k) = \phi_{ii}(f)\,\bar{u}/2\pi$$

where $\bar{u}$ is equal to the mean velocity in the i direction, f is equal to frequency.

To validate this concept, the time scale of the eddy must be much longer than the time taken for the eddy to advect past the point of measurement. For this to be true, it is required that:

[5.17]

$$k\phi_{ii}(k)/\overline{u^2} << 1$$

Stapleton and Huntley (1995)

In practise, this criterion is easily met (Huntley, 1988).

In an environment where there is significant oscillatory flow, Huntley (1988) anticipates that the Taylor hypothesis can become invalid. It has been shown that for isotropic turbulence and horizontal wave velocities much larger than the vertical velocities (Huntley, 1988), the friction velocity needs to be corrected for the influence of wave advection. This is given by the approximation:

[5.18]

$$u_* = (1\text{-}0.16(u_{rms}/\,\bar{u})^2)\,½u\,.$$

To ensure separation between low wave number turbulence production and high wave number dissipation i.e. the inertial sub-range, Tennekes and Lumley (1972) suggested that the turbulent Reynolds number (R_e) must be greater than a critical Reynolds number (R_{ec}), given by :

[5.19]

$$R_e = u_* kz / \nu > R_{ec}$$

Where ν is the kinematic viscosity for sea water. Estimates for R_{ec} range from 2500-4000 (Huntley, 1988). Equation 5.19 can also be rewritten to give a critical height z_{cr} above which measurements must be made to ensure an inertial sub-range (Stapleton and Huntley, 1995), given by:

[5.20]

$$z_{cr} = R_{ec}\,\nu / ku_*$$

As mentioned earlier, it is also a requirement that the measurements are made within the constant stress part of the logarithmic layer. In some circumstances, there is no height at which the instrument is positioned high enough to satisfy the Reynolds criterion, i.e for low Reynolds numbers (Xu *et al.*, 1994), whilst also being within the constant stress layer. For this situation, Huntley (1988) introduced a correction for the shear velocity.

For a sensor at height z above the bed, the peak turbulent energy is expected to be close to $k = \pi/z$. If the assumed Kolmogarov constant αii (0.69) is to be valid, it is suggested that wave numbers greater than twice the expected peak wave number must be used. The lower limit of the $K^{-5/3}$ sub-range is chosen to be given by:

[5.21]

$$k = 2\pi / z$$

The upper wave number limit for the sub-range depends on the physical size of the turbulent motions, and the limit to which these motions can be monitored by the sensor. Soulsby (1980) estimated that the physical dimensions of the electromagnetic current meters (EMCM) would determine the upper limit of the sub-range by:

[5.22]

$$k = 2.3 / d$$

where d is equal to distance between the electrodes on the sensing head of the EMCM (in our case 0.055m). Since frequency is measured and not wave number, it is necessary to convert from wave number to frequency by using:

[5.23]

$$k = 2\pi f / \bar{u}$$

Stapleton and Huntley (1995)

where f is frequency. Two new equations were then devised by Stapleton and Huntley (1995) to determine the upper and lower limits of the sub-range, by substituting equation 5.23 into equations 5.21 and 5.22, that is;

[5.24]

$$f = \bar{u} / z \quad \text{Lower Limit} \quad (a)$$

$$f = 2.3\pi / 2\pi d \quad \text{Upper Limit} \quad (b)$$

which are linearly dependent on the magnitude of the mean velocity at a given height. These limits are given in figure 5.2 for typical maximum velocities of 0.6ms^{-1}.

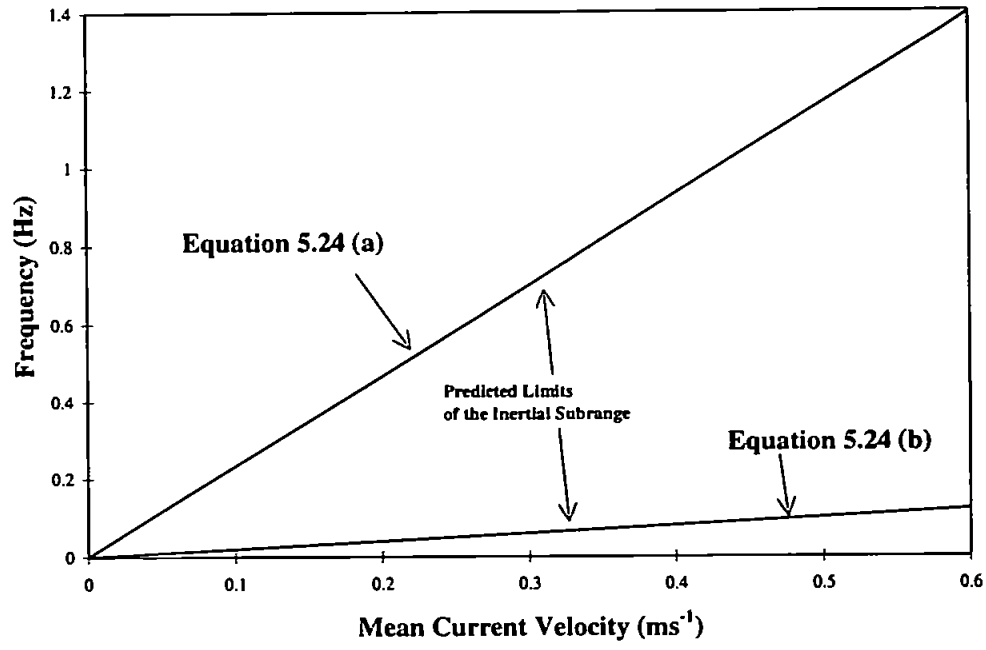

Figure 5.2 Limits on the inertial sub-range for the EMCM's on BLISS using the IDM

5.6 Significant Wave Height

Pressure transducer data was used to provide information on the mean surface elevation (water depth) and surface elevation variance, from which the significant wave heights (H_{sig}) were calculated. Significant wave height is defined as *"the average of the highest one-third of the wave heights"*, and can also have the notation of $H_{1/3}$. For BLISS data analysis, H_{sig} was approximated in two ways.

5.6.1 Time-Series Analysis

For every pressure data run (17 minutes, logging every 0.2 seconds), the data was firstly detrended to remove any tidal signature from the data set, before computing the standard deviation of the surface elevation time series denoted as σ_η. The significant wave height was then calculated using the relationship:

[5.25]

$$H_{sig} = 4 \bullet \sigma_{\eta}.$$

5.6.2 Spectral Analysis of Time Series

The power spectral density (PSD) of the pressure data was computed using Welch's Periodogram method, with the application of a Hanning Window, to reduce spectral leakage. The boundary between the infragravity and gravity band frequencies was arbitrarily chosen as 0.05 Hz following Russell, (1993). The total variance between 0.05-0.33Hz (the gravity wave band), was obtained by summing the spectral estimates across the frequency bins and calculating the area under the curve, using the Trapezium rule (equation 5.10). Significant wave heights were then computed from the total, following equation 5.25 where σ is the variance over the specified frequency band. The spectral method of estimating H_{sig}, is the recommended procedure outlined by the IAHR, (1987).

5.7 Wave Orbital Velocity and Direction

The u and v components of wave variance were calculated using the spectral splitting technique outlined in section 5.5.3, and combined to give a single non-directional measure of the root mean-squared orbital velocity σ_w (Soulsby and Humphrey, 1989; Hannay *et al.*, 1994).

[5.26]

$$\sigma_w = \left(\overline{u'^2_w} + \overline{v'^2_w}\right)^{0.5}$$

The mean direction of wave propagation, θ_w, is measured relative to the coastline because BLISS velocity measurements were rotated to align with the coastline, since it is known that the tidal ellipse off Holderness is essentially rectilinear and runs parallel to the coastline in a North West - South East direction. θ_w is calculated from:

[5.27]

$$\theta_w = \tan^{-1}\left(\overline{v'^2_w} / \overline{u'^2_w}\right)^{0.5}$$

The direction of the waves relative to the mean current is given by :

[5.28]

$$\theta diff. = \theta_w - \phi_c$$

where ϕ_c is the direction of the mean current.

5.8 Re-orientation of the EM Current Meters With Respect to Alongshore and Cross-shore Flow

When considering flux estimates of sediment transport in response to tidal and oscillatory flow, re-alignment of the measured EM current velocities (EMX1 and EMX2) to alongshore and cross-shore flow is crucial. It is assumed that tidal flow off the Holderness coast is nearly rectilinear and is dominated by the M_2 tidal ellipse. This implies that the alongshore current is 90° out of phase to the cross-shore current. Because of the near-rectilinear nature of the flow, the cross shore velocities will also be very small. It was decided to use M_2 tidal flow as the main determinant for alongshore current, based in part on the fact that cross-shore velocities measured by the BLISS tripods were near to the seabed. This suggests that the cross-shore flow may not travel in the same direction as the surface currents, which are influenced by other parameters for example, the wind. Therefore, it is advisable to use the M_2 tidal constituent in the North Sea because it is essentially barotropic and does not change direction with depth.

Three methods have been used to determine the correct angles for aligning the current meters to alongshore and cross-shore flow. They are:-

1. A method proposed by Pugh (1987).
2. Covariance
3. Geometry of the BLISS tripods using the compass information.

5.8.1 Pugh's Estimation (1987)

Pugh (1987) devised a method by which current ellipse parameters were determined from resultant amplitudes and phases of known current velocities. Taken from Pugh (1987) the basic parameters of a current ellipse are in the following diagram (figure 5.3).

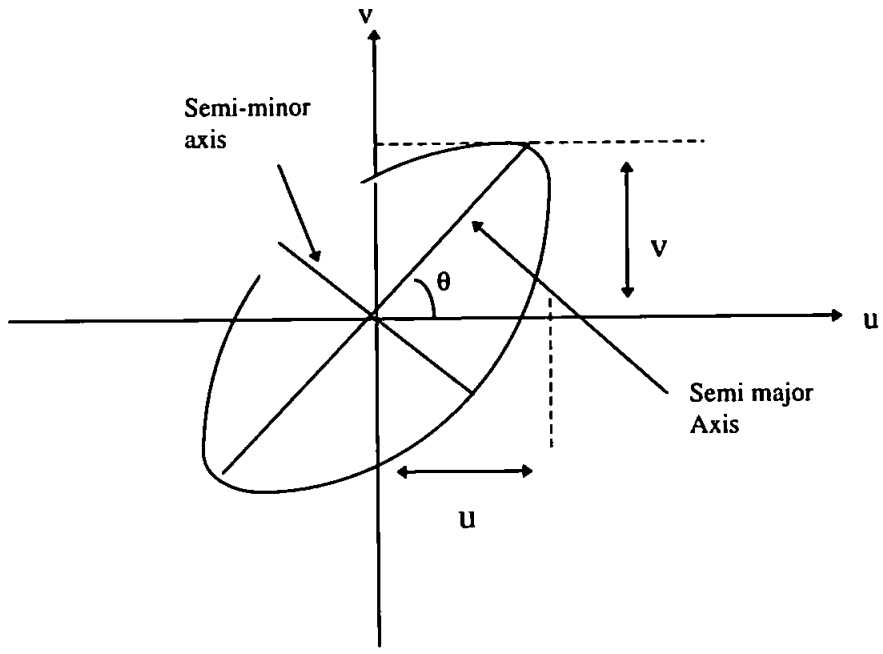

Figure 5.3 Basic parameters of a current ellipse

Consider a harmonic constituent whose East-going and North-going components are:

[5.29]

$$U \cos(\omega t - g_u)$$
$$V \cos(\omega t - g_v)$$

In Cartesian co-ordinates the direction of flow and the current speed are given as:

[5.30]

$$\text{direction } \theta = \arctan \frac{V \cos(\omega t - g_v)}{U \cos(\omega t - g_u)}$$

[5.31]

$$\text{speed } q = \{U^2 \cos^2(\omega t - g_u) + V^2 \cos^2(\omega t - g_v)\}^{1/2}$$

From equation 5.31, q may also be written as:

[5.32]

$$q^2 = \tfrac{1}{2}(U^2 + V^2 - \alpha^2) + \alpha^2 \cos^2(\omega t - gu + \delta)$$

where

[5.33]

$$2\delta = \text{actan} \frac{V^2 \sin 2(g_u - g_v)}{U^2 + V^2 \cos 2(g_u - g_v)}$$

and

[5.34]

$$\alpha^2 = [U^2 + V^2 \cos 2(g_u - g_v))^2 + (V^2 \sin 2(g_u - g_v))^2]^{1/2}$$
$$= [U^4 + V^4 + 2U^2V^2 \cos 2(g_u - g_v)]^{1/2}$$

The maximum value of the current speed is then determined from equation 5.32 as:

[5.35]

$$q_{max} = \left(\frac{U^2 + V^2 + a^2}{2}\right)^{1/2} = \text{semi major axis}$$

and the minimum value is given as:

[5.36]

$$q_{min} = \left(\frac{U^2 + V^2 - \alpha^2}{2}\right)^{1/2} = \text{semi minor axis}$$

The direction of the maximum current speed (θmax) is then given by:

[5.37]

$$\theta_{max} = \arctan \frac{V \cos(g_u - g_v - \delta)}{U \cos(\delta)}$$

rewriting equation 5.30 as:

[5.38]

$$\theta = \arctan K$$

the sense of the ellipse vector rotation can be determined by differentiating with respect to time:

[5.39]

$$\frac{d\theta}{dt} = \frac{1}{(1 + K^2)} \frac{\omega UV}{U^2 \cos^2(\omega t - g_u)} \sin(g_v - g_u)$$

$$= \frac{\omega UV}{q^2} \sin(g_v - g_u)$$

Hence:

if $\frac{d\theta}{dt}$ is positive, the sense of the ellipse is anti-clockwise

$\frac{d\theta}{dt}$ is negative, the sense of the ellipse is clockwise

$\frac{d\theta}{dt}$ zero, the ellipse is rectilinear.

The amplitude and phase components at the M_2 tidal frequency were extracted from the mean time series of EM1X and EM2X by Fourier analysis. The (u) component was taken in all cases (but for the outer station in February 1996 deployment) as EM1X and similarly, EM2X was taken as (v).

Using the FFT function in the mathematical package Matlab, the amplitude and phase of the M_2 tidal constituent at 12.42 hours, were obtained for both the EM1X and EM2X current meter data. To obtain accurate estimates of M_2, care must be taken to ensure that a Fourier harmonic occurs close to a period of 12.42 hours. For example, taking an hourly time series record of 271 hours (July inner station 1995), the 22nd Fourier harmonic will represent the relevant constituents, i.e, (271÷12.42). For a time series of 355 hours, the amplitude and phase of the M_2 tidal harmonic will arise on the 29th harmonic. Once obtained, the amplitude and phase of u and v were inserted into programme 8, appendix B, using equations 5.34 - 5.39, to derive the angles needed for rotating the current velocities to alongshore and cross-shore flow.

For the February 1996 outer station data set, the M_2 signal was extracted from the first 80 runs. The rotation angles derived using Pugh's estimation were then altered in accordance with the actual compass readings, because the tripod shifted from its initial position a number of times during the deployment in response to a large storm (see table 5.2 for rotation angles used). During the February outer station deployment, the BLISS 2 tripod shifted its position in the horizontal 15.44°. This was recorded by the compass, and the first change in position at hour 89 coincided with a large storm which lasted for 55 hours (2.29 days). The current velocity data were then rotated following basic rules of trigonometry (refer to appendix A4 for details).

To test whether the rotated cross-shore and alongshore velocities were in fact 90° out of phase with each other, cross-spectral analysis was performed on the burst averaged values of surface elevation (p) and each velocity component (u and v). The phase angle at the M_2 tidal frequency (12.42 hours) (figure 5.4 and 5.5) was then extracted from the co-spectrum, and the difference between the phase angles were recorded. It was also noted during computation, that the phase angle is very sensitive to the rotation angle used (i.e. a 1 degree change in rotation angle can lead to a large shift in the phase). In addition, spurious points in the data, also increase the phase angle, so it was crucial that all spikes in the data were removed before producing the co-spectrum.

Table 5.1 shows the rotation angles derived by Pugh's estimation and also the phase difference between each velocity component. The phase angles produced by Pugh's method (1987) for p-u and p-v were within ± 7° of the required 90°. A 10% margin of error in the phase was the acceptable limit chosen (Pers. comm., Huntley, 1997). Therefore, Pugh's estimation gave a suitable method for aligning the u-v current values to alongshore and cross-shore flow.

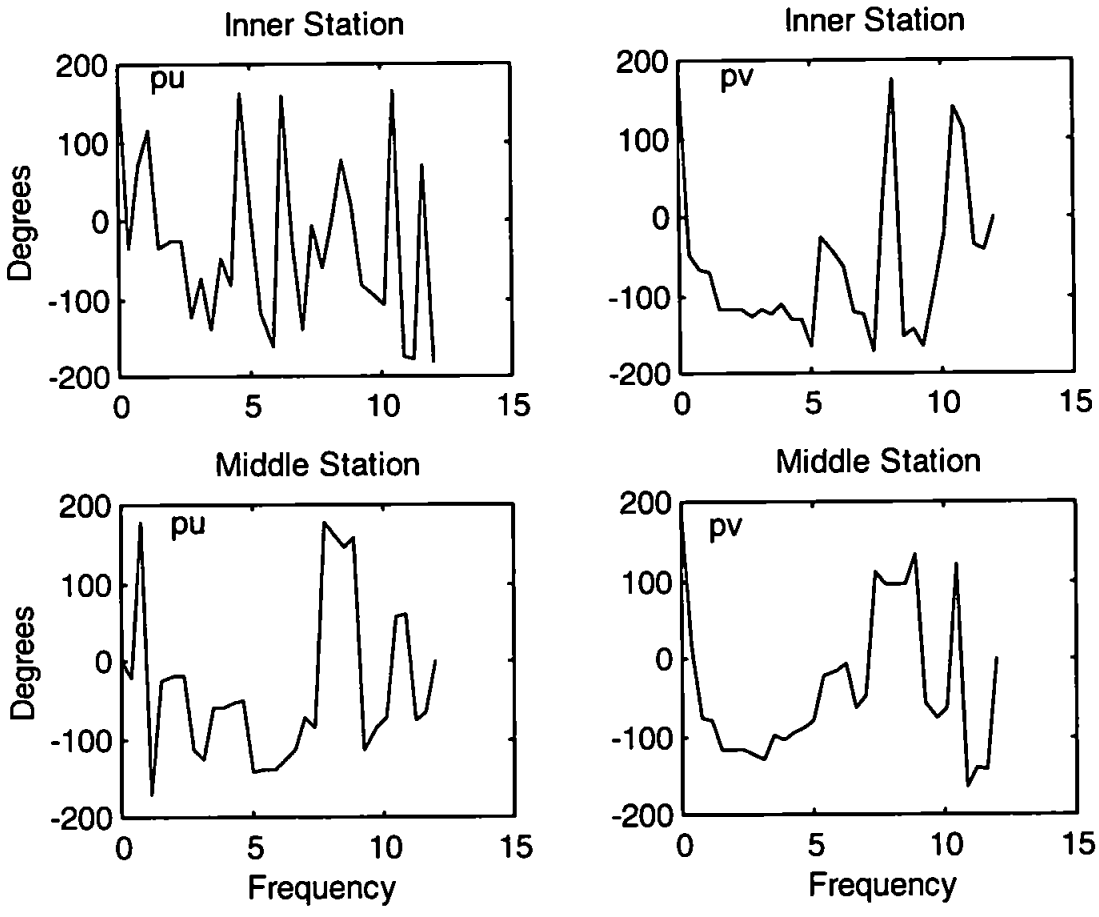

Figure 5.4 June/July 1995 deployment - Resultant transfer function phase between surface elevation and each velocity component (u, v)

Table 5.1 Rotation angles and phase angles derived by Pugh's estimation

Station	Angles used for Rotation	Co-Spectrum of Elevation-Cross-shore Velocity Resultant Phase (°)	Station	Co-Spectrum of Elevation-Alongshore Velocity Resultant Phase (°)	Phase Difference (°)
July Inner	65.9 24.1	-23.79	July Inner	118.26	94.47
July Middle	80.1 9.9	-19.98	July Middle	117.19	97.21
February Inner	72.8 17.2	144.69	February Inner	61.62	83.07
February Middle	51.8 38.2	-25.79	February Middle	-119.31	-93.5
February Outer	See Table 4.10	-23.24	February Outer	-118.64	-95.4

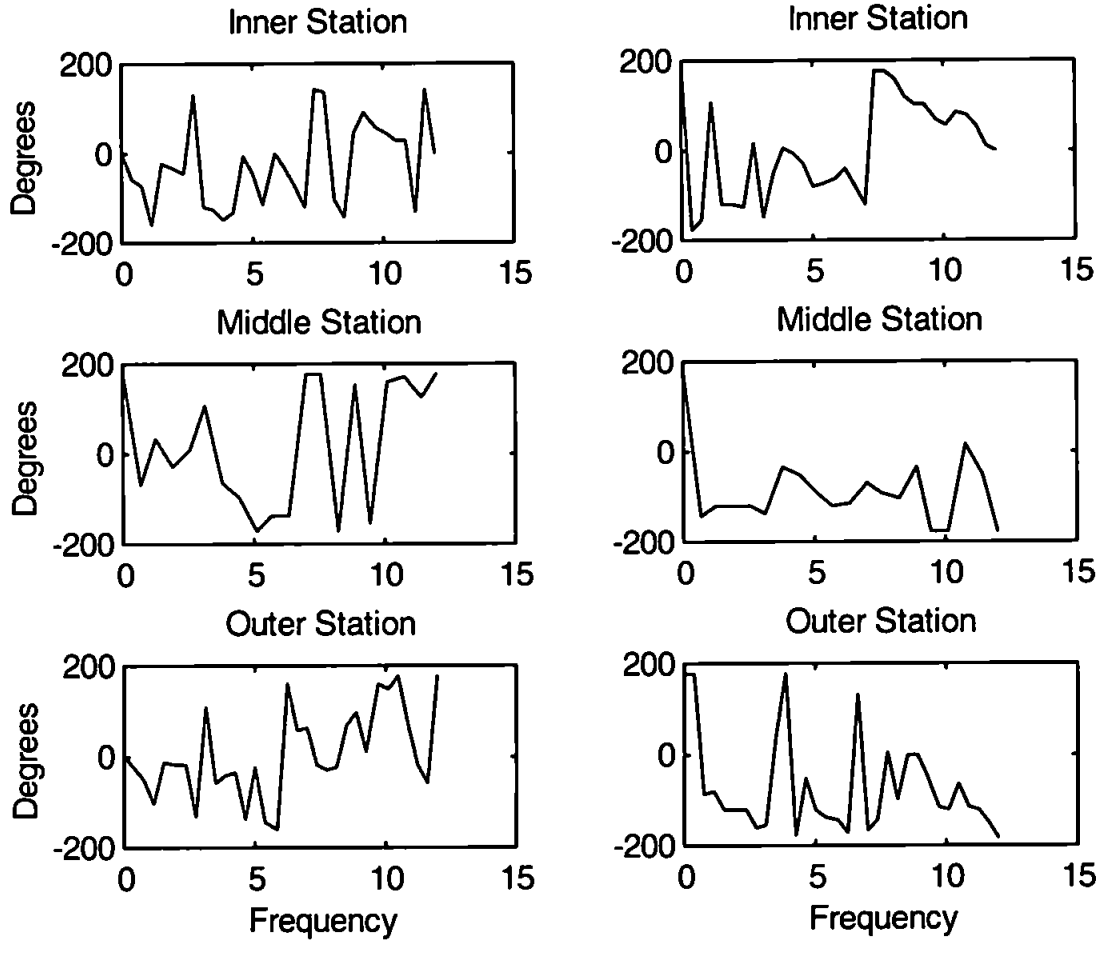

Figure 5.5 February 1996 deployment - Resultant transfer function phase between surface elevation and each velocity component (u, v)

Table 5.2 Angles used to rotate February 1996 outer station data

Runs in Hours	Amount of Tripod's Movement in degrees (°)	Rotation angles used in degrees (°)
1-88	stable	82.4 , 7.6
89	1.66	80.8 , 9.2
90-95	3.09	77.7 , 12.3
96-98	0.71	76.9 , 13.02
99-109	0.95	76.02 , 13.9
110	2.38	73.7 , 16.4
111-112	0.24	73.4 , 16.6
113	0.24	73.2 , 16.8
114-115	1.43	71.8 , 18.3
116-181	1.9	69.9 , 20.2
182-211	0.24	69.6 , 20.4
212-271	0.24	69.4 , 20.6
272-331	1.19	68.2 , 21.8
332-355 End	1.19	66.99 , 23

5.8.2 Covariance Method

Another approach to obtaining the rotation angles for cross and alongshore velocity was to treat the two horizontal components of flow, EM1X and EM2X, as two separate column vectors. The idea here is to use the concept of principal components analysis, 'to look for directions in the data space in which the n points are most spread out', in other words, to rotate the original co-ordinate system of the data space to a new one, where the new co-ordinate system is measured along the direction in which the observations have the most separation. What is meant by the data points being 'spread out' along a direction is that the variance of the observations in that direction is largest. The procedure begins with determining the covariance matrix of u and v, computed by using the function COV(u,v) in Matlab. This function removes the mean from each column of data and reorders the data into the covariance matrix given as:

$$\begin{bmatrix} \overline{U^2} & \overline{UV} \\ \overline{VU} & \overline{V^2} \end{bmatrix} = A$$

Once formed, the eigen values and the eigen vectors are computed for the covariance matrix, by using the Matlab function [EV D]=eig(A).. Here D in the Matlab formula is the

diagonalised matrix of eigen values $D=\begin{bmatrix} U^2 & 0 \\ 0 & V^2 \end{bmatrix}$ which conveniently, are the variances of the observations in each of the new directions. EV is a full matrix whose columns are the corresponding eigenvectors. These eigenvectors are the cosine angles used in diagonalising (rotating) the covariance matrix to its new orientation.

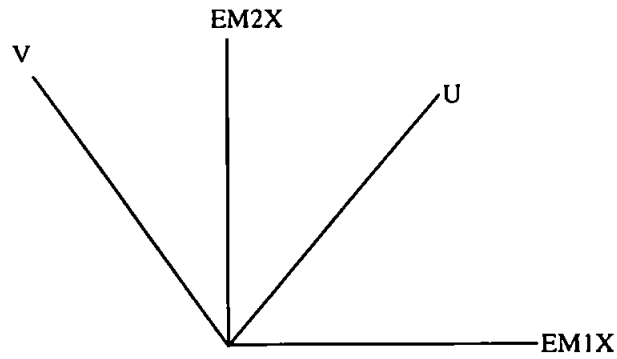

For example if EM1X was treated as u and EM2X was treated as v, and the resultant eigen vectors EV included the four values $\begin{matrix} 0.91 & -0.43 \\ 0.43 & 0.91 \end{matrix}$, then the corresponding rotation angles would be 24.49° ($\cos^{-1}(0.91)$) and 64.53° ($\cos^{-1}(0.43)$) respectively, and cross-shore and alongshore velocities would be calculated as follows.

$$\textbf{Cross-shore} = 0.91 * EM1X + 0.43 * EM2X$$

$$\textbf{Alongshore} = 0.43 * EM1X + 0.91 * EM2X$$

To test whether the covariance method rotated the current velocities so that they were 90° out of phase with each, the same process was employed as for Pugh's estimation. Thus, by computing the co-spectrum between elevation and each flow component, the resultant phase angles were obtained. These phase angles coupled with the phase difference are illustrated in table 5.3.

The phase angles derived from the co-spectrum of elevation and velocity, clearly are not 90° out of phase, although the rotation angles derived using covariance and eigenvectors are similar to the angles derived by Pugh's estimation. It is clear that a 1° change in orientation produces a large phase shift in the resulting cross-shore flow. Cross-shore flow will be most sensitive to shift in orientation, because the cross shore velocities are very small in comparison to the alongshore velocities which are tidally dominated.

Table 5.3 Rotation angles and phase angles from Covariance method

Station	Angles used for Rotation	Co-Spectrum of Elevation-Cross-shore Velocity Resultant Phase (°)	Station	Co-Spectrum of Elevation-Alongshore Velocity Resultant Phase (°)	Phase Difference (°)
July Inner	64.42 25.58	-90	July Inner	-130	-40
July Middle	75.94 14.06		July Middle		
February Inner	73.04 16.96	165	February Inner	60	105
February Middle	52.63 37.37	35	February Middle	-120	-155
February Outer (1-80 runs)	83.41 6.59	-10	February Outer	60	70

The conclusion is that the covariance method, though producing a rotation angle similar to the Pugh method, is less accurate, probably because it uses total variance rather than flows at the M_2 frequency alone.

5.8.3 Geometry Method (angles derived from compass information on the BLISS tripods)

The success of this method is based entirely on how accurately the attitude sensors on BLISS, have recorded the tripod's position, whereas the other two methods discussed above were based on the data itself. The nominal positions and direction of the sensors relative to the compass bearing on the BLISS tripods were noted before deployment. The configuration of the sensors were the same for each tripod, in that each sensor was aligned with respect to the leading bow leg. The compass bearing reads magnetic North at 90° (right angles), to the direction of the leading bow leg. So, to determine the position of the leading leg with respect to magnetic North, 90° must be added to the compass bearing recorded on BLISS. On knowing the position of the bow leg, the position of the current meters can then be determined easily, as we know the angle of the EM current meters with respect to the leading leg (in the horizontal).

Starting with the assumptions that:

1 The coastline is aligned 41° to the west of true North (running in a North West-South East direction) based upon the admiralty chart of the region.

2 Alongshore flow is positive towards the North West.

3 Cross-shore flow is positive offshore.

The angle required to realign the current meters to alongshore and cross shore flow can then be determined by plotting the positions of the EM current meters with respect to the leading bow leg and to the coastline (taken as 41°), and deducing by trigonometry the angle between each current meter and the coastline. This method has been employed for BLISS rigs 2 and 3 in the July 1995 deployment and for BLISS rigs 2, 3 and 4 in the February 1996 deployments. For computations of the rotation angles, refer to appendix A4.

BLISS 2 at the February 1996 outer station shifted 15.4375° clockwise from its initial point during the deployment. Movement was initiated by a large storm which arose after 85 hours into the deployment. The compass worked adequately throughout the deployment, recording the new position of the tripod to within 2 decimal places. Table 5.4 gives the alteration in the rotational angles during deployment, and also which runs the angles correspond to.

Table 5.4 Angles used to rotate February outer station current meter data to alongshore and cross-shore flow

Feb 96 Outer Station Rig 2				
run	**compass**	**degrees**	**Angles used for rotation (°)**	**change in degrees**
			Clockwise rotation	
2	1224	363	81.8 8.2 (runs 1-88)	3
32	1225	363.24		3.24
62	1226	363.48		3.48
78	1227	363.71		3.71
81	1227	363.71		3.71
87	1227	363.71		3.71
89	1234	365.38	84.4 5.7	5.38
90	1247	368.46	87.49 2.51 (90 - 95)	8.46
92	1247	368.46		8.46
96	1250	369.18	88.20 1.79 (96-98)	9.18
99	1254	370.13	90.84	10.13

			0.85 (99 - 109)	
107	1256	370.6		10.6
108	1254	370.13		10.13
			Anticlockwise rotation	
110	1264	372.5	91.77 1.77 (110 - 113)	12.5
111	1265	372.74		12.74
113	1266	372.98		12.98
114	1272	374.4	93.43 3.43 (114-115)	14.4
116	1280	376.3	95.39 5.39 (116-271)	16.3
122	1278	375.83		15.83
182	1281	376.54		16.54
212	1282	376.78		16.78
272	1287	377.96	96.99 6.99 (272-331)	17.96
332	1292	379.15	98.179 8.18 (332-end)	19.15

5.8.4 Summary

Table 5.5 gives all the angles of rotation derived from the three different methods. The geometry method was largely dependent on the accuracy of the compass readings. Because the compass was faulty during the February 1996 inner station and middle station deployment, a decision was made not to use the geometry method for rotating the EM1X and EM2X components, to cross-shore and alongshore flow. Taking the assumption that alongshore flow is 90° out of phase to the cross-shore flow, Pugh's estimation was decidedly the best method for rotating the current velocities.

Table 5.5 Rotation angles derived from each method for each deployment

Deployment	**Pugh's Method in degrees (°)**	**Covariance Method in degrees (°)**	**Geometry Method in degrees (°)**
July 1995 inner station (NI)	65.9016 24.0984	64.42 25.58	75.2 24.8
July 1995 middle station (N2)	80.08 9.92	75.94 14.06	83.97 16.03
February 1996 inner station (NI)	72.81 17.19	73.04 16.96	compass broken
February 1996 middle station (NM)	51.84 38.17	52.63 37.37	compass broken
February 1996 outer station (NO)	see table 5.2	83.41 6.59	see table 5.4

Chapter 6

6. BLISS Field Results

6.1 Introduction

The movement of materials, which remain in suspension in sea water, or which are dissolved in it, are determined entirely by the residual water movements, but the transport of shelf-sea sediments which are alternately taken into suspension and deposited on the seabed depends very much on the nature of the turbulent flow near to the seabed (Harvey and Vincent, 1977). The main focus of the BLISS experiment was to identify the temporal and spatial physical processes which control the movement of sediment both along and across the Holderness coast. Time series results obtained from the June/July 1995 field campaign to characterise summer conditions, and from the February 1996 deployment which typifies winter conditions, are presented in this chapter. The first part begins by giving a detailed account of the BLISS time series data taken from the optical instruments, the electromagnetic current meters, the pressure sensors and the temperature and salinity sensors. Sediment suspension events will be discussed in the context of tidal flows and storm activity over two week spring / neap tidal cycles.

In the second part, the u,v,w velocity components are used to derive shear stress estimates from the three methods described in sections 5.5.2/3/4. The friction velocity, a quantity which expresses shear stress in the form that has dimensions of a velocity, is compared under different wave/current conditions, to determine threshold conditions for sediment transport. Bed stress comparisons are then made between summer and winter, and with results from other field data using the drag coefficient relationship and roughness length.

6.2 Time Series

Time series data allow us to obtain a good overall picture of the processes occurring at different time scales during the BLISS deployments. Anomalous data points taken as >3 x Std from the mean were removed from every 17 minute data burst. The data were then detrended before calculating the means. Each BLISS deployment covered approximately a two week spring/neap tidal cycle. Data overlap between tripods was achieved in the June/July 1995 summer deployment[1], with the BLISS inner station (NI) tripod beginning logging 3.96 days later than the middle station (NM). The optical sensors malfunctioned at the middle station, so that description of the sediment response in summer was confined to results from the inner station only. In February 1996, the inner and middle station BLISS tripods were deployed at the same time, but there was a two hour time delay, with the inner station logging first. The outer station (NO) tripod was deployed 11 days later than the inner station. Data overlap in the February 1996 deployment therefore only occurred for all three tripods at the end of the inner station deployment. The middle station suffered damage during the deployment and was non-operational for much of the inner station data period. Current velocities were recorded for the first 2 days of the deployment, after which the tripod was dragged onto its side apparently by a fishing trawler. The data collected are summarised in table 4.4.

6.2.1 Tidal Conditions in June/July 1995 and February 1996

A characteristic of tidal currents in mid-latitudes is the predominance of the semi-diurnal lunar M_2 and solar S_2 constituents with periods 12.42 hour and 12 hour respectively. Their observed amplitude ratio in shelf seas is close to 1:0.33 (Prandle, 1997). The small difference in their periods produces the widely observed 15 day spring (in phase) and neap (out of phase) MS*f* tidal cycle.

Pressure records (17 minute burst averages) shown for the June/July '95 deployments (figure 6.1a), produced an average water depth of 11.88m for the NI station and 14.33m for the NM station. Tidal range varied from ~3.8m at neaps to ~6m during springs. Time series pressure records (17 minute burst averages) for the February 1996 deployments are given in figure 6.1b.

[1] For deployment sites off the Holderness coast please refer to figure 4.1.

Mean water depths were NI = 12.80m, NM = 14.54m and NO = 17.6m.

The February 1996 deployment phase spanned over two spring/neap tidal cycles. Storm surge was most noticeable during the outer station deployment, which in the following sections, was dominated by a significant winter storm event.

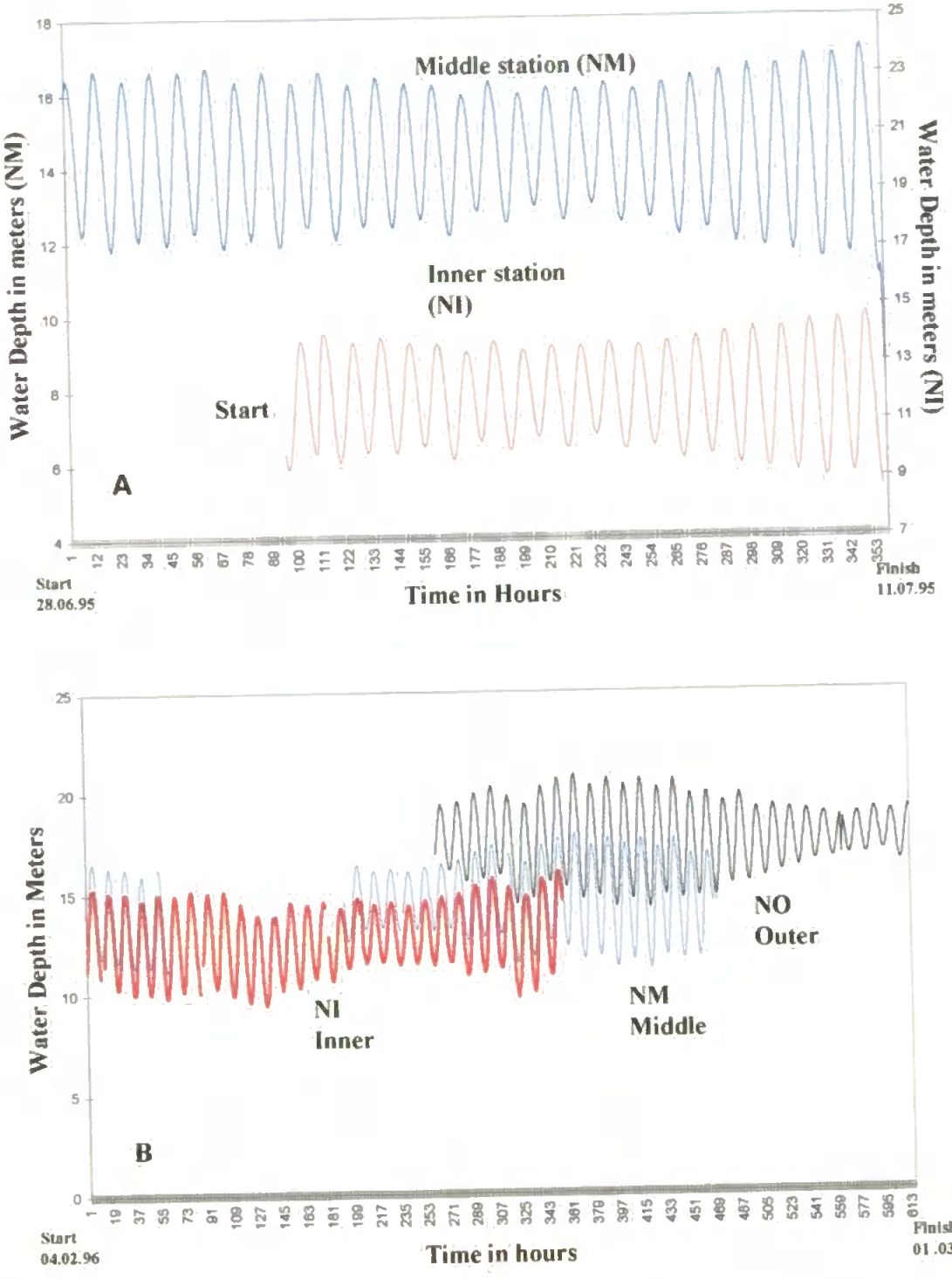

Figure 6.1a,b BLISS Pressure data recorded from (a) June/July 1995 (b) February 1996 deployments (17 minute burst averages).

Taking the February outer station as an example for tidal conditions, the rotated u and v current velocity components were plotted against each other to produce a tidal ellipse (figure 6.2) characteristic of the Holderness coast. The ellipse was almost rectilinear and ran parallel to the coastline in a North West, South East direction. The ellipse rotated in a clockwise direction and the tidal currents flowed towards the North West on ebb and toward the South East on flood. Alongshore velocities were much larger than the cross-shore velocities. Maximum velocities in the alongshore were ~0.5ms^{-1}, whereas in the cross-shore, maximum velocities were ~0.1ms^{-1}. There was a distinct curvature to the ellipse at the northern end which suggests the presence of a non-harmonic component. Curvature in shallow water tidal ellipses have been observed (Pugh and Vassie, 1976) on the North East coast of England just offshore of the Wash estuary. Pugh and Vassie (1976) noticed that the deflected elliptical curvature was most pronounced for very strong current flows and suggested that the deflection in the ellipse was due to increased area of water collected in the Wash on spring tides, which required a greater water input for a unit increase in sea level. It may be hypothesised for the Holderness coast that alongshore tidal currents are deflected towards the North East by the large amount of water which is discharged out of the Humber estuary on ebb tide.

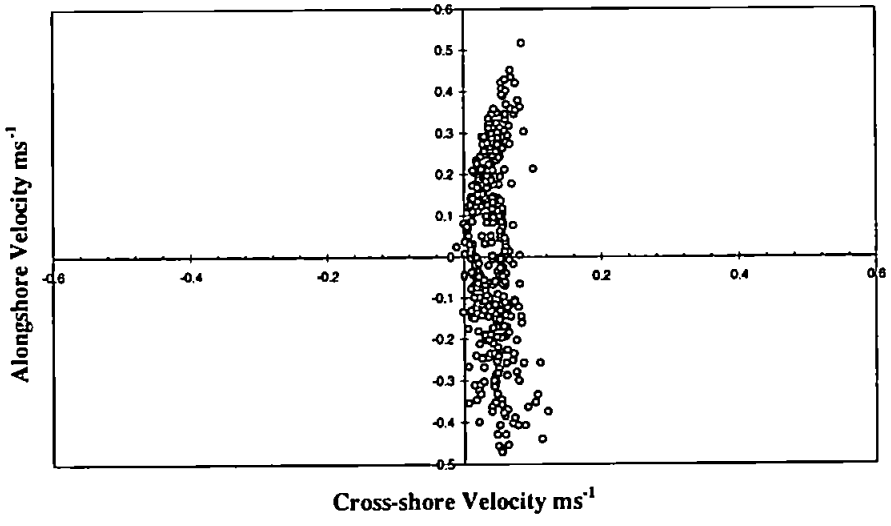

Figure 6.2 Scatter plot of burst averaged flow components u and v rotated (ms^{-1}) to show tidal ellipse characteristic of the Holderness coast. Data taken from February 1996 outer station deployment (15.02.96 - 01.03.96).

6.3 Time Series Results

Burst averaged (over 17 minutes) time series plots of suspended sediment concentration, alongshore and cross-shore current velocities and significant wave height for June/July 1995 and February 1996 are discussed in the following sections.

6.3.1 June/July 1995 Deployment - Weather Conditions

Over the deployment period for July (28.06.95 - 11.07.95), the winds were mainly North Easterly. At the start of the deployment a high pressure system with its centre to the North West of Scotland dominated the meteorological conditions, and generated light North Easterly winds (5 Knots). On 29.06.95, a weak low pressure system formed over the U.K. and caused the winds to veer North/ North West, although still light in strength (5-10 Knot). As the low pressure system moved eastwards, a high pressure system once again controlled the weather over the U.K. Winds at this time were still North/North West and light in nature. This pattern of weather conditions remained until 4.07.95 where a more pronounced low pressure system developed over the U.K, with winds strengthening in the Northern North Sea. Winds were North East although still relatively light. The increased wave conditions shown on figure 6.4a & b as storm number 2, was the product of swell waves travelling down from the Northern North Sea and Norwegian Sea. On 6.07.95 a low pressure system deepened over the U.K., causing the winds to shift West / South West, and slightly increasing in strength. The weather pattern then altered again to produce very light easterly winds, with little wave activity, shown in figures 6.4a & b between hours 110-150 and hours 210-250 respectively. A North Easterly swell developed with increased wave height and winds increased in strength from the North East. Winds remained North East, and on the 10.06.95, winds increased in strength to 25 Knots in the Central and Southern North Sea, causing a swell which accounts for the last storm on figures 6.4a & b. In general terms, the summer storms were mainly generated by North East winds and swell generated from the North East.

Significant wave heights were determined from pressure spectra using the Trapezium Rule (see section 5.5.3). Four storms occurred over the two week period. Maximum wave heights reached 0.4m - 0.45m.

6.3.2 June/July 1995 Time Series - Inner Station

The burst averaged suspended sediment concentrations shown in figure 6.3 were taken from the optical backscatter sensors 0.41m and 0.9 meters above the seabed. Comparisons between the two sensors, showed that suspended sediments increased in background concentration with height above the seabed.

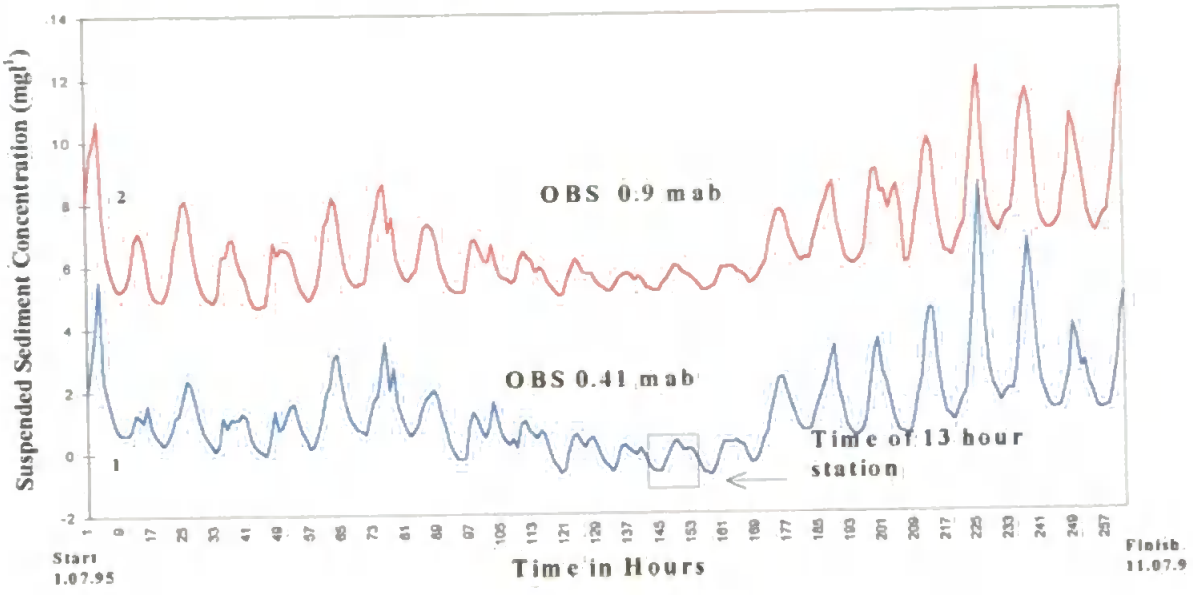

Figure 6.3 Suspended sediment concentration measurements taken from June/July inner station 1995

In situ water samples taken on 07.07.95 - 08.07.95 (during the 13 hour station, figure 6.3, table 6.1) gave low concentration values between 1.37 mgl^{-1} and 13.08 mgl^{-1}. Lowest levels of SSC were seen to arise at maximum tidal streaming. To determine whether the increase in sediment with height is genuine, or the difference in background levels is simply an offset problem in the OBS sensor, water samples taken near to the upper OBS (bottle 2) revealed low concentrations, for example 1.48 mgl^{-1} (sample 6) at maximum tidal streaming and were very similar to the water sample taken at the same time (sample 6) to represent the lower OBS (bottle 4). This confirmed that the upper OBS did have an offset problem. For descriptive purposes, the lower OBS record (0.41mab) will be analysed.

Table 6.1 *In situ* measurements of suspended sediment concentration taken at June/July 1995 inner station.

	Bottle No.	1	2	3	4	5	Time	Depth
Sample		mgl^{-1}	mgl^{-1}	mgl^{-1}	mgl^{-1}	mgl^{-1}		(m)
1	Total	13.79	3.52	2.2417	3.39	8.5743	20.41	11.89
2	Conc.	5.9703	3.9406		13.0837	15.6733	21.57	14.63
3		3.126	7.501		10.8129	5.3259	22.48	14.63
4		7.7841	8.2002	3.3856	4.4599	6.7699	0.38	15.91
5		2.1493	14.8713		3.3768	5.3234	1.45	15.18
6		3.56	1.4796	2.7363	1.8922	2.8867	3.11	14.45
7		2.3087	1.61	0.8649	1.3759	4.6571	4.33	14.45
8		2.5068	3.1373		2.6585	5.6956	6.04	13.72
1	Inorganic	12.14	2.74	0.3021	2.55	4.8119	20.41	11.89
2	Conc.	4.1584	3.3564		12.197	13.0693	21.57	14.63
3		2.0822	6.6198		8.4818	4.0999	22.48	14.63
4		5.004	6.4245	2.1973	3.0302	4.4085	0.58	15.91
5		1.4328	14.07		2.4949	3.4726	1.45	15.18
6		2.38	0.2487	1.771	0.9019	2.1281	3.11	14.45
7		1.565	0.99	0.4257	0.3414	3.0476	4.33	14.45
8		1.9976	2.2317		1.9861	4.545	6.04	13.72

Comparing the suspended sediment concentration time series to current velocity and wave activity for the June/July inner and middle station (figure 6.4a & b), it is noted that the overall background sediment concentration was greater during springs than at neap tides because of the larger tidal excursion. At spring tides, peaks in sediment concentration were modulated by the tide. Comparisons with the alongshore current velocity showed that the peaks occurred just after low water slack only, giving rise to an advective signal. The semi-diurnal sediment signature is a recognised feature, which indicates advection past the mooring site of a horizontal turbidity gradient (see discussion) (Jones *et al.*, 1994 and Weeks and Simpson, 1991).

Superimposed on this advective signal was the influence from wave activity. The waves albeit not very large in summer, appeared to influence the sediment signal in two ways. Firstly, the concentration of suspended sediment over a tidal cycle was increased. A good example of this can be seen between hours 180 - 190, figure 6.4a. Secondly, the waves caused an enhancement in the background concentration levels probably caused by increased current shear stress.

With regards to this thesis, a storm is defined as: *An increase in wave activity for a prolonged time period >12 hours but < 3 days.* In the summer storms wave heights are significantly lower than the winter storms. The summer storms in combination with increasing tidal amplitude towards springs, will initiate enough turbulence near to the seabed to lift both coarse sand and fine material up into the water column. The finer grains would be suspended higher in the water column, and following their initial suspension would settle more slowly than the coarser grains close to the seabed. This situation may account for the distinct time lag for the suspended sediment signal to reach pre-storm background levels after a storm had passed. A clear example of this sediment time lag can be seen in the sediment signal following storm 2 and 4 (figure 6.4a). This suspension time lag was a distinct feature in the winter time series. The combination of storms 3 and 4 (figure 6.4a), with the tides moving towards spring conditions, greatly enhances the background concentration levels, with the largest peaks arising just after the highest waves in storm 4, although the wave heights in summer were at a maximum of only 50cm high.

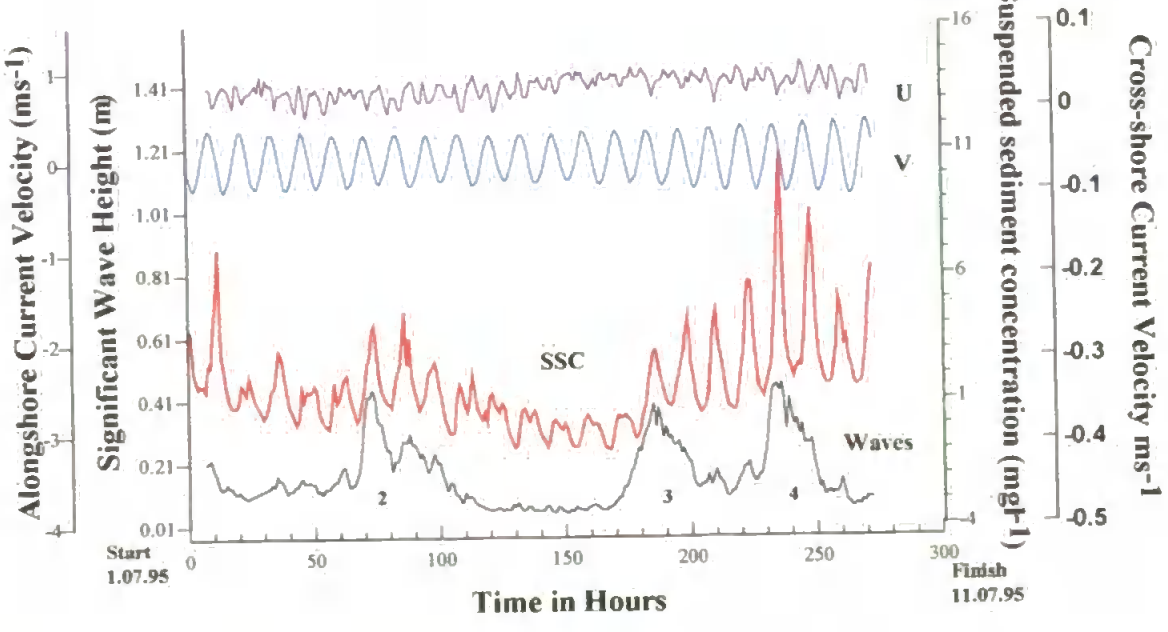

Figure 6.4a Burst averaged time series of SSC, wave activity and u, v flow components for June/July 1995 inner station.

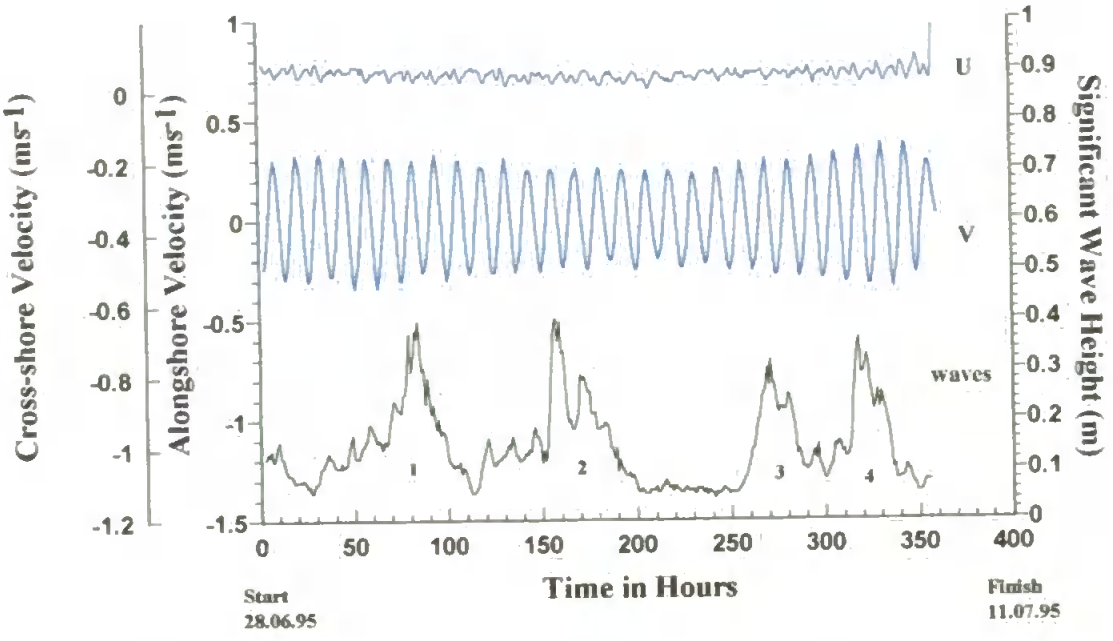

Figure 6.4b Burst averaged time series of wave activity and u, v flow components for June/July 1995 middle station.

In addition to the semi-diurnal concentration signal present, a quarter-diurnal sediment suspension variation associated with local tidal resuspension (Jones *et al.*, 1994, Weeks and Simpson, 1991) could be seen during the neap tidal conditions when wave activity was negligible. Lining up the suspension peaks between hours 115 - 180 (figure 6.4a), with current velocity (figure 6.4c), it was noted that over a complete tidal cycle, local resuspension of the near bed material in the vicinity of tripods occurred on both flood and ebb stages of the tide at maximum tidal streaming. The dip between the peaks was in-phase with slack water, which suggested that material resuspended on flood was given time at slack water to settle out, only to be resuspended again on the next phase of the tide giving rise to the second peak.

6.3.3 February 1996 Deployment - Weather Conditions

The February 1996 deployment occurred from 04.02.96 to 01.03.96. In total ~600 hours of data were collected from the three mooring sites. Wave activity during this time off the Holderness coast from each mooring site is shown in figure 6.5.

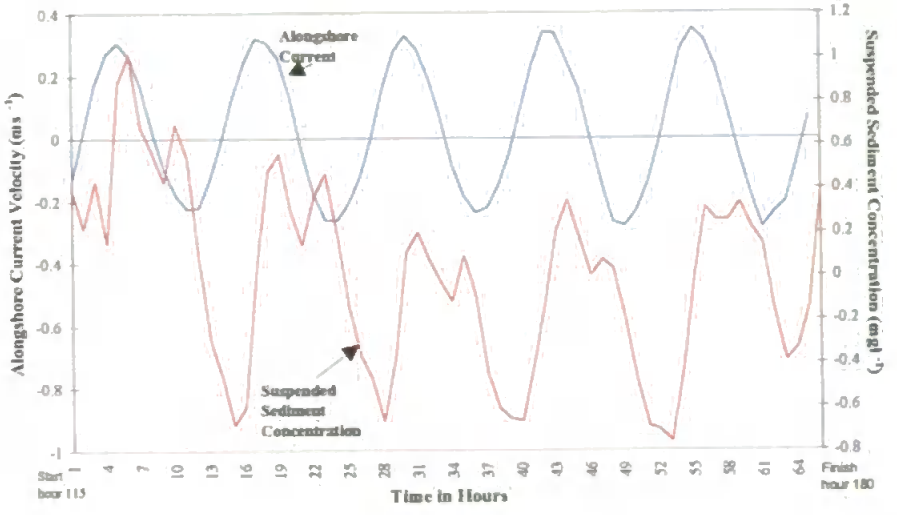

Figure 6.4.C Expanded view of SSC and alongshore current velocity between hours 115-180 - July 1995 Inner Station Deployment.

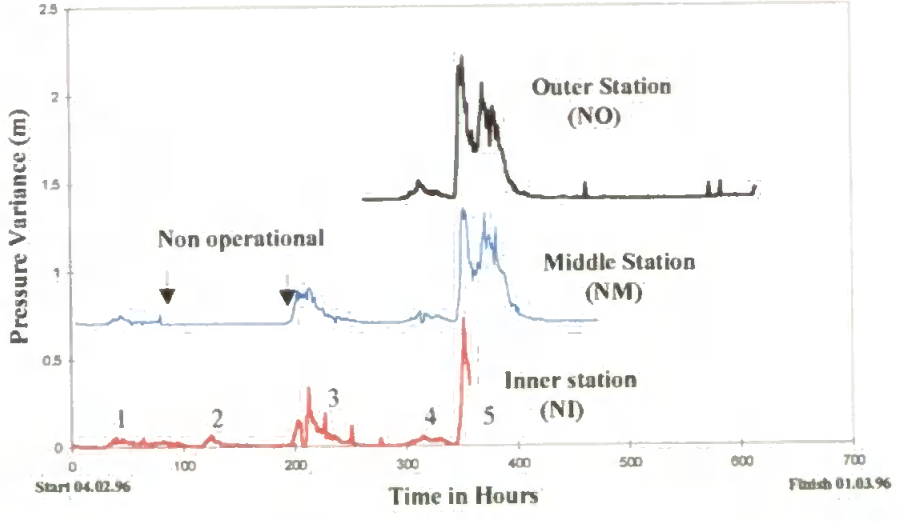

Figure 6.5 Wave activity during the February 1996 BLISS deployments

Deliberate offsets were added to the pressure variance data for the February middle and outer stations, so as to show clearly the period of data overlap between each of the BLISS February deployments.

Five energetic wave events which are characterised as storms following the definition on page 134, occurred during the February 1996 BLISS deployment phase between 04.02.96 - 01.03.96. These events were individually defined as storms because of the time period of wave event was greater than 12 hours. A persistent low pressure system to the North East of the UK was responsible for the production of the swell waves in the first three storms. On the 10.02.96 winds were predominantly from the South, with speeds reaching 20 Knots in the inshore waters off Holderness. On 11.02.96 the winds were still 20 Knots and had veered South West. By the 12.02.96 the winds had backed to Southerly off Holderness and had dropped to 10 Knots. On 13.02.96, a high pressure system developed with its centre over Iceland. Winds then shifted North / North East and increased in strength to 20 Knots down the North East coast of Britain. A quiet period followed as a result of the high pressure system with the winds being light and variable off Holderness. The first and third storm events were recorded by both the inner station and the middle station. The forth and fifth much larger storms were covered by all three BLISS moorings, although the inner station tripod stopped recording 6 hours into the fifth storm. Winds were predominantly from the North West on 17.02.96. In the Northern North Sea winds of 40 knots were recorded. Wave direction off Holderness was predominantly from the North East. Off Holderness winds were 20 Knots. On 18.02.96 a region of low pressure covered the U.K, and the winds veered towards the South West. On 19.02.96 at the peak of the fifth storm, the winds were Northerly and had increased to 30 Knots in the inshore regions off Holderness. On the 20.02.96, winds backed North East and dropped to 15 knots off Holderness, although in the Northern North Sea, winds were still as high as 40 Knots. The period following the fifth storm was controlled by high pressure systems. Winds during this time were light and variable in direction. Wave heights during the first two storm events reached a maximum of ~1m. The third storm reached wave heights of 1.5m and in the fifth storm wave heights of 3m were recorded. Attention will focus on the SSC and velocity data recorded from the February 1996 inner and outer station only. Time series data from the middle station BLISS tripod will not be examined because only 51 hours of data were collected before it was dragged onto its side.

6.3.4 February Inner Station - Time Series

The time series recorded by the two OBS sensors are shown in figure 6.6. Peaks in suspension occurred at the same time at both levels and both sensors recorded similar concentration levels. Between hours 8 - 21, the lower OBS (1) did not function correctly.

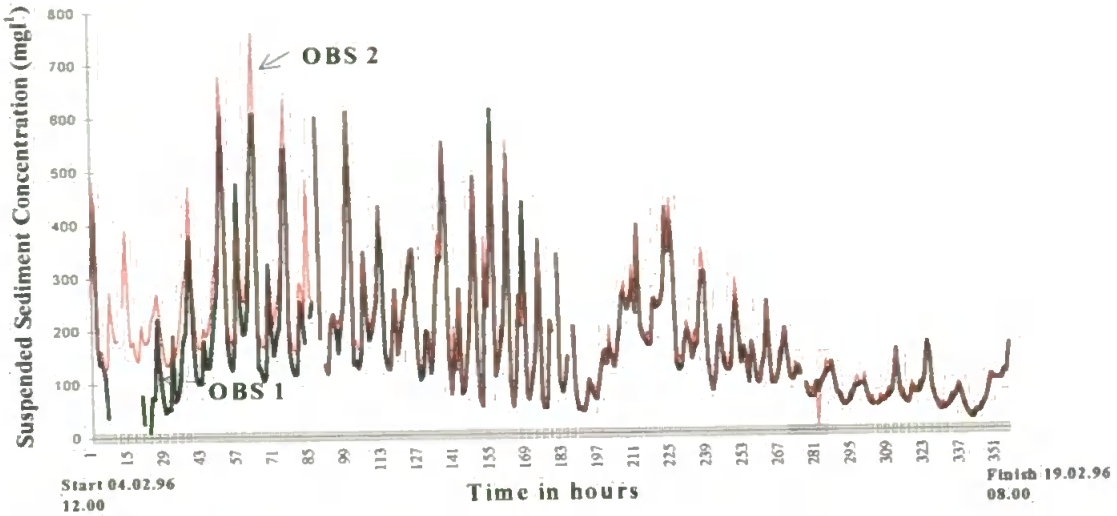

Figure 6.6 Suspended sediment concentration taken from 0.41 and 0.9 meters above the seabed during February 1996 inner station deployment.

In figure 6.7, results from the upper OBS (0.9mab) are shown against current velocity and wave activity. Background levels of suspended sediment were clearly much higher than seen in July 1995 (figure 6.4a). Maximum concentrations reached up to ~780 mgl^{-1} in some cases, and there was a 2 orders of magnitude increase in the suspended concentrations from summer to winter. Peaks in sediment concentration were controlled again by strong M_2 tidal forcing.

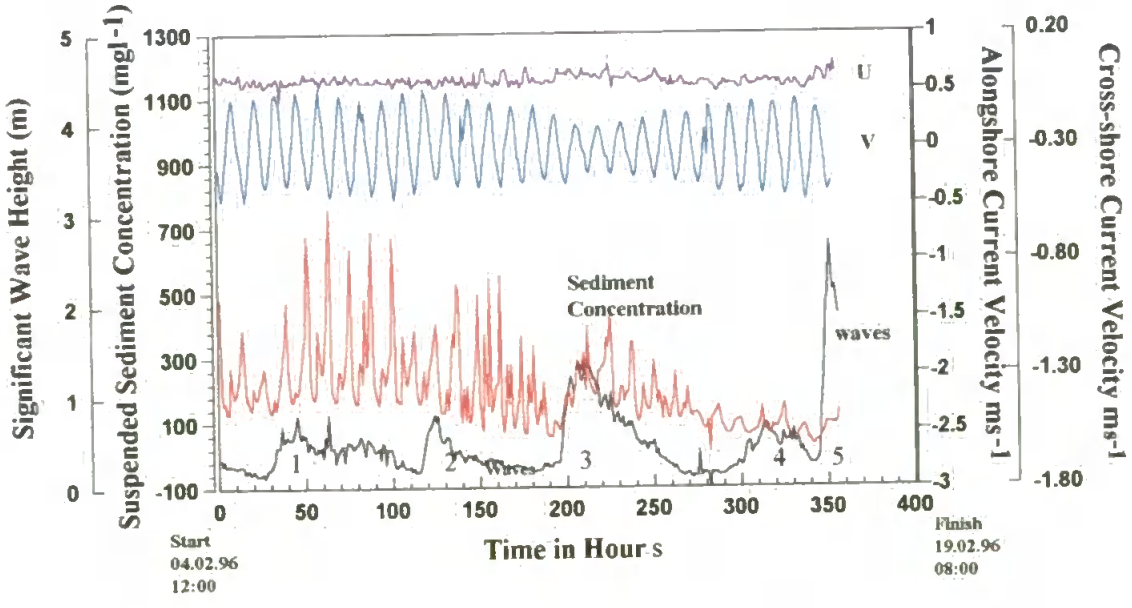

Figure 6.7 Burst averaged time series of SSC, wave activity and u, v flow components for February 1996 inner station.

Suspension peaks occurred at both high water and low water slack (observe peaks between hours 50-80), with maximum peaks again associated with the maximum tidal excursion to the North West, which was consistent with advection of a SSC gradient, increasing in concentration towards Spurn Head. There was a distinct decrease in background sediment concentration from 250 mgl^{-1} during springs to 150 mgl^{-1} during neaps, although the neap storm (storm 3) which occurred between hours 200 - 250 significantly increased the background levels. There was then a characteristic time delay to which the fine sediment settled out of suspension after this storm event.

6.3.5 February 1996 Outer Station - Time Series

A significant storm occurred 86 hours into the February '96 outer station deployment, lasting three days (figure 6.8). The fifth storm in the February 1996 deployment phase had a profound impact on the suspended sediment concentration. Background concentration levels prior to the storm were ~20 mgl^{-1}. These levels were noticeably lower than the levels monitored at the inner station, reflecting the formation of a concentration gradient, which suggests that suspended sediment decreased in concentration seawards. At the onset of the storm, background concentration levels peaked to ~120 mgl^{-1}. Higher suspension peaks ~230 mgl^{-1}, were then seen to occur after the storm, coinciding with the maximum spring tide.

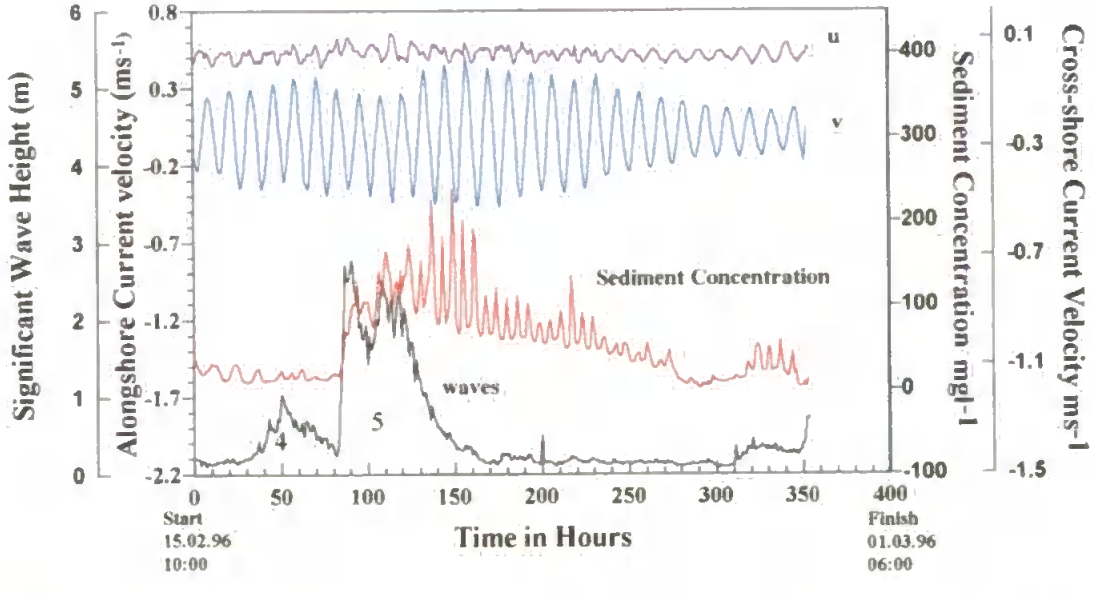

Figure 6.8 Burst averaged time series of SSC, wave activity and u, v flow components for February 1996 outer station.

Energy produced from the storm waves would have increased shear stresses felt at the seabed so that with increased shear stress more sediment could be resuspended. One hypothesis is therefore: the sudden sediment increase at the start of the storm could have been caused by local resuspension of the bed material. Another hypothesis is put forward that the sudden increase in the background concentration levels could have arisen due to the advection of a horizontal concentration gradient originating from the Humber estuary on the ebb tide. It is not obvious from the sediment concentration time series what process was the controlling factor for the sudden increase in background levels of SSC at the start of storm 5. To determine whether the increase in SSC is due to resuspension or advection some way of separating out the two signals from the SSC time series must be established. More of which will be discussed in the next section.

Interestingly, suspension peaks after the storm occurred a short time before maximum tidal streaming. These sediment peaks could not be the result of an advective process, since advection peaks exhibit M_2 tidal variation and arise near to or at slack water (see July 1995 inner station time series, figure 6.4a). The suspension peaks near to maximum tidal streaming could however be caused by resuspension of a surficial veneer of very fine non organic "fluff" material which would have settled out of suspension after the storm. This feature was recorded from the mooring data during the North Sea Project (Jago *et al.*, 1994) although the "fluff" they recorded was of a biogenic origin. Shear stresses would have dropped after the storm and only the finest material would have been resuspended by the maximum currents. Hence it is not the actual seabed material which is being resuspended but the fine background material which is normally in long-term suspension. Sediment resuspension from the activity of the tides gives rise to a quarter-diurnal sediment signal.

6.3.6 Satellite Imagery and *In Situ* Measurements to Support the Hypothesis That Sediment Peaks Occur Due to Advection

6.3.6.1 *Satellite Imagery*

This section considers the possibility that sediment peaks at or near to slack water seen in July 1995 and February 1996 time series, are due to advection of a concentration enriched plume which originates from the Humber estuary. It is postulated that the plume advects around Spurn Head and moves up past the Holderness coast on ebb tide into the vicinity of

the BLISS moorings. Data obtained from satellites can provide some of the synoptic data needed to study suspended sediments in estuaries and coastal shelf seas (Stumpf and Pennock, 1989). Several researchers have shown that total suspended matter or seston can be correlated with radiance data collected from satellite. For example; the Coastal Zone Color Scanner (CZCS) (Tassan and Sturm, 1986), and the advanced very high resolution radiometer (AVHRR) (Curtin and Legeckis, 1986; Stumpf, 1987). With regards to this thesis, AVHRR images of the Holderness Coast and Humber Estuary were obtained from the NERC Image Analysis Unit and examined for sea surface temperature and water colour.

The AVHRR is on board the NOAA TIROS-N (Television and Infrared Observation Satellite) platforms, which are polar-orbiting and sun-synchronous satellites that have one daytime and one night-time pass each day. The sensor scans from right to left in a line orthogonal to the direction of travel and the instantaneous field of view (IFOV) is 1.4 milliradians (1.1 km) and the distance between pixels is 0.8 km across track and 1.1 km along track. AVHRR measures radiation in five different wavebands, and table 6.2 gives the wavelengths measured by the AVHRR sensors aboard the NOAA series of satellites.

Table 6.2 Wavebands of the Advanced Very High Resolution Radiometer

Channel	**TIROS - n**	**NOAA 6,8 and 10**	**NOAA 7, 9, 11, 12**
1. Visible	0.55 - 0.9 μm	0.58 - 0.68 μm	0.58 - 0.68 μm
2. Near Infra-red	0.725 - 1 μm	0.725 - 1.1 μm	0.725 - 1.1 μm
3. Middle Infra-red	3.55 - 3.93 μm	3.55 - 3.93 μm	3.55 - 3.93 μm
4. Thermal Infra-red	10.5 - 11.5 μm	10.5 - 11.5 μm	10.3 - 11.3 μm
5. Thermal Infra-red	10.5 - 11.5 μm	10.5 - 11.5 μm	11.5 - 12.5 μm

Ocean colour is interpreted in terms of water quality parameters by the amount of light that is reflected from the sea surface in the visible wave band between 0.58-0.68μm. Contributions to ocean colour can be divided up into two areas; case 1 waters whereby the optical properties of the sea are dominated by phytoplankton and their degradation products only (open ocean), and case 2 waters, which have non-chlorophyll-related sediments or yellow substance *'gelbstoff'* instead of, or in addition to, phytoplankton, i.e. coastal waters (Robinson, 1985). The AVHRR has a radiometric resolution and dynamic range which is

favourable for studying moderately turbid to highly turbid waters (Gagliardini *et al.*, 1984). Sea surface temperature (SST) is determined from emitted radiance in the thermal infra-red or microwave spectral regions. The AVHRR has been designed especially to measure sea surface temperature and operates between 10.5 - 11.5 μm in the thermal infra-red.

It is difficult to obtain cloud free satellite images in winter. During February 1996 there were no clear images of the Humber - Wash area. However, two images were extracted from the January 1996 archive, to represent flood tidal conditions (28 January 1996) and ebb tidal conditions (14 January 1996). Plate 6.1 and 6.2 are colour scale images in °C to show sea surface temperature using the thermal infra-red wave band. The purple and blue areas depict zones of colder water. The SST image on 28 January 1996 (Plate 6.1) clearly shows a plume of much colder water spreading out from the Humber estuary and hugging the coastline down past the Wash, which is consistent with the southwards movement of the tidal current during flood. Plate 6.2 taken on 14 January 1996 illustrates ebb tidal conditions where the colder Humber water flows out of the estuary around Spurn head and advects up past the BLISS mooring sites. Note that the low surface temperatures measured by the AVHRR were ~3°C on both images and are similar to the bottom temperatures measured by the BLISS tripods in February 1996 (figure 6.9b). The SST image (plate 6.2) indicate that on ebb tide Humber plume water flows up past the BLISS moorings. If the Humber plume water has a high suspended sediment content, then this suspended sediment will be advected past the BLISS moorings on ebb tide as postulated at the start of the section.

Corresponding reflectance images for the 28th and 14th January 1996, plate 6.3 and 6.4 respectively were processed from the AVHRR visible wave band, to show the colour of the surface waters. The wavelengths used by the AVHRR in the visible band are such that the reflectance effects from chlorophyll in phytoplankton are minimal. In January, the concentration of phytoplankton in the Southern North Sea will be low, and correspondingly the reflectance from chlorophyll will also be low. The presence of suspended sediment on the other hand will have a high reflectance ratio and will overpower the chlorophyll signal. Notably the measured reflectance in plate 6.3 and 6.4 is more likely to be due to suspended sediment concentration than any other material.

High levels of sediment concentration will be proportional to high reflectance. In plate 6.3 high levels of suspended sediment which appear yellow to red on the reflectance scale,

correlate spatially with the colder water on the SST image which represents the Humber plume water(plate 6.1). It may be said therefore, that on ebb tide (as seen in plate 6.2), the concentration enriched Humber plume water seen in image of plate 6.3, will advect up past the BLISS moorings. Plate 6.4 shows the corresponding reflectance image taken on 14th January 1998. Notably, higher reflectance is measured around Spurn Head and is associated with the colder waters of the Humber plume. Unfortunately, the presence of cloud cover along the Holderness coast (which appears in black on the image, plate 6.4) masks the true colour of the water in this region.

Nevertheless, the SST images (plate 6.1 and 6.2) show that the colder waters of the Humber plume advects both north and south of the Humber estuary on ebb and flood respectively, and is associated with concentration enriched water as seen in the reflectance images (plate 6.3 and 6.4).

Plate 6.1 28th January 1996 - Humber, Wash region - SST - Thermal infra-red- AVHRR

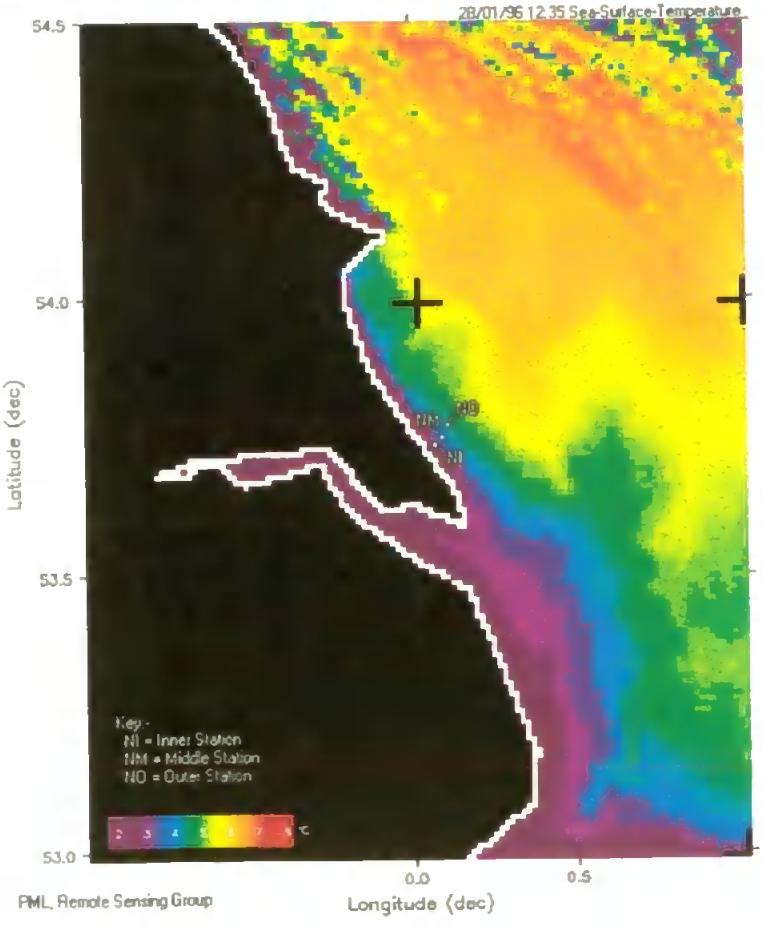

Plate 6.2 14th January 1996 - Humber, Wash region - SST - Thermal infra-red - AVHRR

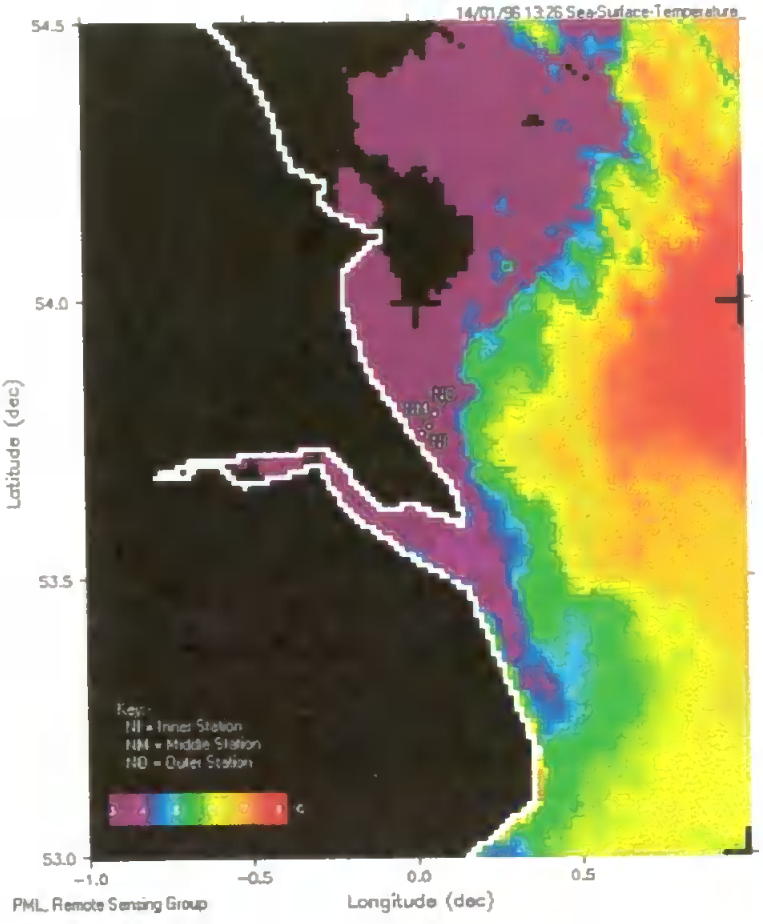

Plate 6.3 28th January 1996 - Humber-Wash region - Reflectance - visible band - AVHRR

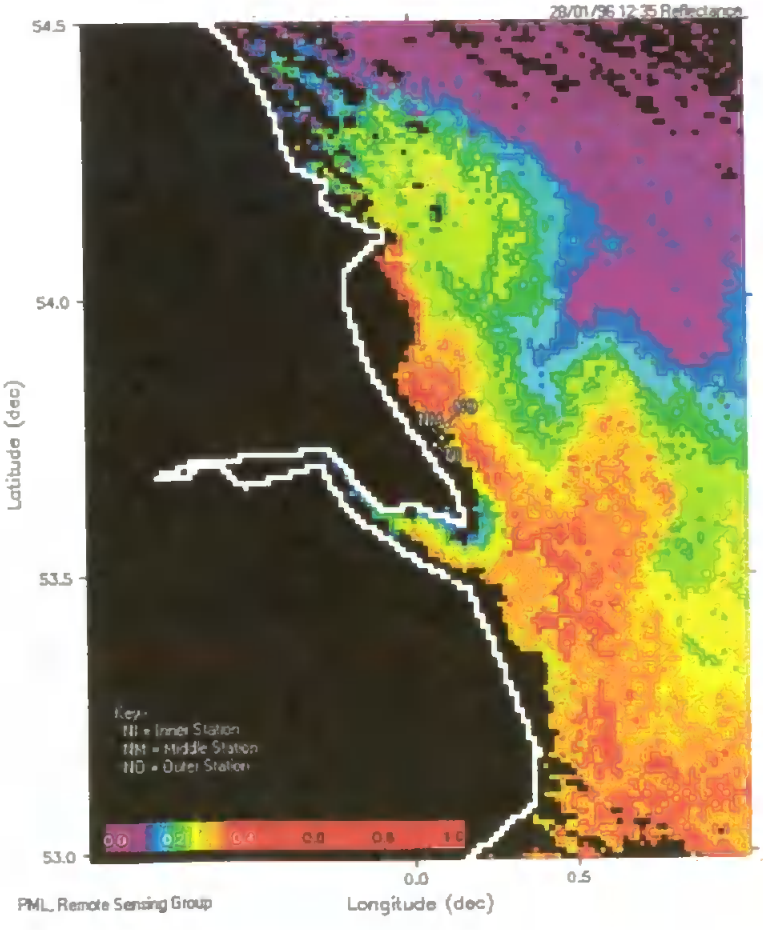

Plate 6.4 14th January 1996 - Humber-Wash region - Reflectance - visible band - AVHRR

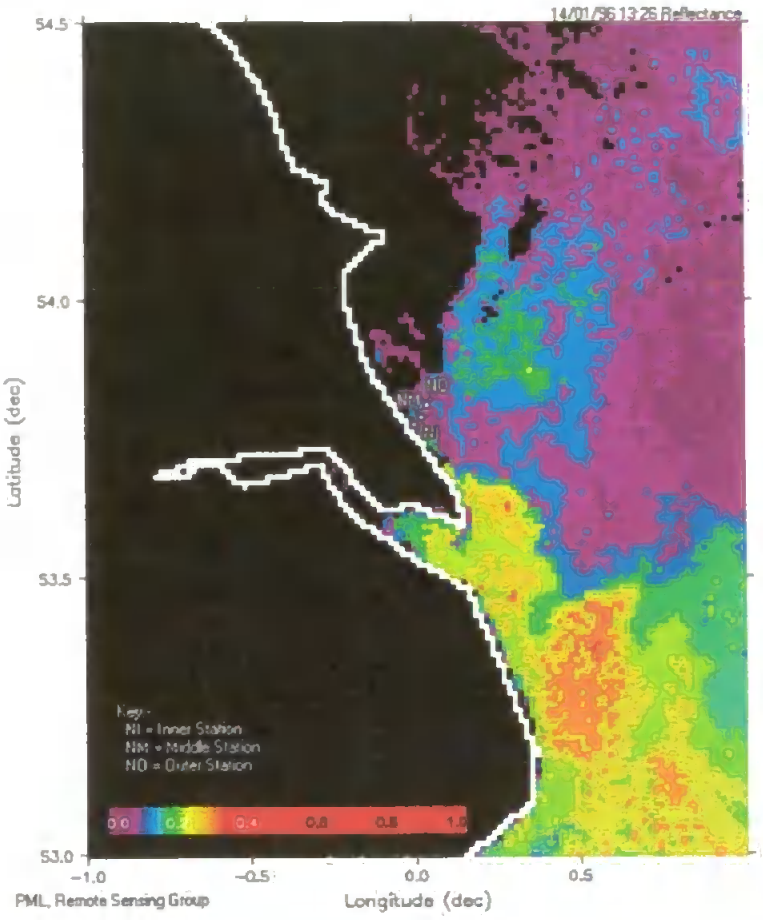

6.3.6.2 *In Situ Measurements*

In situ BLISS time series measurements of temperature, salinity and suspended sediment concentrations were analysed for June/July 1995 and February 1996 deployments. Figure 6.9a and 6.9b represent scatter plots of salinity Vs temperature for each summer and winter deployment respectively. As expected, a negative correlation was produced in summer (figure 6.9a), as opposed to a positive correlation in winter (figure 6.9b), due to the larger thermal inertia of the deeper, more saline waters.

a. Summer (June/July 1995 inner station)
Low salinity - water warmer

b. Winter (February 1996 outer station)
Low salinity - water cooler

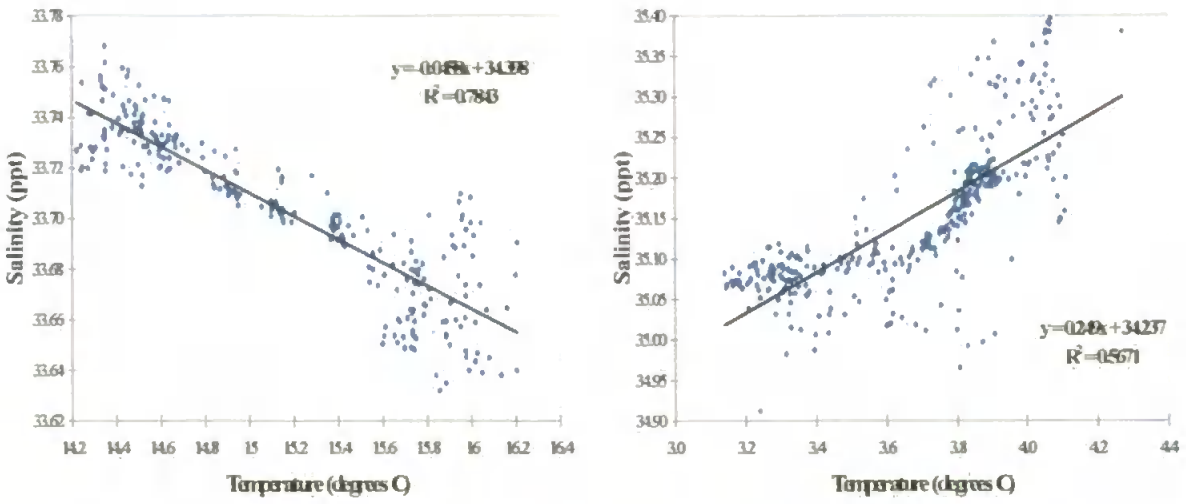

Figure 6.9a & b Scatter plot to show salinity Vs temperature for summer and winter BLISS deployments.

The increase in temperature experienced over the two weeks at the inner station in June/July 1995, was either attributed to solar heating at the surface (figure 6.10) or due to warmer water being present in the Humber plume, or both. In winter, the BLISS inner and outer station salinity measurements suggested that there was a bottom salinity gradient from the inshore station to the offshore station (29.8‰ to 35.4‰) respectively.

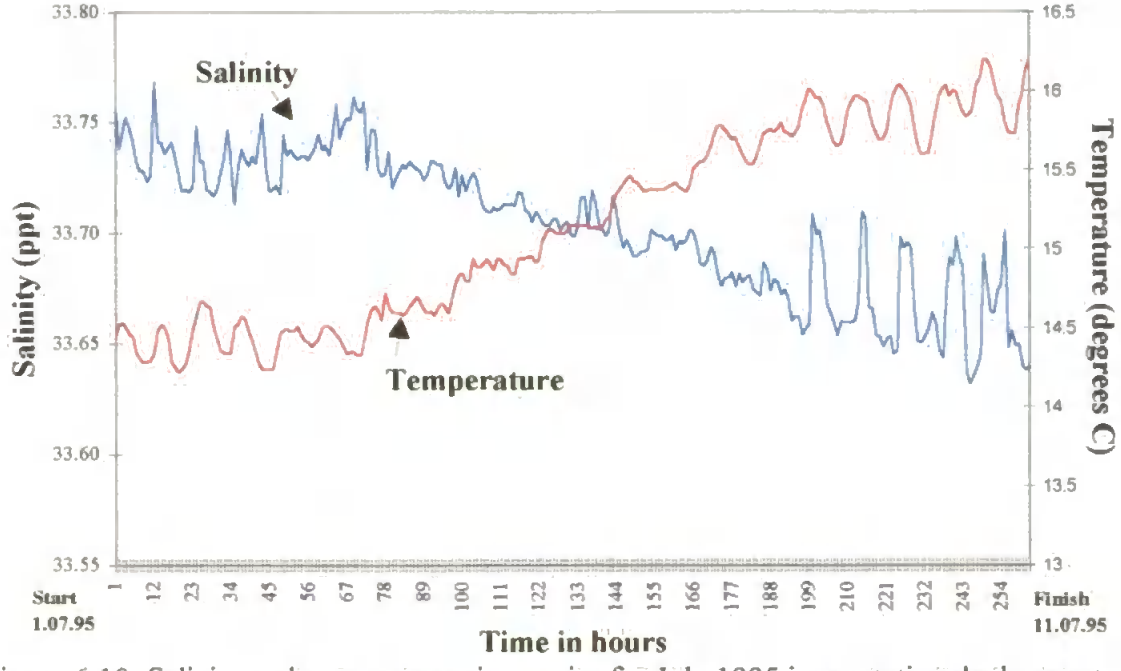

Figure 6.10 Salinity and temperature time series for July 1995 inner station deployment

Salinity and temperature are two independent parameters in sea water which exhibit conservative properties such that below the surface there are no significant processes by which either quantity is changed except by mixing. Assuming that suspended sediment concentration is highest in low salinity waters (for example at the turbidity maximum of an estuary) and decreases in concentration with increasing salinity to pure sea water, a sudden increase in concentration and a decrease in salinity seen at the outer station in February 1996 (figure 6.11A) may suggest advection of a plume of less saline water which has a high sediment content. It is hypothesised that the plume of less saline sediment enriched water originates from the Humber estuary seeing that there is no obvious relationship to salinity from cliff erosion and sediment resuspension.

Figure 6.11B is a scatter plot of salinity and concentration taken for the full February 1996 outer station time series, assuming that there is a correlation between salinity and concentration. February outer station was chosen because this deployment recorded the largest storm (storm 5). It is clear that the correlation between salinity and concentration varies during the deployment. To determine the variation over the deployment, the salinity and concentration time series data for February 1996 outer station was split up into five sections. Section 1 (figure 6.12a) was a scatter plot of salinity and concentration to represent pre storm (0-30 hours) no wave conditions. Section 2 (figure 6.12b) represented storm 4 (31-85 hours) wave conditions.

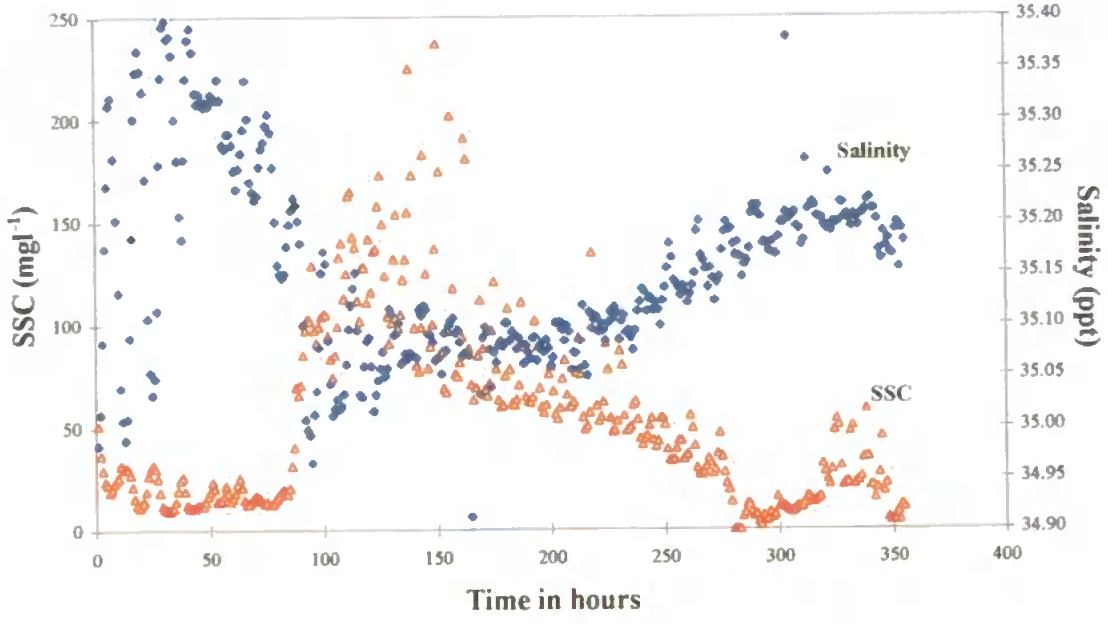

Figure 6.11A Plot to show suspended sediment concentration (0.41mab) against salinity for February 1996 outer station.

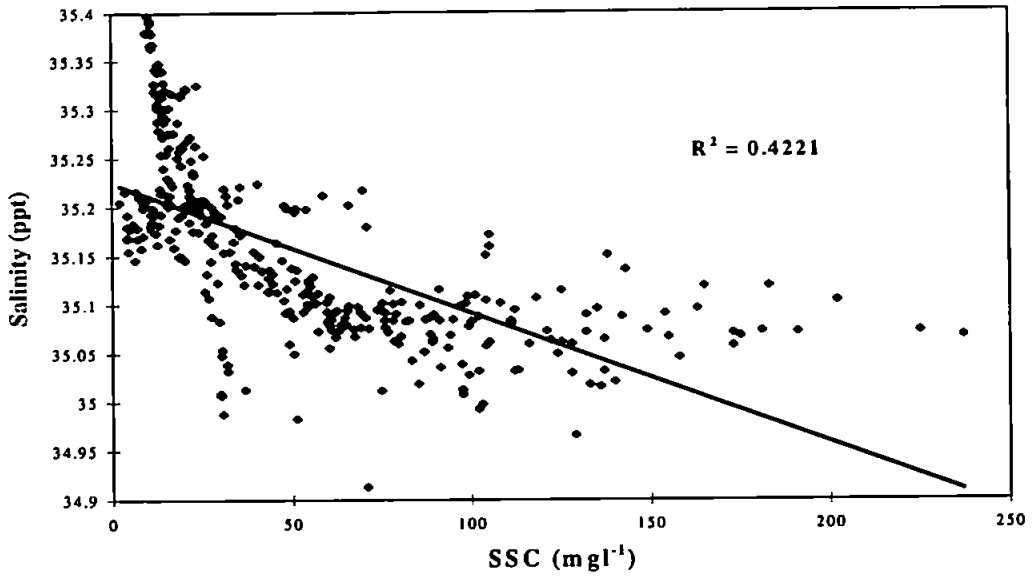

Figure 6.11B Scatter plot to show correlation between salinity and concentration for February 1996 outer station time series

Section 3 (figure 6.12c) showed storm 5 conditions (85-150 hours). Section 4 represented post storm conditions (151-280 hours). The optical sensor then malfunctioned for some reason at hour 281 giving no output for 4 hours. It started working again at hour 285, so the last section represents post storm conditions between hours 285-356.

There was a negative correlation between salinity and concentration before the storm (figure 6.12a) although the background sediment concentrations remained constant between 10 - 30 mgl^{-1}. The second storm section (figure 6.12b) again showed a negative correlation between concentration and salinity but this time the data was more scattered. Referring back to the time series plot of concentration and salinity (figure 6.11), the salinity at which the concentration suddenly increased was ~35.2 ‰. It is suggested that this value characterises the coastal waters off Holderness. Values below 35.2 ‰ suggest the presence of Humber plume water. The possibility that the reduction in salinity was the result of mixing of water from the surface was ruled out by CTD profiles, conducted during the 13 hour stations, which showed a vertically well-mixed water column at all times. There is evidence to suggest therefore that the sudden increase in the background concentration could be due to advection of the sediment rich Humber plume water into the mooring site, although this suggestion is not clear cut, because from the time series plot (figure 6.8) it is clear that the waves also play an important role.

a) Pre storm no wave conditions

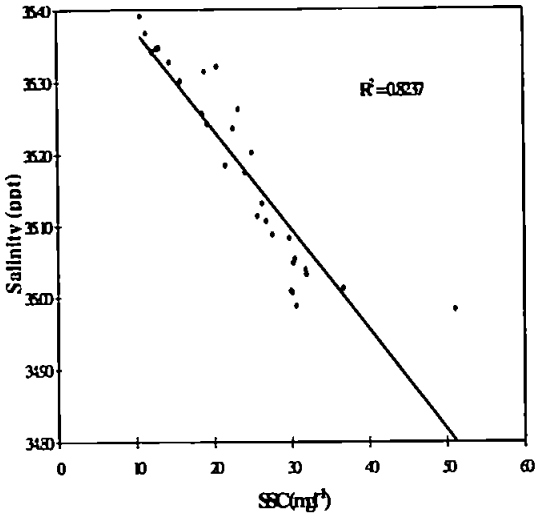

b) Pre storm small wave conditions

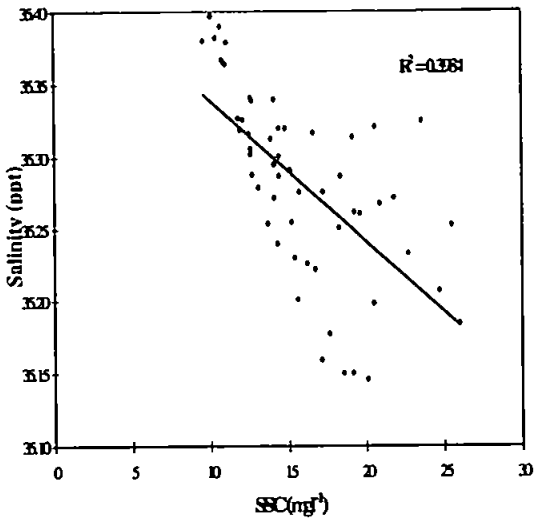

c) Storm conditions

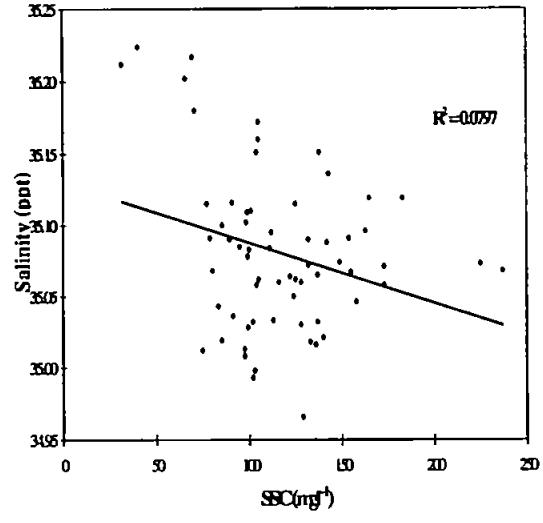

d) Post storm conditions

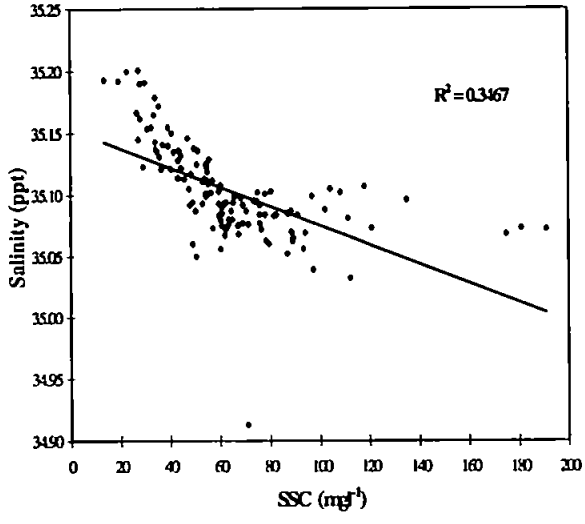

e) Post storm conditions

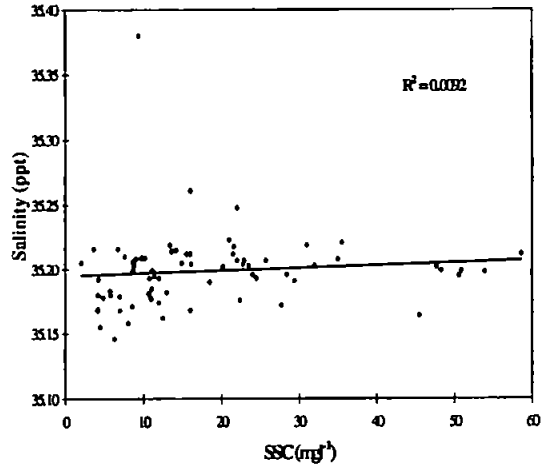

Figure 6.12 February 1996 outer station salinity and concentration time series; b) scatter plot of salinity Vs concentration pre-storm (a and b) storm (c) and post storm conditions (d and e).

Whether the waves resuspend the bed material locally or whether the waves enhance the levels of suspended sediment to the south of the mooring which is then advected into the BLISS site is not so obvious from this means of extracting advection from resuspension using salinity as an indicator of advection.

A resuspension signal is however separated out successfully during the storm. The salinity maintains a steady value between 34.95‰ and 35.1‰ (figure 6.12c) which characterises the salinity of the Humber plume water. A further increase in the concentration peaks occurred during the storm but the salinity stayed the same. This material could not therefore be advective material but was probably material being resuspended from the seabed by wave activity. After the storm (figure 6.12d) the salinity increased and the suspended sediment decreased at the mooring site as the Humber plume retreated. Whereas there was a large reduction in sediment concentration, the salinity increased only a small amount which suggested that the turbidity plume front was much sharper than the salinity plume front. The last scatter plot (figure 6.12e) shows background concentrations varying between 3 mgl^{-1} and 50 mgl^{-1} with a constant salinity value of 35.2‰.

6.3.7 Decay Time and Settling Velocity

Most prominent in the February 1996 outer station SSC time series (figure 6.8) was the characteristic time lag for the sediment in suspension to reach pre-storm levels again once the fifth storm had passed and after the spring tides. Two exponential curves were fitted to the SSC time series between hours 110-279 and hours 88-End (figure 6.13). Assuming an exponential decay rate for suspended sediment concentrations (Prandle, 1997) as:

[6.1]

$$C(t) = C_0 e^{-\alpha t}$$

where α = decay rate = 1/e folding time

t = time

C_0 = Concentration at time $t = 0$

The exponential folding time also known as the e-folding time, is the time it takes for the sediment to settle out of suspension to reach the concentration C_0/e and was calculated from the equations as follows:

(Hours 110 - 279), the exponential curve forms the equation:

$$\text{Concentration} = 154.8e^{-0.0092(169-n)}$$

$$C = 154.8e^{-0.0092 \times 169}e^{-0.0092n}$$

where n = folding time (time of 50% loss).

therefore:

$$e^{-1} \text{ occurs at } 0.0092n = 1$$

$$n = 1/0.0092$$

$$\text{e-folding time} = \mathbf{108.7} \text{ hours}$$

(Hours 88 - 355), the exponential curve forms the equation:

$$\text{Concentration} = 173.9e^{-0.0099(267-n)}$$

$$C = 173.9e^{-0.0099 \times 267}, e^{-0.0099n}$$

therefore:

$$e^{-1} \text{ occurs at } 0.0099n = 1$$

$$n = 1/0.0099$$

$$\text{Exponential folding time} = \mathbf{101} \text{ hours}$$

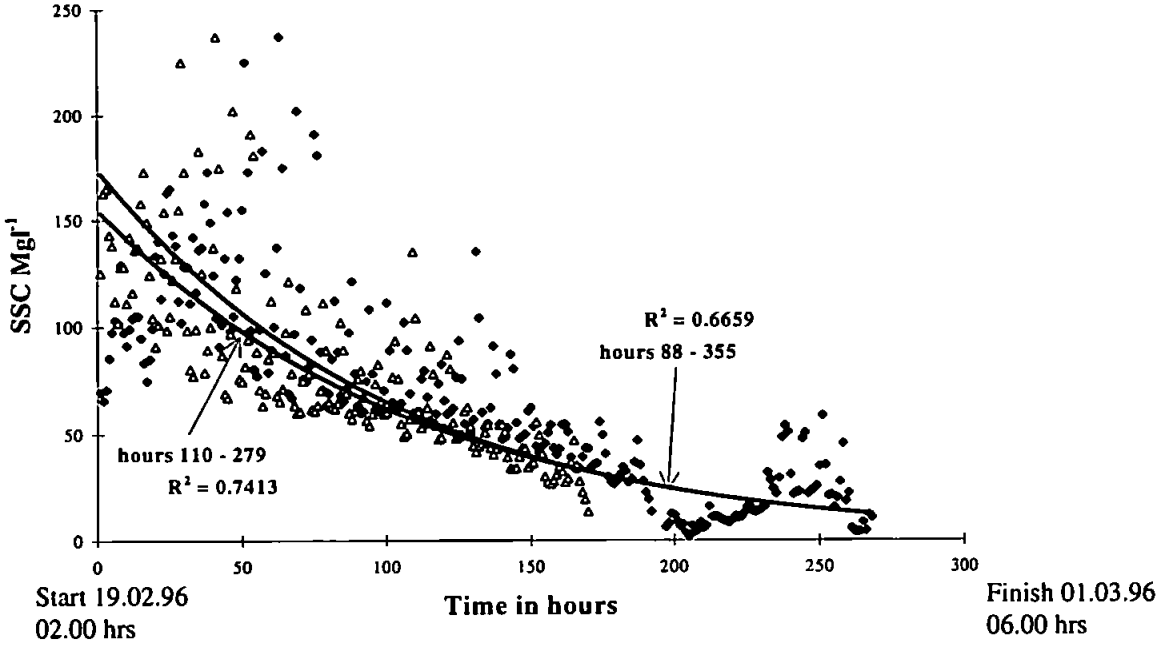

Figure 6.13 Exponential decay curves fitted to February 1996 outer station SSC time series

The exponential folding times of 108.7 and 101 hours represent sediment loss equivalent to 1/e of 39.99% and 37.16% respectively, of the initial SSC.

Taking a value of 0.6 ms^{-1} to represent the maximum tidal amplitude at the outer station, and an average water depth of 18m, it was possible to derive a value for the vertical eddy dispersion coefficient E of ≈ 0.02 m^2s^{-1} from figure 6.14, calculated by Prandle (1997).

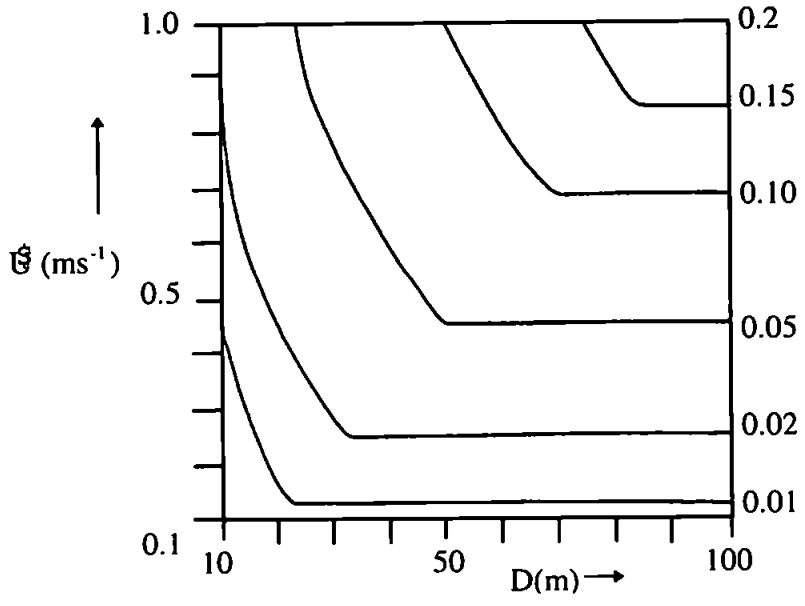

Figure 6.14 Vertical eddy dispersion coefficient E in m^2s^{-1}
(From: Prandle, 1997).

Taking Prandle's derivation for the decay rate α, as:

[6.2]

$$\alpha = 0.693 \frac{w_s^2}{E}$$

where w_s = settling velocity (ms^{-1})

the settling velocity for the SSC at the outer station could be determined by rearranging the equation as follows:

Hours (110-279)

[6.3]

$$0.0092 = 0.693 \frac{w_s^2}{E}$$

$$w_s = \left[\frac{0.0092}{0.693} \times \frac{0.02}{3600} \right]^{\frac{1}{2}} ms^{-1}$$

$$= \left[\frac{1.84}{0.693 \times 3600}\right]^{\frac{1}{2}} \times 10^{-4}\ ms^{-1}$$

$$w_s = 2.71 \times 10^{-4}\ ms^{-1}$$

Hours (88-End)

$$0.0099 = 0.693\frac{w_s^2}{E}$$

$$w_s = 2.81 \times 10^{-4}\ ms^{-1}$$

Comparing these settling velocities to (Dyer, 1986, figure 4.2, p. 111), suggests that much of the sediment in suspension off Holderness is composed of a very fine silt and clay like structure. Adopting the same procedures as above, the SSC exponential folding times and settling velocities were also calculated for the February 1996 and June/July 1995 inner station storm conditions (Table 6.3). The first storm in the July 1995, data set (hour 65, figure 6.4a) was chosen to represent the sediment conditions, primarily because it was followed by a period of zero wave activity. In the February 1996 inner station data set there was one significant storm event which occurred during neap tides between hours 190-260 (figure 6.7). Maximum tidal amplitude was taken as 0.5 ms^{-1} and 0.45 ms^{-1} for the February and July inner stations respectively, and water depth for the inner station was taken as 12m. These values gave a vertical eddy dispersion coefficient E of 0.01 m^2s^{-1}.

The e-folding times and settling rates calculated for February 1996 inner station, showed negligible variation with height above the seabed. The results did vary depending on whether the exponential decay curves were fitted to the concentration data at the start of the storm or in the middle of the storm. The effect from the former case to the latter case was to reduce the e-folding rates from ~129 hours to 95 hours and to cause a small increase in the calculated settling velocities. Both the February inner station and February outer station storm conditions produced similar settling velocities and e-folding times. Higher settling velocities were experienced at the outer station.

Table 6.3 E folding times and settling velocities calculated for February 1996 inner /outer stations and June/July 1995 inner station

February 1996 inner Station (figure 6.7)				
	Height above bed (m)	Equation	E Folding time (in hours)	Settling Velocity Ws (ms^{-1})
Storm (190-356)	0.43	$C=198.41 \exp^{-0.0077x}$	129.87	1.7568×10^{-4}
	0.93	$C=206.46 \exp^{-0.0077x}$	129.87	1.7568×10^{-4}
Storm (210-356)	0.43	$C=221.83 \exp^{-0.0105x}$	95.24	2.05152×10^{-4}
	0.93	$C=231.46 \exp^{-0.0106x}$	94.34	2.06127×10^{-4}
February 1996 outer station (figure 6.8)				
Storm (110-279)	0.43	$C=154.8 \exp^{-0.0092x}$	108.7	2.71×10^{-4}
Storm (88-355)	0.43	$C=173.9 \exp^{-0.0099x}$	101	2.81×10^{-4}
June/July 1995 inner station (Figure 6.4a)				
Storm (65-150)	0.43	$C=1.522 \exp^{-0.0258x}$	38.76	3.21582×10^{-4}
	0.93	$C=6.4631 \exp^{-0.0022x}$	454.5	9.3906×10^{-5}

From these results it can be suggested that during February 1996, settling velocities in the nearshore zone off Holderness ranged from ~1.7×10^{-4} to $2.8 \times 10^{-4} ms^{-1}$ depending on the severity of the storm. E-folding times ranged from 95 to 129 hours depending on whether the data was taken from the start of the storm or the middle of the storm to the end of the record.

In response to a summer storm, the SSC exhibited marked variation in the e-folding time and the settling velocities with different heights above the seabed. Measurements taken at 0.41mab showed a short e-folding time of ~39 hours, whereas at 0.9mab the e-folding time was calculated to be ~ 454 hours. As mentioned already in section 6.3.2, SSC measurements were greater at 0.9mab, but it was not clear whether the higher values experienced at 0.9 mab were due to offset error or were in fact a genuine phenomena. The

particular storm in question was not very large (H_{sig} 0.41m), and clearly did not suspend sediment high up into the water column. The sediment in suspension appeared to reach pre-storm levels quickly (figure 6.4) and in light of this, the lower e-folding time of ~38 hours seemed the most credible for a summer storm at the inner station. The corresponding settling velocities were also noticeably different, being typically much smaller in response to the higher e-folding time. What is clear from these results, is that winter storms suspend significant amounts of sediment up into the water column, so increasing the amount of sediment available for sediment transport, which is further aided by the amount of time it takes for the sediment to settle out to pre-storm levels. In winter therefore, significant sediment transport will occur in response to the storms, but in summer, it is clear that the e-folding time is very sensitive to the absolute values of SSC, and with offset problems, doubt is cast on the validity of the values.

6.4 Bed Shear Stress Estimates

Measurements of the near bed turbulent velocities u', v' and w' taken from the EMCMs on BLISS were used to calculate bed shear stresses following the three procedures outlined in sections 5.5.2/3/4. Results presented are from the June/July 1995 and the February 1996 deployments. Intercomparisons were made between the three methods, so that a choice could be made on which method or combination of methods was the most suitable to represent the BLISS data.

The current velocity data were rotated in the horizontal, using Pugh's estimation (1987) (section 5.8.1). No vertical rotations were performed on the data, because the pitch and roll measurements from each deployment, indicated that each tripod was within 1° of vertical, suggesting that the tripods were sitting horizontally on the seabed. The Reynolds stress (RS) method is sensitive to sensor alignment (Huntley, 1988) and the Inertial Dissipation (ID) method does have a small dependency on orientation, but is generally insignificant (Pers. Comm., Huntley, 1997). The Turbulent Kinetic Energy (TKE) is not affected by sensor alignment because it is based on a different theoretical approach.

There are uncertainties with all three methods, and there is no one method which we can say is the most suitable to calculate shear stress. Sensor alignment plays a major role in the accuracy of the Reynolds stress method. Complete separation of the fluctuations due to the

waves from the fluctuations due to turbulence is important for the accuracy of the TKE method, and is achieved for the BLISS data by interpolating across the base of the wave band as suggested by Soulsby and Humphrey (1989) (figure 5.1). The ID method estimates shear stress by using the spectra of the turbulent fluctuations to find a $K^{-5/3}$ run-off relationship between wave number (K) and spectral energy within a sub-range of the spectrum to infer turbulence (Huntley, 1988). Uncertainty in the IDM results may arise when the ID method, regardless of whether the turbulent spectrum shows a $K^{-5/3}$ runoff, still looks for a $K^{-5/3}$ runoff in the data.

The horizontal (u, v) velocities derived from both the EMCM horizontal velocity measurements were combined with the vertical velocities (w) on each EMCM to calculate bed shear stress. If the EMCM sensors were aligned properly on the BLISS tripod with the vertical sensor pointing positive upwards, then the velocities measured by each current meter should in theory be very similar in magnitude. The vertical velocity component on EMCM 1 did not operate during the February 1996 outer station deployment because of a faulty connector. As a result, all shear stresses were calculated using the horizontal velocities (u v) derived from both EMCMs together with the vertical velocities measured by EMCM 2. In the July 1995 inner station deployment, the vertical velocity component on EMCM 2 malfunctioned so all shear stresses were calculated using the u v velocities (determined using x and y horizontal velocities from EMCM 1 and 2) and the vertical velocities from EMCM 1. For the February 1996 inner station and the July 1995 middle station deployments, the vertical velocity probes on EMCM 1 and 2 were working correctly. Shear stress measurements were taken for each vertical velocity component, by combining with the same horizontal rotated velocities (derived from both EMCMs).

6.4.1 Comparison of the Reynolds Stress, Turbulent Kinetic Energy and Inertial Dissipation Methods for Calculating Bed Shear Stress and Friction Velocity

Figure 6.15 shows a representative velocity spectra of the cross-shore velocity from which the wave and turbulence variance bands are defined in the TKE method. The area above the line is taken to be the wave variance and the area below the line to be the variance due to the turbulence.

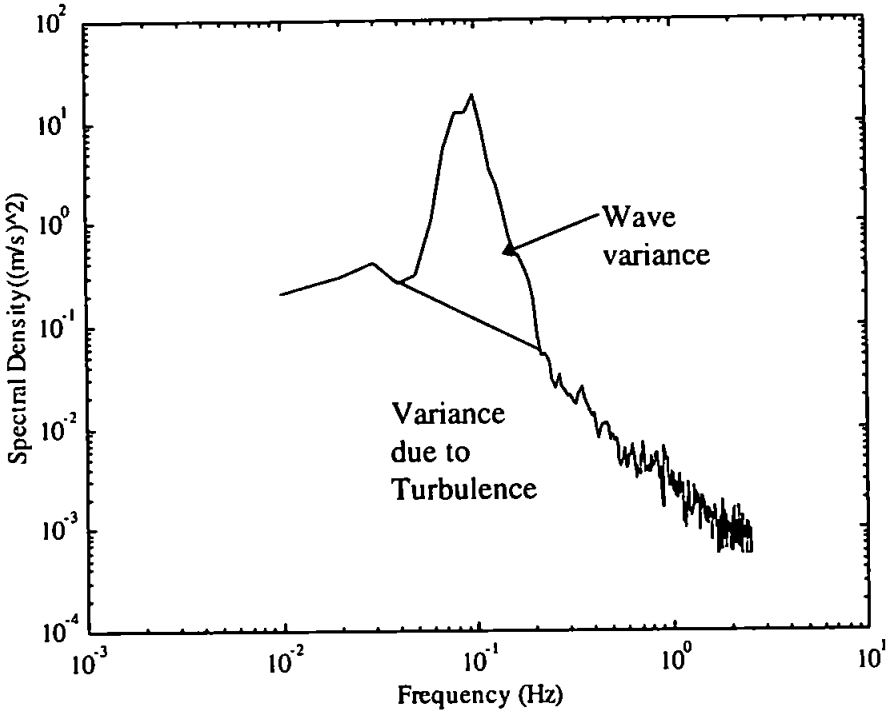

Figure 6.15 Spectrum of cross-shore velocity time series showing areas of variance due to waves and to turbulence.

Separation of the wave and turbulence variance was achieved by following the procedure outlined by Stapleton and Huntley, (1995) (see appendix B for programme details) whereby the limits of the incident wave band are determined by visual inspection of the cross shore velocity spectrum. However, there were at times, in some of the data runs, uncertainty to whether all the wave variance was removed from the spectrum, because the limits are actually defined by eye, and may vary from person to person.

The ID method calculates shear stress by using only a small part of the vertical spectrum in the inertial sub-range which gives a $K^{-5/3}$ roll-off. The method is subject to errors if the lower limit of the inertial sub-range encroaches into part of the wave band region. Conversely, errors may also arise if the upper limit of the inertial sub-range is close to the Nyquist Frequency which then interferes with the flow meter roll-off settings. Figure 6.16 represents a typical vertical velocity spectra taken from the February 1996 outer station data set showing the expected inertial sub-range limits.

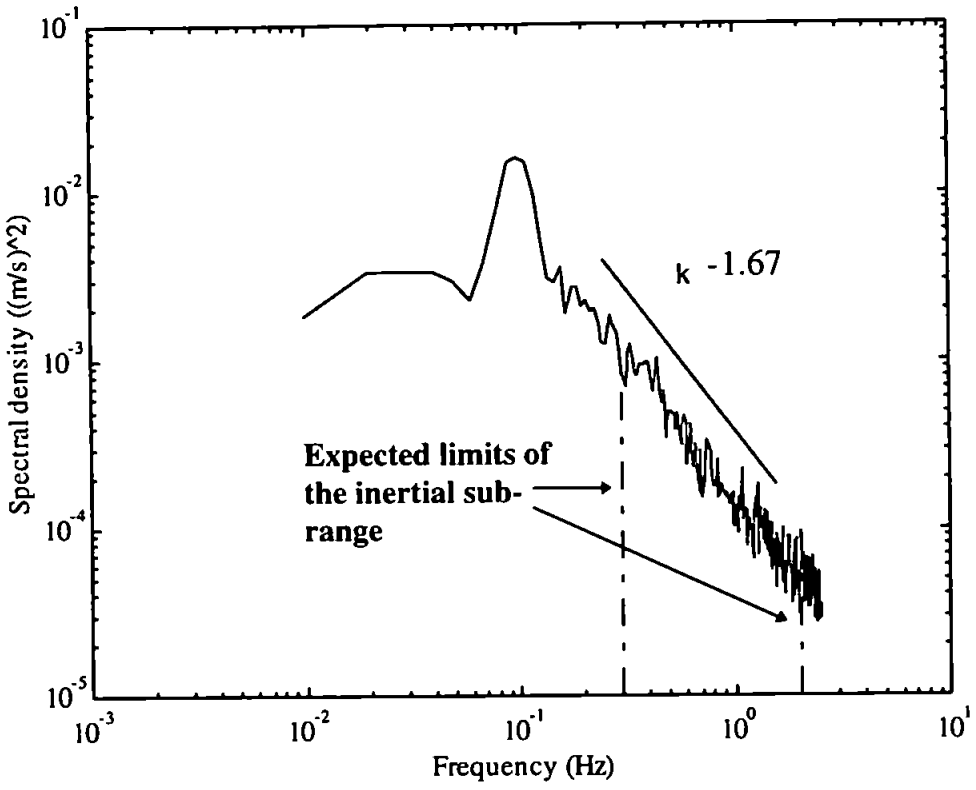

Figure 6.16 Spectrum of vertical velocity time series showing expected limits of the inertial sub-range and -5/3 roll-off.

A suitable cut-off frequency which marks the lower limit of the inertial sub-range is taken from figure 6.16 to be 0.3 Hz and the upper limit taken as 2 Hz. These limits were incorporated as an "if" statement into the ID programme (see Appendix B for details), whereby for example if the predicted limits were less than 0.3 or greater than 2, the limits were reset to 0.3 and/or 2. Computing the ID shear stress in this way ensured that the values taken from the vertical spectrum to calculate the ID shear stresses were within the inertial sub-range limits.

Figure 6.17 shows a scatter plot of u_* derived from the ID and TKE methods for February 1996 outer station. There is correlation between the two methods although there is some scatter with the TKE results. The u_* time series for the RS, TKE and ID methods (figure 6.18) indicated that most scatter in the TKE method arose during the large storm (figure 6.8, hr 85-150) which may be the result of insufficient separation between the fluctuations due to the waves and the fluctuations due to turbulence. The RS method produced the largest u_* results.

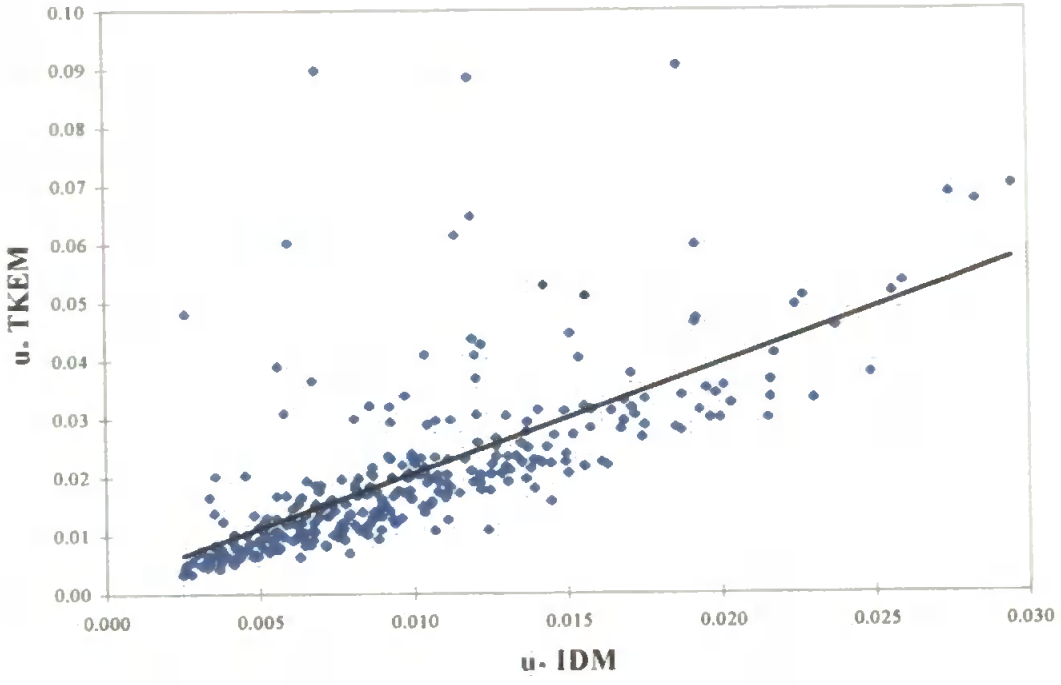

Figure 6.17 Scatter plot to show friction velocity u_* derived from the TKE and ID method - BLISS data taken from February 1996 outer station.

Figure 6.19 a and b show time series of u_* calculated for the February 1996 inner station period. Largest variation between each method occurred during wave conditions (refer to figure 6.7) between hours 200-250. There was close correlation between each of the TKE u_* estimates with an R^2 value of 0.99 which suggested that the vertical velocities measured by each EMCM were very similar in magnitude.

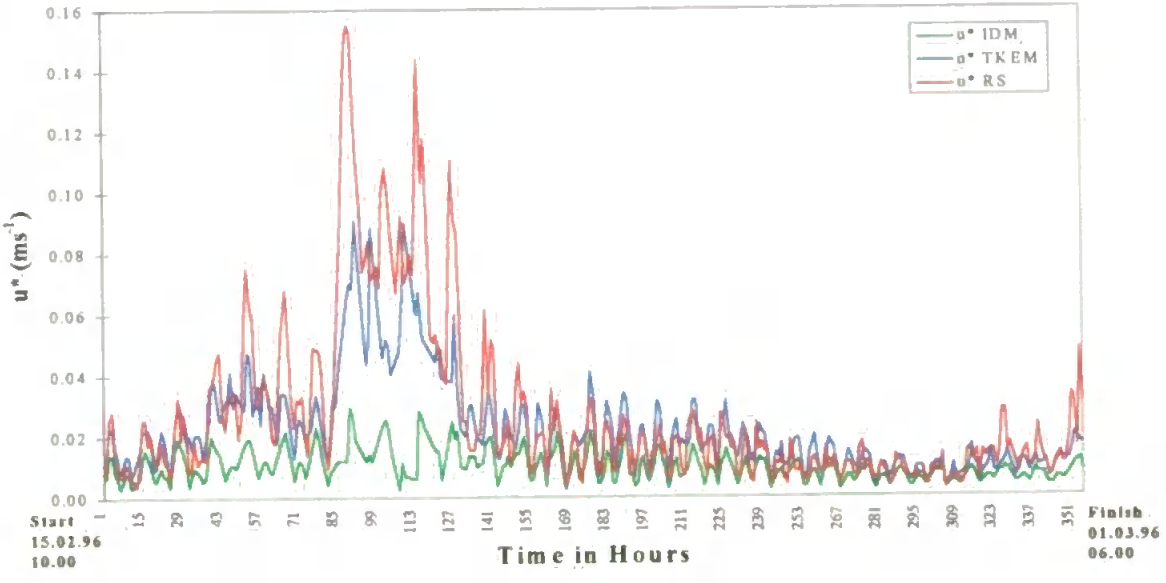

Figure 6.18 Time series to show u_* derived from the RS, TKE and ID method. BLISS data taken from February 1996 outer station.

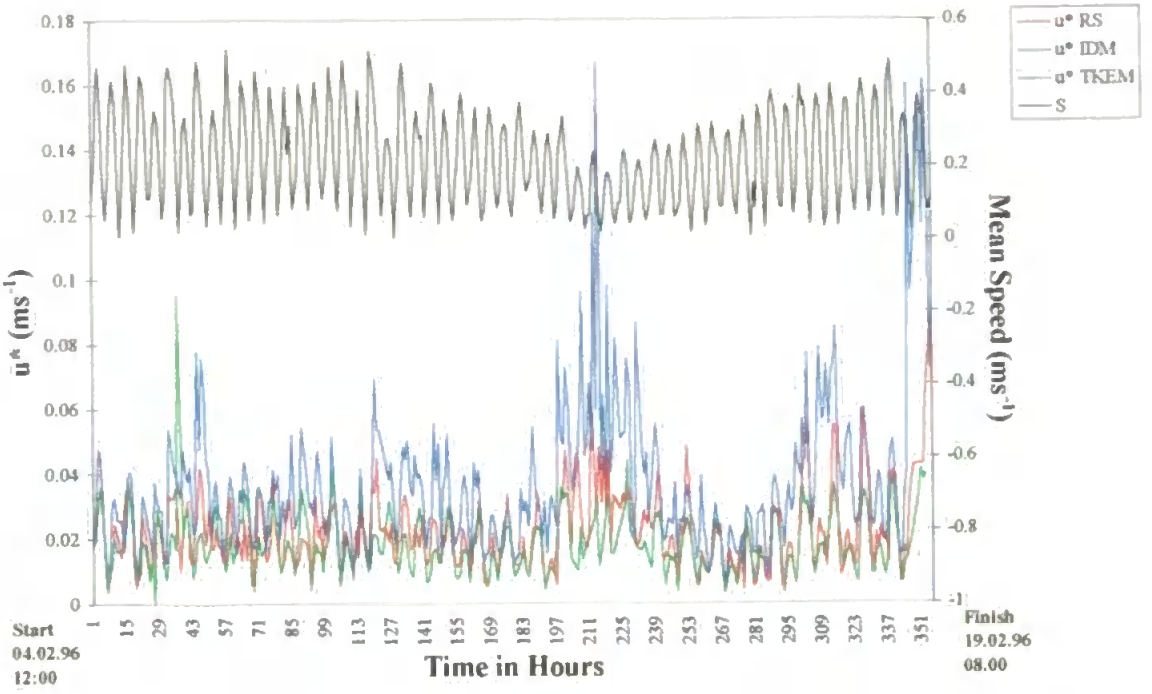

Figure 6.19a Time series to show u* derived from the RS, TKE and ID method. BLISS data taken from February 1996 inner station (the vertical velocity was measured by EMCM1).

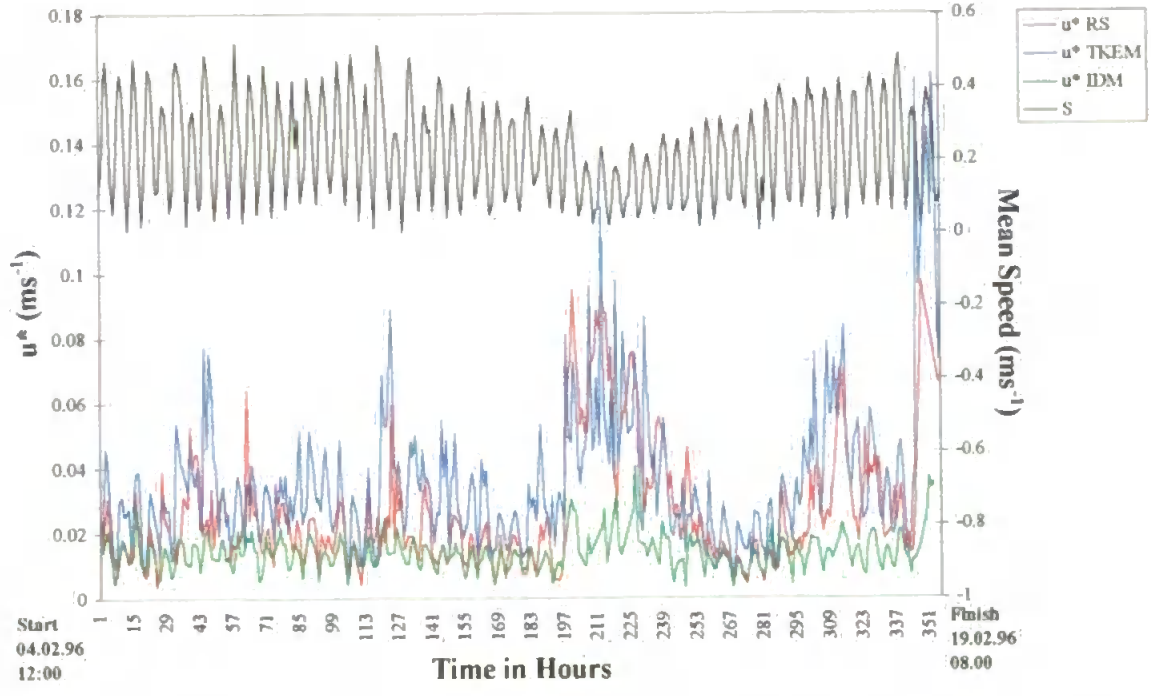

Figure 6.19b Time series to show u* derived from the RS, TKE and ID method. BLISS data taken from February 1996 inner station (the vertical velocity was measured by EMCM2).

Clearly from the February 1996 inner and outer station time series, the value of u_* increased during storms in all three methods. A strong semi-diurnal signal was prominent for all methods and peak stresses occurred either before or just after maximum tidal streaming.

Figure 6.20 show time series of u_* derived for the June/July 1995 inner station deployment which typifies a period of calm summer conditions. u_* is seen to vary with the spring/neap tidal cycle being greatest at springs. The values also showed strong semi-diurnal signature with maximum u_* values arising at maximum current velocity as expected. Similar to the outer station results (figure 6.18), the RS method produced the largest u_* values. There was significant correlation between the TKE and IDM methods with an R^2 value of 0.8.

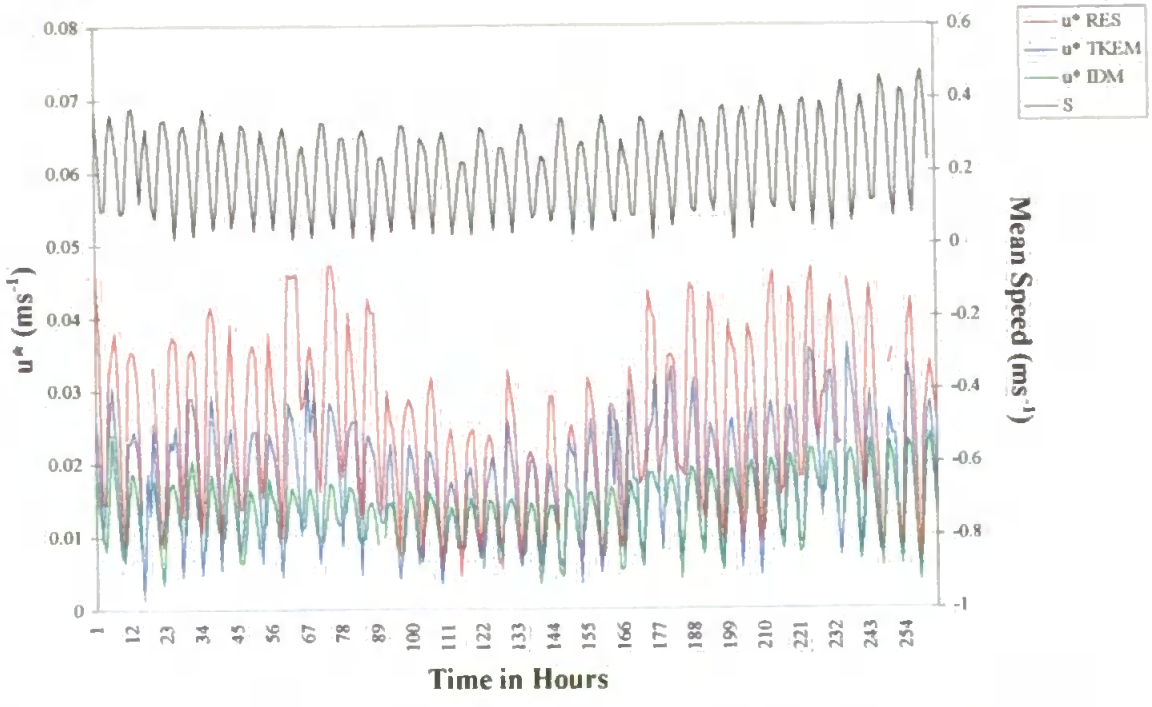

Figure 6.20 Time series to show u_* derived from the RS, TKE and ID method. BLISS data taken from July 1995 inner station.

6.4.2 Discussion of Three Methods

The Reynolds Stress method consistently produced the largest u_* values. The Turbulent Kinetic Energy method produced results that ranged between the Inertial Dissipation u_* values and the RS u_* values. Largest variation between the three methods occurred during storms. This was most noticeable in the February 1996 outer station data set. Because the RS method is so sensitive to sensor alignment, i.e. in combined wave-current flows, a 1°

RS method is so sensitive to sensor alignment, i.e. in combined wave-current flows, a 1° shift in the vertical will induce errors in the shear stress estimation as large as 156% (Soulsby and Humphrey, 1989), it was decided not to use the RS u_* results for any further calculations, knowing that the February outer station BLISS rig for example, shifted a total of 16° in the horizontal and ~ 2° in the vertical in response to the large storm starting at hour 85 (figure 6.8). There are uncertainties with both the TKE and ID as mentioned earlier in the section. The TKE method may incorporate some wave band variance into its calculations, which may cause an over-estimation to the u_* values, although by looking at the velocity spectra for every data run should minimise this uncertainty. The ID method in some cases may not produce the necessary $k^{-5/3}$ roll-off in the vertical velocity spectra, which may cause an under-estimation or an over-estimation in the u_* values. Both methods gave reasonable u_* results, and were similar in magnitude during the calm conditions, although they differed most noticeably during storm conditions. It was therefore decided to combine the u_* results from both TKE and ID method and take the average u_* values for future calculations.

All three shear stress methods made an assumption that the velocity measurements were taken within the constant stress layer of the bottom boundary layer (eg. Huntley, 1988). The assumption of a logarithmic distribution of average velocity with height is found to be still valid for wave plus current conditions (Kemp and Simons, 1983). The boundary layer thickness in neutrally stratified water (i.e. mixed) on the continental shelf can be estimated by Grant and Madsen, (1986) as

$$\delta = 0.4u_*/f \qquad [6.4]$$

where u_* is the friction velocity obtained from the relationship $\tau_0 = \rho u_*^2$, and f is the Coriolis parameter. At the latitude of the Holderness coast f = 1.169 x 10^{-4} sec^{-1}. Typical peak shear stress values determined from the BLISS data using the three methods were approximately, 1.2 - 3.5 Nm^{-2}.

$$u_* = \sqrt{\frac{\tau_0}{\rho}} \Rightarrow u_* = \sqrt{\frac{1.2}{1025}} = 3.4 \text{ cms}^{-1} \text{ or } u_* = \sqrt{\frac{3.5}{1025}} = 5.8 \text{cms}^{-1}$$

for ρ = 1025 kgm^{-3}. Given the above measurements, the boundary layer thickness δ is given as:

[6.5]

$$\delta = \frac{0.4 \times 3.4 \times 10^{-2} ms^{-1}}{1.169 \times 10^{-4} s^{-1}} = 116.34 \text{ m}$$

assuming that the bottom boundary layer was non-stratified. From laboratory results, the logarithmic velocity layer holds up to approximately 10% of the boundary layer thickness (Grant and Madsen, 1986). The constant stress layer is considered to be half the thickness of the logarithmic layer, and is given by Huntley (1988) to be approximately:

[6.6]

$$z_r = (0.013 \text{ to } 0.030)u_*/f$$

For the above friction velocity values ranging from 3.4 - 5.8cms^{-1}, the constant stress layer, following the above equation for each, are:

[6.7]

$$u_* = 3.4\text{cms}^{-1} = z_r = \frac{0.013 \times 3.4 \times 10^{-2}}{1.169 \times 10^{-4}} = 3.78 \text{ m}$$

$$u_* = 5.8\text{cms}^{-1} = z_r = \frac{0.013 \times 5.8 \times 10^{-2}}{1.169 \times 10^{-4}} = 6.45 \text{ m}$$

Measurements of current velocity taken by the BLISS tripods were at 0.41mab, well below the required depths, for accurate shear stress estimations. For minimum shear stresses τ_0 = 0.01Nm^{-2}, u_* = 0.3cms^{-1}, δ = 10.3m, z_r = 0.77m, which is still above the height of the BLISS EMCMs.

In the nearshore zone off the Holderness coast, the Coriolis parameter is not a controlling factor which determines the height of the boundary layer. The height of the boundary layer is limited by the water depth. An assumption is made therefore, that the constant stress layer is within 1/10 of the water depth, which is consistent with other studies off the Holderness coast (Williams *et al.*, 1996). This criterion also confirms that the BLISS measurements were well within the constant stress layer.

6.4.3 Determination of Resuspension Events

The friction velocity u_* had already been introduced in the previous section as an important component for calculating the boundary layer thickness. In this section, u_* has been

contour plotted against wave orbital velocity σ_w (section 5.7) and mean current speed, using the relationship $\overline{S} = \left(\overline{U}^2 + \overline{V}^2\right)^{0.5}$ to determine the possibility that resuspension of the bed material in the vicinity of the BLISS tripods occurred during storm events or at maximum tidal streaming.

Attention will focus on the February 1996 inner and outer station deployments. Comparisons were also made between the BLISS u_* values and STABLE[2] data collected off the Holderness coast by the Proudman Oceanographic Laboratory (POL) in October 1994 and January/February 1995 (Williams *et al.*, 1996a&b). The STABLE deployments were in very close proximity to the outer station BLISS mooring (figure 4.1) and were deployed in 25-27m water.

6.4.3.1 *February 1996 Inner and Outer Station Deployments*

Figures 6.21 and 6.22 show u_* contours plotted against wave and current velocity for February inner and outer stations respectively. Both the winter stations exhibited an expected increase in u_* with increasing current velocity and wave orbital velocities. Observation data points of u_* are included in figure 6.21, to show that most of the u_* values occurred at orbital velocities $<0.4ms^{-1}$, and only a few data points reached u_* values > 0.04 ms^{-1}. Resuspension events will normally occur at maximum tidal streaming or at high wave orbital velocities or both. Figure 6.23 shows the sediment response to the same wave-current conditions for February 1996 inner station. No suspension peaks occur at maximum current velocity or at maximum wave orbital velocity, but peaks in concentration do arise at low current speeds $<0.3ms^{-1}$. These peaks must be due to concentration enriched water being advected into the vicinity of the BLISS tripods.

u_* values for the February 1996 outer station (figure 6.22) were not greater than 0.04 ms^{-1} even at maximum current-wave velocities. Peaks in sediment concentration (figure 6.24) occurred at low current speeds $<0.2ms^{-1}$ and at wave orbital velocities $>0.4ms^{-1}$. These peaks are probably caused by advective material rather than resuspended material. At orbital velocities between $0.55ms^{-1}$ and $0.75ms^{-1}$ and at current speeds $<0.1ms^{-1}$ there was a distinct band in increased sediment concentration at the outer station, that could be due

[2] STABLE stands for Sediment Transport And Boundary Layer Equipment. For further information refer to Humphrey, (1987), see References at back of Thesis.

partly to sediment resuspension in response to the higher orbital velocities but could also be due to advection of Humber plume material as suggested earlier in section 6.3.6.

The corresponding u_* values for the suspension peaks to occur at both stations were between 0.02 ms^{-1} and 0.03ms^{-1}.

In summary, the SSC contour plots did not reveal any resuspension events at maximum tidal streaming or at high wave orbital velocities which we would expect, but suggested that the sediment peaks were due to advection. Since the sediment peaks occurred at low current velocities, the findings give support to the hypothesis that a plume of concentration enriched water originating from the Humber estuary is being advected into the region of the BLISS moorings.

Accuracy was determined by the standard deviation of the residual value, obtained by calculating the difference between the interpolated data of u_* shown on the contour plots and the u_* observational data. Standard deviations for the February inner and outer station deployments are given in table 6.4. Both standard deviations are small which suggest that the interpolated contour lines of u_* match the observations closely.

Table 6.4 Standard deviations of the difference between the u_* contour values and the observations for the February 1996 inner and outer station deployment.

Station	**u_* Standard deviation of the residual value (ms^{-1}) difference between interpolated and observational data**
February 1996 inner	0.00809
February 1996 outer (Fig. 5.21)	0.00408

6.4.4 Determination of Stable Stratification

In high sediment suspension concentrations during storms, such as experienced at the February 1996 outer station, the suspended sediment produces a vertical gradient of density which must have a stabilising effect on the flow, so inhibiting vertical exchange by turbulence (Dyer, 1986). With the right combination of particle settling velocity and turbulent mixing, the added mass of the suspended load could act to stably stratify the boundary layer (Glen and Grant, 1987). The suppressed turbulence will then lead to a reduction in the amount of material being resuspended from the seabed.

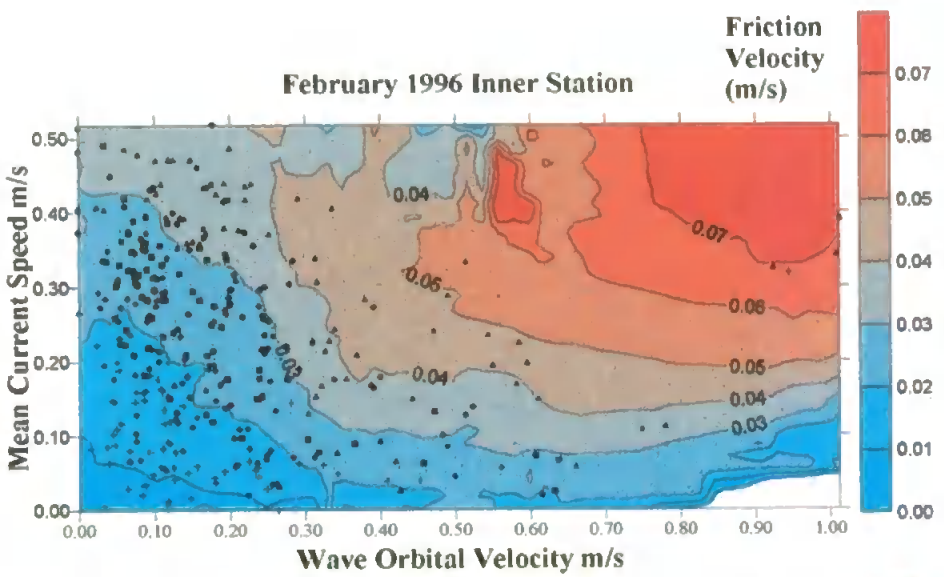

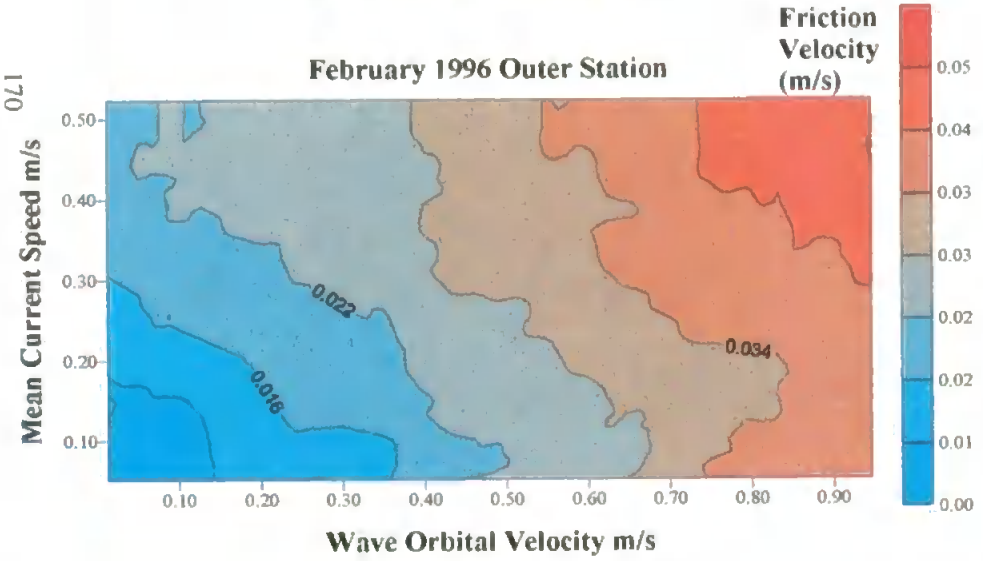

Figure 6.21 & 6.22 Contours of u_* for February '96 inner & outer station plotted against concurrent mean current speed and wave orbital velocities

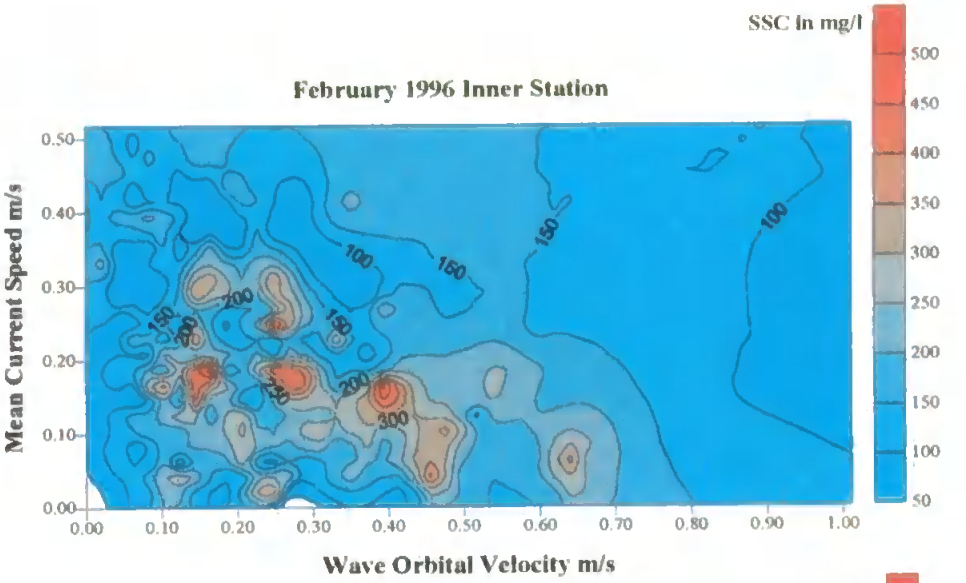

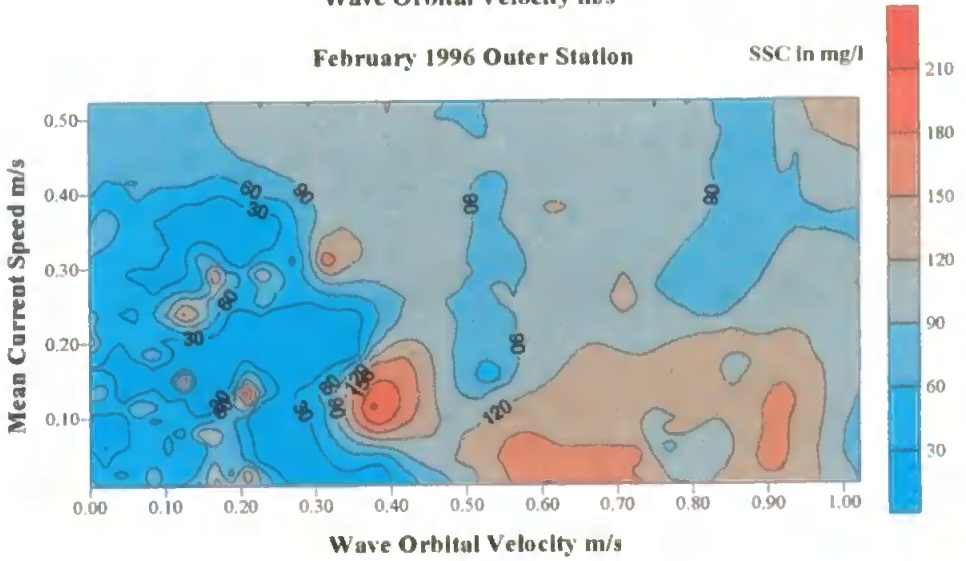

Figure 6.23 & 6.24 Contour plots of SSC February 1996 inner & outer station

To determine whether conditions during the storm were of the right order to stably stratify the boundary-layer flow, the stability parameter z/L (equation 6.8) (Glen and Grant, 1987) was applied to the February 1996 outer station data, defined as:

[6.8]

$$z/L = \frac{zkg(\rho_s/\rho - 1)w_s C_z}{u_*^3}$$

where L is the Monin Obukhov length, k = von Karman's constant 0.4, z is height above the seabed bed (0.41m), g is acceleration due to gravity (9.81 ms^{-1}), w_s is the settling velocity (2.81×10^{-4} ms^{-1}), ρ is water density 1025 Kgm^{-3}, ρ_s is sediment density (assumed to be 2.65 gm cm^{-3} for quartz sand), u_* is the friction velocity (0.0191 ms^{-1}) and C_z is the time averaged suspended sediment concentration (119×10^{-4} Kgl^{-1}). Sediment concentration was taken to be the average over the storm, w_s was taken from table 6.2 (hours 88-355) and u_* was chosen as the average over the storm. The stability parameter is predicted on a buoyancy flux that is due wholly to a vertical turbulent flux of suspended sediment that is, in turn, balanced by an opposite directed sediment settling flux $w_s C_z$ (Glenn and Grant, 1987). The stability parameter during the outer station storm was estimated to be z\L = 0.00199 and was < 0 (10^{-1}). According to Green *et al.*, (1995) the stability parameter should be > 0 (10^{-1}) if stable stratification of the boundary layer is to occur. Therefore, it is evident that stable stratification did not occur at the February outer station during the North Easterly storm.

6.4.5 Estimating Drag Coefficient (C_{d100}) and Roughness Length (z_0) - Comparisons with Other Field Results

It is well recognised that wave and current boundary layers interact non-linearly near the seabed (Soulsby and Humphrey, 1989), and when tackling the subject of sediment transport, their combined effect must be taken into account. In other words, when waves and currents exist together, the shear stresses identified with the wave and with the current are altered, because the nature of the turbulence generated by the waves affect the currents, and vice versa (Grant and Madsen, 1979). The result is that the current in the region above the wave boundary layer, experiences a shear stress which depends not only on the physical bottom roughness but also on the wave boundary layer characteristics. Consequently, combined flows may initiate sediment motion at lower velocities than that predicted for waves alone (Hequette and Hill, 1993).

Direct comparisons of the BLISS shear stress results with other field campaigns off the Holderness coast, were not possible, because current velocity measurements were not taken at the same height above the seabed. To enable comparisons between different data sets, many authors take the mean velocity from a reference point 100cm above the seabed, commonly termed u_{100}. Taking the mean current speed S, u_{100} was calculated from the measurement height of 0.41mab by extrapolation using the logarithmic profile (Ch 2. section 2.2.3), given as:

[6.9]

$$\frac{\bar{u}(z)}{u_*} = \frac{1}{k}\ln\frac{z}{z_0}$$

where, the friction velocity u_* is related to shear stress through $\tau_0 = \rho u_*^2$, z is height above sea bed, z_0 is the roughness length, which is related to the physical roughness of the seabed under pure current conditions, but it can be assumed that z_0 includes wave enhancement under wave-current conditions, and k is von Karman's constant taken as 0.41.

Substituting u_{100} into the above equation gives:

[6.10]

$$\frac{u_{100}}{u_*} = \frac{1}{k}\ln\left(\frac{100}{z_0}\right)$$

substituting u_{41} into equation 6.9 gives

[6.11]

$$\frac{u_{41}}{u_*} = \frac{1}{k}\ln\left(\frac{41}{z_0}\right)$$

u_{100} is calculated as:

[6.12]

$$\frac{u_{100}}{u_{41}} = \frac{\ln 100 - \ln z_0}{\ln 41 - \ln z_0}$$

where

$$\ln z_0 = \left[\ln z - \frac{k u_z}{u_*} \right]$$

The drag coefficient C_d was calculated from the quadratic stress law relationship $\tau = \rho C_d u|u|$ (Huntley *et al.*, 1994), and relates the bed friction to the velocity at some height above the seabed, in this case 100 cm, where:

[6.13]

$$C_{d\ 100} = \tau_0 / \rho U_{100}^2$$

or

[6.14]

$$C_{d\ 100} = \left(\frac{u_*}{U_{100}} \right)^2$$

By presenting shear stress estimates in this non-dimensional form, enables us to determine the importance of the wave enhancement of τ_0, which is noted by Soulsby and Humphrey (1989) to increase the frictional resistance felt by the tidal currents and notably the frictional force acting on the seabed sediments. Alternatively, the drag coefficient can be expressed as the physical bed roughness length z_0, which was evaluated by back calculation from the mean value of C_d through:

[6.15]

$$z_0 = z \exp\left(-k / C_d^{\frac{1}{2}} \right)$$

where z = height above the seabed (100cm).

The drag coefficient was calculated for the June/July 1995 and February 1996 BLISS deployments and compared to STABLE data taken off Holderness during October 1994 and January 1995. The C_{d100} values were then split into two groups depending on whether the corresponding $u_{100} < 0.2 ms^{-1}$ or $u_{100} > 0.2 ms^{-1}$ ($<0.2 ms^{-1}$ was the chosen velocity bracket to separate out the effects which current acceleration near to slack water, had on the value of C_{d100}) and plotted against the wave:current ratio σ_w/u_{100}. Corresponding roughness lengths were also determined and their values were compared to results from other field experiments.

6.4.6 Discussion of Drag Coefficient C_{d100} and Roughness Length z_o

C_{d100} values representing summer conditions off Holderness (figure 6.25) revealed that there was a large amount of scatter at the inner station, with C_{d100} values ranging from 0.0001 to 1. At the middle station (figure 6.26), the spread in the data was much reduced, with C_{d100} values falling between 0.001 and 0.1. Clearly at both stations, the highest C_{d100} values occurred when the corresponding u_{100} values were $<0.2ms^{-1}$, although the inner station produced C_{d100} values an order of magnitude greater than the middle station. C_{d100} values with U_{100} values $>0.2ms^{-1}$ for both stations were within the same order of magnitude, although again there was more scatter at the inner station. The general trend in the BLISS data was observed to follow a linear line, not consistent with the exponential line of fit suggested by Soulsby and Humphrey, (1989). The lines shown are linear lines of best fit applied to each section of data.

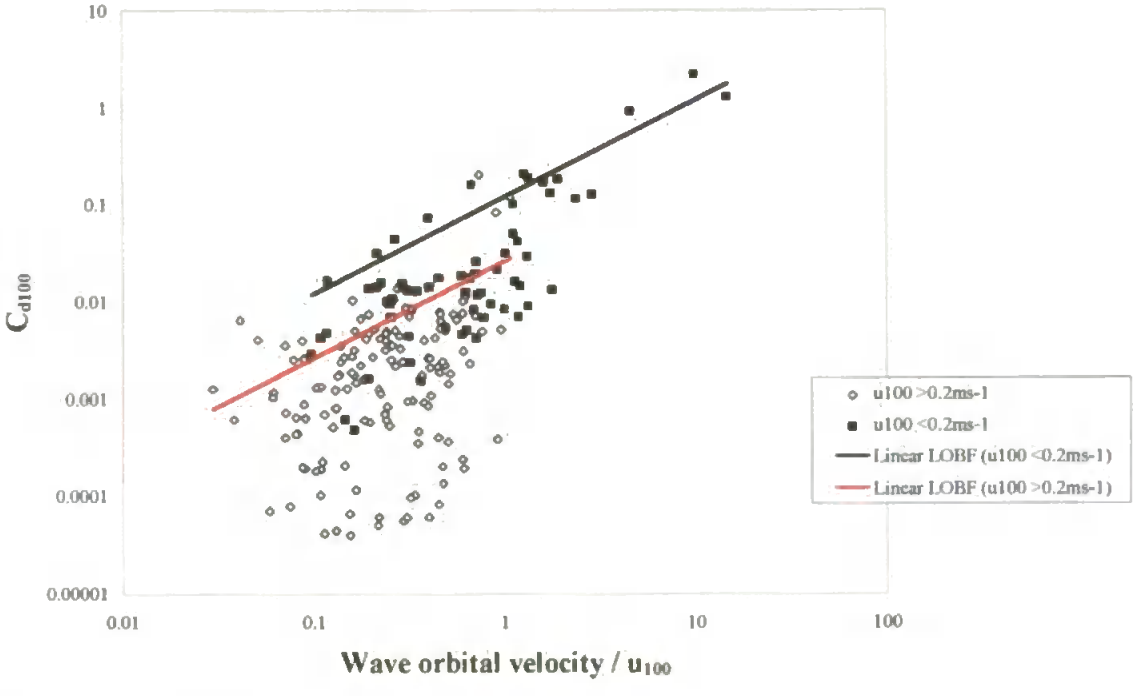

Figure 6.25 Scatter plot to show C_{d100} plotted against wave:current ratio σ_w/u_{100} - BLISS July 1995 inner station.

High C_{d100} values occur when the wave:current ratio is large. This may be due to additional turbulence generated at the seabed through the action of wave motion, or maybe to the formation of bedforms such as ripples which will induce an increase in the physical roughness of the seabed and enhance the shear stress estimates. However, it has also been recognised that large C_{d100} values occur close to slack water, when tidal acceleration effects are likely to introduce an unrelated physical process which acts to enhance turbulence levels

and the shear stress (Soulsby and Humphrey, 1989). This situation may account for why the inner station data set had such high C_{d100} values when compared to the middle station, especially as during the deployments relatively calm weather conditions prevailed, with significant wave heights being in the order of ≤ 0.5m.

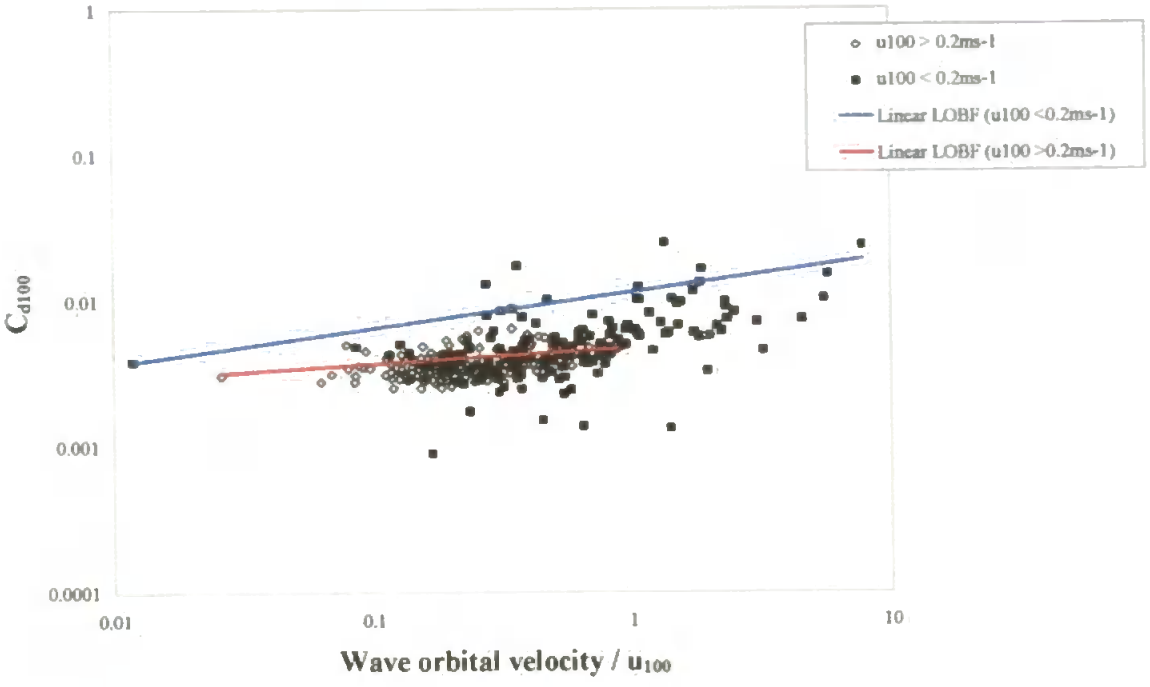

Figure 6.26 Scatter plot to show C_{d100} plotted against wave:current ratio σ_w/u_{100} - BLISS July 1995 middle station

At the middle station, the behaviour of C_{d100} was such that a constant value for C_{d100} of ~0.006, was maintained until the wave:current ratio reached 1. At this point, C_{d100} increased.

C_{d100} measurements taken by Soulsby and Humphrey, (1989) and Hannay *et al.*, (1994), portrayed the same phenomena, and attributed the increase in C_{d100} to wave-generated turbulence close to the bed, being diffused up into the flow from the wave boundary layer. This increase in C_{d100} suggests that waves play a significant role in altering the stress value. It also implies that numerical models based upon a constant drag coefficient are likely to be inappropriate when significant horizontal wave velocities are present (Huntley *et al.*, 1994).

Winter values of C_{d100} for BLISS and STABLE (figures 6.27 and 6.28) were not dissimilar to the summer BLISS results, in that all data sets exhibited an increase in C_{d100}, in response to an increasing wave:current ratio. The highest BLISS C_{d100} values were again seen to

arise when U_{100} values were <0.2ms^{-1}. The largest scatter was again seen to occur at the inner station. In comparison, the STABLE data (all data <0.2ms^{-1} omitted) had similar values to BLISS, with a consistent value around 0.001. However, the STABLE C_{d100} values corresponded to much smaller wave:current ratios than observed in the BLISS data. STABLE data collected in autumn 1994 displayed a consistent C_{d100} of ~0.0008 upto a wave:current ratio of 0.01 when the values started to increase to reach levels consistent with the lowest BLISS values. In January 1995, STABLE results as mentioned, showed a consistent C_{d100} of 0.001, but the corresponding wave current ratios were significantly smaller than the other STABLE and BLISS deployments. The point where the data started to increase was ~0.01. The general trend of the STABLE data was an exponential curve, which was consistent with the line of fit suggested by Soulsby and Humphrey (1989).

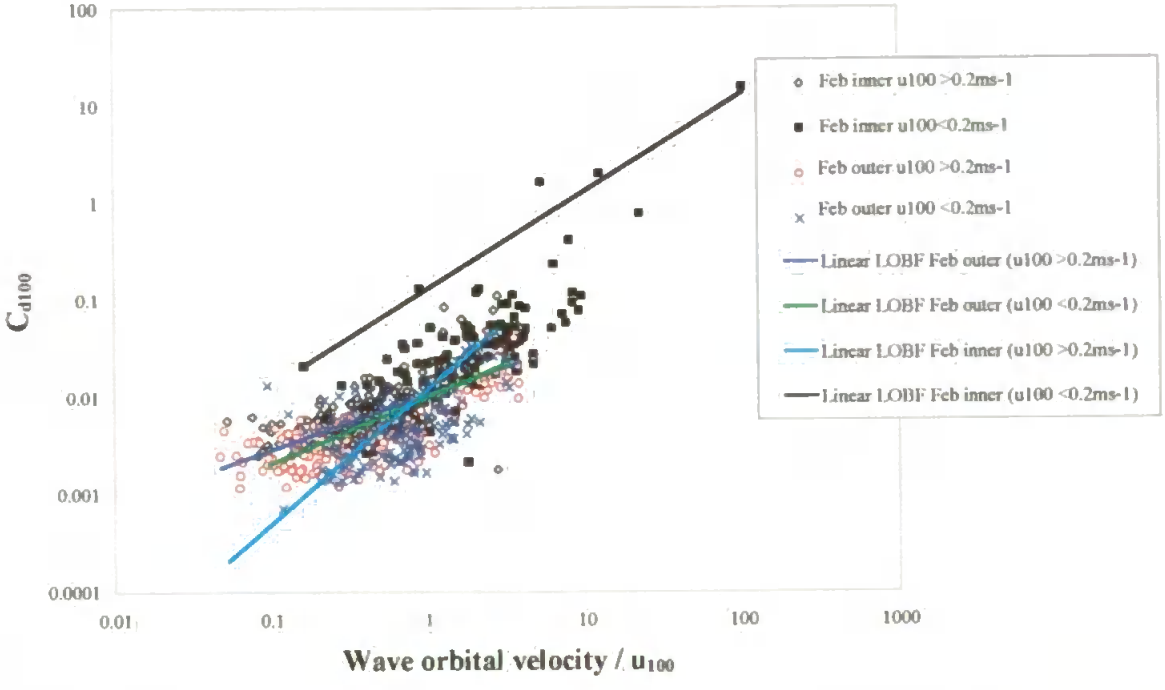

Figure 6.27 Scatter plot to show C_{d100} plotted against wave:current ratio σ_w/u_{100} - BLISS February 1996 inner and outer station

Table 6.5 shows the equations for each line of best fit. The highest drag coefficients occurred as expected when u_{100} was <0.2ms^{-1}. The largest variations in the drag coefficients from u_{100} <0.2ms^{-1} to u_{100} >0.2ms^{-1} arose at the July 1995 and February 1996 inner station. As expected , the STABLE results were lowest in value, even though they were furthest off-shore.

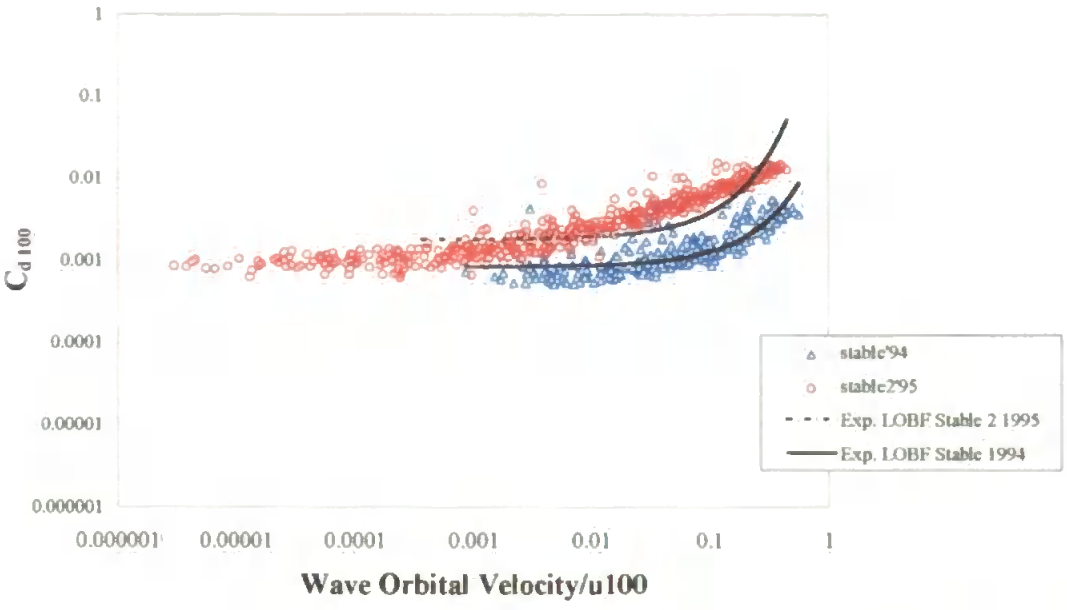

Figure 6.28 Scatter plot to show C_{d100} plotted against wave:current ratio σ_w/u_{100} - STABLE 1994 and 1995.

From the drag coefficient time series and from the C_{d100} constants derived from the equation of the lines of best fit, the corresponding roughness lengths z_o for each station were derived by applying equation 6.15. The results yielded that the highest roughness lengths (excluding z_o values from u_{100} <0.2ms^{-1}) occurred at the inner station in July 1995 and February 1996. The largest storm occurred during the February 1996 outer station deployment, and comparisons of z_o with significant wave height and water depth during this time (figure 6.29), showed significant enhancement to z_o during the storm. There was a distinct over estimation in the z_o value due to acceleration effects after slack water, which gives support to Soulsby and Humphrey's observations (1989). It was unlikely that the observed roughness increase was caused by a major change in the physical roughness due to storm-wave production of large bedforms, because grab samples taken at the time of the deployment, suggested a seabed surface overlay by gravel. However, all the fine sediment and sand which is settled between the interstices of the gravel in calm conditions, was in suspension during the storm. It is suggested that by removing the sand and fine sediment from the gravel, the z_o values could increase (Pers. Comm., Dyer, 1997).

Table 6.5 The equations of the lines of best fit for the data presented in figures 6.25 to 6.28.

Field Station	Equation	Std	R^2 value	Roughness Length z_0 (cm) 100 cm above bed
June/July '95 Inner BLISS <0.2ms^{-1}	$C_d = 0.1239\sigma_{wave}/U_{100}$	0.304	0.75	31
June/July '95 Inner BLISS >0.2ms^{-1}	$C_d = 0.0271\sigma_{wave}/U_{100}$	0.021	0.14	8.3
June/July '95 Middle BLISS <0.2ms^{-1}	$C_d = 0.002\sigma_{wave}/U_{100}+0.0039$	0.004	0.34	0.01
June/July '95 Middle BLISS >0.2ms^{-1}	$C_d = 0.0018\sigma_{wave}/U_{100}+0.0032$	0.0007	0.14	0.006
Feb '96 Inner BLISS <0.2ms^{-1}	$C_d = 0.1344\sigma_{wave}/U_{100}$	0.013	0.9	32
Feb '96 Inner BLISS >0.2ms^{-1}	$C_d = 0.0188\sigma_{wave}/U_{100}-0.0008$ $\sigma_{wave}/U_{100} = 1,\ C_{d100} = 0.01$ $\sigma_{wave}/U_{100} = 0,\ C_{d100} = 0.005$	1.357	0.53	5
Feb '96 Outer BLISS <0.2ms^{-1}	$C_d = 0.0066\sigma_{wave}/U_{100}+0.0014$	0.006	0.44	0.5
Feb '96 Outer BLISS >0.2ms^{-1} Prestorm Storm Post-storm	$C_d = 0.0056\sigma_{wave}/U_{100}+0.0017$ $\sigma_{wave}/U_{100} = 1,\ C_{d100} = 0.0045$ $\sigma_{wave}/U_{100} = 0,\ C_{d100} = 0.0025$ $C_d = 0.0089\sigma_{wave}/U_{100}$ $C_d = 0.0067\sigma_{wave}/U100-0.0011$ $C_d = 0.0006\sigma_{wave}/U_{100}+0.0025$	0.007 0.003 0.0099 0.001	0.64 0.05 0.5 0.005	0.4
STABLE '94	$C_d = 0.0018\exp 7.5391\sigma_{wave}/U_{100}$	0.002	0.68	0.006
STABLE '95	$C_d = 0.0009\exp 4.2218\sigma_{wave}/U_{100}$	0.005	0.65	0.0001

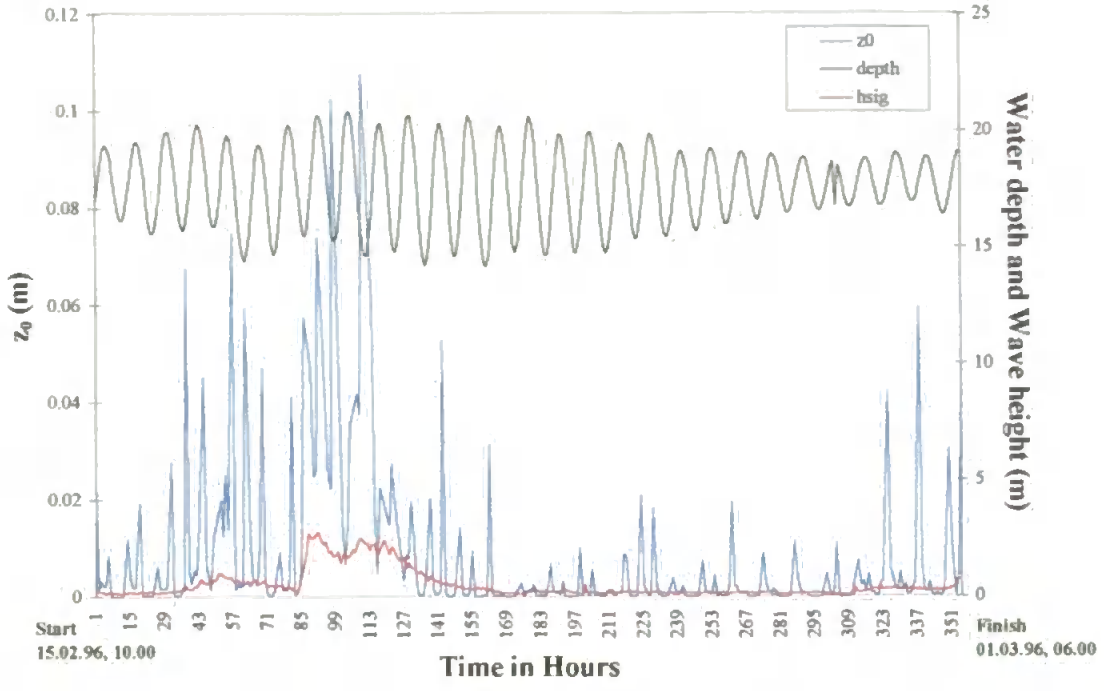

Figure 6.29 Time series of roughness length, wave activity, and water depth - February 1996 outer station

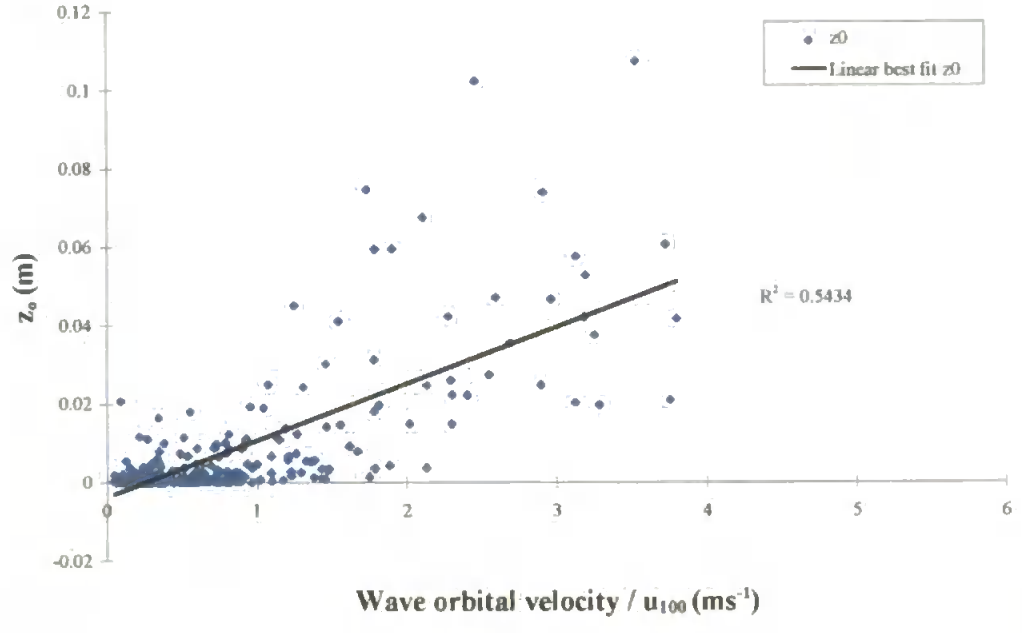

Figure 6.30 Scatter plot to show correlation between roughness length and wave:current ratio - February 1996 outer station

As shown in figure 6.30 for the February 1996 outer station, there was good correlation between σ_w/u_{100} and z_0. When σ_w/u_{100} was low the roughness felt by the current declined to ~0.1 cm. The scatter in the value of z_0 increased when the ratio of σ_w/u_{100} was >1.

Since the wave-orbital velocity was at least the same order as the steady current speed, wave-current interaction should have affected the boundary-layer dynamics (Green *et al.*, 1995).

Over estimated z_0 values were clearly apparent at the June/July 1995 inner station (figure 6.31), but in this case, z_0 was not enhanced by wave activity. The over estimations in z_0 probably account for the large C_{d100} coefficient representative of conditions <0.2ms^{-1} (table 6.5). Notably, the rapid variation of z_0 over the tidal cycle may be the result of a very unstable estimate of the drag coefficient near to slack water (Pers. Comm., Huntley, 1997).

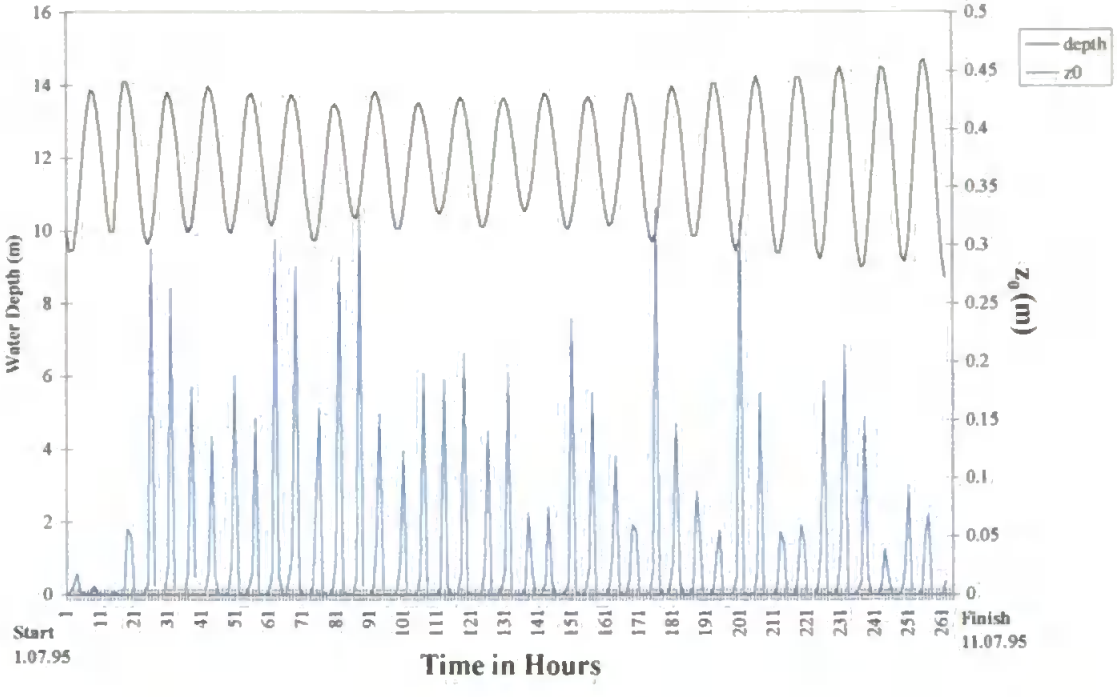

Figure 6.31 Time series to show roughness length against water depth - July 1995 inner station

The nature of the seabed in the vicinity of the BLISS tripods during the deployments was unknown because there was no facility on the tripods to take bottom photographs. Grab samples taken in the June/July 1995 deployment are given in table 6.6, along with typical values of roughness length z_0 and drag coefficient C_{d100} taken from Soulsby, (1983).

Table 6.6 Sediment samples taken during June/July 1995 deployment with corresponding z_0 and C_{d100} values taken from Soulsby (1983).

Station June/July 1995 Deployment	Location	Sediment Size	Total %	Roughness Length z_0 (cm)	Drag coefficient C_{d100}
Inner	53° 45.844'N 00° 00.181'E	≤ 125 µm fine sand/silt	92	0.04 - 0.005	0.0026 - 0.0016
Middle	53° 47.190'N 00° 02.497'E	2-2.8mm granular course/very coarse sand 500 µm - 1mm	77 21	0.3 - 0.03	0.0047 - 0.0024
Outer	53° 47.666'N 00° 03.275'E	1 to 2.8 mm pebbles/granular	90	>0.3	>0.0047

Comparisons of the derived C_{d100} and z_0 results (table 6.5) with the typical results expected from the grab samples (table 6.6) showed that there was good agreement at the outer station suggesting that the outer station is composed of coarse material. The C_{d100} and z_0 values obtained at the July 1995 inner station did not agree with the expected values. The C_{d100} and z_0 results taken for the middle station in July 1995 (table 6.5) suggested a seabed composed of fine sand/silt, and were not consistent with the grab samples results (table 6.6). Derived C_{d100} and z_0 values ($u_{100} > 0.2ms^{-1}$) taken from the February 1996 inner and outer stations suggested a seabed that was composed of coarse sand and granular material.

The STABLE results from table 6.5, suggest that further offshore, according to Soulsby (1983), the seabed surface was composed of fine sand and silt material. This could be possible as there was little wave activity during the STABLE deployments, and under calm conditions the fine material in suspension (as seen in February 1996), would have settled onto the seabed to produce a relatively smooth surface. Notably, mixtures of grain sizes have relatively small values of z_0, as the fine grains fill the spaces between the coarse grains (Soulsby, 1983).

In summary, the drag coefficient and roughness length showed large variations depending on the current speed, wave activity and seabed composition. Over estimated values of C_{d100} and z_0 were seen to arise in all the BLISS deployments after slack water. This feature was attributed to the effects of tidal acceleration, which introduced an unrelated physical process, and acted to enhance the turbulence levels and the shear stress. Roughness length

values were seen to increase significantly during the winter storms. It was postulated that the fine material which is settled between the interstices of the gravel overlay in calm conditions at the outer station was in suspension during the storm, and by removing the fine sediment from the gravel, caused the value of z_0 to increase. These results illustrate the dangers of using a constant drag coefficient for all substrates, especially in shallow shelf sea waters where bed friction is significant.

6.5 Threshold for Sediment Transport

Sediment movement will not occur until the combined lift and drag forces exerted by the fluid exceed the gravitational and cohesive forces acting on a sediment grain. Cohesive forces are only important for fine grained material (Dyer, 1986). The velocity at which movement begins is referred to as the threshold velocity or critical velocity, that can also be expressed in terms of a critical friction velocity. Dyer, (1986) states:

> *"If the flow velocity is increased in small increments, motion will first occur of a few particularly exposed grains, but it will die away after a time as they come to rest in new equilibrium positions. With increasing velocity, movement will become more general and prolonged".*

The threshold of motion is consequently a difficult thing to define. For the BLISS data, the threshold was determined by those events during the sampling period when the SSC suddenly increased above previous sustained background levels. This procedure has been adopted elsewhere (Larsen *et al.*, 1981). The threshold velocity (u_{*c}) was determined for each deployment, by comparing the observed SSC time series with the u_* time series. This technique, however, of defining threshold velocity, gives the threshold for the mobile sediment, which may be only one fraction of the seabed (Dyer, pers comm., 1997). The method however is acceptable for the BLISS data because there was no clear evidence to suggest that resuspension of the bed material alone was the cause for the SSC peaks (section 6.4.3). Figure 6.32 shows u_* plotted against SSC for the February 1996 outer station deployment. It has been suggested (section 6.3.6) that the sudden increase in SSC at hour 85 was due mainly to advection of fine material into the vicinity of the BLISS tripod but also due to seabed resuspension. The sediment peaks after the storm have been attributed to resuspension of the very fine sediment which had already settled out of

suspension (section 6.3.5). To more accurately determine the threshold velocities for the storm and post storm conditions, a section of the time series to cover the storm period was plotted (figure 6.33). Each data point of u_* and SSC represented the same time period, because all the data was recorded on the same acquisition system. By lining up the u_* and SSC data points, the sudden increase in SSC at hour 85 (figure 6.33) corresponded to a threshold u_* value 0.02 ms^{-1}. Just before the onset of each resuspension peak after the storm, the threshold u_* values varied between ~0.009 ms^{-1} and 0.02ms^{-1}, depending on where one defines the point of sediment increase.

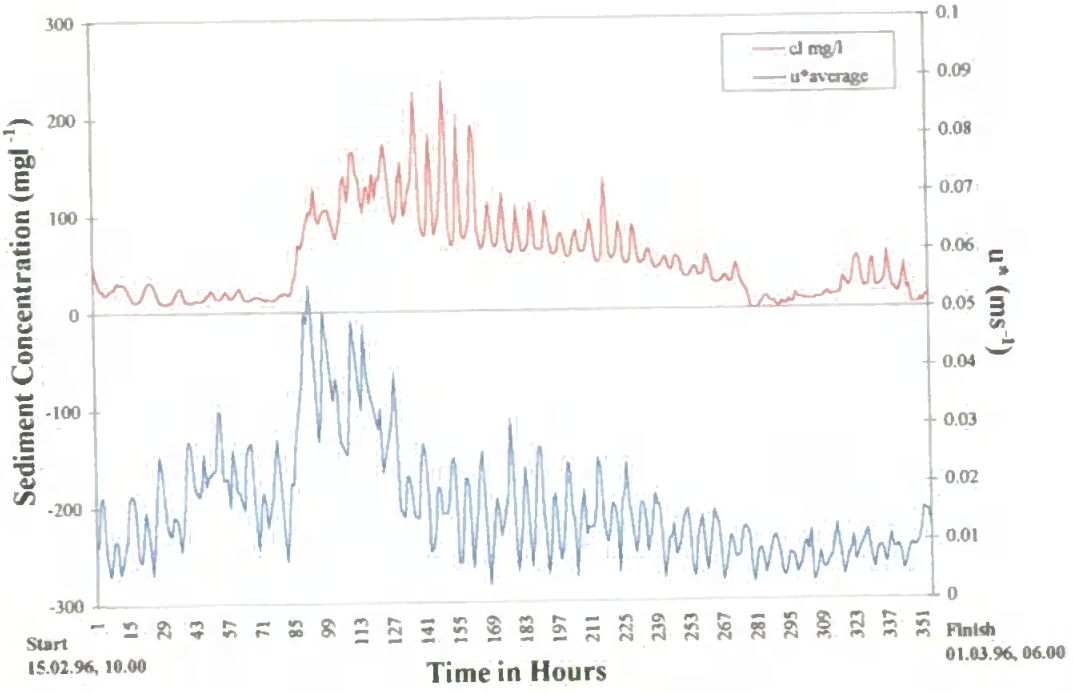

Figure 6.32 Time series of u_* and SSC for February 1996 BLISS outer station deployment.

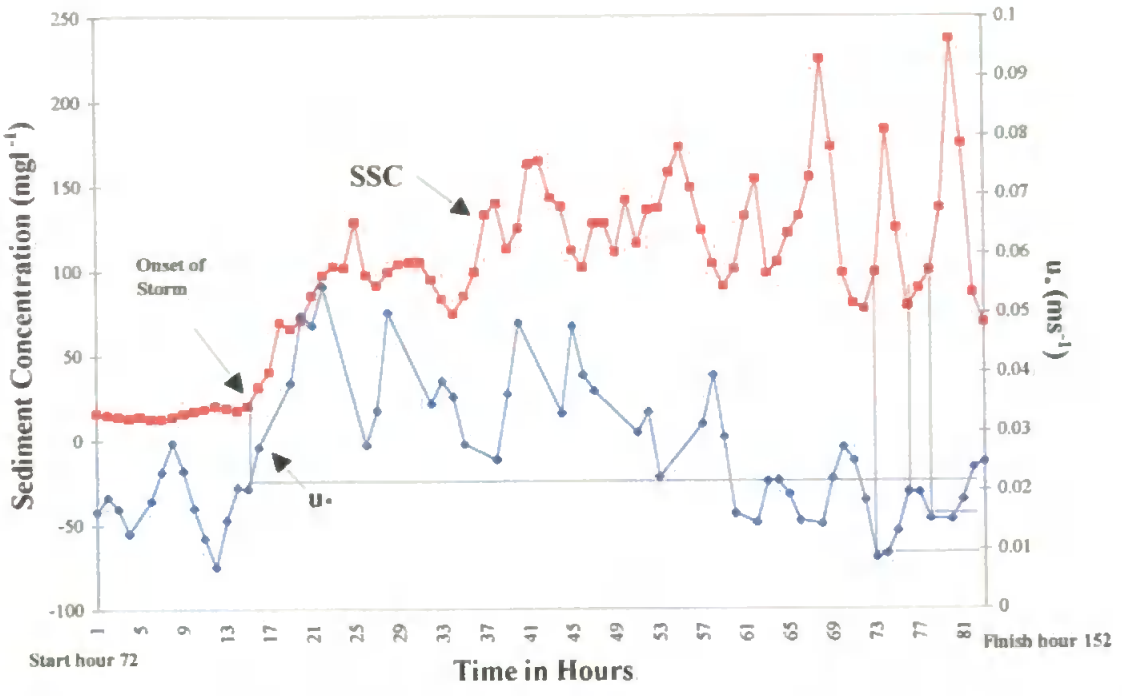

Figure 6.33 Time series of u_* and SSC between hours 72-152 - February 1996 outer station deployment

The same procedure to determine threshold velocity was performed on the July 1995 inner station time series (refer to figures 6.4a and figure 6.34) and the February 1996 inner station time series (refer to figures 6.7 and 6.35). Threshold velocity results for each deployment are given in table 6.7.

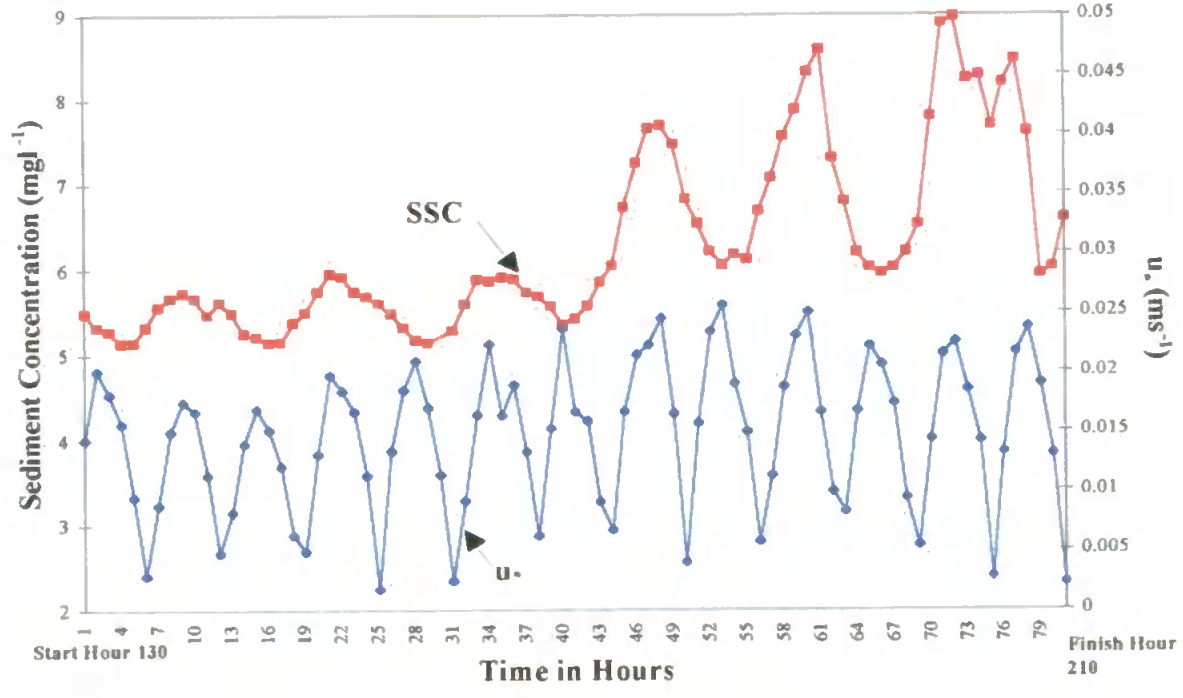

Figure 6.34 Section of July 1995 inner station time series (hour 130 - 210) of u_* and SSC to determine threshold velocity.

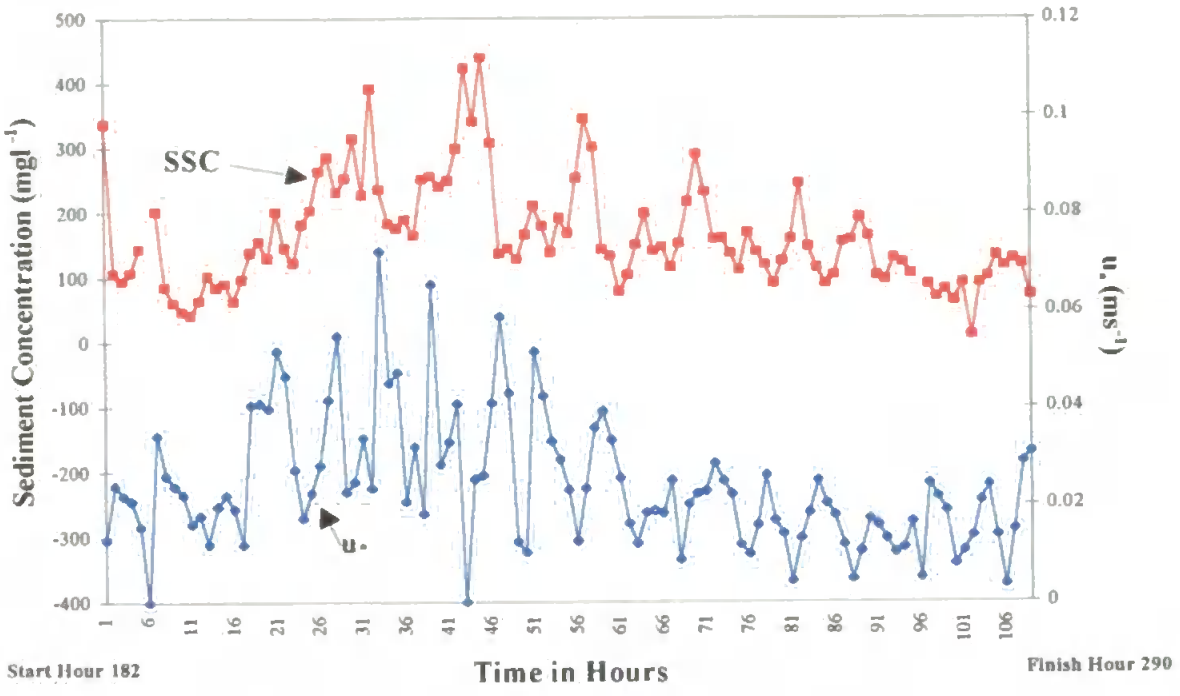

Figure 6.35 Section of February 1996 inner station time series (hour 182 - 290) of u_* and SSC to determine threshold velocity.

The section of data chosen in July 1995 (figure 6.34) represented the second half of the calm neap period leading into the spring tidal cycle. Figure 6.35 for February 1996 inner station covered the duration of the neap storm.

Sediment movement is determined principally by the fluid velocity and the grain size. The dependence of the critical velocity on the grain size is normally expressed in terms of a threshold diagram or a threshold curve (for more details refer to section 2.2.7). To obtain an idea on the size of the seabed sediments, the derived threshold velocities were compared to figure 6.36 after Miller *et al.*, (1977). Observed thresholds and suggested grain sizes are given in table 6.7.

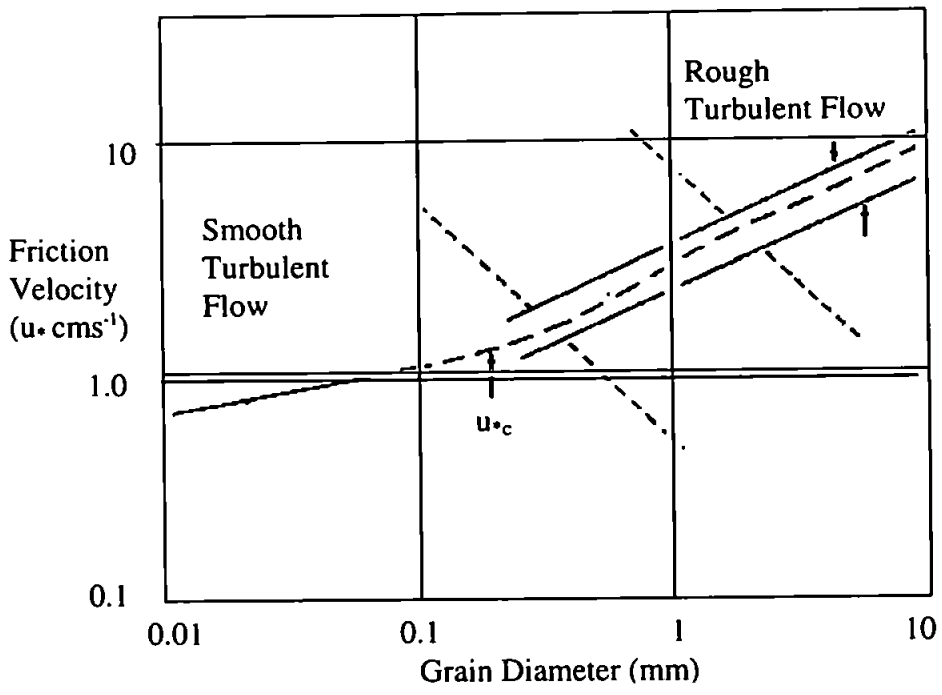

Figure 6.36 Threshold friction velocity for grain movement (Miller *et al.*, 1977)

Table 6.7 Threshold values (u_{*c}) derived for sediment resuspension

BLISS station	**Observed threshold friction velocity (u_{*c}) cms^{-1}**	**Grain size derived from threshold curve (Miller *et al.*, 1977)**
July Inner 1995	0.8 cms^{-1}	0.05mm (50 μm)
February Inner 1996	1.4 cms^{-1}	0.2 mm (200 μm)
February Outer 1996	Onset of storm (hour 85) = 2.0 cms^{-1} Post storm (no waves) = 0.9 cms^{-1} to 2cms^{-1}	0.4mm (400μm) 0.07 mm (70μm) to 0.4mm (400μm)

The threshold velocity given for July 1995 suggested that the seabed sediments were composed of coarse silt (refer to Wentworth grain size scale, P. 16-17, Dyer, 1986). Threshold velocities derived for the February 1996 inner station, depicted a seabed composed of fine sand. The most dramatic change in the threshold was seen for the outer station. During the storm conditions, the threshold velocities were significantly higher at 2 cms^{-1}, this suggested an equivalent grain size of medium sand (table 6.7). After the storm,

the threshold velocity values ranged from 0.9cms^{-1} to 2cms^{-1} with an equivalent shear stress of 0.083 - 0.41 Nm^{-2}. Given the persistence of the high levels of SSC beyond the storm conditions in both the February inner and outer station, it is unlikely that these grain sizes are actually in suspension. These threshold values are not dissimilar to critical shear stresses derived for cohesive sediment from inter-tidal mud flat areas during the LISP (Littoral Investigations of Sediment Properties) study (Christie, 1997, Widdows, 1996).

Corresponding settling velocities derived for the post-storm conditions at the outer station (section 6.3.7) were calculated as 0.281 mms^{-1}. When compared to settling velocities derived in the Tamar Estuary for cohesive sediments (Fennessy *et al.*, 1994), the value of 0.281 mms^{-1} represented a floc size of 200 μm which is also the same size non-cohesive grain derived from the velocity threshold curve of Miller *et al.*, (1977) (table 6.7). The value of threshold velocity u_* for cohesive sediments is variable, depending on the degree of consolidation, but it is clear that the non-cohesive grain sizes produced by Miller's threshold curve could in fact represent different floc sizes of cohesive material. In the case for the February 1996 outer station, the threshold velocity above which there was a massive increase in suspension occurred at a $u_* = 2$ cms^{-1}, or 0.41 Nm^{-2}. Shear stress measurements taken on the mud flats at Skeffling, Spurn Bight, a macro-tidal estuary, in April, 1995, produced a mean erosion stress for the exposed mud flats of 0.31 Nm^{-2} (Christie, 1997). Notably, then, at the outer station, the sudden increase in suspension, could be due to the erosion of material from a muddy seabed exhibiting cohesive properties. At the July 1995 inner station, the lower measured threshold velocities suggested that the increase in suspension was due to suspension of the already mobile sediment, which is moving freely under the tidal forces (Dyer, 1986), and is consistent with the threshold for erosion of an unconsolidated 'fluff' of fine sediment at the seabed. The much calmer conditions in July, with periods between storms to allow the deposition of such a fine layer, makes the interpretation of the threshold friction velocity extremely plausible. It should be acknowledged however that finding the threshold of sediment suspension is difficult when the advection signal is strong, and this is likely to be particularly the case for the July data.

6.6 Discussion

The suspended sediment concentration (SSC) time series data recorded by the BLISS tripods, indicated several components of variability. In the July 1995 inner station time series (figure 6.4a), background levels in SSC were 2 orders of magnitude smaller than

observed in the February 1996 time series (figure 6.7). SSC was strongly influenced by the tidal flow, with concentration peaks exhibited both M_2 and M_4 variation. The strong SSC semi-diurnal signal (M_2), only occurred on the ebb tide and just after slack water. This prominent feature has been explained most successfully (Weeks and Simpson, 1991) as due to the effect of tidal advection past the mooring, of a horizontal suspended concentration gradient. Time series of this nature have also been observed in other well-mixed areas of the Southern North Sea, such as the Dover Strait (Jones *et al.*, 1994), North of Flamborough Head (Jago & Jones, 1993) and in the Irish Sea (Weeks and Simpson, 1991, Weeks *et al.*, 1993) (see chapter 2 for more details).

One theory for horizontal advection is that on ebb tide, a plume of fine sediment which is homogenous throughout the water column is discharged out from the mouth of the Humber estuary, and extends around Spurn Head towards Holderness (visual surface sighting by Millward, 1995 Pers. Comm.). It is hypothesised that this turbidity gradient of fine material which increases in concentration towards Spurn Head was advected into the vicinity of the BLISS bottom moorings on ebb tide, and maximum suspension peaks were observed when the tidal excursion had reached its maximum extent towards the North West. Further evidence to suggest that the sediment plume exists came from surface AVHRR satellite imagery of the Holderness and Humber region (section 6.3.6).

To examine further the possibility of an advection of concentration enriched water towards the North West on ebb flow, tidal displacement over a complete spring tidal cycle was calculated using the alongshore velocity from the July 1995 inner station time series, detrended, and plotted against the suspended sediment concentration (figure 6.37). The strong tidal SSC signal is consistent with the alongshore advection of a gradient in SSC, increasing towards the south, since it is in quadrature with the current and in-phase with the tidal alongshore advection. Comparing tidal displacement to water depth, (figure 6.38), showed that maximum displacement occurred one hour after low water and maximum concentration occurred 1 hour after maximum displacement. There is the suggestion that the amplitude of this tidal signal, and the background levels of SSC decrease during neap conditions (figure 6.4a, the middle of the deployment period) but it is clear that both the tidal signal and the background levels increase significantly during even the small wave conditions experienced.

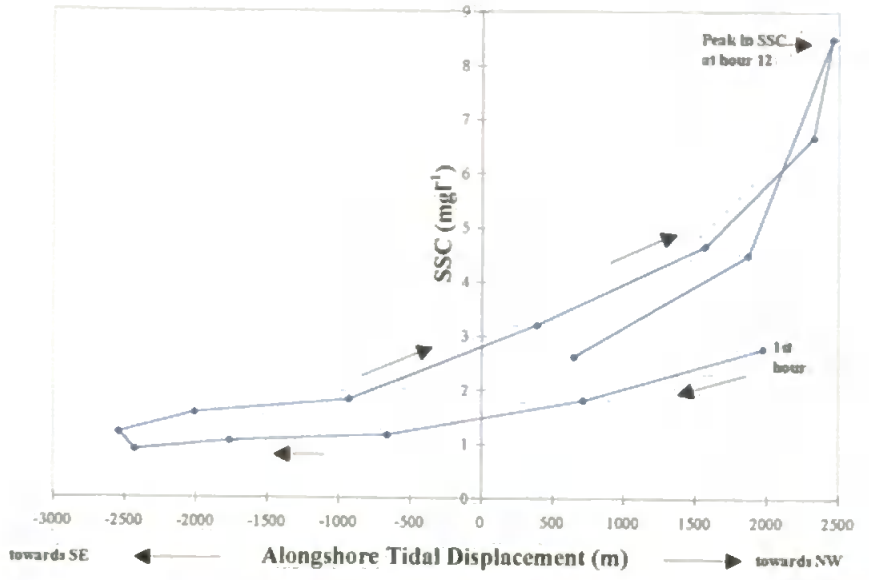

Figure 6.37 Plot to show tidal displacement Vs concentration over a complete tidal cycle (hour 226-239 , the start of storm 4 (figure 6.4a)) - July 1995 inner station

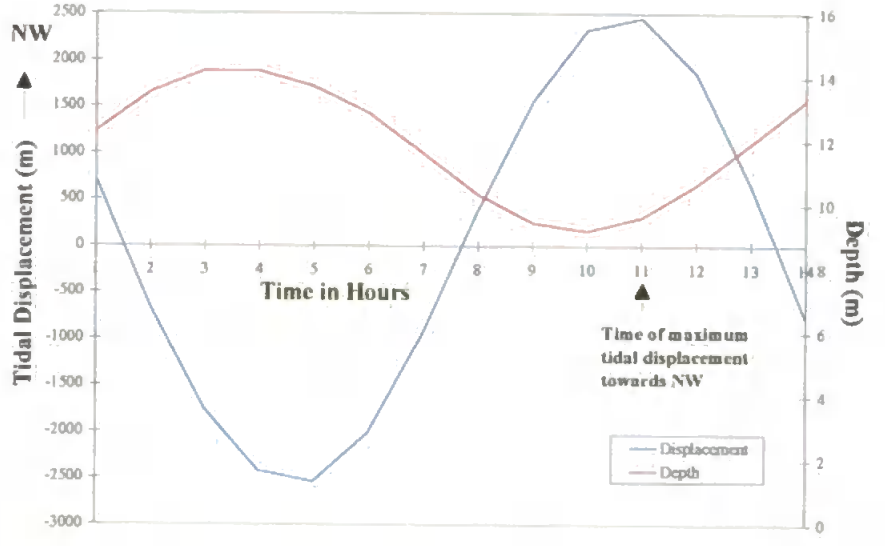

Figure 6.38 Water depth plotted against tidal displacement - July 1995 inner station (hour 226-239)

The double-peaked SSC signals, most prominent between hours 100 and 150 in the July 1995 time series (figure 6.4a), are characteristic of resuspension from the seabed and subsequent deposition during successive tides of the bed material in the locality of the BLISS moorings, with small peaks coincident with maximum tidal current speeds. It is perhaps unexpected that these peaks are most prominent during the smaller neap tidal currents, but it is likely that the stronger advective signal at other times swamps this resuspension signal. Two significant factors determining SSC dynamics at the BLISS sites from the July 1995 deployment are ascertained; firstly, the tidal currents were responsible

for resuspending the bed material at the BLISS site at maximum tidal streaming when there were no waves, and secondly, the resuspended material had a settling velocity fast enough for most of it to be re-deposited between times of maximum flow. Combination of the M_2 advective signal and the M_4 resuspension signals in the February '96 inner station, produced the characteristic *'twin-peak'* signature in the concentration time series, originally noted by Weeks and Simpson, (1991) and Jones *et al.*, (1994), to be characteristic of SSC time series in shelf seas where tidal resuspension occurs.

At the February 1996 inner station (figure 6.7), the tidal signal in SSC was still evident, but clearly more complex, with periods of quarter-diurnal oscillations. To investigate what processes were operating at the February 1996 inner station, tidal displacement was taken between hours 57-70 and correlated to SSC (figure 6.39). To determine the state of the tide in context to the sediment peaks, tidal displacement was plotted against water depth (figure 6.40).

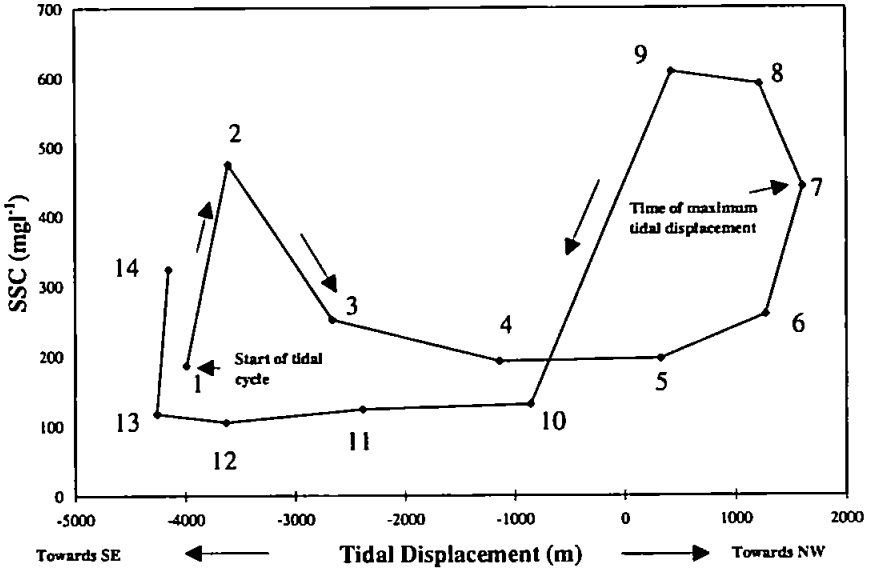

Figure 6.39 Plot to show tidal displacement Vs concentration over a complete tidal cycle (hour 57-70 , - February 1996 inner station

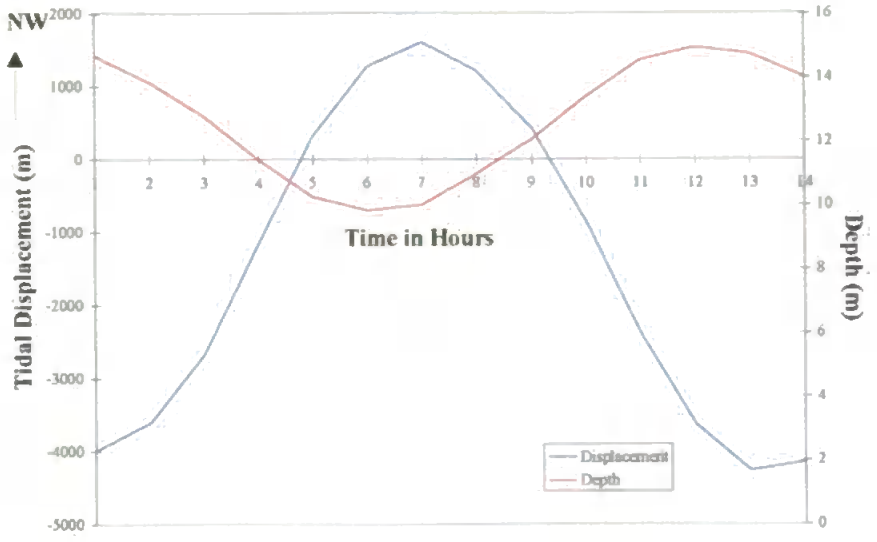

Figure 6.40 Water depth plotted against tidal displacement - February 1996 inner station (hour 57-70)

There was a distinct increase in concentration with tidal displacement towards the North West and a smaller increase in sediment concentration associated with the return displacement towards the South East, which suggests that there may be a secondary source of sediment being advected with the flood tide. The sudden increase in sediment concentration from hour 6 to hour 7 occurred at maximum tidal displacement, one hour after slack water. At hour 8, the sediment concentration increased further one hour after maximum displacement. Interestingly at hour 9, the highest sediment signal coincided with maximum tidal streaming which may suggest sediment resuspension. This may be the case, because from hour 9 to 10 there was a rapid decrease in sediment concentration, suggesting that the concentration enriched water had been displaced away from the BLISS tripods to the Southeast. One other hypothesis is a turbidity gradient which if inclined at an angle to the axes of the tidal ellipse, can create a complex relationship between the advective signal and the tidal displacement as seen in figure 6.39, (eg R. Wood, PML and D. Huntley - Pers. Comm., 1997). The phase between the flow and the SSC is not a straightforward indication of the relative importance of advection and resuspension. If this hypothesis is true, then the simple advection/resuspension modelling used by Weeks and Simpson, (1991) and Jago and Jones, (1993) must be treated with caution in a region such as Holderness where the concentration gradients may have both alongshore and cross-shore components. In the case of our Holderness measurements, the spatial structure of the SSC was not known and could only be inferred from the fixed tripod locations. We cannot

therefore distinguish between advection and resuspension purely on the basis of the phase of the SSC signal relative to the flow, or on the basis of the frequency of the SSC signals.

From the burst averaged time series plots (figure 6.4a, 6.7 and 6.8) it can be seen that wave conditions clearly have a major influence on the levels of SSC off the Holderness coast. This was most dramatically illustrated at the February 1996 outer station (figure 6.8) but was also clear in the other deployments (figure 6.4a and 6.7). Although some of the increase in SSC during storms may come from cliff erosion, it also seems likely that resuspension from the seabed plays a significant role.

From CASI images (Pers. Comm., Morris, 1997) there is evidence to suggest that there is a distinct turbidity zone marking the extent of the eroded beach and cliff material off shore. In the summer most of this fine material had settled out, to give very low SSC concentrations. In the winter the SSC were much higher at the inner station than at the outer station suggesting that a distinct turbidity gradient existed, decreasing in concentration towards the offshore. Cliff material eroded during the winter period, would have been carried in suspension by the currents both offshore and alongshore. The lower SSC levels measured at the outer station suggests that a significant amount of cliff material had either settled out from suspension or had been carried away from the Holderness region by the alongshore currents.

Corresponding roughness lengths (z_o) were increased during the winter storms, which are noted to increase the resuspension and dispersion of particles from the seabed (Jago *et al.*, 1994). A C_{d100} value of 0.0045 and 0.0025 was noted (table 6.5) during the February 1996 outer station storm when $\sigma_w/u_{100} = 1$ and 0 respectively, so taking the average between the two values, 0.0035 was used as a representative drag coefficient for the outer station storm. This value although slightly larger, was within the same order as 0.0025 which is the value traditionally employed in shelf-circulation models (Green *et al.*, 1995). Green *et al.*, (1990) noted, in agreement with the February 1996 outer station, that observed roughness lengths taken just North of the Holderness Coast, in Marsden Bay, were significantly greater during a storm, and were coincident with the higher levels of wave energy.

Separating the resuspension effects from advection effects in a local time series of SSC is clearly very difficult, especially during storm events. Two other ways were devised in

which these features could be identified in the BLISS data. Under some circumstances, alongshore advection was revealed by the strong correlation between salinity and SSC. Figure 6.12a represented such a correlation at the February 1996 outer station during pre-storm conditions (first 30 hours of figure 6.8). Low salinity, high turbidity water from the south, was advected past the tripod and was illustrative of the plume from the Humber estuary. The reduction in salinity was not caused by mixing because the CTD profiles showed a vertically well-mixed water column at all times. In contrast, during the storm at the same station (figure 6.12c), the very high values of SSC observed were insignificantly correlated with salinity and were therefore unrelated to the advection process. These high SSC values were likely due to resuspension from the seabed.

The second way of separating advection from resuspension effects was to use the burst current data to estimate the seabed stresses imposed by the combined waves and currents, and to compare these with the expected threshold values for sediment resuspension. Referring to figure 6.32 and 6.33, the sudden increase in SSC at the February outer station coincided with a significant increase in the friction velocity, and suggested a threshold friction velocity of $0.02ms^{-1}$. Similar analysis conducted for the February and July inner station data provided the implied thresholds given in table 6.7, along with equivalent grain diameters for non-cohesive sediments derived from the threshold curve of Miller *et al.*, (1977). However, given that high levels of SSC persisted for some time after storm conditions (seen in all cases), it is unlikely that the proposed grain sizes in table 6.7 are what was actually in suspension. It is more likely that the threshold friction velocities related to the erosion of cohesive, or partially cohesive, beds of fine sediments. The threshold friction velocities in February 1996 were entirely consistent with other observations of threshold for the bulk erosion of partially consolidated cohesive seabeds (Widdows et al., 1997). The much smaller July values were consistent with the threshold for erosion of an unconsolidated 'fluff' of fine sediment at the seabed. Hence the much calmer conditions in July, with periods between storms to allow the deposition of such a fine layer, makes this interpretation of the threshold friction velocity entirely plausible.

The time it took for the background suspension levels to reach pre-storm levels again depended on the severity of the storm and on continued wave activity after the storm. The larger the storm, the longer the settling time of the sediment. Settling velocities derived from the SSC decay curves for February outer station (section 6.3.7) estimated w_s values of 2.81×10^{-4} ms^{-1}. Similar calculations for the inner station data lead to the settling velocity

estimates given in table 6.3. These estimates in the range of 1.8 to 2.81 x 10-4 ms-1, correspond to fine silt particles or equivalently to typical settling velocities for fine sediment flocs with a diameter of <200μm in a tidally-dominated environment (Fennessy, 1994). They also correspond well to settling velocity measurements made by ship-based settling velocity tubed in the Holderness region (Pers. Comm., Jago, 1997). It is difficult to determine exactly the source of the sediment (due to lack of grain size measurements), but the size of the particles, calculated from the settling velocities, may suggest that the sediment originated from the Holderness Cliffs, since 67% of the cliffs are composed of sediments <63μm (McCave, 1987). The seabed surface sediments were highly variable in the nearshore zone of the Holderness coast, changing quite dramatically from summer to winter. In summer, grab samples taken from the inner site (~ 10m depth) revealed a thick covering of fine silt and clay material overlying sand. It is possible that ripples were formed at the July 1995 inner station by wave activity in low current velocities, which may suggest why larger roughness length values were produced in current velocities <0.2ms^{-1}. At high current velocities it is postulated that the ripples were washed out to produce a smooth seabed surface, which will explain the lower roughness lengths measured at higher velocities. In the winter, at the inner and outer station, the nature of the seabed surface, according to the derived C_{d100} and z_0 values, revealed a seabed composed of gravel and coarse sand >500μm. During calm weather periods the fine sediment in background suspension is thought to settle in between the interstices of the coarse grains, so creating a smooth surface and so lowering the z_0 values.

Analysis of the BLISS data has shown that there is clear evidence to suggest resuspension of the seabed, although the SSC signals are influenced greatly by changes due to the advection of ambient turbidity gradients. There is a strong link between variations in SSC and changes in salinity in the absence of resuspension, so confirming the advective nature of these changes. However, it is apparent during winter storm events, that resuspension is dominant. Evidence of resuspension is strongest at the BLISS outer station in February 1996, which recorded a storm with significant wave height of 3m. Here, the background SSC and the consequent advective effects appear to be less prominent than at the inner BLISS station. Hence a large increase in SSC was coincident with an increase in friction velocity above a threshold of 0.02ms^{-1}, and the resulting decay of SSC suggests the resuspension of fine, cohesive material with a settling velocity between 1.8 to 2.81 ms^{-1}. Similar values were noted at the February 1996 inner station.

Our results have important implications for estimating sediment fluxes in this region. The difficulty of distinguishing advective effects from resuspension effects, and the recognition that phase between flow and SSC cannot be used for this purpose means that direct estimation of flux from a single station is not possible without a detailed knowledge of the spatial variation of SSC around the station. Our results also imply that the advective component of SSC due to advection of the Humber plume can be identified by its strong correlation between SSC and salinity, and therefore in principle, can at least, be removed. This procedure might be useful in isolating the resuspension effects in certain circumstances (February 1996 outer station data), but advection of a cross-shore turbidity gradient caused by cliff erosion, cannot be identified in this way since there is no obvious relationship to salinity from cliff erosion

Finally, our results provide important parameters such as threshold shear stress for resuspension and sediment settling velocity as inputs into numerical models. In the winter data sets these sediment parameters are reasonably robust, but in the summer they are more difficult to estimate due to the relative importance of advection.

Chapter 7

7. Sediment Flux Transport - Results

7.1 Introduction

Simultaneous time series measurements of suspended sediment concentration (SSC), current velocity and elevation taken from 0.41m and 0.9m above the seabed, (chapter 6 figs. 6.4a, 6.7 & 6.8) revealed that suspension events at the BLISS sites were either a result of resuspension of material from the activity of the waves or currents, or from material which had been tidally advected into the region of the BLISS tripods. The effect from storm events were such that background levels of SSC were significantly increased. After the storm there was a distinct time lag after which the elevated suspended sediment settled out to the pre-storm levels. The emphasis of this chapter will be on deriving single point estimates of sediment flux from the BLISS measurements. Long-term fluxes and net transport will be discussed first. The second part will focus on the time series flux due to the waves and tides. The last part then considers instantaneous fluxes over short time scales (within burst activity). From concentration and velocity spectra, the net sediment transport contributions at different frequencies will be determined, and the relative importance and directions of sediment transport due to incident waves, long period motion and tidal burst averaged flows will be addressed.

7.2 Estimation of Sediment Flux

The product of the instantaneous sediment concentration and velocity measured at a point gives the local instantaneous sediment flux $c(t)u(t)$. SSC measurements taken every 0.2 seconds for 17 minute bursts at 0.41mab and 0.9mab, were multiplied with concurrent

current velocity (u,v) measurements at 0.41mab, (assuming the same instantaneous velocity at 0.9mab). The product of the instantaneous fluxes were then time averaged over 17 minutes to produce the total net sediment transport flux $\overline{c(t)u(t)}$ or the local net sediment transport rate at the measurement height (Osborne and Greenwood, 1992). The single over bar denotes a time average over 17 minutes (burst average). Multiplying the concentration and velocity before time-averaging preserved the fluctuating quantities. If one or both of c and u were constant, independent of time, then the net sediment transport rate would simply be the product of the mean concentration and the mean current (Huntley and Hanes, 1987). However, in the nearshore zone it is well recognised that the value of c and u fluctuate, and that net sediment transport can occur even in the absence of a mean flow (Huntley and Hanes, 1987). Hence, the total hourly sediment flux $\overline{c(t)u(t)}$ may be split up into steady, and unsteady, fluctuating components (Beach and Sternberg, 1991; Osborne and Greenwood, 1992; Russell, 1993).

[7.1]

$$\overline{cu} = \overline{c'u'} + \bar{c}\,\bar{u}$$

1. The fluctuating components of current velocity and suspended sediment concentration $\overline{c'u'}$ represent the flux contribution from waves and turbulence, which give rise to intra-burst variability.

2. The burst averaged flow components $\bar{c}\,\bar{u}$ (averaged over 17 minutes) represent the flux contribution from tidal effects and mean flows which give rise to the inter burst variability.

$\bar{c}$ and $\bar{u}$ may be further split up into its mean value (given as $\bar{c}$ averaged over the deployment i.e. $\bar{\bar{c}}$) and its tidal component c_t defined as; $c_t = \bar{c} - \bar{\bar{c}}$. Therefore, $\bar{c} = \bar{\bar{c}} + c_t$ and $\bar{u} = \bar{\bar{u}} + u_t$. As a result, $\bar{c}\,\bar{u}$ averaged over a deployment will include:

[7.2]

$$\overline{\bar{c}\,\bar{u}} = \bar{\bar{c}}\,\bar{\bar{u}} + \overline{c_t u_t}$$

The total flux transport over the complete time series $\overline{\overline{cu}}$, (double over bar denoting time averaged over whole deployment, or total flux over a storm or calm event) is then given by:

[7.3]

$$\overline{cu} = \overline{\bar{c}\,\bar{u}} + \overline{c_t u_t} + \overline{c' u'}$$

Where, $\overline{\bar{c}\,\bar{u}}$ are the overall means, $\overline{c_t u_t}$ is the tidal oscillatory flux and $\overline{c' u'}$ is the wave and turbulent oscillatory flux.

Results for July 1995 inner station and February 1996 inner and outer stations are discussed. For the inner station, fluxes from two different heights (0.41mab and 0.9mab) are presented.

In the following section, the contribution of the mean flux $\overline{\bar{c}\,\bar{u}}$ (long-term average) components to the net flux will be addressed.

7.3 Long Term Fluxes and Net Transport

Suspended sediment concentrations, fluxes and net transport are summarised in tables 7.1, 7.2 and 7.3. The summer and winter deployments were split up into storm events and calm periods. A positive sign indicates northwards transport in the alongshore direction and a positive sign in the cross-shore indicates offshore transport. It is assumed that sediment transport off Holderness is controlled not only by the waves and tides but also by the mean flow (i.e. long-term current average). By calculating the net mean flux and comparing the values to the net tidal flux will determine whether the mean flow is important in transporting the sediment.

The net transport results are summarised as follows. At the July 1995 inner station (table 7.1), storms occupied 120 hours of the total deployment time. The suspended sediment concentrations were higher during the storm events, but overall, were very low in comparison to winter SSC levels (table 7.2) at the same station. Measurements taken at 0.9mab were consistently higher than at 0.41mab. As discussed earlier (section 6.3.2) the optical sensor at 0.9 meters above the seabed probably had a calibration problem, which could explain the higher values. Net transport of the mean (long-term average flux, i.e. net mean transport) was consistently different to the tidal net transport. During the first storm, in the alongshore direction, net mean transport was directed towards the South and offshore, whereas for the tidal net flux, transport was directed towards the North and

onshore. In the calm period, the net mean flux changed direction to the North, and the tidal net flux changed direction to the South. The cross-shore directions remained the same. Directions again changed during the second storms for the tidal net flux, towards the North and onshore at 0.41mab and towards the North and offshore at 0.9mab, whereas the mean net flux stayed the same. Net transport averaged over the whole deployment, revealed that net transport due to the mean flow and that due to the tides was the same in the alongshore, towards the North, but in the cross-shore differed, being offshore (mean) and onshore (tidal) respectively.

For the February 1996 inner station and outer station, the deployments were split up into four categories; pre storm, storm activity, post storm activity and total deployment period. Suspended sediment concentration levels were significantly higher at the inner station than at the outer station. At the inner station, maximum concentrations were higher at 0.9mab in all events. The difference in the concentration values may be due to an offset problem, although the differences between each sensor are not consistent at each time period.

At the February 1996 inner station (table 7.2), the magnitude of the net mean flux averaged over the deployment were consistently higher than the net tidal flux in the alongshore and cross-shore direction. Directions of flow were again inconsistent. In the pre-storm period activity (to incorporate detail from storms 1 and 2, figure 6.7), the net mean flux was directed towards the North and offshore, whereas the tidal net flux was directed towards the South and onshore at both heights. During the neap storm (storm 3, figure 6.7), directions in the alongshore and cross-shore remained the same for the net mean flux. The tidal net flux however, changed direction towards off-shore transport although, in the alongshore the net transport was still towards the South. After the neap storm (to incorporate details of storms 4 and 5, figure 6.7), both the net mean flux and the net tidal flux changed direction for the alongshore transport. The net overall flux, showed that the mean flow contributed to a northward sediment movement and was generated onshore, and the tidal flux contributed to a northward and southward transport at 0.41 and 0.9mab respectively. The cross-shore net tidal flux was generated offshore.

The outer station deployment was dominated by a strong North Easterly spring tide storm (storm 5, figure 6.8) which lasted over a period of 108 hours. Maximum concentrations before the storm were 51.1 mgl^{-1} (table 7.3). The effect of the storm was to increase the SSC to a maximum level of 236.9 mgl^{-1}. Before and during the spring storm, the net mean

flux alongshore was towards the South and in an offshore direction. In the period that followed the storm, net mean transport alongshore changed towards the North, but remained offshore. The net tidal flux again opposed the direction of the mean flux in the alongshore and cross-shore before the storm. During the storm, sediment transport by the tides was towards the North and generated offshore. After the storm, transport alongshore reversed towards the South, but was still offshore. However, even though the signs were different for mean and tidal flux for each event, the overall net transport was the same, whereby net flux was generated towards the South and in an offshore direction.

What is clearly apparent from the net flux results is that a very small velocity of $0.3cms^{-1}$ (for example, the neap storm period, (table 7.2)) will produce a net mean flux which is larger than the net mean and tidal flux combined. Hence, even a small residual flow will make a large change to the long-term net fluxes. To accurately separate out the mean flow from the tidal flow over the long-term period, therefore requires a current meter which can measure to $> 3mms^{-1}$ degree of accuracy. Unfortunately, the BLISS electromagnetic current meters used to calculate these fluxes had sensor offset uncertainties that were larger than the accuracy required. For example, the smallest offset (at the February inner station) was $0.02ms^{-1}$. If we suppose a mean concentration of 168 mgl^{-1} (February inner station) an offset of $0.02ms^{-1}$ will produce a mean flux over the deployment period of 356 hours of 4306.2 kg m^{-2}, which is significantly greater than the overall net fluxes calculated. This leads us to the conclusion that we are unable to estimate the mean flow contributions to the fluxes using the BLISS data. This disappointing conclusion prevents us from estimating an overall flux budget at the BLISS stations. The problem is however a general one, since it is notoriously difficult to measure directly the mean flow, from benthic landers like BLISS using electromagnetic current meters, to the accuracy required for realistic long-term net flux estimates. Nevertheless, the BLISS tripods have successfully managed to measure single point fluxes at the tidal and wave frequencies, which can be used as inputs to calibrate numerical models on sediment transport at those levels. It is probably better to use models to calculate the long-term mean flux, rather than relying on observational data, because the current meters presently available cannot measure flow to the accuracy required.

Because of the uncertainty in the mean flow calculations, the remaining sections will concentrate on the flux measurements taken at the tidal and wave frequencies.

Table 7.1 Summary of suspended-sediment concentrations, fluxes and net transport during events at the July 1995 inner station deployment

Event	$\bar{v}$ **ms^{-1}**	$\bar{u}$ **ms^{-1}**	**Conc** $\bar{c}$ **mgl^{-1}**	**Max Conc mgl^{-1}**	**Mean Flux mgl^{-1} ms^{-1}**	**Mean Flux mgl^{-1} ms^{-1}**	**Net Flux due to Means kg m^{-2}**		**Net Flux Means and Tides kg m^{-2}**		**Net Transport at Tidal and Freq. > 1hr kg m^{-2}**	
	mean	mean	mean		$\bar{c}\,\bar{v}$	$\bar{c}\,\bar{u}$	along	cross	along	cross	along	cross
0.41mab	-0.001	0.018	1.4	3.6	-0.002	0.026	-0.27	3.74	1.5	2.9	1.77	-0.84
0.9mab			6.4	8.6	-0.009	0.117	-1.27	16.91	31.2	16.4	32.47	-0.51
storm												
(h 60-100)												
0.41mab	0.032	0.027	0.1	1.6	0.003	0.003	0.80	0.68	-0.2	0.6	-1	-0.08
0.9mab			5.8	6.8	0.187	0.159	46.35	39.42	20.1	37.1	-26.25	-2.32
Calm												
(h 101-169)												
0.41mab	0.015	0.034	1.9	8.5	0.029	0.065	8.3	18.65	34.4	15.0	26.1	-3.65
0.9mab			7.5	12.2	0.114	0.256	32.76	73.6	98.4	74.4	65.64	0.79
2 Storms												
(h 170-250)												
0.41mab	0.024	0.027	1.2	8.5	0.029	0.032	27.75	30.57	34.9	26.7	7.15	-3.87
0.9mab			6.7	12.2	0.163	0.179	155.01	170.67	186.2	167.3	31.19	-3.37
Total (h 264)												

Table 7.2 Summary of suspended-sediment concentrations, fluxes and net transport during events at the February 1996 inner station deployment

Event	$\bar{v}$ ms^{-1}	$\bar{u}$ ms^{-1}	Conc $\bar{c}$ mgl^{-1}	Max Conc mgl^{-1}	Mean Flux $mgl^{-1}\ ms^{-1}$	Mean Flux $mgl^{-1}\ ms^{-1}$	Net Flux due to Means $kg\ m^{-2}$		Net Flux Means and Tides $kg\ m^{-2}$		Net Transport at Tidal and Freq. > 1hr $kg\ m^{-2}$	
	mean	mean	mean		$\bar{c}\,\bar{v}$	$\bar{c}\,\bar{u}$	along	cross	along	cross	along	cross
0.41mab	0.019	0.007	189.1	610.9	3.593	1.276	2328.3	827.1	1544.5	-345.2	-783.8	-1172.3
0.9mab			237.7	760.4	4.516	1.605	2926.4	1039.7	1683.9	-676.2	-1242.5	-1715.9
Pre-storm												
(h 1-180)												
0.41mab	0.003	0.007	171.9	422.6	0.584	1.118	168.1	322	159.7	631.9	-8.4	309.9
0.9mab			191.4	439.3	0.649	1.245	187.1	358.6	59.9	687.6	-127.2	329
Neap storm												
(h 181-260)												
0.41mab	-0.031	-0.016	82.1	245.1	-2.55	-1.299	-881.3	-448.9	-712.7	-335.4	168.6	113.5
0.9mab			94.5	256.5	-2.966	-1.495	-1025.2	-516.7	-869.4	-445.4	165.75	71.3
Post storm												
(h 261-356)												
0.41mab	0.004	-0.006	168	610.9	0.638	-1.058	817.7	-1356.4	991.5	-48.7	173.8	1307.7
0.9mab			189	760.4	0.718	-1.191	920.5	-1526	874.4	-433.9	-46.1	1092.1
Total (h 356)												

Table 7.3 Summary of suspended-sediment concentrations, fluxes and net transport during events at the February 1996 outer station deployment

Event	$\bar{v}$ **ms^{-1}**	$\bar{u}$ **ms^{-1}**	**Conc** $\bar{c}$ **mgl^{-1}**	**Max Conc mgl^{-1}**	**Mean Flux mgl^{-1} ms^{-1}**	**Mean Flux mgl^{-1} ms^{-1}**	**Net Flux due to Means kg m^{-2}**		**Net Flux Means and Tides kg m^{-2}**		**Net Transport at Tidal and Freq. > 1hr kg m^{-2}**	
	mean	mean	mean		$\bar{c}\,\bar{v}$	$\bar{c}\,\bar{u}$	along	cross	along	cross	along	cross
0.41mab **Pre-storm (h 1-85)**	-0.001	0.04	18.6	51.1	-0.009	0.748	-3.02	228.9	24.7	218.3	27.72	-10.6
0.41mab **Spring storm (h 86-170)**	-0.026	0.056	106.5	236.9	-2.74	5.89	-847.4	1823.2	-578.8	2032.3	268.6	208.9
0.41mab **Post storm (h 171-355)**	0.006	0.039	41.1	135.1	0.23	1.63	156.1	1082.4	100.6	1099.4	-55.5	17
0.41mab **Total (h 355)**	-0.003	0.04	51.7	236.9	-0.171	2.255	-218.5	2881.6	-453.5	3350.1	-234.9	468.5

7.4 Sediment Fluxes - Time Series Results

Time series of flux and net transport resulting from the single-point estimates and the corresponding wave conditions are shown in figures 7.1 to 7.7. The wave conditions are presented as significant wave heights and wave orbital velocities. Total flux magnitude shown in panel D is the resultant of the tidal and wave burst averaged flux (over 17 minutes) alongshore $\overline{cv}$ and cross shore $\overline{cu}$. The resultant tidal and wave oscillating flux components are presented as vectors (panel E and F) to show not only the magnitude of the flux but also the direction. For these vectors a positive value in the alongshore represents flux directed towards the North West and positive in the cross-shore represents flux moving off-shore. The bottom panel G, shows the cumulative flux transport due to the waves and tides, split into alongshore and cross-shelf components.

7.4.1 July 1995 Inner Station

Weather conditions for July 1995 were described in detail in Chapter 6, section 6.3.1. The storms depicted in panel A, figure 7.1 and 7.2, were generated from a North Easterly swell. Peak wave heights of 0.45 - 0.5m related to wave orbital velocities 0.25 - 0.29ms^{-1} respectively. Flux magnitude calculated at 0.41mab (figure 7.1, D) were highest during the summer storms, with peak values reaching up to 1.1 x10^{-3} kgm^{-2} s^{-1}. The tidal and wave oscillating vectors representing flux transport, showed that sediment transport due to the tides (panel E) was stronger towards the North West, whereas sediment transport in response to the waves (panel F) was generated onshore. The tidal fluxes were an order of magnitude greater than the fluxes due to the waves, although in comparison to the winter conditions shown in figures 7.3 - 7.5 the summer fluxes were very small. During the no-wave period between hours 110 to 160, there was negligible flux transport. The net transport given as the cumulative flux of the combined tidal and wave oscillating components in the alongshore and cross-shore, (panel G) showed that over the deployment period significant transport only occurred when there was prolonged wave activity. The same time corresponds to spring tidal conditions.

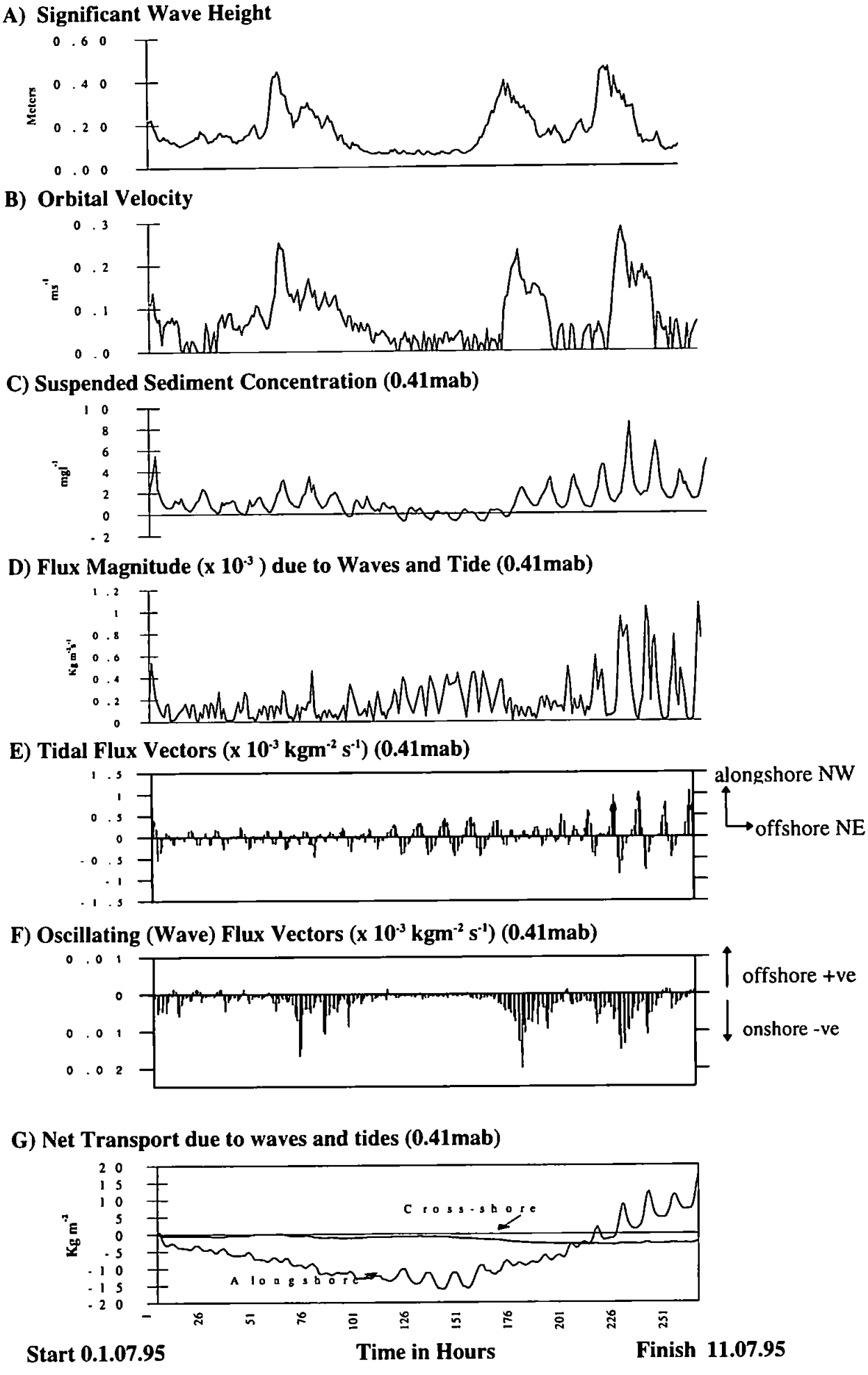

Figure 7.1 Sediment fluxes and net transport - July 1995 inner station (0.41 m above bed)

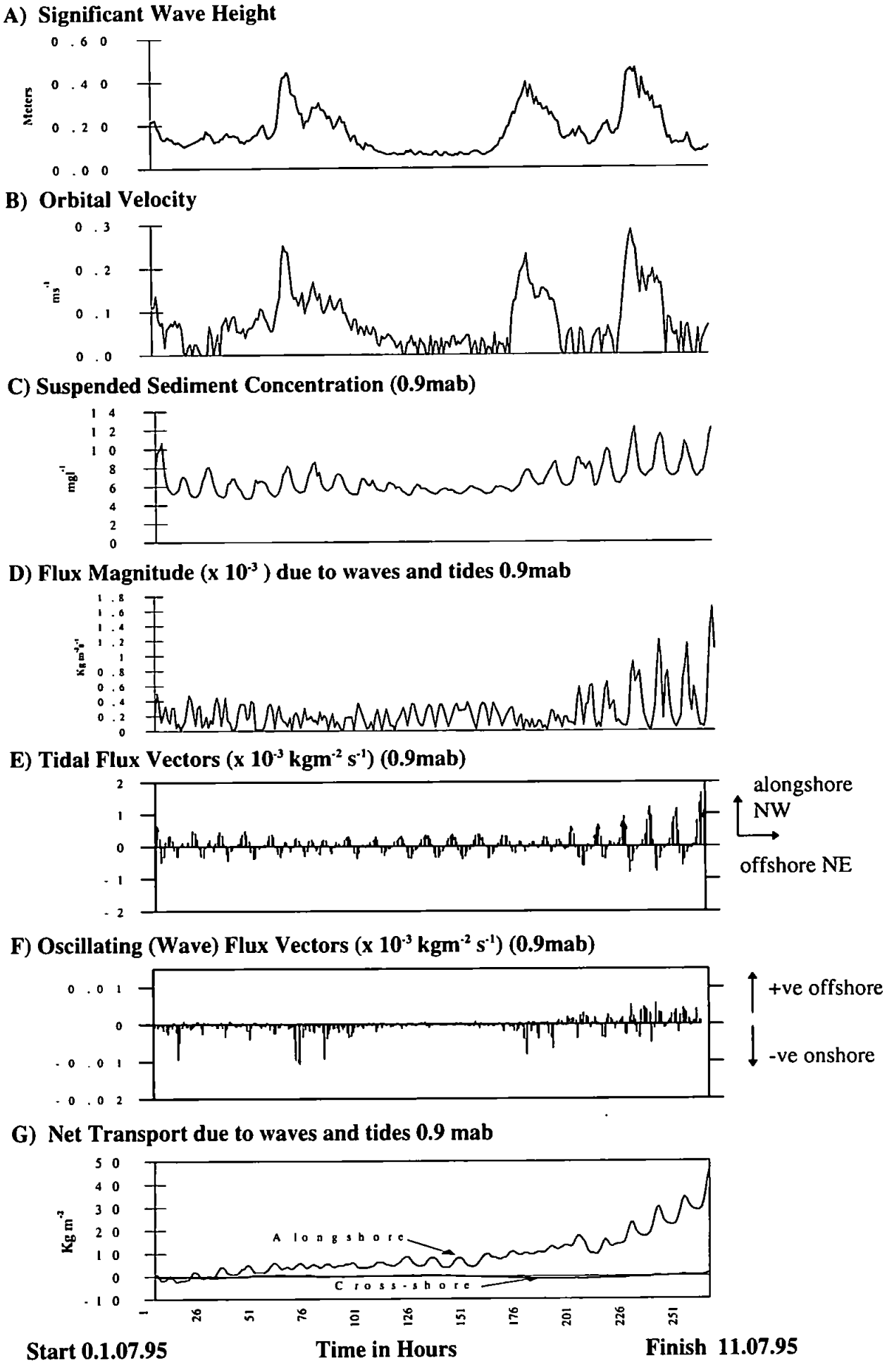

Figure 7.2 Sediment fluxes and net transport - July 1995 inner station deployment 0.9mab

In the cross-shore sense, ~ 1 to 5 Kgm^{-2} was transported onshore past the measurement point during the storms. In the alongshore sense, ~15 Kg m^{-2} was transported towards the South East during the first storm. After the calm period (hour 160), net transport was towards the North West. At the end of the deployment ~ 30 Kgm^{-2} of sediment had been transported past the mooring point towards the North West. Although the waves (both in the alongshore and cross-shore) generated sediment flux movement onshore, the tidal influence on moving the sediment was significantly stronger.

Fluxes calculated at 0.9mab (figure 7.2) used velocity measurements taken from 0.41mab and SSC measurements taken from 0.9mab. It was assumed that there was no change in the velocity field between 0.41m and 0.9m. The flux magnitudes maintained a value of ~0.4 x 10^{-3} kgm^{-2} s^{-1}, increasing to a maximum of ~1.8 x 10^{-3} kgm^{-2} s^{-1} during the two latter storms (after hour 160), noticeably greater in magnitude than the fluxes measured nearer to the seabed. The tidal fluxes both in the cross-shore and alongshore were significantly stronger towards the North West after hour 160. Wave induced fluxes indicated both on shore and off shore flux movement, and although they were within the same order of magnitude as the lower (0.41mab) fluxes, they were smaller. As a result, net transport was negligible in the cross-shore direction and dominant towards the North West, to reach a maximum net flux transport of 45 kg m^{-2} alongshore. The alongshore flux calculated at 0.9mab was 3 times greater than net alongshore flux at 0.41mab and was notably in the opposite direction. As mentioned in 6.3.2 the upper OBS at 0.9mab was thought to have an offset problem. Comparisons of the burst averaged concentration time series at both heights for the July inner station (panel C, figures 7.1 & 7.2), showed that there was a difference of ~5.1 mgl^{-1} between each time series being greater at 0.9mab. The smaller wave fluxes measured at 0.9mab may have influenced the direction of the net cumulative flux transport in the alongshore when the values were combined with the tidal fluxes. In fact, these net transport results show that accurate long-term averages would need to be much longer in time and more comprehensive in the vertical.

7.4.2 February 1996 Inner Station

There was continuous wave activity during the inner station deployment. Storm waves at hour 200 were generated by a North Easterly swell (see section 6.3.3 for weather details) and reached peak heights of 1.5m. Corresponding peak wave orbital velocities were

0.7ms^{-1}. At the end of the deployment the onset of a much bigger storm was recorded. Wave heights and orbital velocities at the start of this storm were 3m and 1.2ms^{-1} respectively and were generated by swell from the North and North East. Flux estimates taken from 0.41mab (figure 7.3) and 0.9mab (figure 7.4) were very similar in magnitude and direction. The high SSC levels were characteristic of winter conditions and total flux magnitudes measured at each height appeared to be greater before the neap storm. The tidal vector plots (figures 7.3, 7.4 E) illustrated this point and also showed that the fluxes were greater in magnitude towards the South before the neap storm. After the storm, the flux magnitude was slightly greater towards the North West. The wave flux vectors showed clearly for both 0.41 and 0.9mab (figures 7.3 and 7.4, F) that during the two storm events, sediment transport was in an offshore direction, although, the alongshore flux was still greater by an order of magnitude. Net (cumulative) sediment transport due to the tides and waves at 0.41mab and 0.9mab (figure 7.3 and 7.4, G) showed a general trend towards the South in the alongshore direction before the neap storm, with a consistent off-shore movement of sediment in the cross-shore direction. At the onset of the neap storm, alongshore flux stopped progressing towards the south and maintained a constant value upto ~ hour 190 when the net transport reversed direction and moved towards the North West. The cross-shore fluxes clearly increased in the offshore direction as a result of the storm waves.

Figure 7.5 shows alongshore and cross-shore flux transport split up into its wave and tidal components. The results clearly illustrate that offshore transport was controlled by the tide and by the waves. Waves alongshore generated a North West movement which may account for the reversal of the alongshore flux after the neap storm (storm 3, figure 6.7) and during the spring storm (storm 5, figure 6.8). Crude estimates from looking at the net transport time series (figure 7.3 and 7.4, G) suggests that the amount of sediment transported offshore over the whole deployment at both heights above the seabed was between 1000-1500 kg m^{-2}. Close to 1500 kg m^{-2} was transported towards the South over the first 150 hours. In reaction to the neap storm and the spring storm ~1000 kg m^{-2} was carried in the alongshore back towards the North West.

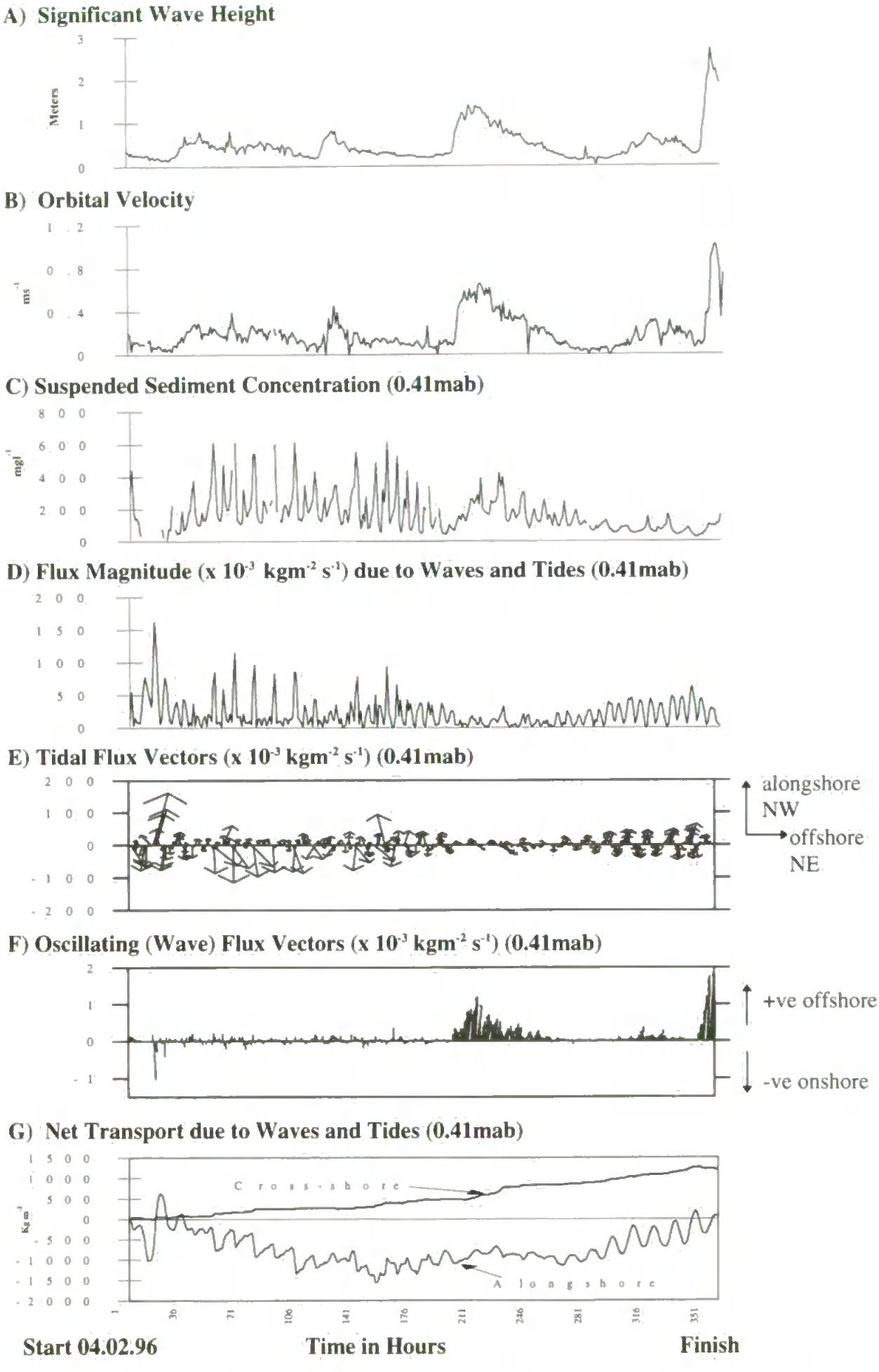

Figure 7.3 Sediment fluxes and net transport - February 1996 inner station 0.41m above bed

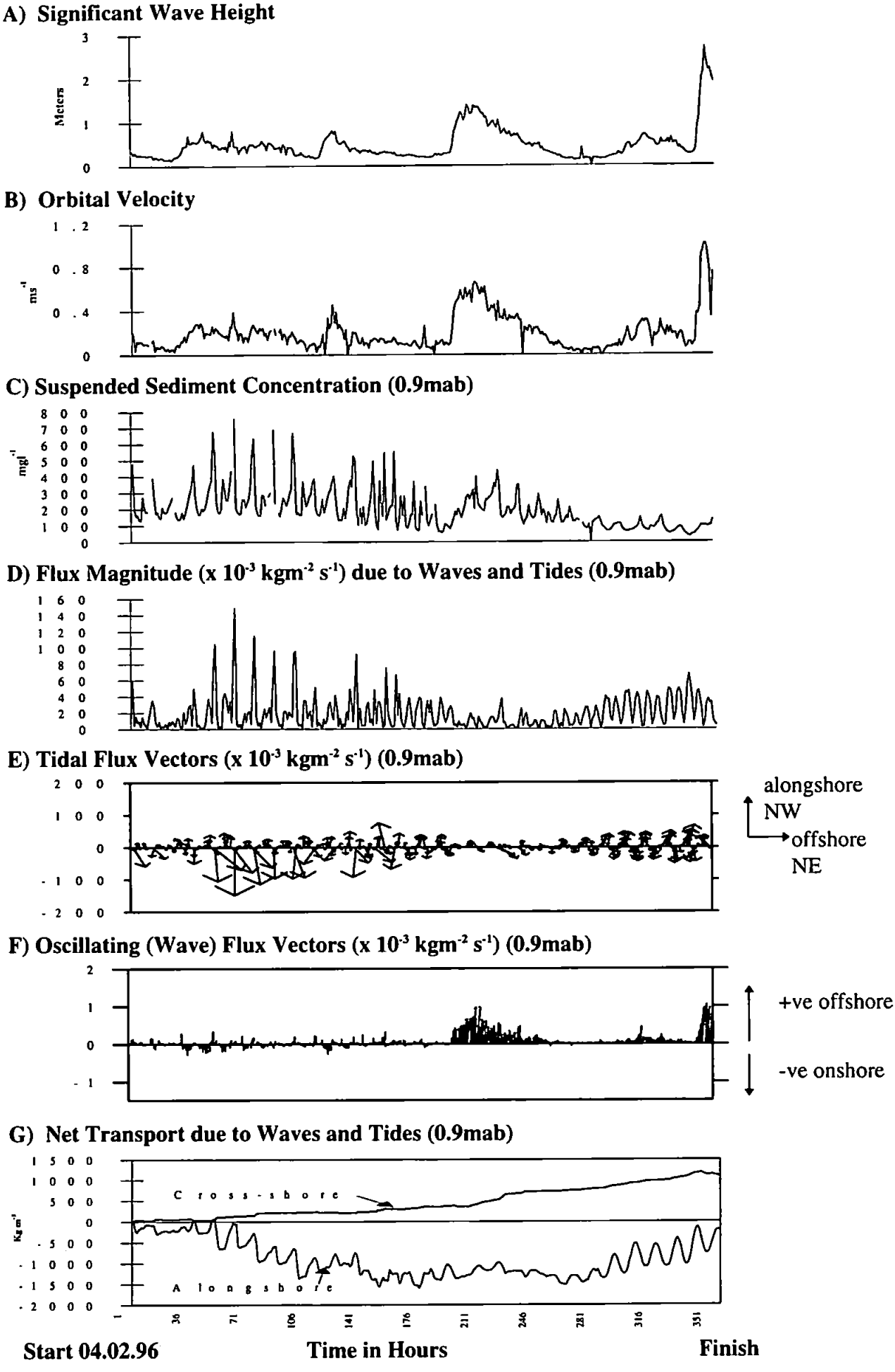

Figure 7.4 Sediment fluxes and net transport - February 1996 inner station 0.9 m above bed

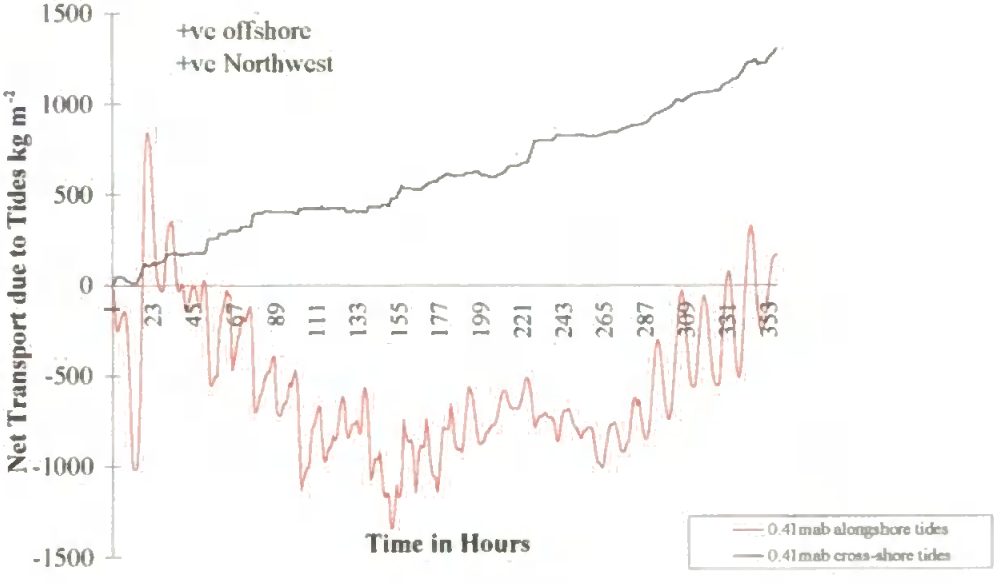

Figure 7.5 Alongshore and Cross-shore flux transport separated into its wave (a) and tidal components (b) - February 1996 inner station deployment

7.4.3 February 1996 Outer Station

The spring storm, just discussed at the end of the inner station deployment, was recorded at the outer station. Wave heights and wave orbital velocities before the storm reached peaks of 1m and 0.4 ms^{-1} respectively (figure 7.6 A and B). During the storm (hours 85 - 160) peak wave heights were 2.9m and peak orbital velocities were 1 ms^{-1}. Flux measurements represent conditions at 0.41mab only. Flux magnitudes (figure 7.6 D) elevated from ~ 15 x 10^{-3} kgm^{-2} s^{-1} to ~25 x 10^{-3} kgm^{-2} s^{-1} at the start of the storm and increased further to a maximum of 35 x 10^{-3} kgm^{-2} s^{-1} during the storm. The corresponding tidal flux vectors (figure, 7.6 E) showed a significant increase in the flux magnitudes as a consequence of the storm and showed a distinct movement of the sediment towards the off-shore. In the alongshore direction, the tidal fluxes did indicate a favoured direction towards the South, during the spring storm. The oscillating wave fluxes clearly showed transport towards the off-shore, at the onset of the storm and during the storm. Separating out the cross-shore and alongshore flux into their separate wave and tidal components, figure 7.7a and b showed that the cross-shore wave component was directed offshore, and the tidal component was negative onshore before the spring storm (upto hour 85). At the onset of the storm, the tidal cross-shore flux reversed direction, towards the offshore.

The corresponding alongshore components showed that wave flux alongshore was also directed towards the North West and that the alongshore tidal flux was relatively balanced in a North/South direction before the Spring storm. This feature indicated clearly that there was no preference for sediment movement alongshore in either direction. At the onset of the storm, net flux due to the tide was generated towards the south. The combined net transport due to both the tide and waves (figure 7.6, G) showed that in the event of the storm, the combined effect of an offshore directed flux due to the tides and waves was capable of moving significant amounts of sediment offshore. From the storm to the end of the deployment, ~2500 kg m^{-2} of sediment was moved offshore, but there was much smaller net movement of sediment alongshore (~ 250 kgm^{-2}) towards the South.

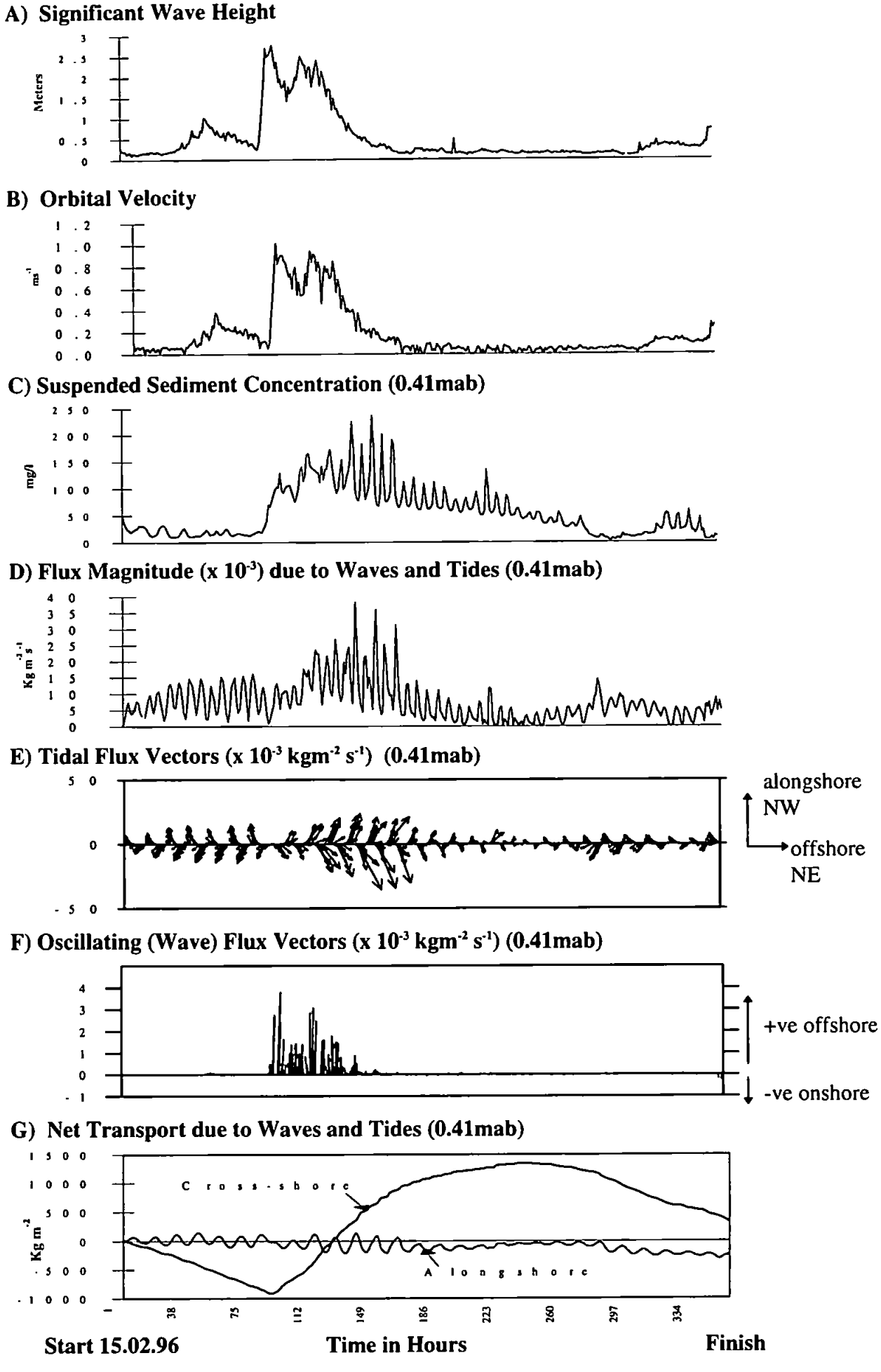

Figure 7.6 Sediment fluxes and net transport - February 1996 outer station 0.41m above bed

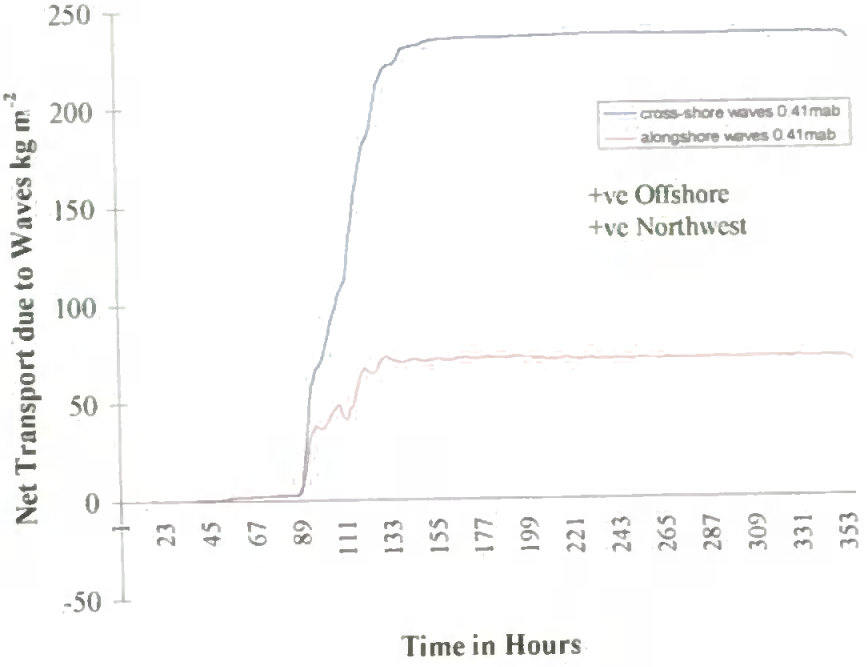

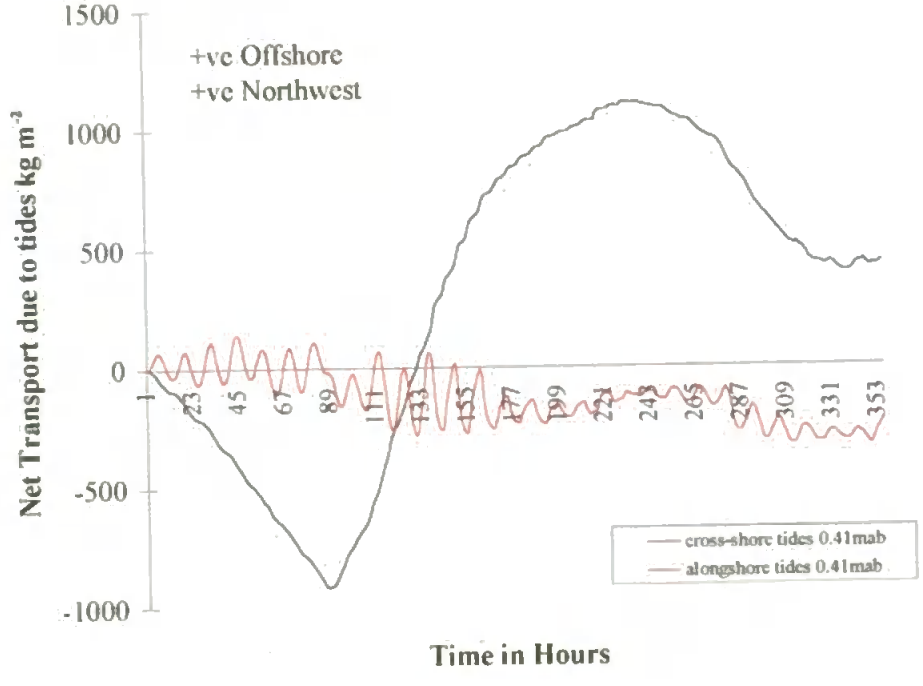

Figure 7.7 Alongshore and Cross-shore flux transport separated into its wave (a) and tidal components (b) - February 1996 outer station deployment

7.5 Suspended Sediment Transport Rates - Contributions at Different Frequencies

So far, we have considered net sediment transport in terms of large time scale events such as storms and the tides. In this section, emphasis is placed on determining what frequencies in the instantaneous fluctuations of concentration c(t) and velocity u(t) (over 17 minutes) are responsible for net sediment transport. It is readily accepted that transport will happen when fluctuations in u(t) and c(t) occur at the same frequency, and are in-phase or are in anti-phase with each other (Huntley and Hanes, 1987). Net transport will not occur if the concentration and velocity fluctuations are in quadrature, or if the c and u fluctuations occur at different frequencies, since their product will then average out to zero over time (Huntley and Hanes, 1987).

Using the intra-burst (17 minutes) instantaneous fluctuating values of c(t) and u(t), an appropriate measure of the net sediment transport contribution (due to waves and turbulence) to any particular frequency, is the co-spectrum between u(t) and c(t). The co-spectrum (refer to section 5.4.1) gives the cross-product between c(t) and u(t) as a function of frequency, and is the in-phase part of the cross spectrum, which also includes the quadrature spectrum. It reveals the relative contributions to the rate and direction of sediment transport of oscillations at different frequencies. Hence, integration of the co-spectrum over all frequencies is equal to the net sediment flux due to the fluctuating components $\overline{c' u'}$ (Jenkins and Watts, 1968, equation 8.3.16; Beach and Sternberg, 1991). The co-spectrum may also be referred to as the fluctuational transport (Hanes, 1988).

In this section, we are concerned mainly with cross-shore sediment transport. Spectra and co-spectra of u and v with concentration c at the two heights (0.41 and 0.9mab), are given for representative burst data during pre-storm, storm and post-storm periods, highlighted in the time series for July 1995 inner station and February 1996 inner and outer station. Since a positive u is considered to be off-shore flow, a positive co-spectrum will imply an offshore transport of suspended sediment, and a negative co-spectrum, will indicate on-shore sediment transport.

The spectra and co-spectra were obtained using the standard MATLAB 'Spectrum' function (section 5.4). A 50% overlapping Hanning data window was used on each data burst.

Sampling frequency was set at 5 Hz, giving a Nyquist Frequency of 2.5Hz. Each burst lasted 17 minutes. Because analysis was for 50% overlapping pieces, the number of degrees of freedom (dof) can be computed using the relationship $\nu = 3.82N_p - 3.24$ (Nuttall, 1971), where N_p is equal to the number of non-overlapping samples, given as; the number of data points divided by the number of non-overlapping segments, i.e the window length. For example, given a burst of 5120 data points (sampling at 5 Hz) and a Hanning window of 512, then $\nu = 3.82*10-3.24 = 34.96$ dof.

To determine whether the spectral peaks in the spectra were 'real' or just a statistical extreme, the 95% confidence intervals for the upper and lower spectral limits were obtained by comparing 34.96 degrees of freedom to the probability graph (Jenkins and Watts, 1968, p.82). The upper and lower limits for 34.92 dof are 1.72 and 0.66 respectively. These numbers define the length of the 95% confidence interval drawn on the spectra. Width of the 95% confidence limits along the spectral density axis will vary depending upon the frequency resolution chosen. Most commonly, at least 20 degrees of freedom are necessary to define a spectrum clearly (Pers. Comm., Huntley, 1995). A biased upper limit for zero coherence was computed using the formula after Goodman (1957),

[7.4]

$$C^2 ubiased = 1 - a^{2/(\nu-2)}$$

where ν = degrees of freedom

a = percentage of confidence i.e. 95% confidence = 0.05.

and was used in conjunction with the following equation [7.4] Jenkins and Watts (1968) to draw the zero coherence line C_u^2. Any coherence peaks below this line is not significant from zero.

[7.5]

$$C_u^2 = C^2 ubiased - \frac{2}{\nu}(1 - C^2 ubiased)$$

The boundary (spectral trough) between the infragravity (long-period motion) and gravity (incident wave energy) band was determined by looking at the pressure spectra for each data run chosen. For the February 1996 inner and outer stations data series the boundary

was chosen to be 0.05 Hz (20 seconds), which is consistent with other observations typical of high energy storm conditions (Osborne and Greenwood, 1992, Russell, 1991, Guza and Thornton, 1982). For the July 1995 inner station data runs, the boundary was chosen to be 0.08Hz (12.5 seconds), and was more typical of a low energy environment (Huntley and Hanes, 1987).

7.5.1 Results of the Cross-Spectral Analysis

Single data runs (17 minute bursts) were chosen in each deployment to represent pre-storm, storm, post-storm and calm conditions over different tidal states. The spectra and co-spectra between u and c of the chosen runs are presented and the similarities and dis-similarities between the events are discussed.

Pre-storm Conditions (Refer to Figures 7.8, 7.9 and 7.10)

The cross-shore velocity spectrum for each deployment (figure, 7.8, 7.9, 7.10) showed that a large contribution of the variance was dominated by the gravity component, with peak contribution centred at the incident wave frequency. Peak frequency varied from 0.15 Hz (6.6 seconds) in July (figure 7.8) to 0.13 Hz (figure 7.9) and 0.09 Hz (figure 7.10) at the February inner and outer stations respectively. The suspended sediment concentration spectra at 0.41 and 0.9mab in July 1995, gave a distinct peak again at 0.15 Hz suggesting that the SSC and cross-shore velocity were closely correlated. SSC spectra at the inner and outer station in February 1996 were noticeably different. No significant peak occurred at the inner station, and at the outer station the SSC spectra showed a prominent peak in the infragravity band at 0.025 Hz relating to long period motion. Coherence (agreement) between u and c were similar for all deployments and showed maximum coherence at the incident wave period. At the February 1996 inner station, coherence was also noted at the infragravity frequencies. The transfer function estimate showed also that at the incident wave frequency and infragravity frequency, c and u were in-phase at 0.41 and 0.9 mab in all deployments, although at the outer station in February 1996 c and u at the lower frequencies were slightly out of phase. The resulting co-spectra between c and u showed marked differences between summer and winter. In July 1995, the co-spectrum showed a strong negative contribution at 0.13 Hz (0.41mab) and 0.13-0.15 Hz (0.9 mab). This implied that the incident wave motion contributed to a net onshore flux of suspended sediment.

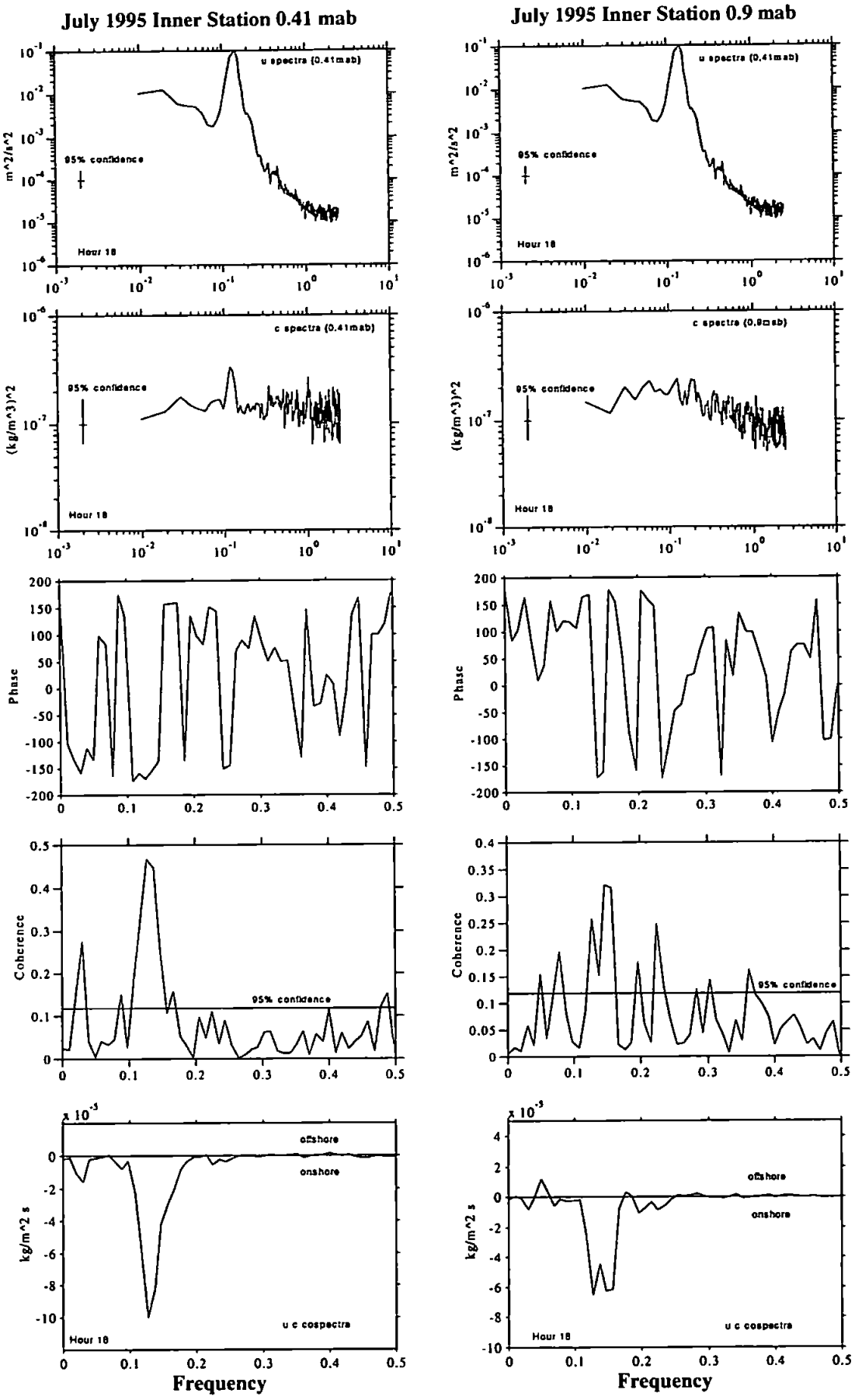

Figure 7.8 Spectra of c and u during a burst in pre-storm conditions (hr 18) at high water slack

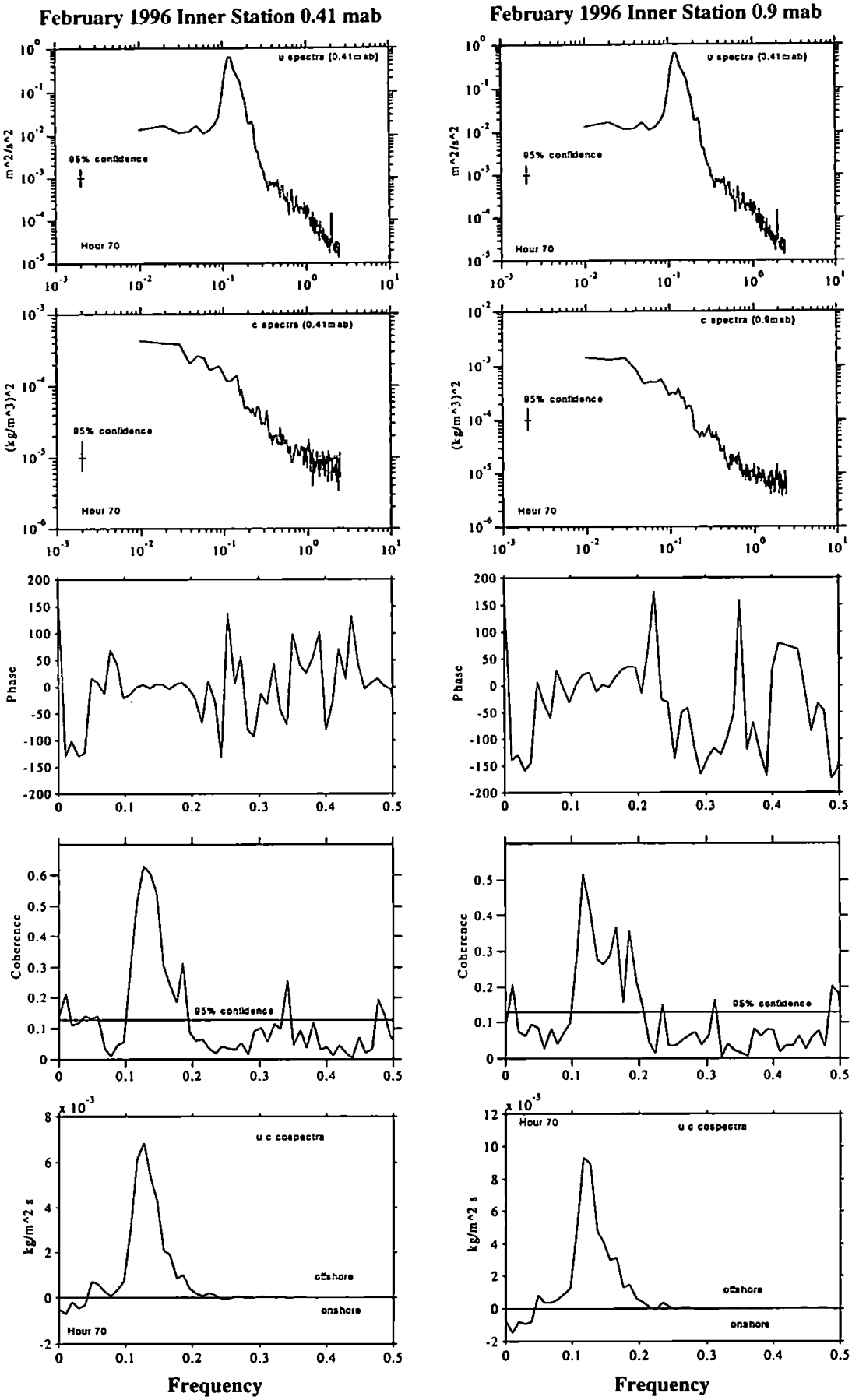

Figure 7.9 Spectra of c and u of a burst, in pre neap storm conditions (hr 70) 4 hours before high water

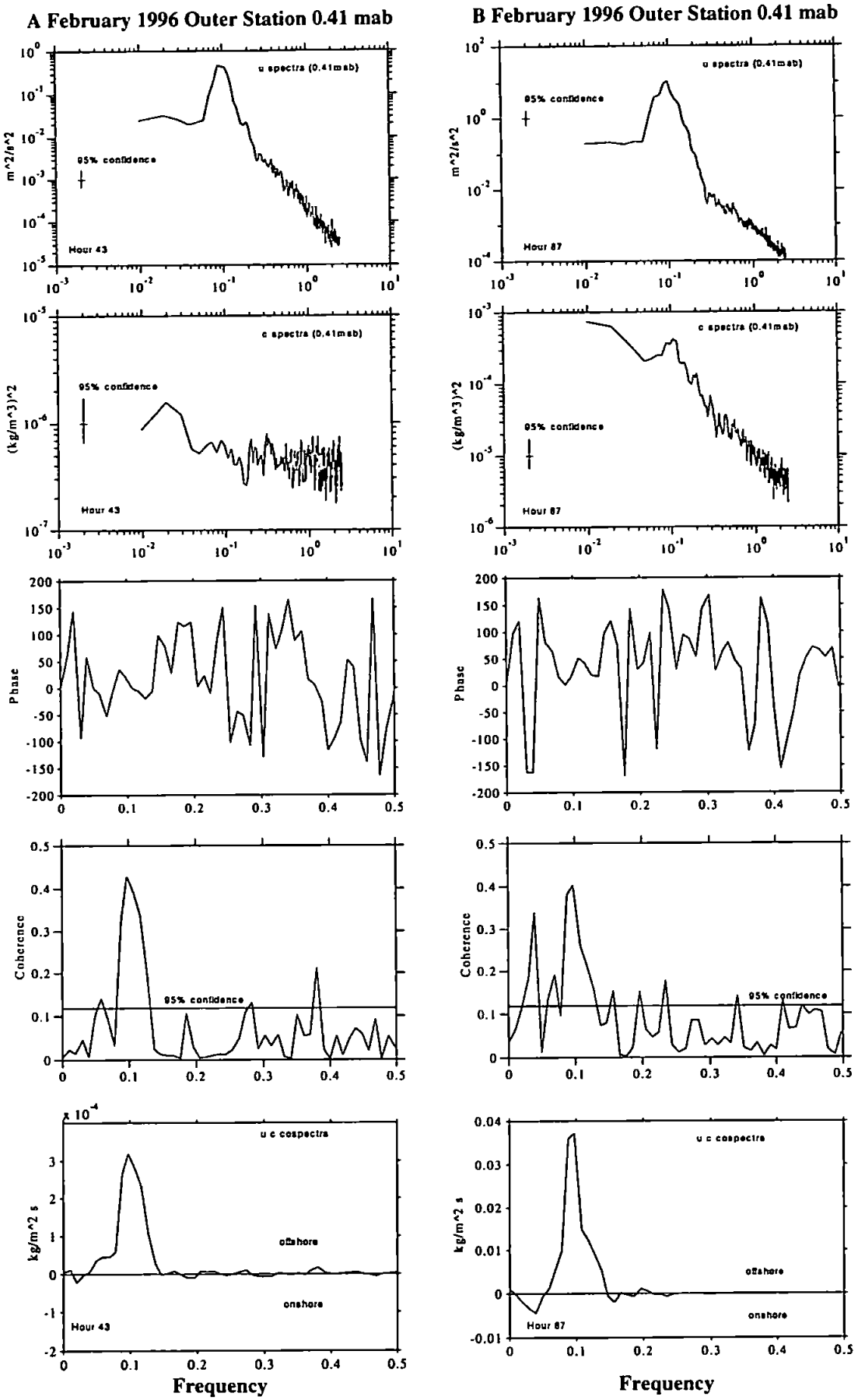

Figure 7.10 Spectra of c and u of a burst, A) pre-storm (hr 43) at high water B) Spring storm (hr 87) at low water slack

There was also a small onshore flux contribution at both heights in July 1995, due to long period motion at 0.03 Hz. In winter, conditions at the February inner and outer station was such that the co-spectra between c and u showed strong offshore sediment transport at the incident wave frequencies. Similar to July, there was a small contribution to onshore sediment transport from long period motion at the infragravity frequencies.

Storm Conditions (Refer to Figures 7.11, 7.12, 7.13, 7.14 and 7.10)

Wave heights in each deployment varied significantly. The smallest storms occurred in July 1995 with H_{sig} of 0.41m. The neap storm at the inner station in February 1996 produced H_{sig} of 1.5 m. The spring storm at the outer station in February 1996 produced H_{sig} of ~2.7m. The resulting spectra of c and u showed marked similarities in all storms. The cross-shore velocity spectra showed a dominant peak in the gravity band centred at the incident wave frequency and at the inner station in both the July 1995 (figure 7.11 to 7.13) and February 1996 (figure 7.14) storms, a much lesser peak arose in the infragravity band at 0.02Hz and 0.01Hz respectively. At the outer station in February 1996 (figure 7.10) there was no contribution in the infragravity wave band. Interestingly, there were no significant peaks in the SSC spectra for the July storms, but in February 1996 at both stations, the SSC spectra showed peaks in spectral energy at both the incident wave band and at the infragravity wave band. Coherence varied depending on the phase relationship between c and u. In all the storms, there was strong coherence between c and u at both measurement heights in the incident wave frequencies, showing an in-phase relationship in the gravity band. Phase relationships in the infragravity frequencies varied from storm to storm. c and u were slightly out of phase at 0.9mab during the February inner station storm (figure 7.14). This feature was also noticed during the July second storm (figure 7.12) where at 0.9mab c and u were out of phase at the infragravity wave band but were in-phase at 0.41mab. In the other storms for July and at the outer station in February, c and u were in-phase at both heights in the infragravity frequencies. The resulting co-spectra of c and u again displayed marked differences between summer and winter. The storms in July 1995 showed dominant onshore sediment transport at both measurement heights in the gravity band, with peak transport occurring at ~ 0.15 Hz. During the winter storms at the February 1996 inner and outer stations, sediment transport at the same incident wave frequency was dominant offshore. The direction of sediment transport in response to the infragravity frequencies varied in July with height above the seabed.

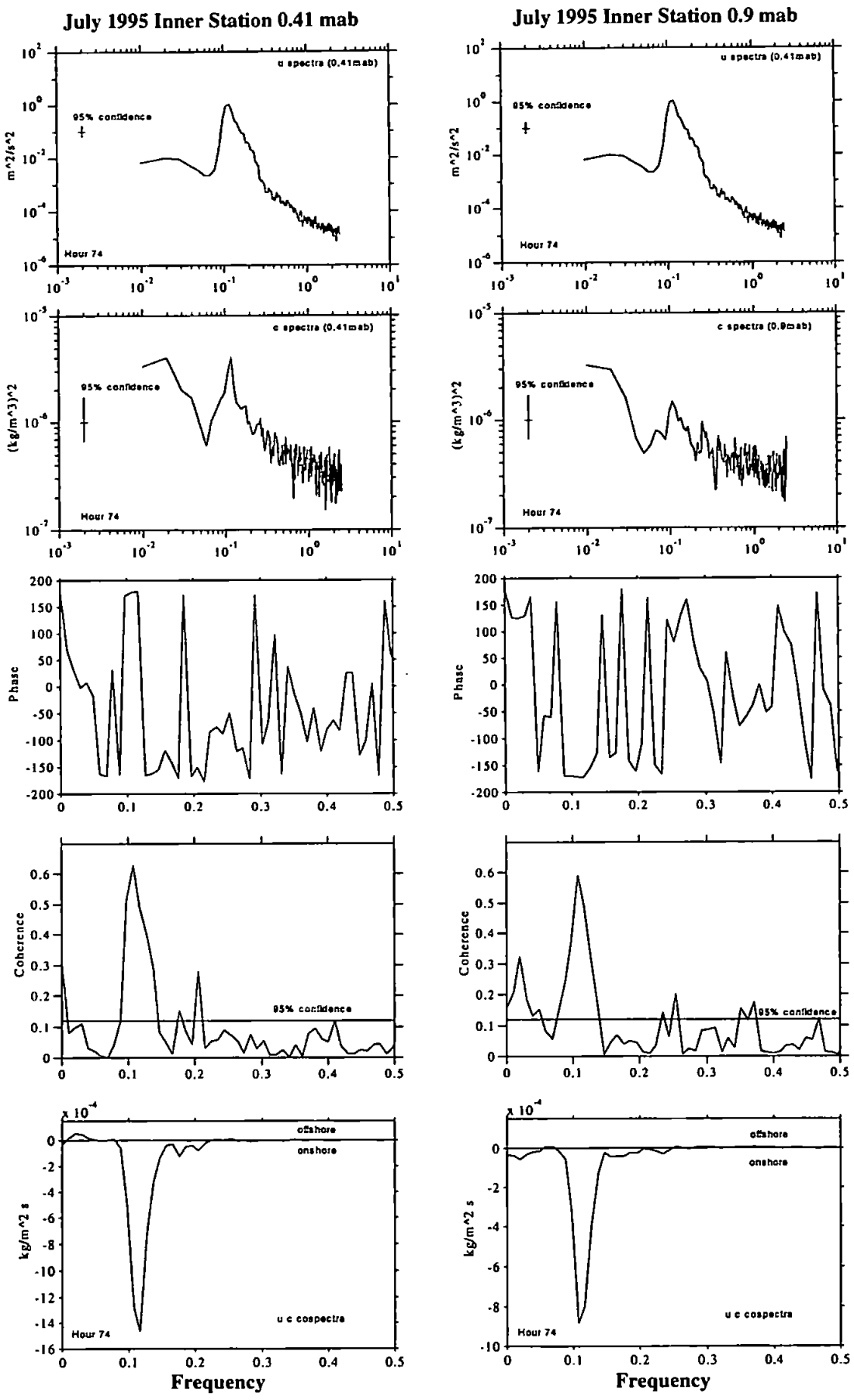

Figure 7.11 Spectra of c and u of a burst, during first storm (hr 74) at maximum tidal streaming on flood

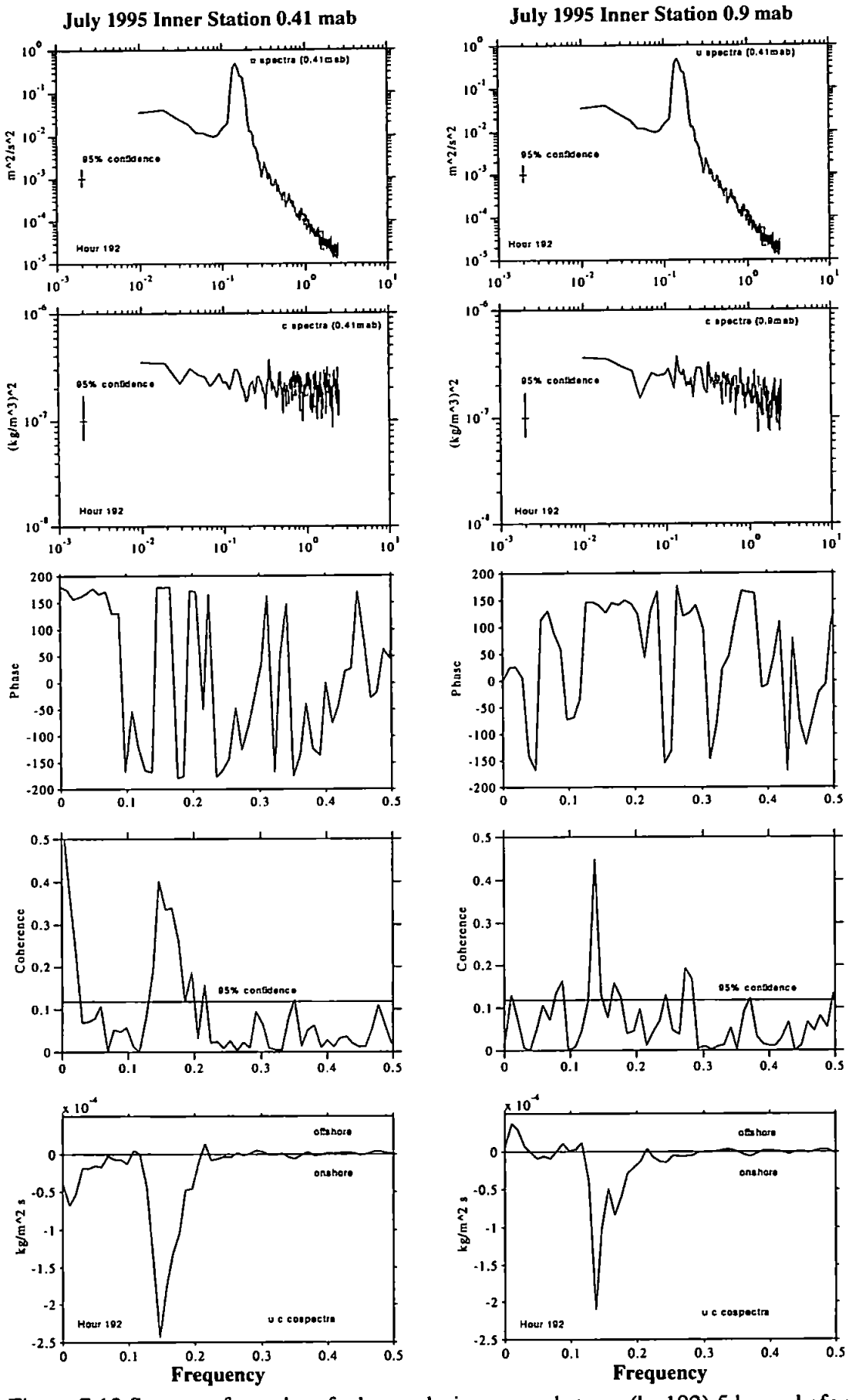

Figure 7.12 Spectra of c and u of a burst, during second storm (hr 192) 5 hours before low water

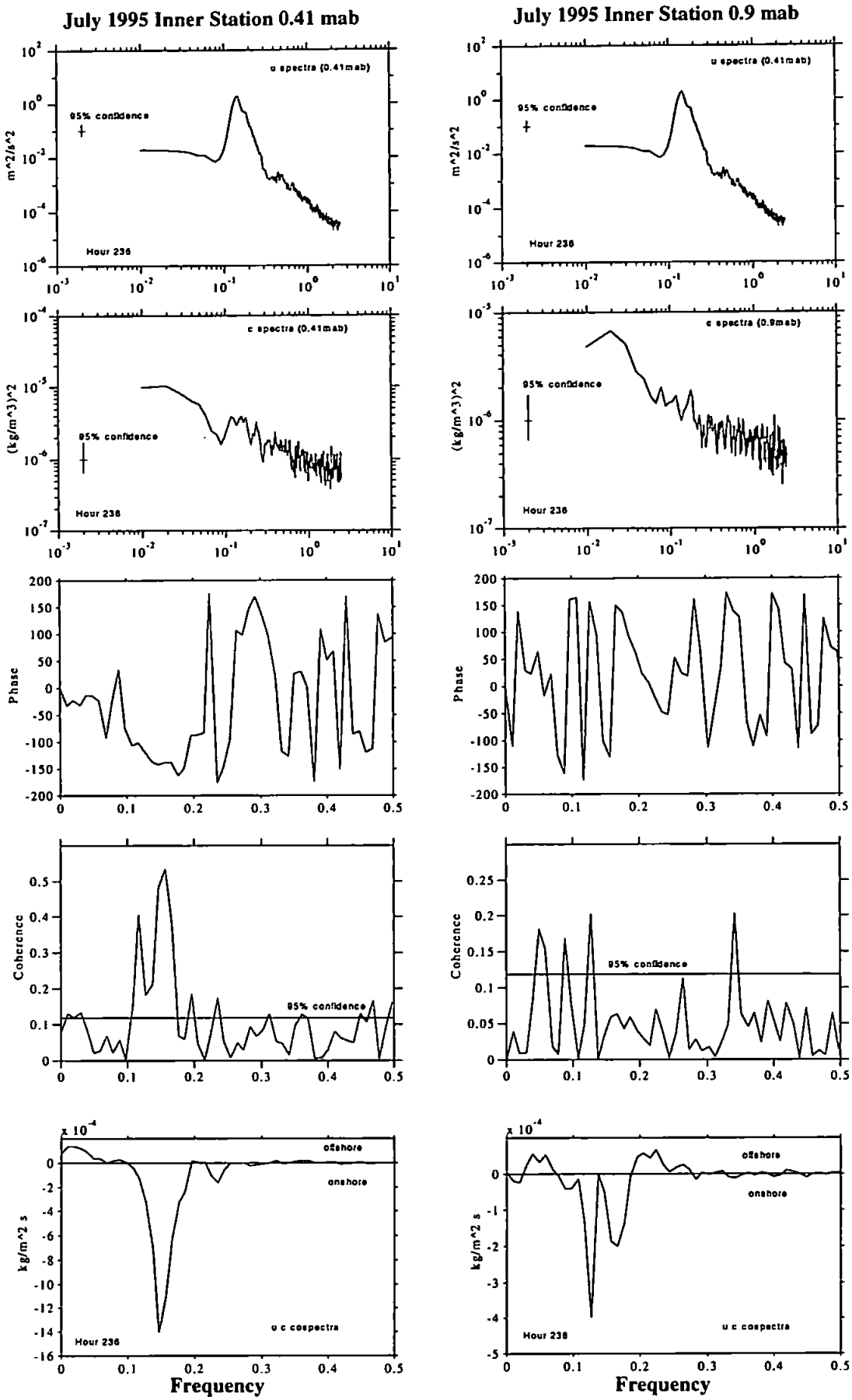

Figure 7.13 Spectra of c and u of a burst, during third storm (hr 236) 5 hours before high water

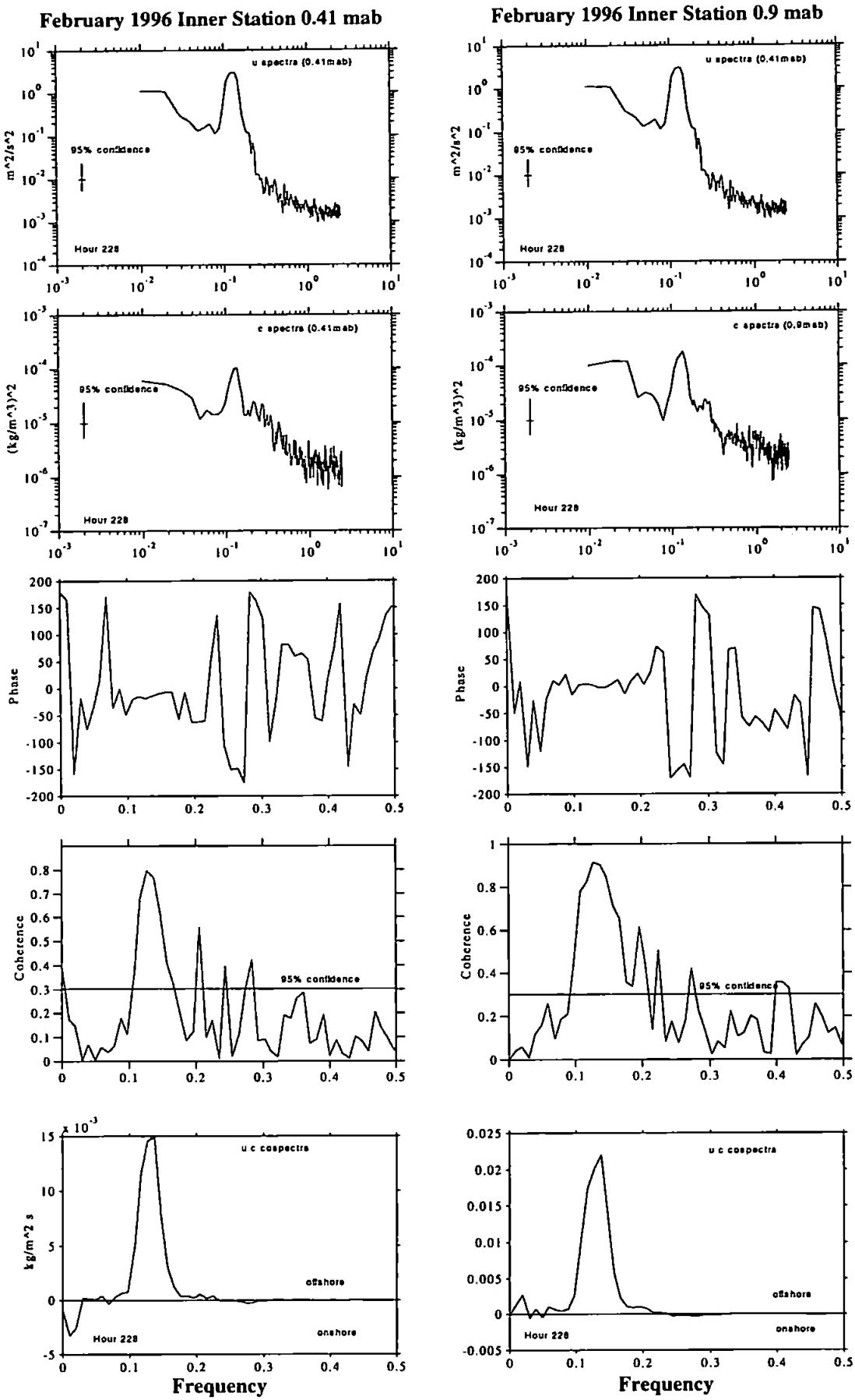

Figure 7.14 Spectra of c and u of a burst, during Neap storm (hr 228) at high water

In the first (figure 7.11) and third storm in July (figure 7.13), cross-shore sediment flux from long period motion was directed offshore at 0.41mab but directed onshore at 0.9mab. In the second storm (figure 7.12) contribution to cross-shore sediment transport from the lower frequencies reversed, and was onshore at 0.41mab and offshore at 0.9mab. The February 1996 inner and outer station storms also showed the same conditions whereby at 0.41mab there was a small on-shore sediment transport contribution at the infragravity wave frequencies. The amount of sediment moving onshore in July 1995 in response to the storm increased by an order of magnitude. In February 1996 the sediment moving offshore increased by two orders of magnitude.

Post Storm Conditions (Refer to Figures 7.15, 7.16, 7.17)

There were clear differences in the spectra and co-spectra of c and u between the post-storm conditions in July 1995 (figure 7.15) and February 1996 (figure 7.16 and 7.17). In July, the cross-shore velocity spectrum exhibited two peaks, the largest at 0.08 Hz, defined earlier as the boundary between the infragravity and gravity bands, and a second much smaller peak at the incident wave frequency. u spectra in February 1996 at the inner and outer station displayed one dominant peak at the incident wave band 0.13 Hz. The SSC spectra for July showed no significant peaks at 0.41mab, but showed two peaks at 0.9mab, one at 0.1 Hz and the second centred at 0.33Hz, which corresponds to the first harmonic of the incident waves (Huntley and Hanes, 1987). In February 1996, SSC spectra showed two prominent peaks; one peak similar to July centred at 0.13 Hz, but a second peak centred at 0.01 Hz in the infragravity wave band. Coherence between c and u in July 1995 was very small, in contrast to conditions in February 1996, where coherence between c and u was high at the incident wave band at the inner and outer station. At the infragravity band, coherence was low at the inner station but high at the outer station. u and c were also in-phase at these frequencies. Co-spectra between u and c showed onshore sediment transport occurring in July 1995 over a broad range between 0.05Hz and 0.15 Hz. Contributions to cross-shore sediment transport from the infragravity wave bands was negligible. In winter, the co-spectra of u and c showed no change and displayed a strong off-shore sediment movement in response to both gravity and infragravity wave motions. The largest off-shore contribution came from incident wave motions at 0.13 Hz, although the amount of sediment being transported had dropped to pre-storm levels once again.

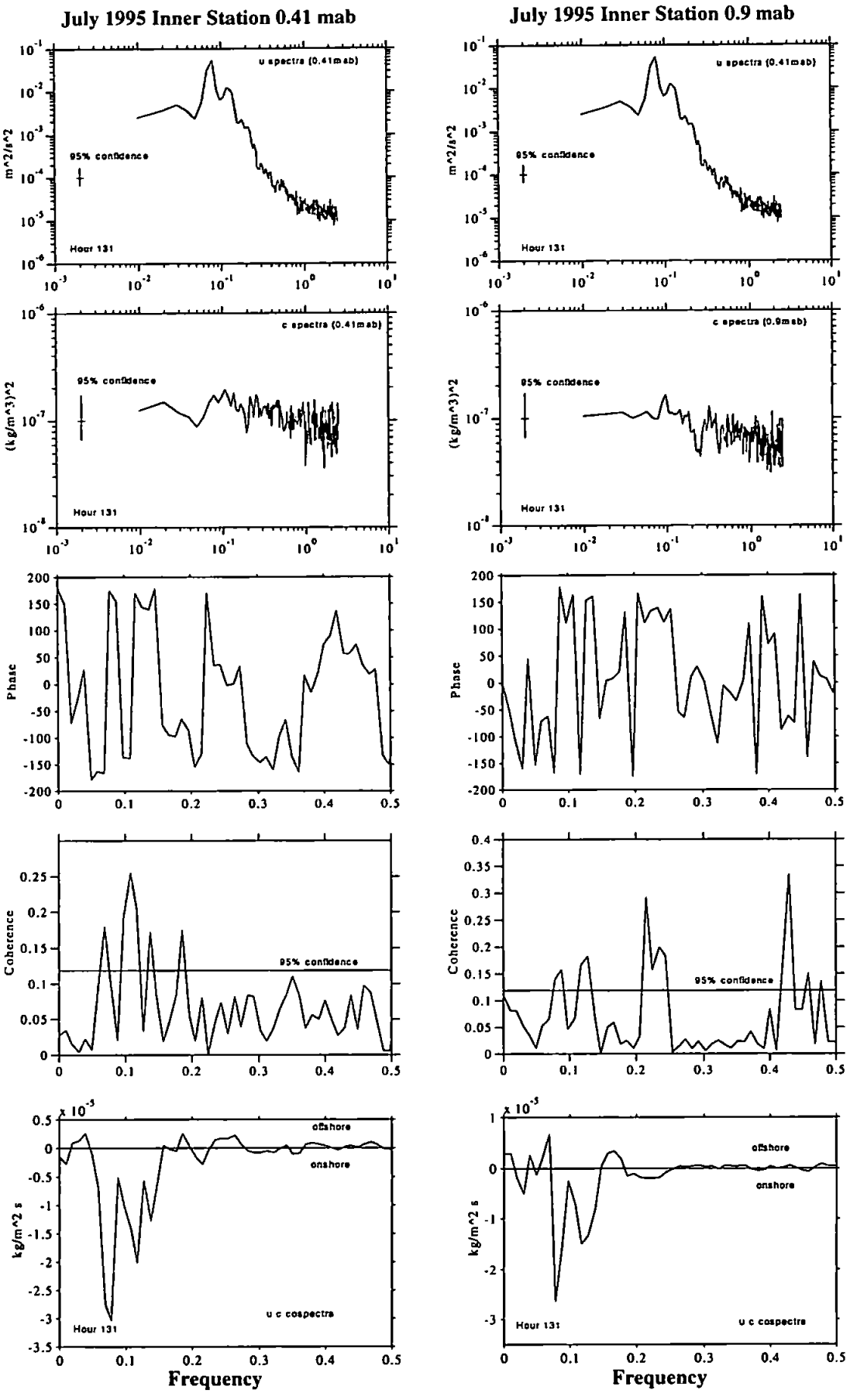

Figure 7.15 Spectra of c and u of a burst, in calm conditions (hr 131) at maximum tidal streaming on ebb

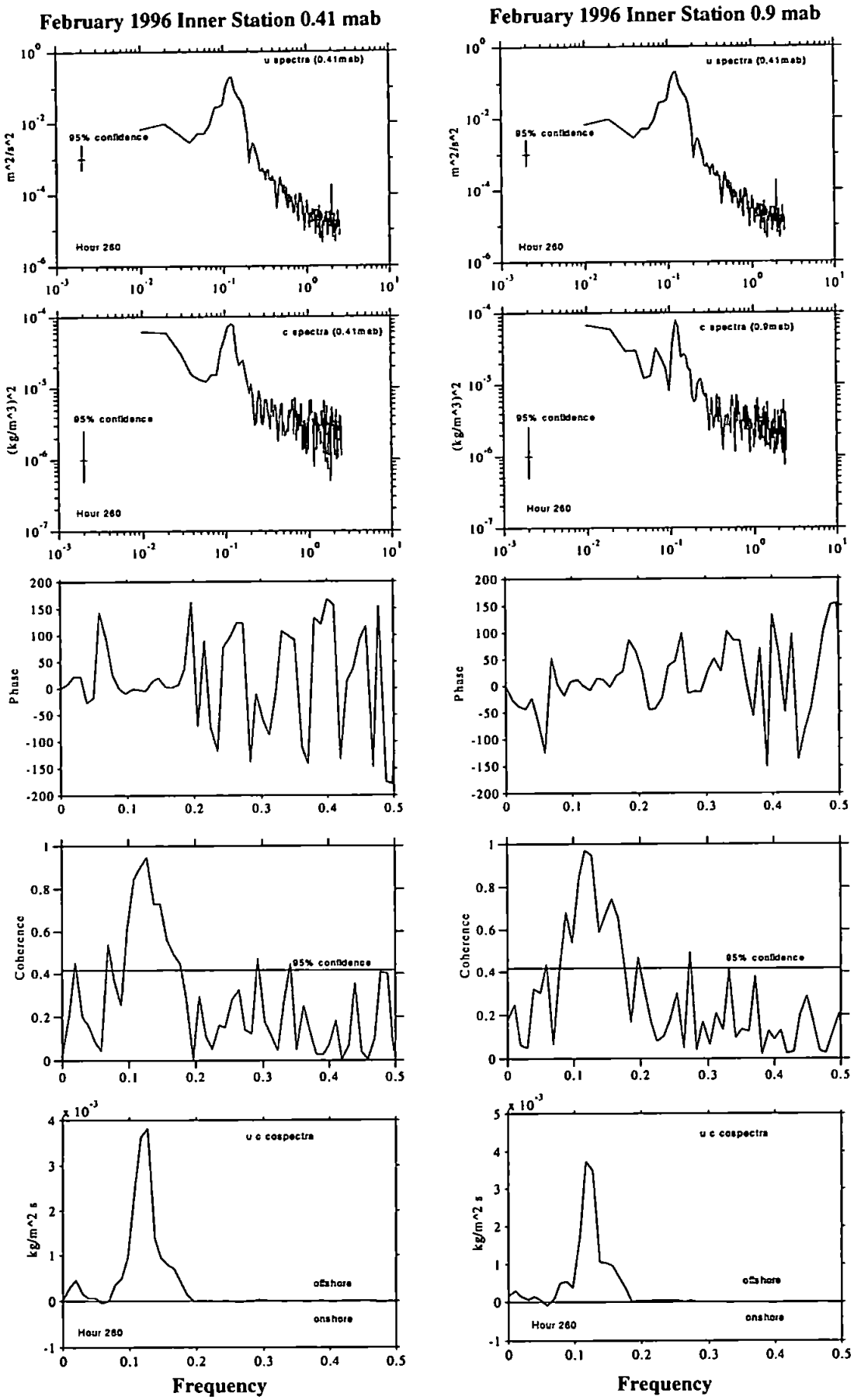

Figure 7.16 Spectra of c and u of a burst, during post storm conditions (hr 260) 4 hours before low water

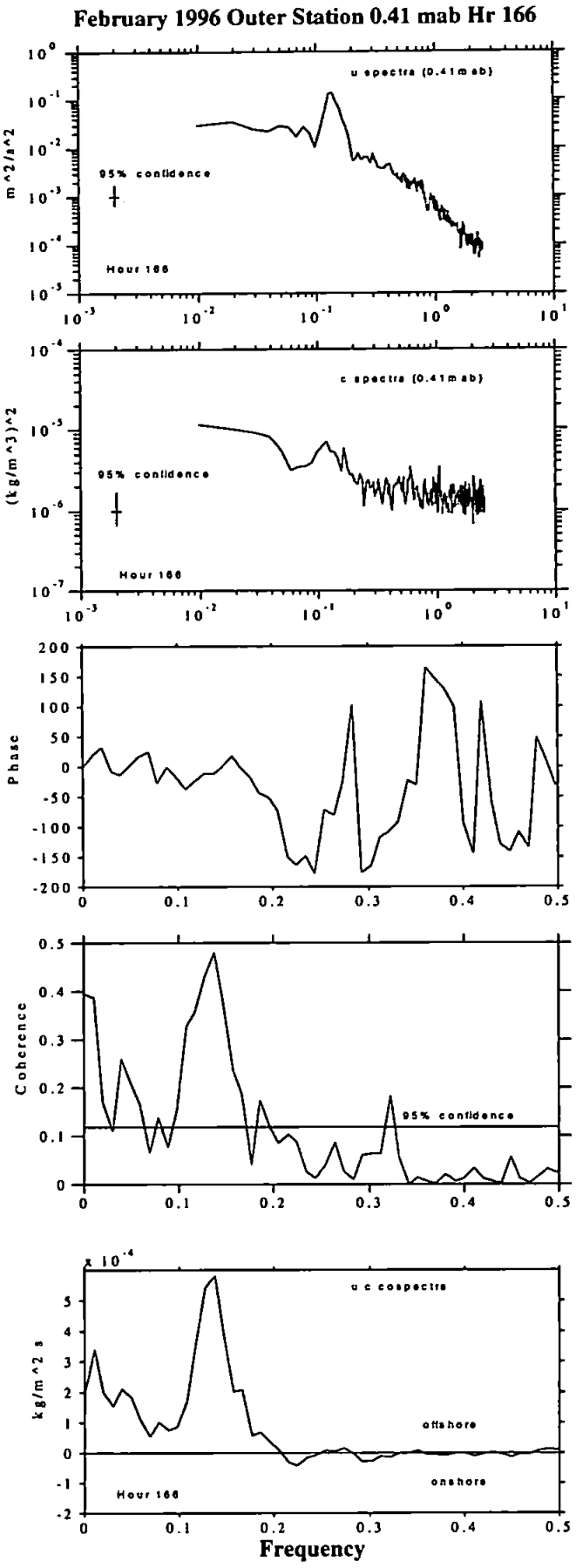

Figure 7.17 Spectra of c and u of a burst, during post storm conditions (hr 166) at maximum tidal streaming on flood

In summary, on-shore sediment transport dominated during the summer deployment (July 1995) and offshore sediment transport dominated in winter (February 1996). Incident wave motions in the gravity wave band contributed to most of the sediment transport, with a much smaller contribution coming from long period motions in the infragravity wave band. The direction of sediment transport (on/off shore) at the infragravity frequencies was not consistent and tended to change direction during the time series in response to the prevailing surface wave conditions. The spectral and co-spectral results will be discussed in more detail at the end of this chapter.

7.5.2 Gross Transport Rates

The relative importance of the burst averaged tidal, infragravity and gravity components to the total cross-shore transport (excluding the mean long-term component) in pre-storm, storm and post storm conditions given by $\overline{c_{t+w}u_{t+w}} = \overline{c'u'}$ (gravity and infragravity) + $\overline{c_t u_t}$ (tide), were assessed for the two measurement heights 0.41m and 0.9m above the seabed. Gross transport rates are presented in tables 7.4 A and B, 7.5 A and B and 7.6.

The total transport rates in the July 1995 deployment were highest during the calm period at 0.41mab and transport was dominated by the tidal (advective) component. During the storms the gravity component controlled the movement of sediment. The effect from the infragravity component on the gross transport rate was negligible during the storms but more significant in the calm period. At 0.9mab, the largest transport rate was measured during the first storm. Transport during the calm period and in the second set of storms was the same. Onshore sediment transport was initiated by the tidal and gravity wave band frequencies throughout the deployment. Offshore sediment transport was dominant in the infragravity frequencies in all cases, except during calm conditions at 0.41mab when infragravity frequencies initiated an onshore transport flux. The total average flux (excluding the long-term mean component) indicated onshore sediment transport throughout the deployment period and was greater at 0.41mab.

During winter, starting first with the February 1996 inner station, the total transport rate was dominated by the tidal component at both measurement heights before and after the neap storm. The gravity wave frequencies also played a significant role, and was most prominent during the neap storm in response to increased wave activity. Sediment transport was directed offshore throughout the deployment by the tidal and gravity

components. The infragravity wave component played a very small role in transporting the sediment. Transport was directed offshore at both heights except during the post storm conditions at 0.41mab when infragravity transport was directed onshore. Transport rates increased by a factor of 2 during the neap storm. Total average transport rates were offshore at all times during the deployment.

At the outer station in February 1996, the transport rate was controlled entirely by the tidal component before and during the spring storm. Sediment transport was directed onshore before the storm but offshore during the storm. After the storm, the influence of the tidal component on the transport rate reduced to almost half, and sediment transport was directed onshore. The effect of the gravity wave component on the transport rate was to cause negligible offshore sediment transport during the pre-storm and storm conditions. Although the influence of the waves in $\overline{u'c'}$ terms is small, their influence in increasing levels of suspended sediment concentration during the storms and contributing to $\bar{c}$ is very important. That is, waves actively stir sediments into suspension even if they do not significantly move the sediment themselves.

After the spring storm, the role of the gravity wave component increased significantly to almost half the contribution of the total transport rate. Onshore transport was initiated by the gravity wave component during post storm conditions. The infragravity frequencies contributed a very small amount to the total transport rate and was directed offshore at all times except during the storm. The total average transport rates was directed offshore during the storm event but onshore before and after the spring storm. Sediment flux magnitudes increased significantly by two orders of magnitude during and after the storm. The outer storm also transported more sediment offshore per m than the neap storm event at the February 1996 inner station.

Table 7.4 Gross transport rates to show the relative importance of the burst averaged tidal, gravity and infragravity components to the total cross-shore sediment transport (July 1995 BLISS deployment)

(A) July 1995 inner station - 0.41mab

Component (0.41mab)	**Storm (hr 60-100) $kgm^{-2} s^{-1}$** x 10^{-5}	**Calm period (hrs 101-169) $kgm^{-2} s^{-1}$** x10^{-6}	**2 storms combined (hrs 160-240) $kgm^{-2} s^{-1}$** x 10^{-5}
Tidal	-0.37 **26.2%**	-1.8 **52.2%**	-0.2 **16.2%**
Infragravity	0.01 **0.5%**	-0.3 **9%**	0.001 **0.75%**
Gravity	-1.02 **73.3%**	-1.3 **38.8%**	-1.1 **83%**
Total	-1.38	-3.4	-1.3

Table 7.4 (B) July 1995 inner station - 0.9mab

Component (0.9mab)	**Storm (hr 60-100) $kgm^{-2} s^{-1}$** x 10^{-5}	**Calm period (hrs 101-169) $kgm^{-2} s^{-1}$** x 10^{-5}	**2 storms combined (hrs 160-240) $kgm^{-2} s^{-1}$** x 10^{-5}
Tidal	-0.1 **15.3%**	-0.2 **68.65%**	-0.046 **14%**
Infragravity	0.002 **0.3%**	0.03 **13%**	0.06 **18.4%**
Gravity	-0.6 **84.4%**	-0.04 **18.4%**	-0.2 **67.6%**
Total	-0.7	-0.21	-0.2

Table 7.5 Gross transport rates to show the relative importance of the burst averaged tidal, gravity and infragravity components to the total cross-shore sediment transport (February 1996 inner station deployment)

(A) February 1996 inner station - 0.41mab

Component (0.41mab)	**Pre-neap storm (hrs 1-180) $kgm^{-2} s^{-1}$ x 10^{-3}**	**Neap storm (hrs 181-260) $kgm^{-2} s^{-1}$ x10^{-3}**	**Post storm (hrs 261-356) $kgm^{-2} s^{-1}$ x 10^{-3}**
Tidal	0.7 **78.7%**	0.74 **37.8%**	0.91 **58.9%**
Infragravity	0.01 **1.3%**	0.02 **0.9%**	-0.02 **1.1%**
Gravity	0.2 **20%**	1.2 **61.3%**	0.6 **40%**
Total	0.91	1.8	1.5

Table 7.5 (B) February 1996 inner station - 0.9mab

Component (0.9mab)	**Pre-neap storm (hrs 1-180) $kgm^{-2} s^{-1}$ x 10^{-3}**	**Neap storm (hrs 181-260) $kgm^{-2} s^{-1}$ x10^{-3}**	**Post storm (hrs 261-356) $kgm^{-2} s^{-1}$ x 10^{-3}**
Tidal	0.43 **56.9%**	0.72 **33.7%**	0.87 **59.2%**
Infragravity	0.02 **2%**	0.01 **0.7%**	0.02 **1.6%**
Gravity	0.3 **42%**	1.4 **65.6%**	0.6 **39.2%**
Total	0.75	2.13	1.49

Table 7.6 Gross transport rates to show the relative importance of the burst averaged tidal, gravity and infragravity components to the total cross-shore sediment transport (February 1996 outer station deployment)

February 1996 outer station - 0.41mab

Component (0.41mab)	**Pre-storm (hrs 1-85)** $kgm^{-2} s^{-1}$ $\times 10^{-3}$	**Spring storm (hrs 86-170)** $kgm^{-2} s^{-1}$ $\times 10^{-3}$	**Post storm (hrs 171-355)** $kgm^{-2} s^{-1}$ $\times 10^{-3}$
Tidal	-3 **99%**	5.52 **99%**	-1.04 **40.5.%**
Infragravity	0.002 **0.09%**	-0.05 **0.95%**	0.004 **0.2%**
Gravity	0.02 **0.6%**	0.002 **0.05%**	-1.5 **59.3%**
Total	-2.98	5.5	-2.5

7.6 Discussion

The suspension and transport of sediment off the Holderness coast is governed by four factors

1. Availability of sediment.
2. Storm wave activity.
3. Current direction.
4. Wind direction and strength.

In summer there was very little sediment in suspension so there was no substantial movement of sediment away from the Holderness coast. In winter, suspended levels were much higher and consequently far more sediment was made available for sediment transport. From the time series flux vector plots, it is clear that during storms sediment transport was directed offshore in winter, but in summer the transport contribution due to the waves was on-shore. The net transport due to a combined action of the waves and tides, indicated for summer that the wave flux and tidal flux both generated onshore sediment transport at both heights above the seabed. Wind direction during the summer deployment was predominantly from the North East. The wave flux coupled with the tidal flux was directed in the alongshore towards the South East at 0.41mab. However, at 0.91mab, sediment transport alongshore was mainly towards the North West even though the wave flux was directed towards the South East. Essentially, at 0.91mab the tidal flux was in a North West direction and clearly illustrated that the prevailing swell had no influence over the tidal flux in moving the sediment at that particular height.

During February 1996, the inner station deployment was dominated again by prevailing North Easterly winds, which varied in strength. From the cumulative net transport values it was evident that sediment transport alongshore was influenced entirely by the tides towards the South East, even though the wave flux was towards the North West. Cross-shore sediment transport was directed offshore at all stages during the deployment, aided by offshore transport from both wave and tidal propagation. The average net transport over the whole deployment due to the tides and waves (table, 7.2) was positive towards the North at 0.41mab but negative towards the South at 0.9mab, even though the cumulative net transport plots in the alongshore direction showed (over most of the deployment) a southerly movement of sediment at both measurement levels. This result illustrates that a

mean overall value may not reflect the true direction of the tidal flux, as it is notoriously difficult to separate out the long-term mean flux from the tide and wave flux (refer to section 7.4.3).

During the February 1996 outer station deployment, significant offshore sediment transport in response to the North East storm did occur. The waves played a significant role in elevating the background suspended sediment levels by an order of magnitude, but it was the offshore directed cross-shore current that maintained the large movement of sediment offshore. The North Easterly swell waves coupled by the alongshore tidal flux also controlled the alongshore sediment movement towards the South.

Co-spectra (which relate concentration to both the wind wave and swell frequencies in the cross-shore velocity spectrum) of individual burst data revealed that sediment fluxes at the incident wave frequencies (0.11 Hz) were seaward at all times during the February 1996 deployments but were directed onshore in the July 1995 deployment. Fluxes at the infragravity frequency were significantly smaller, and in fact gave only a very small contribution to the overall cross-shore sediment flux. In the concentration spectra and velocity spectra, significant peaks corresponded mainly to incident wave frequencies greater than 0.1 Hz (10 seconds) which suggested that sediment concentrations were responding to individual incident waves. Observations have shown that skewed shoaling waves travelling towards the shore suspend sediment during the shore-ward phase of the wave, as the wave crest passes causing onshore transport (Hanes and Huntley, 1986; Hanes, 1988). Consequently, offshore sediment transport arises in the trough of the wave. A smaller but distinctive offshore peak at the lower frequencies <0.05 Hz was associated with offshore transport due to long period waves (Osborne and Greenwood, 1992, Huntley and Kim, 1985). Longuet-Higgins and Stewart (1962, 1964), Larsen (1982) and Shi and Larsen (1984) proposed that incident wave groups (which are characterised by having an alternating sequence of high and low waves), are associated with gradients in the radiation stress which generate a forced long wave at the lower frequencies (infragravity frequency) (Foote *et al.*, 1992). Subsequently, offshore flow coincides with increased suspension due to the larger waves.

The July 1995 co-spectra clearly indicated onshore transport as a result of surface waves. Low frequency waves contributed a small amount to both onshore and off-shore flux transport and in a number of bursts, the direction of the flux reversed with height above the

seabed. For a good example of this refer to the co-spectra of u and c for hour 192 (figure 7.12) where at 0.41mab long period motion was contributing a small but significant role to onshore sediment flux and at 0.9mab to off shore directed flux. This reversal of the transport direction higher in the flow has been seen by Osborne and Greenwood (1992) to reflect the importance of temporal and spatial interdependencies between the sediment concentration and horizontal velocity. It was noted from our data, that onshore transport at the lower frequencies only occurred when the phase between u and c exceeded ± 90° but was less than ± 160°. These findings support other field results obtained from the outer surf zone off Duck, North Carolina (Beach and Sternberg, 1991), where flow reversal onshore was noted to occur below 0.004 Hz at phase between u and c exceeding -90°. They also noted that sediment resuspension was dominated by incident wave processes.

All the c-u co-spectra for the February 1996 period showed large positive spectral densities coincident with the wind wave frequencies, suggesting off-shore transport. Much smaller but still distinct spectral peaks were seen at frequencies <0.05 Hz. Again, these peaks associated with the long period waves were not just indicating offshore transport but were also showing at times on-shore transport at the very low frequencies.

To ascertain what mechanism was causing offshore transport at the incident wave frequencies in the February 1996 data, the pressure, concentration and cross-shore velocity bursts were split up into smaller time series of 100 seconds and compared to the July 1995 data set. Figure 7.18 represents a section taken from the outer station in February, 1996, illustrative of conditions at the start of the spring storm. Peaks in concentration occurred both at minimum and at maximum current velocity, but not at the wave crests. Sediment peaks at maximum cross-shore velocity occurred in the trough of the incident wave crest as expected if the cross-shore velocity and pressure records are 180° in anti-phase. Peaks in concentration at minimum velocity occurred mid-way between the crest and trough of the wave record. These results suggest that onshore sediment transport does not occur as the wave crest passes, but that offshore sediment transport occurred at maximum positive velocity and was opposite to the direction of wave propagation. The SSC record clearly shows the importance of the signal at the wave period. However, the phase between SSC and the cross-shore current shows that the offshore current is associated with maximum SSC. This result reflects that there is a small offshore flow superimposed on the wave oscillations. Notably then in the February deployment, near-bed offshore sediment transport is associated with the steady nearbed offshore flow (undertow) explained by

Stokes theory whereby a net flow in the direction of the wave advance near the water surface will be balanced by net flow in the opposite direction at mid depths. Similar studies off Spurn Head by Davidson *et al.*, (1993) showed that cross-shore sediment transport seaward of the breaker zone was dominated by strong offshore transport at the incident wave frequency on the ebbing tide. He noted that the period of high transport occurred primarily as a result of high sediment suspension at gravity frequencies which interacted coherently and in anti-phase with the incident wave flow field. Davidson *et al.*, (1993) postulated that the observed increased suspension as the tide turned could be due to erosion of a ripple field which formed in the slack waters over high tide. Notably, increased offshore sediment transport under incident waves seen in the BLISS data sets in February 1996 may also suggest a rippled bed in the vicinity of the BLISS tripods, which is destroyed with increasing velocity as the water depth shallows on ebb tide and in the process suspend sand to high elevations where it may be detected by the OBS.

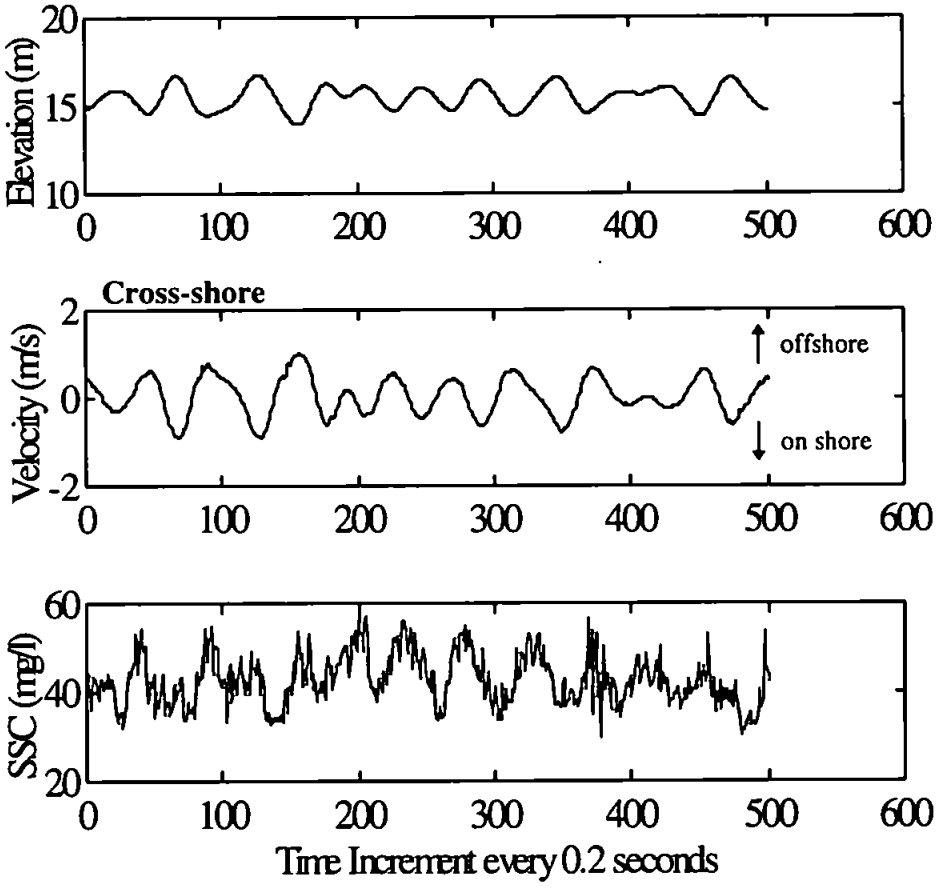

Figure 7.18 Section of SSC, cross-shore velocity and pressure taken from the February 1996 outer station data- Burst number 87 (storm data, between 1000-1500), to determine the mechanism that causes off-shore sediment transport at the incident wave frequencies

Co-spectra produced from the summer deployment suggested that surface waves controlled the sediment flux onshore. Time series from the calm period in July 1995 (figure 7.19) confirmed that peaks in sediment suspension were correlated to peaks in the pressure time series, illustrating resuspension by the wave crest and subsequent onshore transport by the wave.

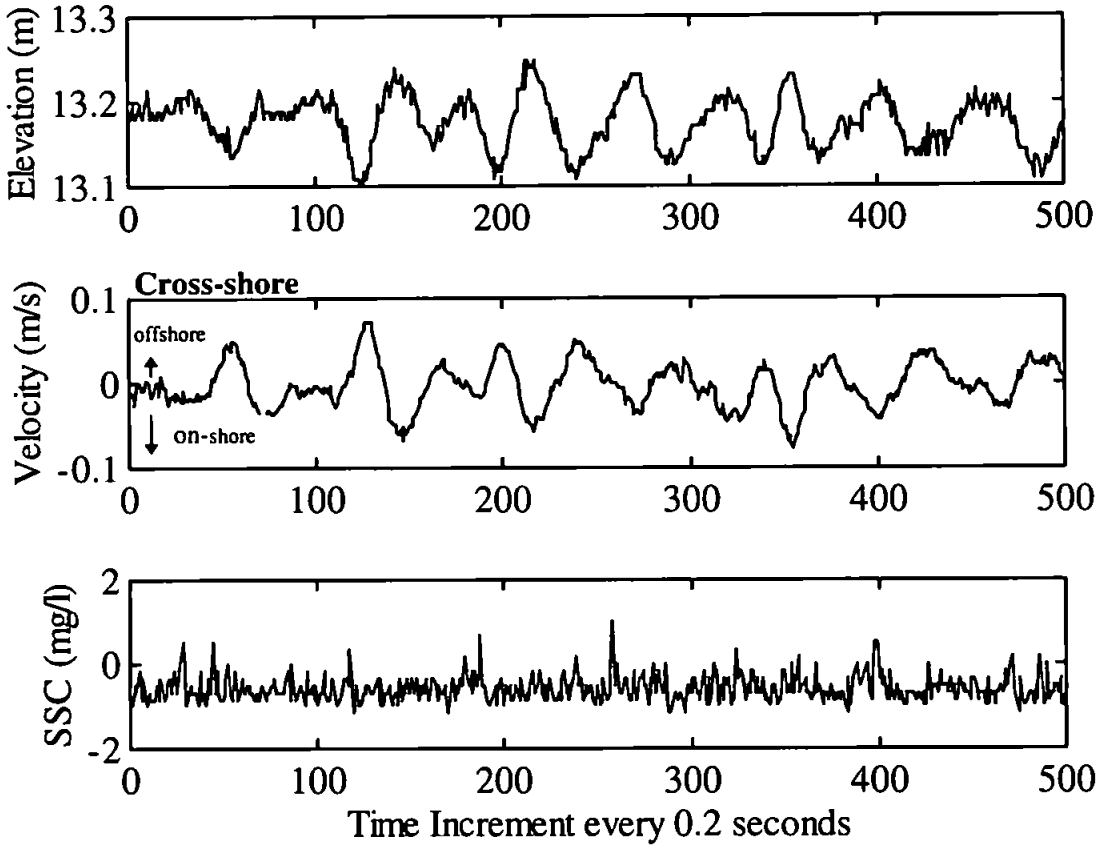

Figure 7.19 Section of SSC, cross-shore velocity and pressure taken from July 1995 inner station - Burst number 131 (1:500) during a calm period, to determine the mechanism that causes off-shore sediment transport at the incident wave frequencies

Our results indicate that cross-shore flows (time averaged and within the burst), although very subordinate to alongshore currents in strength, are extremely important to offshore as well as onshore sediment flux. Incident waves in summer and winter were undoubtedly the primary cause of sediment suspension and in summer, the oscillatory currents dominated the onshore advection of sediment in response to an onshore wind from the North East. In winter, the mean sediment transport became large enough to offset the oscillatory transport, so that offshore sediment transport in response to the return mean current became dominant at both stations. It was clear from the deployment results that low-frequency effects caused

measurable, but not significant, cross-shore sediment fluxes. However, we cannot draw any conclusions as to whether or not the mechanisms hypothesised by Larsen (1982) and Shi and Larsen (1984) contributed to off-shore sediment transport. In fact, our data suggests that low frequency fluxes are just as often directed on-shore as they are off-shore. Fluxes of this nature have been seen in other field results. Wright *et al.*, (1991) suggested that the inconsistency in the low frequency flux directions may be due in part to the presence of another long wave component reflected from the shore.

One aim of the BLISS experiment was to derive flux budget estimates for the Holderness coast from the single point flux measurement taken at one height above the seabed. Unfortunately, the net mean flux over the deployment period could not be calculated with any reliability, because a greater accuracy was required by the electromagnetic current meters of > 0.3 cms^{-1} to separate the mean flux from the tidal flux. The BLISS experiment therefore was able only to calculate accurately the tidal and wave flux transport, the data of which, may be used to calibrate numerical models, so that the models themselves can estimate the mean flux with a better degree of accuracy.

It is normal practice when deriving flux budgets to take many measurements in the region of interest, of current velocity, SSC and depth, at different heights above the seabed and along a grid of known width. A flux budget is normally calculated by vertical integration across the grid. So, the single point measurements taken by the BLISS tripods were only determining flux conditions at that point in time. To achieve an accurate sediment budget calculation for the Holderness coast, measurements should be taken throughout the year along a grid system. Flux measurements taken over 12 months are important for the accuracy of the annual sediment budget estimate, because the cliff erosion rate is likely to vary depending on the storm conditions, and the rate of cliff erosion will not be the same all through the year. Dyer and Moffat (1994) noted from data collected during the North Sea Project, that the sediment flux transported during two winter months, made up 71% of the total annual sediment flux monitored away from the East Anglian coast. In conclusion, storm events increase the rate of cliff erosion off Holderness. During a storm, sediment transport is directed offshore in winter and onshore during summer. Storm waves only play a small role in transporting the sediment offshore, but they are effective stirring mechanisms for increasing the amount of suspended sediment in the water column. It is the cross-shore wave induced currents which actively transport the sediment away from the Holderness coast.

Chapter 8

8. Conclusions and Future Work

A highly successful field campaign was carried out during 1995 and 1996 off the Holderness coast, Southern North Sea to tackle the aims outlined in section 1.2. All the initial objectives have been achieved and a significant contribution has been made to understanding the suspended sediment transport processes in the nearshore zone off the Holderness coast, where the cliffs are renowned for their rapid rate of erosion (1.7m a^{-1}, Valentin, 1971, McCave, 1987). This final chapter will focus on addressing the original aims outlined in section 1.2 and will draw together the main findings of the thesis in a concise and precise manner and then highlight the specific contributions this study has made to the current understanding of shelf sea sediment transport processes in the near-shore zone, off the Holderness coast. Finally, recommendations for future BLISS deployments will be made in context to further studies off the Holderness coast.

8.1 Field Work

With regard to the field work objectives outlined in section 1.2 (Number 1 and 2), the following achievements have been accomplished.

There have been four BLISS deployments conducted along a transect normal to the Holderness coastline at Tunstall, during 1995 and 1996. The BLISS tripods in each deployment were operational for two weeks rather than for one month as originally anticipated. The original deployment depth range of 5-15 m was extended to cover depths between 9-23 m. An extensive and comprehensive data set has been produced from the

BLISS field campaign and each 17 minute data run has been processed and corrected where possible for sensor gain and offset. Measurements of cross shore and alongshore current velocity, suspended sediment concentration, surface wave activity, salinity, temperature and pressure have been successfully recorded during calm conditions and in storms. From the current velocity and suspended sediment concentration data, sediment fluxes have been successfully calculated. Results presented in this thesis were taken from data collected during June/July 1995 and February 1996, which typified summer and winter storm conditions.

1) A 13 hour station was conducted during the June/July 1995 and February 1996 deployments. Over 13 hours, *in situ* water samples were successfully collected in the bottom boundary layer at known heights above the seabed, using a modified version of the bottom landing water sampling system, originally developed by Bale and Barrett (1995). Each mooring site was visited a total of 4 times. The water samples were promptly filtered and their results were then used to convert the optical backscatter sensor output data from FTU to mgl^{-1}. Because FTU is a measure of the cloudiness of the water and not the actual amount of sediment in suspension, this procedure was necessary to calculate the sediment fluxes accurately. A single calibration coefficient was produced in the recognition that sediment in suspension off Holderness was essentially homogeneous throughout the water column. The horizontal current velocity data were realigned to alongshore and cross-shore, using the M_2 tidal flow as the main determinant for the alongshore current.

2) Water column profiles of CTD and SSC were taken using a self logging profiling system at the same time as the water samples, but the results were not presented in the thesis because the profiles showed no change in salinity or temperature with depth over the 13 hour period. The optical sensors on the self logging profiler saturated to full scale and showed no variation in sediment concentration.

8.2 Time Series Results

The main focus of the BLISS experiment was to identify and quantify the temporal and spatial physical processes which control the movement of sediment both along and across the Holderness coast during calm and storm conditions (objective 3). Two week time

series plots over a spring/neap cycle, of suspended sediment, current velocity and wave activity for the June/July 1995 inner station and the February 1996 inner and outer station deployments (described in chapter 6) highlighted the dominant processes operating off Holderness. The main findings are summarised as follows:

1) Tides off the Holderness coast flowed to the North West on ebb and towards the South-East on flood. The tidal ellipse was almost rectilinear in nature and ran parallel to the coastline in a North West, South East direction. Maximum velocities alongshore were $0.5ms^{-1}$, whereas in the cross shore they were $\sim 0.1ms^{-1}$.

2) Background levels of SSC measured at the BLISS stations varied with the tides and the seasons. SSC was greater during springs than neaps and was due to the tidal excursion being greatest at springs. SSC measured at the BLISS inner site showed an increase from summer to winter by two orders of magnitude eg. from ~11 mgl^{-1} to 780 mgl^{-1} respectively. It is suggested that more sediment is mobilised into suspension during the winter period by the activity of waves. Spatially the background SSC levels were lower at the outer station, which suggested the presence of a concentration gradient which decreased in suspended sediment towards the offshore.

3) Over a tidal cycle, the largest SSC peaks occurred at or near to slack water and exhibited strong M_2 tidal forcing, interpreted as an advective signal. This semi-diurnal sediment response was evident in all the BLISS time series, and is a recognised feature, which indicates advection past the mooring site of a horizontal turbidity gradient (Weeks and Simpson, 1991, Jones *et al.*, 1994). It was postulated that a plume of concentration enriched water flowing out of the Humber estuary on ebb tide, advects around Spurn Head and moves up past the Holderness coast into the vicinity of the BLISS moorings. Maximum concentration occurs when the tidal current has reached maximum excursion to the North West. Synoptic evidence to suggest the existence of the Humber plume was obtained from satellite AVHRR sea surface temperature and water colour images of the Humber and Holderness region. Satellites view only the surface water layer whereas BLISS measures the near bed conditions. However, CTD profiles taken in February 1996 show that the water is well mixed throughout the water column. Salinity and concentration scatter plots taken from the February 1996 outer station near to the seabed, suggest that Holderness coastal water is characterised by a salinity above 35.2‰. Salinity below 35.2‰ indicates the presence of Humber estuary derived water.

At the outer station, the sudden increase in concentration with a corresponding decrease in salinity signified the advection of the sediment rich Humber water into the mooring site.

4) Sediment resuspension of the bed material in the vicinity of the BLISS moorings occurred at maximum current velocity. Peaks in sediment suspension occurred on both the flood and ebb stage of the tidal cycle and gave rise to an M_4 or quarter-diurnal variation in the sediment signal. Resuspension peaks were significantly smaller than the advective peaks. At spring tides and during storms in the July 1995 time series, the stronger advective M_2 sediment signal swamped out the M_4 sediment signal.

5) At the February 1996 inner station (figure 6.39) a complex relationship between the advective signal and the tidal displacement arose whereby, there was a distinct increase in SSC with tidal displacement towards the North West and a smaller increase in SSC associated with the return displacement towards the South East. It has been suggested that this relationship may occur when there is a turbidity gradient present which is inclined at an angle to the axes of the tidal ellipse. If this is so, then the phase between the flow and the SSC is not a straightforward indication of the relative importance of advection and resuspension, and simple advection/resuspension modelling used by Weeks and Simpson, (1991) and Jago and Jones (1993) must be treated with caution in a region such as Holderness where the concentration gradients may have both alongshore and cross-shore components.

8.2.1 Shear Stress, Drag Coefficient and Roughness Length Estimates

Three methods based on turbulence were used to determine shear stress. Shear stress measurements presented in the form of a friction velocity u_* showed that agreement between each method reduced during storm events. A strong semi-diurnal signal was prominent for all methods and peak stresses occurred before or just after maximum tidal streaming. There was distinct spring/neap tidal variation in the u_* value in response to the larger velocities experienced during springs. The Reynolds stress method consistently produced the largest u_* values and was not used to represent the BLISS shear velocities because of the method's sensitivity to sensor alignment. The u_* values from the Turbulent Kinetic Energy and Inertial Dissipation method were averaged and the resultant u_* value used to represent the BLISS measurements. The conclusions were:

1) Friction velocity u_* relates to the current gradient above the seabed and was seen to vary with the spring-neap tidal cycle being greatest at springs. u_* values were highest in wave dominated flows during the winter storms.

2) Peaks in sediment concentration at the February 1996 inner and outer stations from figures 6.23 and 6.24 respectively, occurred at u_* values of $0.02ms^{-1}$ and $0.03ms^{-1}$, (figures 6.21 and 6.22). The corresponding current speeds and wave orbital velocities were $<0.2ms^{-1}$ and $<0.4ms^{-1}$ respectively, which suggested that the sediment peaks were caused by horizontal advection of concentration enriched water and not sediment re-suspension which would occur in high wave and current velocity conditions. Nevertheless, for the outer station (figure 6.24) there is some strong evidence to suggest that higher SSC occurs at larger wave flows, which could suggest resuspension.

3) Drag coefficients for both BLISS and STABLE were derived using the quadratic stress law relationship. All data sets exhibited a rapid increase in C_{d100}, in response to an increasing wave:current ratio, which suggests that waves play a significant role in altering the stress value because waves have a thinner boundary layer so the bed appears rougher. It also implies that numerical models based upon a constant drag coefficient are probably inappropriate when significant horizontal wave velocities are present (Huntley *et al.*, 1994).

4) Errors in the value of C_{d100} occur close to slack water because the tidal acceleration effects will introduce an unrelated physical process which acts to enhance turbulence levels and the shear stress. This error accounts for the large scatter in C_{d100} values observed at the July 1995 and February 1996 inner station.

5) C_{d100} for the BLISS and the STABLE results showed similar values between 0.001 and 0.01. However, the STABLE C_{d100} values corresponded to much smaller wave:current ratios than observed in the BLISS data, probably because the STABLE tripod was deployed in deeper water.

6) Comparisons of the C_{d100} and z_o results, with typical results expected from grab samples taken during the BLISS July 1995 deployments based on Soulsby (1983), showed good agreement with the outer station suggesting that the outer site was composed of coarse material of pebbles and shingle which ranged from 1 to 2.8 mm in diameter. There was

no agreement with the expected values at the inner station. Derived values of C_{d100} and z_o for the February 1996 inner station suggested a seabed composed of coarse sand and granular material.

8.3 The Influence of Storms on the Movement of Sediment

Storm events off the Holderness coast monitored by the BLISS tripods, have been categorised into three types according to wind direction, tidal cycle and time of year. Before the characteristics of each event are summarised, there are a number of features which are common to all the storms measured off the Holderness coast. There is an elevated increase in SSC levels at the onset and during a storm. This was most dramatically illustrated at the February 1996 outer station (figure 6.8), where increase in SSC was attributed to two processes: Horizontal advection of the Humber plume water into the vicinity of the BLISS moorings and resuspension of the seabed material by wave activity. Another common feature to note is that after every storm, there was a distinct time lag for which it took the finer material in suspension to settle out to pre-storm levels once again. The e-folding time was longer for winter storms (between 95 and 129 hours) than summer storms (~39 hours). The corresponding settling velocities were between 2.05×10^{-4} ms^{-1} and 1.76×10^{-4} ms^{-1} for the winter storms and 3.22×10^{-4} ms^{-1} for the summer storms.

1) Summer North Easterly Storm - Spring Tidal Conditions

A typical summer storm off the Holderness coast, produces wave heights of 0.4-0.45 m and lasted for approximately 35 hours. Time series vector plots of sediment flux showed onshore sediment transport during the storms. Co-spectra of the cross-shore velocity and SSC clearly suggested onshore transport as a result of surface waves. Maximum coherence between the u and c occurred in the gravity wave band at the incident wave frequency at 0.15 Hz. Time series of SSC and pressure (taken from the 17 minute burst) confirmed that peaks in sediment suspension were correlated to peaks in the pressure time series. From these results it was concluded that in summer, skewed shoaling waves travelling towards the Holderness coast from the North East, suspend sediment during the shore-ward phase of the wave, as the wave crest passes, causing onshore transport. The e-folding time for the sediment to settle out after a summer storm was calculated to be 39 hours, with a settling velocity of 3.2×10^{-4} ms^{-1}, and a grain size corresponding to fine silt < 20 μm.

2) Winter North / North Easterly Storm - Spring and Neap Tidal Conditions

The spring storm produces the highest waves off Holderness. Maximum wave heights of 3m were recorded from the February 1996 outer BLISS deployment. During the neap storm at the February 1996 inner station, wave heights were 1.5m. Time series vector plots of sediment flux for both deployments showed offshore sediment transport in response to the waves. In the spring storm, the tidal flux was one order of magnitude greater than the wave flux. In the neap storm, the magnitude difference between the tidal and wave flux was by an order of 2. Co-spectra of SSC and cross-shore velocity of both deployments, revealed that sediment fluxes at the incident wave frequencies (0.11 Hz) were directed offshore at all times during the February outer station deployment. The phase between SSC and the cross-shore current shows that the offshore current is associated with maximum SSC. This result reflects that near the bed sediment transport is associated with the mean nearbed offshore flow (undertow) explained by Stokes theory whereby a net flow in the direction of the wave advance near the water surface will be balanced by net flow in the opposite direction at mid depths. Increased offshore sediment transport under incident waves seen in the February 1996 BLISS data sets may also suggest a rippled bed in the vicinity of the BLISS tripods, (Davidson *et al.*, 1993).

There was very little net movement of sediment flux alongshore during the February outer station deployment. During the February inner station deployment, net transport alongshore was directed towards the south. The spring storm lasted 84 hours (3.5 days) and the neap storm lasted 65 hours (2.7 days). E-folding times i.e. the time it took for the fine material to settle out of suspension after the storm was recorded as 108 hours for the spring storm and 94 hours for the neap storm. Corresponding settling velocities were 2.81 x 10^{-4} ms^{-1} for the spring storm and between 2.05 x 10^{-4} ms^{-1} for the neap storm. These values suggested that in both deployments very fine silt was in suspension.

To summarise, winter storms suspended significantly more sediment up into the water column than the summer storms, so that more sediment is made available for sediment transport in winter, which is further aided by the time it takes the finer material in suspension to settle out after the storm. Sediment flux transport from waves alone accounted for ~10% of the total flux transported offshore. The storms are in fact, effective stirring mechanisms which increase the amount of sediment available for sediment transport rather than actual transporters of suspended sediment.

8.4 Calculating Sediment Fluxes and a Sediment Flux Budget

From the BLISS single-point measurements of concentration and velocity, tidal and wave fluxes were successfully calculated. However, it was not possible to calculate the mean flux accurately because the electromagnetic current meters were not able to measure to a precision of $>3mms^{-1}$ required to separate the long-term deployment average mean flux from the tidal flux and wave flux. As a result, the mean fluxes presented, did not reflect the true direction and magnitude of the sediment transported. Because of the uncertainty with the mean flux, sediment budget estimates cannot be produced with the BLISS data. However, the tidal and wave flux measurements should be used for calibrating numerical models. The results of the models should then be able to estimate the mean flow with higher degree of accuracy and hence budget estimates could be formulated using these results.

8.5 Relating the BLISS Measurements to Numerical Models

The fifth objective was to relate the BLISS *in situ* measurements to numerical models developed at the University of Plymouth which are able to simulate the BLISS observations and also provide a comprehensive prediction of SPM dynamics off the Holderness coast. A multi-input single output (MISO) time series model was developed to simulate both horizontal advection, local resuspension and the effects of waves and storms which had been ignored from earlier SPM models, such as those by Simpson and Sharples, (1991) and Jago and Jones, (1993). The MISO model took the suspended sediment dynamics to be an unknown stochastic system and considered and included the following as stochastic processes; current velocity, wave variation, tidal displacement and SSC. The first three were set as inputs to the system model, and the last one was considered as the output of the system model. System Identification Theory was then applied in the model, to identify the unknown parameters of the model based on the *in situ* data collected by the BLISS observations. The simulation results from the model showed good agreement with the *in situ* data collected from the Holderness coast. The results from this work has been submitted to the Journal of Marine Systems titled: *Time Series Modelling of Suspended Sediment Concentration on the Holderness Coast* by Chen, Dyke, Blewett and Huntley, (1997).

8.6 Future Work and Recommendations for Future BLISS Deployments

The Holderness coast in the North East coast of England has a history of severe coastal erosion and is the largest coastal source of fine sediment into the North Sea. The single most important factor in cliff erosion is the action of the waves, which are effective mainly during storms at high water springs. The main objective of the BLISS project was to determine the physical processes which control the movement of suspended sediment off the Holderness coast during storm events and in different seasons. The second objective was to measure sediment fluxes and determine a sediment flux budget for the material coming away from the Holderness coast.

Analysis of data collected from the BLISS deployments revealed a number of important features, and noted that an increase in sediment suspension in the vicinity of the BLISS moorings was caused by two processes. Horizontal advection of a concentration enriched plume flowing out of the Humber estuary in ebb tide. Resuspension of bed material at maximum tidal streaming was not an important contributor to the increase in sediment suspension, but resuspension of the bed material was noted to occur during storms. The February outer station storm was a good example of this. The transport of suspended sediment away from Holderness is controlled by the steady (near bed) return seaward flow (undertow) during the winter storms. The storm waves however, only contribute to a small percentage of the actual amount of sediment transported. They are effective stirring mechanisms which increase the amount of sediment available for sediment transport.

Recommendations for future work off Holderness and the necessary ancillary measurements are now described.

1) The hypothesis that concentration enriched water is advected into the region of the BLISS moorings should be examined in more detail. From satellite evidence, it is suggested that the source of the concentration enriched plume originates from the Humber estuary. It is proposed that for any future *in situ* measurements taken off the Holderness coast, in the same way as the BLISS experiment i.e. along a transect normal to the coast, should be complemented with profile measurements of salinity, temperature and SSC taken at predetermined sites from Spurn Head to the vicinity of the mooring sites. In this way the profile measurements can be compared to the BLISS measurements, to determine whether the BLISS measurements are indeed recording

advection of a horizontal concentration gradient which increases towards Spurn Head. All measurements should be complemented with compatible SeaWiFs satellite images and CASI overflights. In addition, current velocity measurements to complement BLISS should be made using other instruments such as the Acoustic Doppler Current Profiler and drifter buoys. These instruments may be more accurate at measuring the mean flow than the electromagnetic current meters, which as already mentioned is crucial for accurate sediment budget calculations.

2) It is postulated that a turbidity gradient which is inclined at an angle to the axes of the tidal ellipse will produce the double peaks in suspension seen in the concentration advective signal and the tidal displacement at the February 1996 inner station. In future BLISS deployments off Holderness, accurate measurements of the two-dimensional spatial structure of turbidity in the vicinity of the BLISS moorings coupled with aerial photography of the surface turbidity is required to validate this suggestion.

3) The distribution of sediment in the vicinity of the BLISS moorings off the Holderness coast was considered to be homogeneous throughout the water column. It is suggested in further experiments using BLISS, whether off Holderness or in other dynamic regions, BLISS optical measurements should be complemented by additional measurements using an *in situ* backscatter particle sizer (Law *et al.*, 1997), which determines particle size distribution.

4) Single-point estimates of sediment flux taken from the BLISS tripods are not suitable measurements to obtain a realistic sediment flux budget for the Holderness coast. Future measurements of sediment flux off the Holderness coast should consider the whole water column. It is proposed that a survey grid is established for the coastal waters of the Holderness coasts from Bridlington to Spurn Head. A survey vessel equipped with a downward looking Acoustic Doppler Current Profiler should take measurements along this grid, coupled with vertical profiles of SSC (from near bed to surface) taken using optical instruments such as a beam transmissometer and optical backscatter sensor, fitted to a CTD *in situ* profiler. In order to calculate the total flux within the grid system, an integration of the fluxes across the grid needs to be made.

5) The difficulty of distinguishing advective effects from resuspension effects, and the recognition that phase between flow and SSC cannot be used for this purpose means

that direct estimation of flux from a single station is not possible without a detailed knowledge of the spatial variation of SSC around the station. This will be a particular problem in estimating cross-shore fluxes in regions where the tidal ellipse is strongly aligned parallel to the coast, as at Holderness. In view of this, it is likely that the best approach to estimating net fluxes will be through numerical modelling, and our model results provide valuable input for such modelling. Firstly, we have shown that the level of SSC is enormously increased by waves, and that storms are therefore of prime importance to the sediment fluxes. Other analysis, shows that the direct effect of waves in driving a net (long-term average) flux is relatively small, so that the primary effect of waves is simply to increase the levels of SPM which can then be moved by tidal and mean flows. Models of flux therefore do not need to include the detailed dynamics of the wave flows but need only include their influence on resuspension, stresses and mixing throughout the water column.

6) The seabed off Holderness is very variable over a year and it was recognised in the previous BLISS deployments, that not enough information was collected regarding the nature of the seabed material. It is recommended that prior to and during every deployment off Holderness, a site survey is conducted between the BLISS moorings, using a side-scan sonar and taking complementary shipek grab samples. In this way, the nature of the seabed and grain size distribution of the seabed material can be determined. Measurements of this kind are necessary for determining threshold conditions for sediment movement and suspension as well as roughness length and corresponding drag coefficient. However, the BLISS results do provide estimates of the threshold values of bed stress (or friction velocity) for resuspension, as well as estimates of sediment settling velocity, which will be important inputs to numerical models.

7) Seabed photography would show bed state and perhaps even determine the presence of settled fine *"fluff"* sediment which is thought to be settle out from suspension during calm periods only to be resuspended at maximum tidal streaming. To ensure a comprehensive investigation of the sedimentation processes using the BLISS tripods, a camera and/or video system should be added to the design of BLISS, offering coverage at timed intervals during the deployment. Manual control of the camera system should be possible via the telemetry link which is already included in the BLISS system, so

that in periods of rough weather, the processes acting at the seabed can be recorded and during prolonged periods of low wave activity, the camera system can be switched off.

8) It was possible in the previous BLISS deployments to calibrate the optical backscatter sensors with Formazin solution and later convert the Formazin Turbidity Units to mgl^{-1} using filtered sediment samples to obtain a single calibration curve. This was possible because off Holderness, the sediment in suspension was considered to be homogeneous and well mixed throughout the water column. This situation may not be the case in other deployment areas and it is recommended that the OBS sensors on the BLISS tripods are calibrated prior to and after the deployment by using sediment and water samples collected from the survey site before and during the deployment.

9) It was recognised during the BLISS deployments that the surface buoys, which carry the UHF radio transceiver to ensure a telemetry link, were vulnerable to fishing activity, and on two occasions were set adrift by trawlers. The BLISS tripods carry an acoustic pinger in the case of such an event happening. The BLISS tripods were located by pinpointing the pinger's signal using a hand held receiver. The tripods however, could only be located to within a square of 50m and therefore the tripods had to be actually located by grappling methods. This system is very hit and miss, and it was only by luck that the tripods were recovered without incurring serious damage. One way of avoiding this from happening in future deployments, is to include an acoustic release buoy system, so that the tripods could be recovered by simply lifting off the seabed without running the risk of dragging the tripods along the ground.

10) The BLISS compass did not operate very well in the previous deployments, so other methods were employed to re-orientate the current meter data to alongshore and cross-shore flow. In future deployments, it is recommended that divers are employed to measure exactly the orientation of the tripods with respect to North and to measure accurately the height of the optical sensors and EM current meters off the seabed. Grab samples and water samples at the tripod site may also be taken.

11) The main role of the BLISS tripods were to monitor the nearbed sedimentary and flow conditions in the bottom boundary layer during storm events. It would have been advantageous during the storm period to extend the deployment coverage to a whole month. In future deployments off Holderness using BLISS, it is recommended that

more use is made of the telemetry link by improving the modem telephone link and by having a larger battery pack and hard drive on the BLISS system.

12) Complementary measurements at the BLISS sites should be conducted with other benthic landers, which carry upward looking ADCPs, such as the PMPs designed by POL, to ensure a comprehensive investigation of the tidal currents throughout the bottom boundary layer.

References

Abbot, V.J. 1992. *Hydrography for the Surveyor and Engineer.* By. A.E. Ingham, 3rd Edition, revised by V.J. Abbot. Blackwell Scientific, London.

Al-Bakri, D. 1986. Provenance of the sediments in the Humber Estuary and the adjacent coasts, Eastern England. *Marine Geology.* Vol. 72, p. 171-186.

Anglian Water. 1988. *Anglian Coastal Management Atlas.* Sir William Halcrow and Partners.

Aubrey, D.G. 1989. Measurement errors for electromagnetic current meters, In Seymour, R.J. (Ed.). *Nearshore Sediment Transport.* Plenhum Press, Hertfordshire p. 67-78.

Aubrey, D.G. and J.H. Trowbridge. 1985. Kinematic and Dynamic Estimates from electromagnetic current meter data. *Journal of Geophysical Research.* Vol. 90, No. C5, p. 9137-9146.

Bagnold, R.A. 1966. Mechanics of marine sedimentation. In: *The Sea.* Vol. 3 (Ed. by M. N. Hill), p. 507-528. Interscience Publishers, New York.

Bale, A.J. and C.D. Barrett. A bottom-landing water sampling system for the benthic boundary layer. 1995. *Netherlands Journal of Sea Research.* Vol. 34, No. 4, p. 259-266.

Bale, A.J. and A. Morris. 1998. Particulate carbon: sediment resuspension and the mixing of suspended particles. *Submitted to Continental Shelf Research in 1993.* In review.

Banner, F.T., Collins, M.B. and K.S. Massie. 1980. Tides on the North West European continental shelf by D.A. Huntley. *In: The North West European shelf seas: The seabed and the sea in motion. II. Physical and chemical oceanography, and physical resources.* Chapter 9, p. 301-350. Elsevier Scientific, Oxford.

Beach, R.A. and R.W. Sternberg. 1991. Infragravity driven suspended sediment transport in the swash, inner and outer surf zone. *Proceedings, Coastal Sediments '91*, A.S.C.E., p. 114-128.

Brenninkmeyer, B.M. 1976. In-situ measurements of rapidly fluctuating high sediment concentrations. *Marine Geology.* No. 20, p. 117-128.

Cacchione, D.A. and D.E. Drake. 1982. Measurements of storm-generated bottom stresses on the continental shelf. *Journal of Geophysical Research.* No. 87, p. 1952-60.

Cacchione, D.A. and D.E. Drake. 1979. A new instrument system to investigate sediment dynamics on continental shelves. *Marine Geology.* No. 30, p. 299-312.

Charnock, H., K.R. Dyer, J.M. Huthnance, P.S. Liss, J.H. Simpson, P.B. Tett. 1994. *Understanding the North Sea System.* The Royal Society, Chapman & Hall. London p. 1-4, 5-15, 53 - 68.

Christie, M. 1997. *The In Situ Erosion of Intertidal Muds.* Ph. D. Thesis, University of Plymouth.

Cunningham, P.M., R.T. Guza and R.L. Lowe. 1979. Dynamic calibration of electromagnetic flow meters. *Proceedings of Oceans '79*, p. 298-301. Institute of Electrical and Electronics Engineers, New York.

Curtin, T.B. and R.V. Legeckis. 1986. Physical observations in the plume region of the Amazon River during peak discharge, I, Surface variability. *Continental Shelf Research.* Vol. 6, p. 31-51.

D & A Instruments. 1989. OBS-1 & 3 Suspended solids and turbidity monitor. *Instruction manual.*

Davidson, M.A., Russell, P.E., Huntley, D.A. and J. Hardisty. 1993. Tidal asymmetry in suspended sand transport on a macrotidal intermediate beach. *Marine Geology*. No. 110, p. 333-353.

Dewey, R.K. and W.R. Crawford. 1988. Bottom stress estimates from vertical dissipation rate profiles on the continental shelf. *Journal of Physical Oceanography*. Vol. 18, p. 1167-1177.

Downing, J.P., R.W. Sternberg and C.R.B. Lister. 1981. New instrumentation for the investigation of sediment suspension processes in the shallow marine environment. *Marine Geology*. No. 42, p. 19-34.

Drake, D.E. and D.A. Cacchione. 1986. Field observations of bed shear stress and sediment resuspension on continental shelves Alaska and California. *Continental Shelf Research*. Vol 6, p. 415-429.

Dyer, K.R. 1986. *Coastal and Estuarine Sediment Dynamics*. Chapter 8, Wiley and Sons. Chichester, England.

Dyer, K.R. 1980. Velocity profiles over a rippled bed and the threshold of movement of sand. *Estuarine and Coastal Shelf Science*. No. 10, p. 181-99.

Dyer, K.R. and T.J. Moffat. 1998. Fluxes of suspended matter in the East Anglian plume, Southern North Sea. *Submitted to Continental Shelf Research in 1994*. In review.

Dyer, K.R. and T.J. Moffat. 1992. Suspended sediment distributions in the North Sea. *Institute of Marine Studies Report*. University of Plymouth.

Dyer, K.R. and R.L. Soulsby. 1988. Sand transport on the continental shelf. *Annual Review of Fluid Mechanics*. No. 20, p. 295-324.

Eisma, D. 1986. "The North Sea". An Overview. Netherlands Institute for Sea Research. *Proceedings of the 2nd North Sea Seminar '86*, p. 11.

Eisma, D. 1981. Supply and deposition of suspended matter in the North Sea. *In. Ed. Holocene Marine Sedimentation in the North Sea Basin.* Nio, S.D. Schuttenhelm, R.T. E. and Van Weering, T.C.E. International Association of Sedimentologists Special Publication, No. 5, p. 415-28.

Eisma, D. 1973. Sediment distribution in the North Sea in relation to marine pollution. In *North Sea Science.* NATO North Sea Science Conference, Aviemore, Scotland, 15-20 November 1971, p. 131-150. Ed. E.D. Goldberg.

Eisma, D. and J. Kalf. 1987. Dispersal, concentration and deposition of suspended matter in the North Sea. *Journal of the Geological Society*, London. No. 144, p. 161-178.

Fennessy, M.J., Dyer, K.R. and D.A. Huntley. 1994. Size and settling velocity distributions of flocs in the Tamar Estuary during a tidal cycle. *Netherlands Journal of Aquatic Ecology.* Vol. 28 (No. 3-4), p. 275-282.

Flather, R.A. 1976. A tidal model of the north-west European continental shelf. *Memorial Society Royal Science Liege Series.* Vol 6, No. 10, p. 141-164.

Foote. Y., Huntley, D.A., Davidson, M., Russell, P.E., Hardisty, J. and A. Cramp. 1992. Incident wave groups and long waves in the nearshore zone. *Coastal Engineering*, p. 974-989.

Fredsoe, J. and R. Deigaard. 1992. *Mechanics of Coastal Sediment Transport.* World Scientific Publishing Co., Singapore.

Furnes, G.F. 1980. Wind Effects in the North Sea. *Journal of Physical Oceanography.* Volume 10, p 978 - 984.

Gagliardini, D.A., Karzenbaum, H., Legeckis, R. and V. Klemus. 1984. Application of Landsat MSS, NOAA / TIROS AVHRR and Nimbus CZCS to study the La Plata river and its interaction with the ocean. *Remote Sensing Environment.* No. 15, P. 21-36.

Glen, S.M. and W.D. Grant. 1987. Suspended sediment stratification correction for combined wave and current flow. *Journal of Geophysical Research.* Vol. 92, p. 8244-8265.

Goodman, N.R. 1957. On the joint estimation of the spectra, co-spectrum and quadrature spectrum of a two-dimensional stationary Guassian process. *Scientific Paper*, 10, Engineering Statistics Laboratory, New York University.

Grant, W.D. and O.S. Madsen. 1986. The continental shelf bottom boundary layer. *Annual Review of Fluid Mechanics*. No. 18, p. 265-305.

Grant, W.D. and O.S. Madsen. 1979. Combined wave and current interaction with a rough bottom. *Journal of Geophysical Research*. Vol. 84, p. 1797-1808.

Green, M.O. and J.D. Boon. 1993. The measurement of constituent concentrations in non-homogeneous sediment suspensions using optical backscatter sensors. *Marine Geology*. No. 110, p. 73-81.

Green, M.O., Vincent, C.E., McCave, I.N., Dickson, R.R., Rees, J.M. and N.D. Pearson. 1995. Storm sediment transport: observations from the British North Sea shelf. *Continental Shelf Research*. Vol. 15, No. 8, p. 889-912.

Green, M.O., Rees, J.M. & N.D. Pearson. 1990. Evidence for the Influence of Wave Current Interaction in a Tidal Boundary Layer. *Journal of Geophysical Research*. V. 95, p. 9629-9644.

Guza, R.T. 1988. Comment on "Kinematic and dynamic estimates from electromagnetic current meter data" by D.G. Aubrey and J.H. Trowbridge. *Journal of Geophysical Research*. No. 93(C2), p. 1337-1343.

Guza, R.T. and E.B. Thornton. 1982. Swash oscillations on a natural beach. *Journal of Geophysical Research*. Vol. 87 (C1), p. 483-491.

Hanes, D.M. 1988. Intermittent sediment suspension and its implications to sand tracer dispersal in wave dominated environments. *Marine Geology*. No. 81, p. 175-183.

Hanes, D.M. and D.A. Huntley. 1986. Continuous measurements of suspended sand concentration in a wave dominated nearshore environment. *Continental Shelf Research*. Vol. 6, No. 4, p. 585-596.

Hanes, D.M., Vincent, C.E., Huntley, D.A., and T.L. Clarke. 1988. Acoustic measurements of suspended sand concentration in the C2S2 experiment at Stanhope Lane, Prince Edward Island. *Marine Geology*. No. 81, p. 185-196.

Hannay, A., Williams, J.J., West, J.R. and L.E. Coates. A Field Study of Wave-Current Interactions over a Rippled Sand Bed. 1994. *EUROMECH 310. Sediment Transport Mechanisms in Coastal Environments and Rivers.* M. Belorgey, R.D. Rajaona and J.A.F. Sleath (Editors). World Scientific, London. P. 345-359.

Hardisty, J. 1993. Time series analysis using spectral techniques: oscillatory currents. *Earth Surface Processes and Landforms*. Vol. 18, p. 855-862.

Hardisty, J. 1986. Engineering Versus Environmental Requirements in Coastal Prediction. *Journal of Shoreline Management*. Vol. 2, p. 65-72.

Harvey, J.G. and C.E. Vincent. 1977. Observations of shear in the near-bed currents in the Southern North Sea. *Estuarine and Coastal Marine Science*. Vol 5, p. 715-731.

Heathershaw, A.D. and J.H. Simpson. 1978. The sampling variability of the Reynolds stress and its relation to boundary shear stress and drag coefficient measurements. *Estuarine and Coastal Marine Science*. Vol. 6, p. 203-274.

Hequette, A. and P.R. Hill. 1993. Storm-generated currents and offshore sediment transport on a sandy shoreface, Tibjak Beach, Canadian Beaufort Sea. *Marine Geology*, No. 13, p. 283-304.

Hill, A.E., James, I.D., Linden, P.F., Matthews, J.P., Prandle, D., J.H. Simpson, Gmitrowicz, E.M. Smeed, D.A., Lwiza, K.M.M., Durazo, R., Fox, A.D. and D.G. Bowers. 1994. Dynamics of tidal mixing fronts in the North Sea. *In Understanding the North Sea System* Edited by Charnock *et al.*, 1994. The Royal Society, p. 53-68. Chapman & Hall. London.

Holligan, P.M., T. Aarup and S.B. Groom. 1989. The North Sea: Satellite Colour Atlas. *Continental Shelf Research*. Vol 9, No 8, p. 667 - 765.

Howarth, M.J., Dyer, K.R., Joint, I.R., Hydes, D.J., Purdie, D.A., Edmunds, H., Jones, J.E., Lowry, R.K., Moffat, T.J., Pomroy, A.J. and R. Proctor. 1994. Seasonal cycles and their spatial variability. *In Understanding the North Sea System.* Edited by Charnock *et al.*, 1994. The Royal Society, p. 5-26. Chapman & Hall. London.

Humphrey, J.D. 1987. STABLE. An instrument for studying current structure and sediment transport in the benthic boundary layer. *Institute of Electronic and Radio Engineers.* No. 72, p. 57-62.

Huntley, D.A. 1988. A Modified Inertial Dissipation Method for Estimating Seabed Stresses at Low Reynolds Numbers, with Applications to Wave/Current Boundary Layer Measurements. *Journal of Physical Oceanography.* 18, p. 347-346.

Huntley, D.A. and D.M. Hanes. 1987. Direct measurements of suspended sediment transport. In. N.C. Kraus (Editor). *Coastal Sediments, 1987.* Am.Soc.Civ.Eng., New Orleans, p.723-737.

Huntley, D.A. and C.S. Kim. 1985. Is surf beat forced or free? *Proc. 19th Coastal Engineering Conference.*, Houston, Texas. ASCE, New York, p. 871-885.

Huntley, D.A., Nicholls, R.J., Chulei Liu and K.R. Dyer. 1994. Measurements of the semi-diurnal drag coefficient over sand waves. *Continental Shelf Research.* Vol. 14, No. 5, p. 437-456.

Hydraulics Research. 1992. Particulate pollutants in the North Sea. *Report SR 292,* Hydraulics Research, Wallingford.

IAHR. 1987. *List of Sea State Parameters.* Presentation by M. Daras.

Jago, C.F., A.J. Bale, M.O. Green, M.J. Howarth, S.E. Jones, I.N. McCave, G.E. Millwood, A.W. Morris, A.J. Rowden and J.J. Williams. 1994. Resuspension processes and seston dynamics in the Southern North Sea. In. *Understanding the North Sea System.* Edited by H. Charnock, K.R. Dyer, J.M. Huthnance, P.S. Liss, J.H. Simpson, P.B. Tett.Chapman and Hall, London.

Jago, C.F. & S.E. Jones. 1998. Dynamics of Suspended Particulate Matter in the Southern North Sea. I. Tidally Mixed Waters. *Submitted to Continental Shelf Research in 1993*. In review.

James, I.D. 1989. A three dimensional model of circulation in a frontal region in the North Sea. *Delft Hydrography*. No. 42, p. 231-247.

Jenkins, G.M. and D.G. Watts. 1968. *Spectral Analysis and its applications*. Holden-Day, San Francisco, New York. Vol. 3, p. 529-533.

Jones, S.E., Jago, C.F., Bale, A.J., Chapman, D., Howland, R. & J. Jackson. 1998. Dynamics of Suspended Particulate Matter in the Southern North Sea. II. Seasonally Stratified Waters. *Submitted to Continental Shelf Research in 1993*. In review.

Jones, S., C.F. Jago, D. Prandle and D. Flatt. 1994. Suspended sediment dynamics: measurement and modelling in the Dover Strait. In. *Mixing and Transport in the Environment*. Edited by, K.J. Beven, P.C. Chatwin and J.H. Millbank. John Wiley and Sons Ltd. Chichester, England.

Jones, S., C.F. Jago and J.H. Simpson. 1996. Modelling suspended sediment dynamics in tidally stirred and periodically stratified waters: progress and pitfalls. Mixing in Estuaries and Coastal Seas: *Coastal and Estuarine Studies*. Vol. 50, p. 302-324.

Jonsson, I.G. 1980. A new approach to oscillating rough turbulent boundary layers. *Ocean Engineering*. No. 7, p. 109-152.

Kapdasli, M.S. and K.R. Dyer. 1986. Threshold conditions for sand movement on a rippled bed. *Geo-Marine Letters*. Vol. 6, p. 161-164.

Kemp, P.H. and R.R. Simons. 1983. The interaction of waves and a turbulent current: waves propagating against the current. *Journal of Fluid Mechanics*. Vol. 130, p. 73-89.

Kineke, G.C. and R.W. Sternberg. 1992. Measurements of high concentration suspended sediments using the optical backscatterance sensor. *Marine Geology*. No. 108, p. 253-258.

Komar, P.D. and M.C. Miller. 1975. Sediment threshold under oscillatory waves. *Proceedings Conference on Coastal Engineering*, p. 756-775.

Kundu, P.K. 1990. *Turbulence in Fluid Mechanics*. Chapter 12, p. 416-473. Academic, San Diego, California.

Larsen, L.H. 1982. A new mechanism for seaward dispersion of mid-shelf sediments. *Sedimentology*. No. 29, p. 279-284.

Larsen, L.H., Sternberg, R.W., Shi, N.C., Marsden, M.A.H., and L. Thomas. 1981. Field investigations of the threshold of grain motion by ocean waves and currents. *Marine Geology*. No. 42, p. 105-132.

Law, D. J., Bale, A.J. and S.E. Jones. 1997. Adaption of focussed beam reflectance measurement to in situ particle sizing in estuaries and coastal waters. *Marine Geology*. No. 140, p. 47-59.

Longuet-Higgins, M.S. and R.W. Stewart. 1964. Radiation stress in water waves: a physical discussion, with applications. *Deep Sea Research*. No. 11, p. 529-562.

Longuet-Higgins, M.S. and R.W. Stewart. 1962. Radiation stress and mass transport in gravity waves, with application to 'surf-beats'. *Journal of Fluid Mechanics*. No. 13, p. 481-504.

Lynch, J.F., Gross, T.F., Sherwood, C.R., Irish, J.D. and B.H. Brumley. 1997. Acoustical and optical backscatter measurements of sediment transport in the 1988-1989 STRESS experiment. *Continental Shelf Research*. Vol. 17, No. 4, p. 337-366.

Madsen, O.S., and W.D. Grant. 1975. The threshold of sediment movement under oscillatory waves: a discussion. *Journal of Sediment Petrology*. No. 45, p. 360-361.

McCave, I.N. 1987. Fine sediment sources and sinks around the East Anglian Coast (UK). *Journal of Geological Society*, London. No. 144, p. 149-152.

McCave, I.N. 1973. Mud in the North Sea. In: Goldberg E.D. (ed.) *North Sea Science.* M.I.T. Press, Cambridge, London., p. 75-100.

McCave, I.N. 1972. Transport and escape of fine-grained sediment from shelf areas. *In: Shelf Sediment Transport: Process and pattern.* Swift, D.J.P., Duane, D.B., Pilkey, O.H. (eds). Dowden, Hutchingson and Ross, Stroudsberg, p. 225 - 248. Pennsylavania. John Wiley and Sons. England.

McCave, I.N. 1971. Wave effectiveness at the seabed and its relationship to bedforms and deposition of mud. *Journal of Sediment Petrology.* No. 41, p. 89-96.

McCave, I.N. 1970. Deposition of fine-grained suspended sediment from tidal currents. *Journal of Geophysical Research.* Vol. 75, No. 21, p. 4151-4159.

McManus, J.P and D. Prandle. 1997. Development of a model to reproduce observed suspended sediment distributions in the southern North Sea using principal component analysis and multiple linear regression. *Continental Shelf Research.* Vol. 17, No. 7, p. 761-778.

Miller, M. C., I. N. McCave and P. D. Komar. 1977. Threshold of sediment motion under unidirectional currents. *Sedimentology.* Vol. 24, p. 507-527.

Mork, M. 1981. Circulation Phenomena and Frontal Dynamics of the Norwegian Coastal Current. *Philosophical Transaction for the Royal Society of London.* A 302, p. 635-647.

Myrhaug, D., Lambrakos, K.F. and O.H., Slaattelid. 1992. Wave boundary layer in flow measurements near the seabed. *Coastal Engineering.* No. 18, p. 153-181.

Myrhaug, D., O.H. Slaattelid and K.F. Lambrakos. 1994. Suspended sediment concentrations near the seabed in North Sea storms. In: M. Beloreg et al. (editors), *Euromech 310. Sediment Transport Mechanisms in Coastal Environments and Rivers*. World Scientific Publishing Co. Singapore, p. 397-412.

Nielson, P. 1992. *Coastal Bottom Boundary Layers and Sediment Transport*. Advanced Series on Ocean Engineering. Vol. 4. World Scientific, Singapore, p. 62-91.

Nuttall, A.H. 1971. Spectral estimation by means of overlapped FFT processing of windowed data. *Naval Underwater System Centre*. Report No. 4169. New London CT USA (and supplement in USCTR - 4169S.

Osborne, P.D., B. Greenwood. 1992. Frequency dependent cross-shore suspended sediment transport. A non-barred shoreface. *Marine Geology*. Vol. 106, p. 1-24.

Osborne, P.D., C.E. Vincent and B. Greenwood. 1994. Measurement of suspended sand concentrations in the nearshore: field intercomparison of optical and acoustic backscatter sensors. *Continental Shelf Research*. Vol. 14, No. 2/3, p. 159-174.

Owen, M.W. 1976. Determination of the settling velocities of cohesive muds. *Report No. IT 161, Hydraulics Research Station, Wallingford.*

Pearson, N.D. and M.R. Thomas. 1991. An instrument to measure seabed boundary-layer processes. *Journal of Oceanic Engineering*. Vol. 16, No. 4, p.338-342.

Pingree, R.D. and D.K. Griffiths. 1978. Tidal fronts on the shelf seas around the British Isles. *Journal of Geophysical Research*. No. 83, p. 4615 - 4622.

Prandle, D. 1997. Tidal characteristics of suspended sediment concentrations. *Journal of Hydraulic Engineering*. Vol. 123, No. 4, p. 341-350.

Prandle, D. 1994. Holderness Experiment. the observational programme. *LOIS Newsletter*. Issue No. 2.

Pringle, Ada W. 1985. Holderness Coast Erosion and the Significance of Ords. *Earth Surface Processes and Landforms*. Vol. 10, p. 107-124.

Pugh, D.T. 1987. *Tides, Surges and Mean Sea Level.* John Wiley & Sons, Chichester, England. P. 166 - 170.

Pugh, D.T. and J.M. Vassie. 1976. Tide and surge propagation off-shore in the Dowsing Region. *Deutsche Hydrographische Zeitschrift, Jahrgang*. Vol. 29., No 5, p. 162 213.

Reynolds, O. 1883. An experimental investigation of the circumstances which determine whether the motion of water shall be direct or sinuous, and of the law of resistance in parallel channels. *Philosophical Transaction Royal Society, London*. No. 18, p. 819-832.

Robinson, I.N. 1985. *Satellite Oceanography: an introduction for oceanography and remote sensing scientists*. Ellis Howard Limited, Chichester, England.

Russell, P.E. 1993. Mechanisms for beach erosion during storms. *Continental Shelf Research*. Vol. 13, No. 11, p. 1243-1265.

Russell, P.E. 1991. *Field Studies of Suspended Sand Transport on a High Energy Dissipative Beach*. PhD Thesis. University of Wales, Swansea.

Shi, N.C. and L.H. Larsen. 1984. Reverse sediment transport induced by amplitude modulated waves. *Marine Geology*. No. 54, p. 181-200.

Simpson, J.H. 1994. Introduction to the North Sea Project. *In Understanding the North Sea System*. Edited by Charnock *et al.*, 1994. The Royal Society, p. 1- 4. Chapman & Hall. London

Simpson, J.H and J.R. Hunter. 1974. Fronts in the Irish Sea. *Nature*, London. No. 250, p. 404-406.

Simpson, J.H. & J. Sharples. 1991. Dynamically-active Models in the Prediction of Estuarine Stratification. *In coastal and Estuarine Studies,* p. 101-113. Editor David Prandle. Dynamics and Exchanges in Estuaries and the Coastal Zone. American Geophysical Union. Springer Verlag. New York.

Smith, J.D. 1977. Modelling of sediment transport on continental shelves. *The Sea.* Ed. Goldberg and co-editors. Vol. 6. Wiley-Interscience, Chichester, England. P. 529-577.

Soulsby, R.L. 1983. The bottom boundary layer of shelf seas: *Physical Oceanography of Coastal and Shelf Seas*, B. John Ed., Elsevier Oceanography Series, 35, Oxford. P. 189-266.

Soulsby, R.L. 1980. Selecting record length and digitisation rate for near-bed turbulence measurements. *Journal of Geophysical Research.* Vol. 10, p. 208-219.

Soulsby, R. L. 1977. Sensors for the measurement of sand in suspension. A survey of requirements and possibilities for development. *Report No. 27.* Institute of Oceanographic Sciences, Taunton.

Soulsby, R.L. and J.D. Humphrey. 1989. Field observations of wave-current interactions at the seabed. *Proceedings of the NATO Advanced Workshop on Water Wave Kinematics*, A. Torum & O.T. Gudmestad (eds), 22-25 May, 1989, Molde, Norway, Kluwer Academic Publication, Dortrecht, Netherlands, p. 413-428.

Soulsby, R.L. and B.L.S.A. Wainwright. 1987. A criterion for the effect of suspended sediment on near-bottom velocity profiles. *Journal of Hydraulic Research.* Vol. 25, No. 3, p. 341-356.

Stapleton, K.R. 1996. *Wave and Current Interaction in the Coastal Zone.* PhD. Thesis University of Plymouth.

Stapleton, K.R. and D.A. Huntley. 1995. Seabed stresses determinations using the inertial dissipation method and the turbulent kinetic energy method. *Earth Surface Processes and Landforms.* Vol. 20, p. 807-815.

Sternberg, R.W., N.C. Shi and J.P. Downing. 1984. Field investigation of suspended sediment transport in the nearshore zone. *Proceedings of the Int. Conf. of Coastal Engineering*. 19th Am. Soc. Civ. Eng., p. 1782-1798.

Stride, A.H. 1973. Sediment transport by the North Sea. *In North Sea Science*. NATO North Sea Science Conference, Aviemore, Scotland, 15-20 November 1971. p. 131-150. Ed. E.D. Goldberg. Wile and Sons, Chichester, England.

Stumpf, R.P. 1987. Application of AVHRR satellite data to the study of sediment and chlorophyll in turbid coastal water. *Tech. Memo. NESDIS AISC 7*. p. 50. National Environmental Satellite Data and Information Service, National Oceanic and Atmospheric Administration. Washington D.C.

Stumpf, R.P. and J.R. Pennock. 1989. Calibration of a general optical equation for remote sensing of suspended sediment in a moderately turbid estuary. *Journal of Geophysical Research*. Vol. 94, N0. C10. P. 14,363 - 14,371.

Sundermann, J. 1993. Suspended particulate matter in the North Sea: field observations and model simulations. *Philosophical Transactions-Royal Society of London*. A 343, p. 423-430.

Tassan, S. and S.B. Sturm. 1986. An algorithm for the retrieval of sediment content in turbid coastal waters from CZCS data. *International Journal of Remote Sensing*. Vol. 7 (5), p. 643-655.

Tennekes H. and J.L. Lumley. 1972. *A First Course in Turbulence*, MIT Press. Cambridge, Mass.

Ternberg, A., F. De Bovee, P. Hall, W. Bearetson, D. Chadwich, G. Ciceri, P. Crassous, A. Devol, S.E. Mason, J. Gage, R. Glud, F. Graziothini, J. Gundesen, D. Hammond, W. Helder, K. Hinga, O. Holby, R. Jahnke, A. Khripounoff, S. Lieberman, V. Nuppenau, O. Pfannkuche, C. Reimers, G. Rowe, A. Sahami, F. Sayles, M. Schurter, D. Smallman, B & P. Wehrli, DeWilde. 1995. Benthic Chamber and Profiling Landers in Oceanography. a review of design, technical

solutions and functioning. *Progress in Oceanography.* Vol. 35, p. 253-294. Elesvier Science, LTD. Oxford.

Thorne, P.D., Hardcastle, P.J. and R.L. Soulsby. 1993. Analysis of acoustic measurements of suspended sediments. *Journal of Geophysical Research.* Vol. 98, No. C1, p. 899-910.

Thorne, P.D., C.E. Vincent, P.J. Hardcastle, S.Rehman and N. Pearson. 1991. Measuring suspended sediment concentrations using acoustic backscatter devices. *Marine Geology.* No. 98, p. 7-16.

UNESCO, 1991. *Processing of Oceanographic Data*, p. 9-11. Published by the United Nations Educational, Scientific and Cultural Organisation. Paris, France.

Valentin, H.. 1971. Land loss at Holderness. *Applied Coastal Geomorphology.* Edited by J.A. Steers. Macmillan. London.

Van Rijn, L.C. 1993. *Principles of Sediment Transport in Rivers, Estuaries and Coastal Seas.* Chapters 2, 3, 4, 9. Aqua Publications. Oxford.

Weeks, A. & J.H. Simpson. 1991. The Measurement of Suspended Particulate Concentrations from Remotely Sensed Data. *International Journal of Remote Sensing.* V. 12, p. 725-737.

Weeks, A, Simpson, J.H. and D. Bowers. 1993. The relationship between concentrations of suspended particulate material and tidal processes in the Irish Sea. *Continental Shelf Research.* Vol. 13, No. 12, p. 1325-1334.

Widdows, J.W. 1996. Summary report on: *Use of In situ benthic annular flume to investigate particle flux at the sediment-water interface in relation to changes in current velocity and macrofauna community.* In: Preliminary results, LISP - Littoral Investigation of Sediment Properties. LOIS RACS (C) Special Topic 122. Compiled by K. Black and D. Patterson.

Williams, J.J., Humphrey, J.D., Moores, S.P. and D. Clipson. Analysis of STABLE data from deployment 1, Holderness, UK. October 1994. 1996a., *Proudman Oceanographic Laboratory, Report No. 42.*

Williams, J.J., Humphrey, J.D., Moores, S.P., Wilson, D. 1996b. Analysis of STABLE Data from Deployment 2, Holderness, UK. January - February 1995. *Proudman Oceanographic Laboratories, Report No. 43.*

Williams, J.J., Thorne, P.D., O'Connor, B.A., Humphrey, J.D., Hardcastle, P.J., Moores, S.P. & Cooke, J.A. 1998. Interactions between Currents, Waves and Sediment in Calm and Storm Conditions. *Submitted to Continental Shelf Research in 1996.* In Review

Wimbush M. and W. Munk. 1970. The benthic boundary layer. In: *The Sea*, Vol. 4, Part 1 (Ed A.E. Maxwell), Wiley-Interscience, Chichester, New York, p. 731-758.

Wright, L.D., Boon, S.C. Kim and J.H. List. 1991. Modes of cross-shore sediment transport on the shoreface of the Middle Atlantic Bight. *Marine Geology*, No. 96, p. 19-51.

Xu, J.P., Wright, L.D. and J.D. Boon. 1994. Estimation of bottom stress and roughness in Lower Chesapeake Bay by the inertial dissipation method. *Journal of Coastal Research.* Vol. 10, No. 2.

Personal Communications

Barrett, Colin. 1996. Plymouth Marine Laboratory Electronics group. West Hoe, Plymouth, Devon. Tel: (01752) 633100

Bull, Chris. 1997. University College of North Wales, Bangor. School of Ocean Sciences Menaii Bridge, Anglesey. LL59 5EY. Tel: (01248) 351151

Dyer, Keith. 1997. University of Plymouth, Institute of Marine Studies. Drake Circus. Plymouth, Devon. PL4 8AA. Tel: (01752) 232400

Huntley, David. 1997. University of Plymouth, Institute of Marine Studies, Drake Circus, Plymouth, Devon. PL4 8AA. Tel: (01752) 232400

Jago, Colin. 1997. University College of North Wales, Bangor. School of Ocean Sciences Menaii Bridge, Anglesey. LL59 5EY. Tel: (01248) 351151

Millward, Geoff. 1995. University of Plymouth, Department of Environmental Science. Drake Circus. Plymouth, Devon. PL4 8AA. Tel: (01752) 232400

Morris, Kevin. 1997. Plymouth Marine Laboratory Electronics group.West Hoe, Plymouth, Devon. Tel: (01752) 633100

Appendix A

Instrument Calibrations and Geometry Rotation

A.1 Electromagnetic Current Meters

Table A.1 Results of pre-deployment 2 calibrations

BLISS Rig 2			BLISS Rig 3			BLISS Rig 4		
	Sensor 1			Sensor 3			Sensor 5	
Date, Time	Sensor axis	Offset (bits)	Date, Time	Sensor axis	Offset (bits)	Date, Time	Sensor axis	Offset (bits)
20/6/95 09:35	1x 1y	-20 9	20/6/95 13:27	1x 1y	88 -854	18/6/95 14:09	1x 1y	-348 -311
						20/6/95 17:26	1x 1y	-360 -300
	Sensor 2			Sensor 4			Sensor 6	
Date, Time	Sensor axis	Offset (bits)	Date, Time	Sensor axis	Offset (bits)	Date, Time	Sensor axis	Offset (bits)
20/6/95 09:35	2x 2y	-5 61	20/6/95 13:27	2x 2y	-31 -64	18/6/95 13:49	2x 2y	380 533
						20/6/96 17:26	2x 2y	387 525

Sensors 1 and 2 on BLISS 2 appeared to work sufficiently, with small offsets likely due to the proximity effects. BLISS 3 was similar, except that sensor 3 appeared to have a different offset fault on the y-axis. Both sensors on BLISS 4 still had substantial and repeatable offsets on both axes, suggesting that Valeport had not eliminated the problem in these sensors. Monitor values logged during the launches for Deployment 2 were consistent with the above offsets still present after the frames had settled on the seabed.

Post deployment 2 checks were made using the same procedure as above. Each data entry is the mean of 30 monitor scans logged at 1s intervals. The low standard deviations and the small change between successive means shows that, for a given setup, the readings were steady to within the Valeport specified noise levels of the sensors. The offsets were then calculated by taking the average of the given means.

A.2 Optical Backscatter Sensor

A.2.1 Calibration Procedure using Formazin

1. Clean the apparatus i.e. container, stirring mechanism, glassware with detergent and rinse with filtered water.

2. Calibration standards are made by diluting stock turbidity solutions with filtered distilled water. Prepare 10 litre Formazin solutions in buckets with different concentrations (25 FTU, 100 FTU and 400 FTU), by using a 4000 FTU standard solution.

3. Place the OBS sensors in the different solutions (25,100, 400 FTU). Take readings, recording the average voltage output each time. Repeat this exercise ~20 times.

4. Plot FTU against bits values and perform linear regression to obtain the linear equations to perform the calibrations.

A.2.2 Deployment 2 - Pre and Post Calibrations

Diluted Formazin suspensions prepared in June were not significantly different from those freshly prepared for the post calibrations. The sensors after deployment had very little, if any, visible fouling, and cleaning (rubbing in dilute detergent with a soft cloth, followed by rinsing in tap water) had little or no significant effect. I.e. uncleaned OBS ≡ cleaned OBS. The OBS was at room temperature (~18°C) so it had to be placed into tap water at ~5°C where it settled to a steady value within ~ 30s. This indicated that there were no long thermal time constants. There was no significant difference between readings in tap water at ~5°C and ~16°C. This showed that temperature compensation is effective. All these tests were performed on Rig 3 OBS sensors. Later, it was confirmed that with Rig 2

sensors, compensation was effective between ~9°C and ~19°C at high turbidity, 400 FTU. I.e. the sensor did not function below ~9°C.

Although readings within any one calibration setup are constant to within ± 2 bits, differences ~ ± 10 to 20 bits resulted when one attempted to repeat a setup. The cause for this is unknown. This apparent small degree of non-repeatability is only likely to be important when dealing with low turbidities, when it could amount to a large % error.

A.2.3 Deployment 3 - November 1995

OBS 2/1

Used as slave OBS 2/2 in deployment 2 and possibly damaged by being run with a faulty master OBS 2/1. However, when re-tested by itself it appeared to work OK, though with reduced sensitivity, and so was used as master OBS 2/1 in deployment 3.

OBS 2/2

Fitted as master OBS 2/1 in deployment 2, when it went faulty, apparently with broken connection to temperature compensation in probe itself. Reconfigured, following the advice from D & A, with fixed temperature compensation and fitted as slave OBS 2/2 for deployment 3.

Calibration Coefficients (highlighted = calibrations used)

Rig 2 OBS 2/1

Pre 2	Did not function.
Post 2/Pre 3:	Full calibration (at approx. 9°C, washed).
	Turbidity (FTU) = 0.34454 x bits - 13.370
Pre 3	Functional checks: air 38 bits finger: 4095 bits (test full range of sensor).
Post 3	Functional checks: in water tank: 255 bits, finger: 4095 bits
	Calibration used: **Turbidity (FTU) = 0.34454 x bits - 13.370**
Pre 4	Functional check: finger 4095 bits

Post 4	Full calibration, new standards
	Turbidity (FTU) = 0.33376 x bits - 14.683

Rig 2 OBS 2/2

Pre 2	Full calibration
	Turbidity (FTU) = 0.19109 x bits - 28.071 (used for deployment 2)
Post 2/Pre 3:	Full calibration (at ~19°C, washed, temp. compensation set for 10°C):
	Turbidity (FTU) = 0.23242 x bits -7.7374 (used for deployment 3)
Pre 3	Full calibration at ~9°C to test temperature compensation.
	OK down to ~100 FTU then increasingly too low, going -ve at ~25 FTU
Pre 3	Partial recalibration (at ~5 to 8°C temp. compensation set for 7°C.
	Comparisons show consistency with higher FTU and better
	performance at lower FTU. Combining the high FTU value with low
	FTU value, gives the best calibration equation:
	Turbidity (FTU) = 0.23378 x bits + 1.1172
Post 3	Functional check: Sensor dead: open circuit in probe.
Post 4	There was no OBS 2/2 for deployment 4

Rig 3 OBS 3/1

Pre 2	**Turbidity (FTU) = 0.2156 x bits -10.758**
Post 2	Turbidity (FTU = Turbidity (FTU) = 0.1881 x bits -5.201
Post 4	Full calibration with new FTU standards
	Turbidity (FTU) = 0.2225 x bits - 1.0754

Rig 3 OBS 3/2

Pre 2	**Turbidity (FTU) = 0.2033 x bits - 5.1678**
Post 2	Turbidity (FTU) = 0.2484 x bits - 23.898
Post 4	Full calibration with new FTU standards
	Turbidity (FTU) = 0.2395 x bits - 10.219

Rig 4 OBS 4/1

Pre 2	Turbidity (FTU) = 0.2167 x bits - 12.993 (not deployed)
Post 2	**Turbidity (FTU) = 0.1992 x bits - 12.273**
Post 4	No OBS response for post calibrations so need to examine the data and apply a previous calibration. The sensor worked for our initial post deployment checks and hopefully has worked during the deployment.
Post 4 (2nd)	One final test of this sensor showed it to work, so a full calibration was completed. Corrosion of the connector (contacts) may have caused the initial failure. However, the following calibration had taken place some time after the rig was actually recovered, and the sensor had been sat in the lab since. The new Formosan standards were used (1 month old).
	Turbidity (FTU) = 0.1925 x bits - 9.140

Rig 4 OBS 4/1

Pre 2	Turbidity (FTU) = 0.2249 x bits - 13.104 (not deployed)
Post 2	Turbidity (FTU) = 0.2217 x bits - 15.486
Post 4	Full calibration with new FTU standards
	Turbidity (FTU) = 0.2564 x bits - 15.171

A.3 Procedure for filtering water samples containing suspended sediment. Results used in OBS calibration

1) Use a Glass microfibre filters of diameter 5.5cm (100 in a box) and pore size 0.4μm. The filter is a disc of compressed glass fibre forming a 'depth filter rather like a piece of felt. The Whatman GF/C filters of 47mm diameter are 260μm thick, weigh ~100mg and have a nominal minimum particle retention size of 1.2μm. They have a high flow rate and take a high load. They can also be pre-combusted to remove any traces of organic carbon. They tend to shed fibres so are not completely weight-stable.

2) Weigh untreated filters and number them 1 to 100. It is acceptable to mark the filters with a felt tip pen.

3) Place untreated filters in an oven set at 90° C for 24 hours.

4) Cool in a desiccator and reweigh filters. For work of this nature, a balance reading to is acceptable. Only in situations with heavily loaded filters and/or where order of magnitude results are satisfactory will a 10^{-4} balance suffice.

5) Place the reweighed filters in an oven set at 500° C for 24 hours. This acts to ash dry the filters.

6) Cool and weigh the ash dried filters.

7) Set up apparatus using the suction method of filtering.

8) Turn system on and wash through with distilled water. All beakers etc. to be washed thoroughly with distilled water.

9) Take a measurement of the amount of water sample to be filtered to the nearest ml. Note this in litres. One problem which must be guarded against is the particle settling in a sampling bottle or measuring flask. The bottle or flask needs to be shaken up to ensure filtration of a homogeneous and representative suspension is achieved. Also, rinse the sampling bottle with distilled water to get out all the sediment and also rinse the empty beaker previously holding the water sample.

10) NB There may be so much material in suspension that the filters clog before all the water is filtered. In this case, it is particularly important to ensure that what is filtered is a homogenised sub-sample of the whole.

11) Filter the water samples. Ensure that at all times, a representative water sample is taken, and that all the apparatus is washed thoroughly with distilled water in between filtration exercises. Note high vacuum pumps should not be used as this tends to pull the particles into the filter, making it clog sooner. Following filtration, wash the sediment sample through with distilled water to get rid of the salt water.

12) Obtain a few blanks filtered with a known quantity of distilled water.

13) Place the filter containing the sediment sample carefully into a petri dish provided using a flat-bladed tweezers.

14) Dry by placing in a drying oven set at 90° C for 24 hours. Do not cover the samples. Cool in the desiccator and immediately weigh the sediment sample so as to prevent the filter from acquiring moisture from the atmosphere. Other means of drying the filters is to place the filters in individual petri dishes with the covers over the dish but not firmly on so that air circulation can be achieved.

15) When the filter is dry, the sample is reweighed to give a value for both organic and inorganic suspended sediment concentration.

16) The dry filters are then placed in a crucible oven and left for 24 hours at 500° C so that the organic content is burnt off.

17) The filters are then cooled and reweighed to give the inorganic sediment content.

A.4 Orientation of Current Meters

June/July 1995 inner and middle station deployments; February 1996 inner and middle station deployments

Cross-shore $EM1X * \cos\theta + EM2X \sin\theta$

Alongshore $EM2X * \cos\theta - EM1X \sin\theta$

A.7.1 Reorientation of current meters using BLISS geometry

Table A.2 Nominal position and directions of sensors - Frame upright

	Height Above seabed			Direction of sensor axis	
	Position of sensor head. Distances along the axes.			Vertical plane ° up from horiz.	Horizontal plane ° CW from +x axis
	mm from origin				
Sensor	**x**	**y**	**z**	**ϕ**	**θ**
Pressure	268	0	700	-	-
Temperature	78	35	480	-	-
Conductivity	78	10	480	-	-
EMC1 (x+)	0	-143	390	0	315
EMC1 (y+)	0	-143	390	90	-
EMC2 (x+)	0	143	410	0	225
EMC2 (y+)	0	143	410	90	-
OBS1	325	-200	410	0	225
OBS2	268	0	900	0	270
Compass (N)	-	-	-	0	270
Pitch (Bow up +)	-	-	-	0	0
Roll (Port up +)	-	-	-	0	270
Transmissometer	-263	-50	927	0	270

Axis Plane

Origin at intersection of rig centre-line and base
x,y,z axes at right angles
x-axis - in plane of base, at rt. angles to y-axis, +ve towards bow foot
y-axis - parallel to line joining port and starboard feet, +ve towards starboard.
z-axis - vertical, +ve upwards.

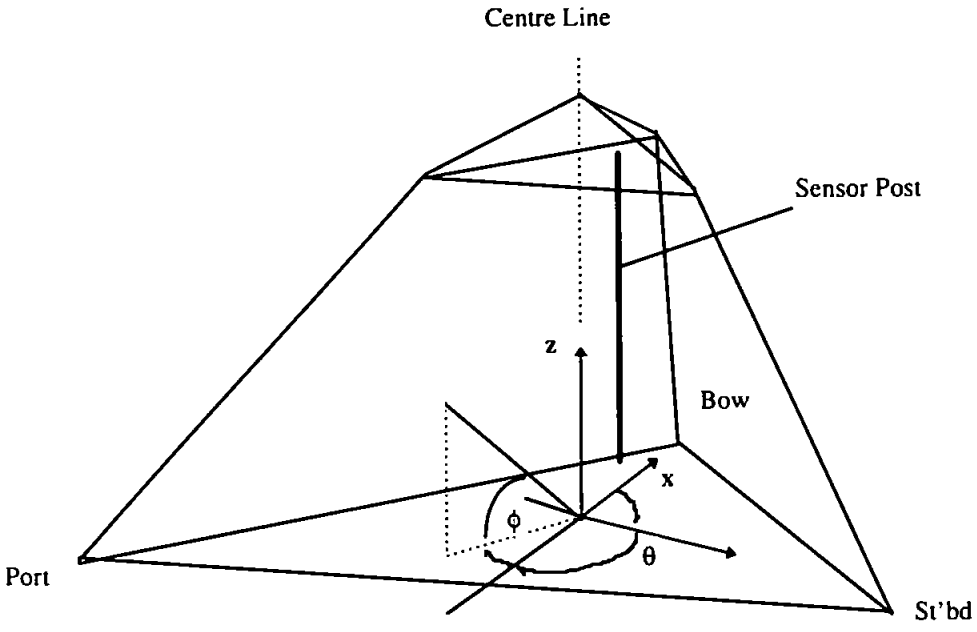

Figure A.1 Nominal position and direction of sensors

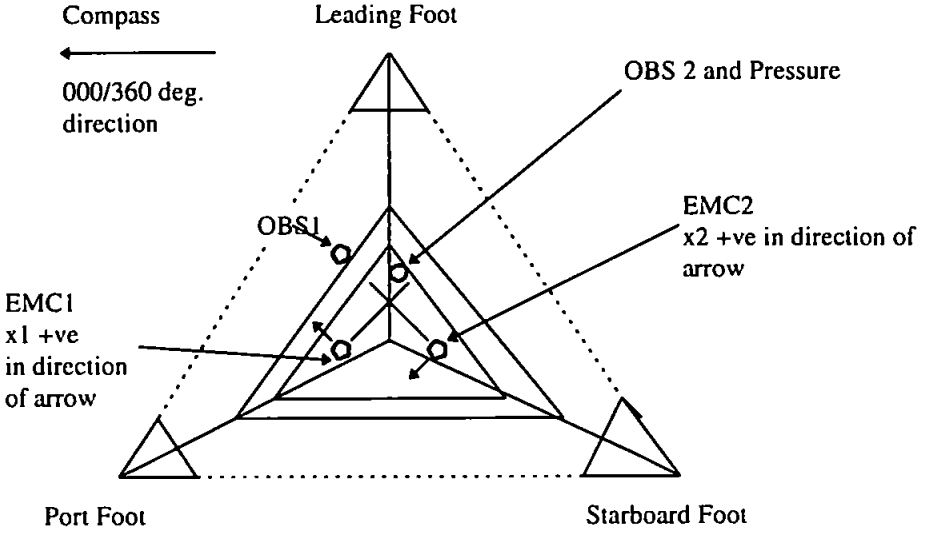

Figure A.2 Plan view

The leading bow leg heading from magnetic North was calculated as 125.8°. Therefore:

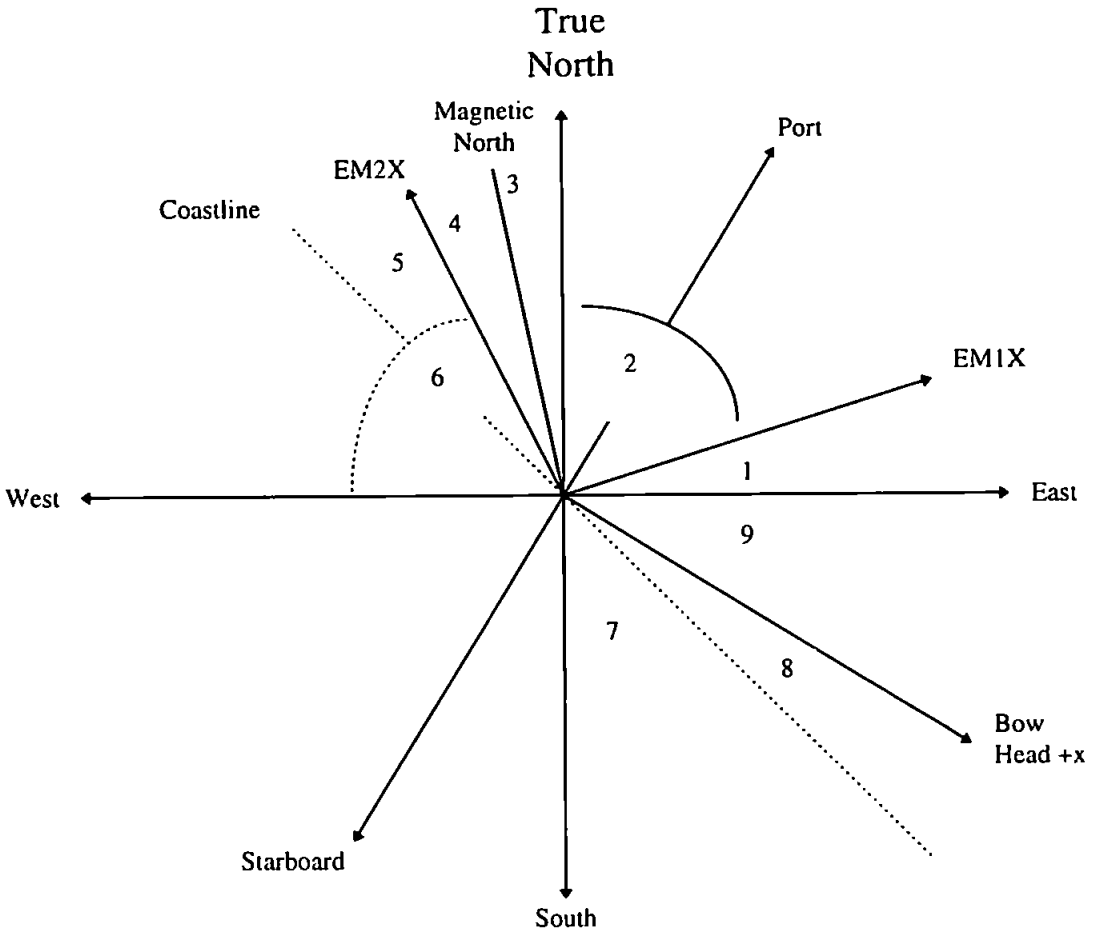

Figure A.3 Position of sensors relative to true North (in degrees)

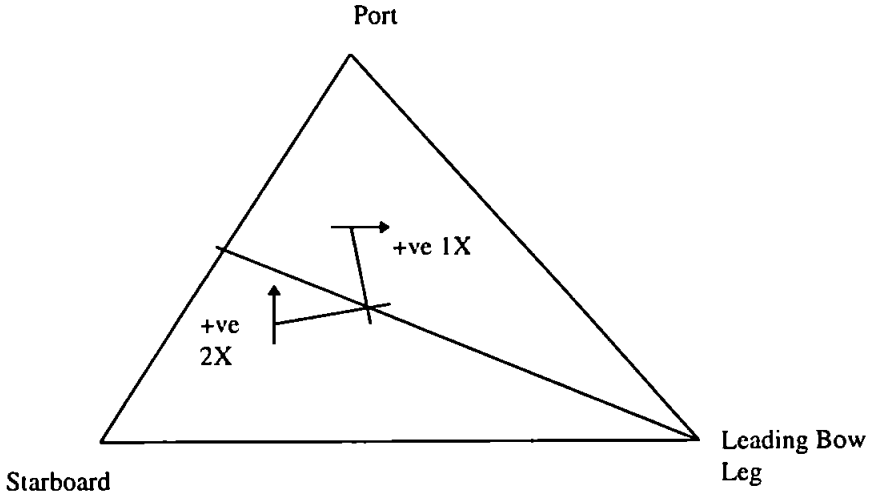

Figure A.4 BLISS 3 tripod orientation - plan view

Angles in Degrees

1. 16.17
2. 73.8
3. 6.97
4. 9.2
5. 24.8
6. 73.8
7. 41
8. 20.17
9. 28.83

Rotation of current meters to alongshore and cross-shore flow for July BLISS 3 inner station data were conducted using trigonometry as follows:

Alongshore = (2x) cos 24.8 - (1x)sin 24.8

Cross-shore = (2x)+sin 24.8 + (1x)cos24.8

June/July 1995 Middle Station Deployment - BLISS 2

The leading bow leg heading from magnetic North was calculated as 117°.

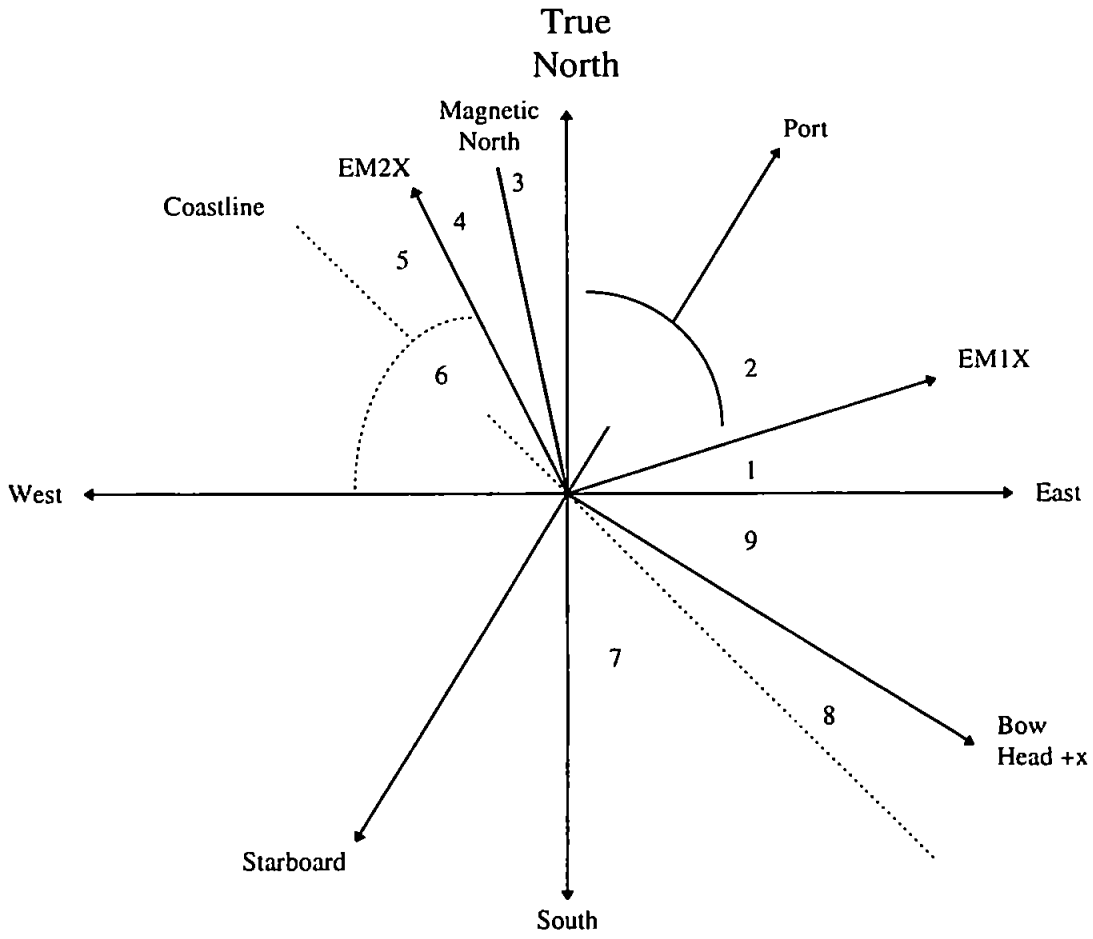

Figure A.5 Position of sensors with respect to true North (in degrees)

Angles in Degrees

1. **24.971**
2. **65.029**
3. **6.971**
4. **18**
5. **16.029**
6. **65.029**
7. **41**
8. **28.971**
9. **20.029**

Rotation of current meters to alongshore and cross-shore flow for July BLISS 2 middle station data were conducted using trigonometry as follows:

Alongshore = (2x) cos 16.029 - (1x)sin 16.029

Cross-shore = (2x)+sin 16.029 + (1x)cos16.029

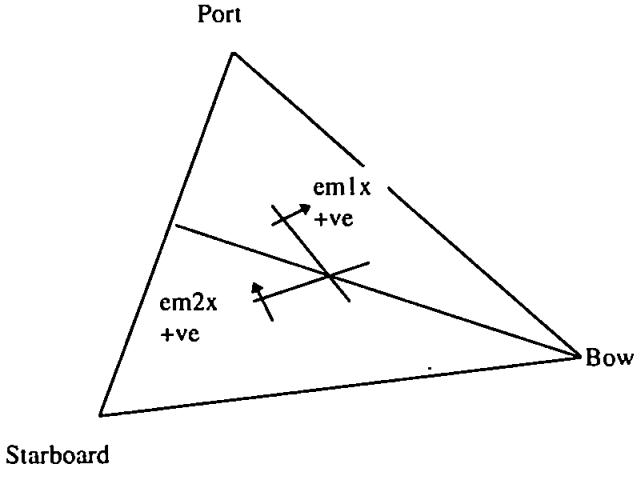

Figure A.6 BLISS 2 tripod orientation - plan view

February 1996 Inner Station Deployment - BLISS 4

The compass during the February Inner Station deployment did not function properly, so it was not possible to determine the angle required for rotation by this method.

February 1996 Middle Station Deployment - BLISS 3

The leading bow leg heading from Magnetic North was calculated as 115.12°.

During this deployment, trawlers operating in the vicinity of the BLISS moorings, snagged BLISS 3 and dragged the tripod onto its side. Before this point, good data was collected and the orientation of the tripod was deduced from the compass measurements, as follows,

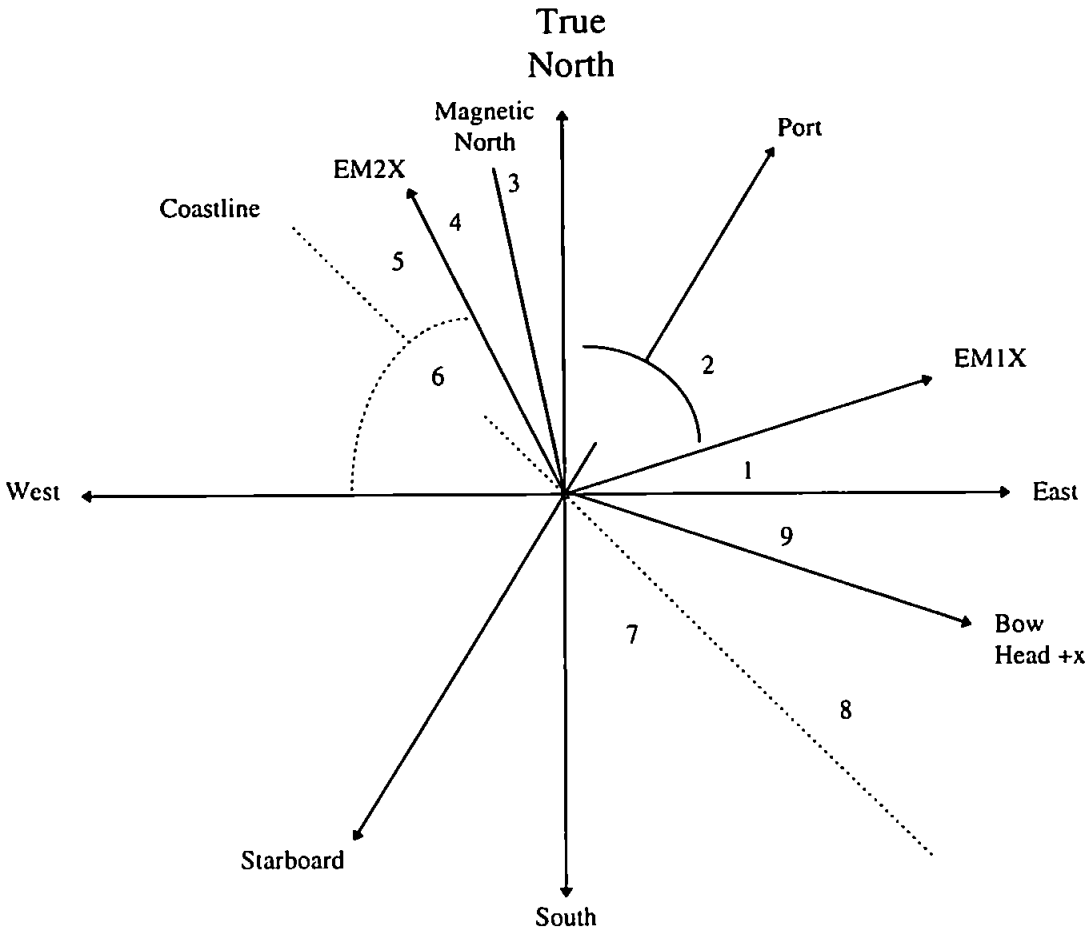

Figure A.7 Position of sensors with respect to true North (in degrees)

Angles in Degrees

1. **26.851**
2. **63.149**
3. **6.971**
4. **19.88**
5. **14.149**
6. **63.149**
7. **41**
8. **30.851**
9. **18.149**

Rotation of current meters to alongshore and cross-shore flow for February BLISS 3 middle station data were conducted using trigonometry as follows:

Alongshore = (2x) cos 14.149 - (1x)sin 14.149

Cross-shore = (2x)+sin 14.149 + (1x)cos14.149

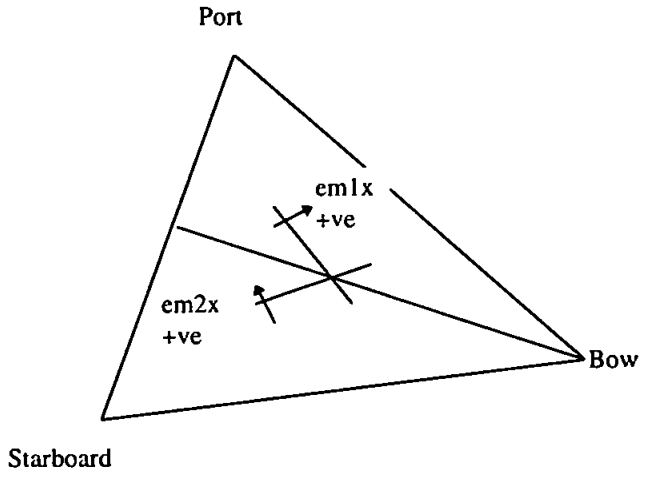

Figure A.8 Tripod orientation - plan view

February 1996 Outer Station Deployment - BLISS 2

The leading bow leg heading from magnetic North was calculated as 2.7625°.

The bow leg heading of BLISS 2 shifted 15.4375° clockwise from its initial point during the deployment period. Movement was initiated by a large storm which arose after 87 hours into the deployment. The compass worked adequately throughout the deployment, recording the new position of the tripod to within 4 decimal places. The position of the tripod before it started to move is given in figure A10, along with the corresponding angles. Table (A3) gives the alteration in the rotational angles during deployment, and also what runs the angles correspond to. The difference with the outer station's position to the other moorings, is that EM1X is measuring alongshore instead of cross-shore and EM2X is measuring cross-shore instead of alongshore

Angles in Degrees

1. **2.7625**
2. **41**
3. **8.2**
4. **40.8**
5. **44.2**
6. **40.8**
7. **41**

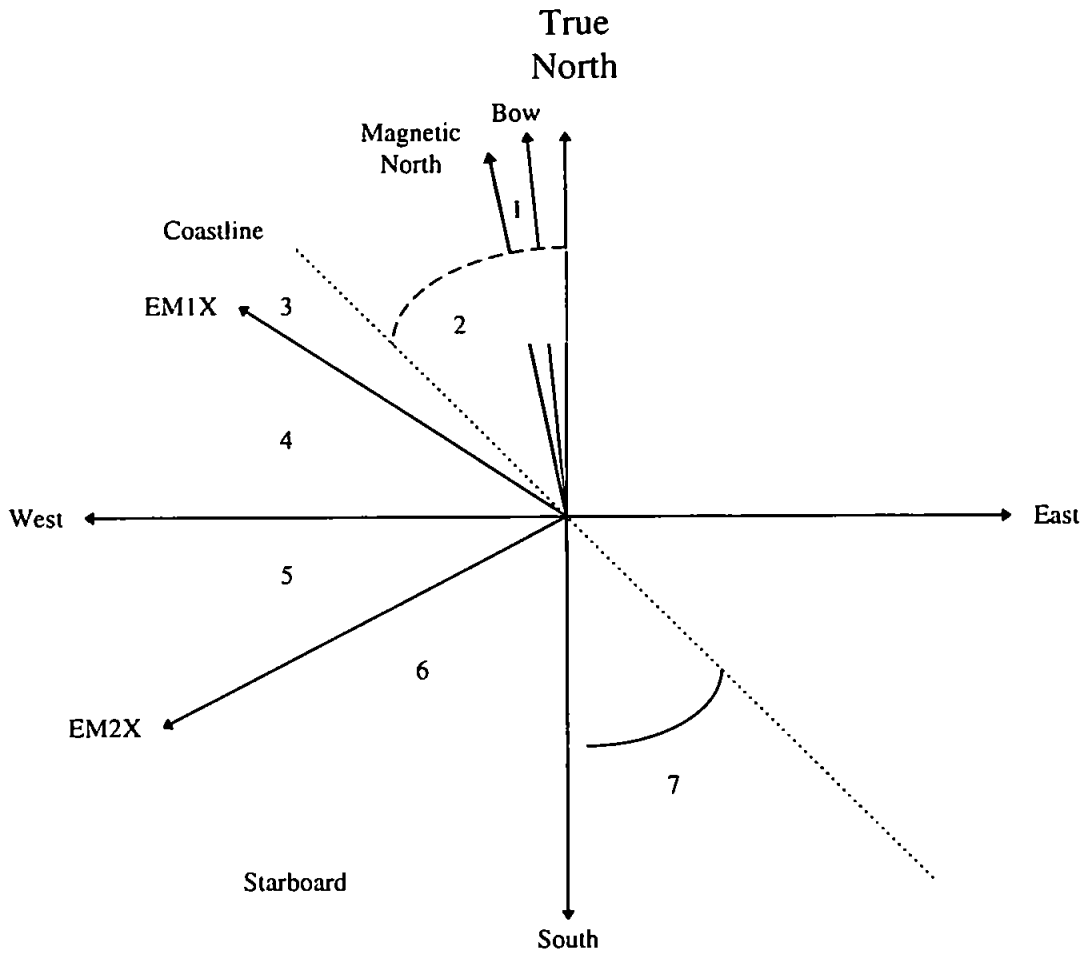

Figure A.9 Position of sensors with respect to true North (in degrees)

Table A.3 Angles used to rotate February outer station current meter data to alongshore and cross-shore flow

Feb 96 Outer Station Rig 2				
run	compass	degrees	Angles used for rotation (°)	change in degrees
			Clockwise rotation	
2	1224	363	81.8 8.2 (runs 1-88)	3
32	1225	363.2375		3.2375
62	1226	363.475		3.475
78	1227	363.7125		3.7125
81	1227	363.7125		3.7125
87	1227	363.7125		3.7125
89	1234	365.375	84.4 5.7	5.375
90	1247	368.4625	87.4915 2.5085 (90 - 95)	8.4625
92	1247	368.4625		8.4625
96	1250	369.175	88.204 1.796 (96-98)	9.175

99	1254	370.125	90.842 0.846 (99 - 109)	10.125
107	1256	370.6		10.6
108	1254	370.125		10.125
			Anticlockwise rotation	
110	1264	372.5	91.7665 1.7665 (110 - 113)	12.5
111	1265	372.7375		12.7375
113	1266	372.975		12.975
114	1272	374.4	93.429 3.429 (114-115)	14.4
116	1280	376.3	95.3884 5.3884 (116-271)	16.3
122	1278	375.825		15.825
182	1281	376.5375		16.5375
212	1282	376.775		16.775
272	1287	377.9625	96.9915 6.9915 (272-331)	17.9625
332	1292	379.15	98.179 8.179 (332-end)	19.15

Rotation of current meters to alongshore and cross shore flow for February BLISS 2 Outer station data were conducted using trigonometry as follows:

Clockwise Rotation (runs 1-109)

Alongshore = (1x) cos 8.2 - (2x)sin 81.8
Cross-shore = (1x)+sin 8.2 + (2x)cos81.2

Anticlockwise Rotation (runs 110-355)

Alongshore = (1x) cos1.7665 + (2x)sin 91.7665
Cross-shore = (1x)sin 1.7665 + (2x)cos91.7665

Start Position

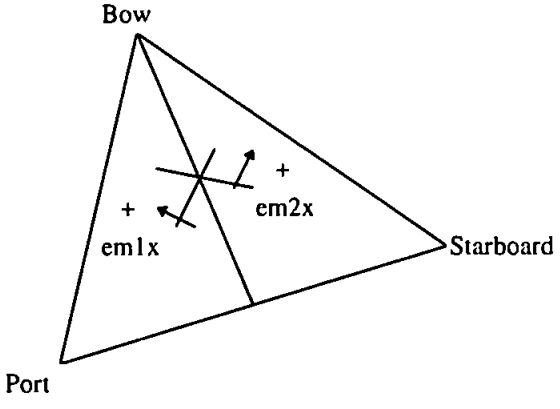

End Position (on day of Recovery)

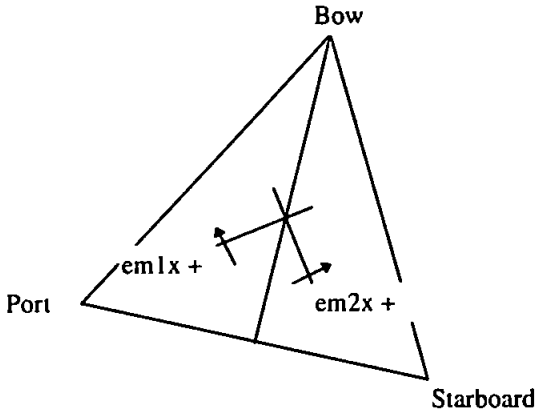

Figure A.10 BLISS 2 tripod orientations - plan view

February 1996 Outer Station Deployment

Cross-shore	EM1X * cosθ - EM2X sinθ
Alongshore	EM2X * cosθ + EM1X sinθ

Appendix B

MATLAB Programmes

B1 Programmes used in Data Processing

1. This is a program to load rig 3 July 1995 raw files and correct with calibration coefficients. It also transposes the files.

```
clear

for i=9
%way=input('directory:','s');
%name=input('name of file:','s');
eval(['load d:\r3raw\r3un',int2str(i),'.dat']);
%data=fscanf(fid,'%e',[5120,51200]);
%fclose(fid)
s=eval(['r3un',int2str(i),'(:,:)']);
st=s';

st(:,2)=(st(:,2)*0.008671)+(-9.955342);
st(:,3)=(st(:,3)*0.0019909)+13.763;
st(:,4)=(st(:,4)*0.0002826)+(-0.0111730);
st(:,5)=(st(:,5)*0.21557)+(-10.758);
st(:,6)=(st(:,6)*0.20331)+(-5.168);
st(:,7)=(st(:,7)-(70))*0.0012209;
st(:,8)=(st(:,8)-(-800))*(-0.0012209);
st(:,9)=(st(:,9)-(-50))*0.0012209;
st(:,10)=(st(:,10)-(-80))*0.0012209;
eval(['save c:\bliss\july\inner\rc3un',int2str(i),'.dat st -ascii -double'])
end
```

2. This is a program to load raw files for rig 2 July 1995 data and correct with calibration coefficients. It also transposes the files.

```
clear

%for i=59
%way=input('directory:','s');
%name=input('name of file:','s');
%eval(['load c:\job\run',int2str(i),'.dat '])
%fid=fopen(['d:\r2\r2un',int2str(i),'.mat']);
%data=fscanf(fid,'%e',[5120,51200]);
%fclose(fid)

%s=run';
load c:\job\run353.dat
t=run353;
b=(t(:,2)*0.008764)+(-10.235295);
c=(t(:,3)*0.0020326)+13.360;
d=(t(:,4)*0.0002826)+(-0.0111730);
e=(t(:,5)*0.21557)+(-10.758);
f=(t(:,6)*0.19109)+(-28.071);
g=(t(:,7)-(-40))*0.0012209;
h=(t(:,8)-(-67))*(0.0012209);
i=(t(:,9)-(-5))*0.0012209;
j=(t(:,10)-(-35))*0.0012209;
save c:\job\rcun353.mat
end
```

3. This is a program that will import the February 1996 rig 4 data and ignore the header information, transpose the files and correct the data using the calibration coefficients.

```
%for i=114
fid=fopen(['c:\job\r4d3b012.dat'])
%fid=fopen(['d:\blissf\r',int2str(i),'un4f.txt']);

dp=0;
while 1==1,
 m=fscanf(fid,'%s ',[1 1]);
 mot=sscanf(m,'%s');
 l=length(mot);
 for j=1:l
  let=mot(j);
  if let==':', dp=dp+1; end
 end
 if dp==2 & mot(l)~=':', break, end
end

m=fscanf(fid,'%e',[10 inf]);
fclose(fid);
m=m';
```

```
m(:,2)=m(:,2)*0.008758+(-10.228);
%m(:,3)=m(:,3)*0.0019194+(13.336);
%m(:,4)=m(:,4)*0.0019194+(13.336);
m(:,5)=(m(:,5)*0.1925)+(-9.14);
m(:,6)=(m(:,6)*0.2564)+(-15.171);
m(:,7)=(m(:,7)-(17))*0.0012209;
m(:,8)=(m(:,8)-(49))*0.0012209;
m(:,9)=(m(:,9)-(-17))*0.0012209;
m(:,10)=(m(:,10)-(49))*0.0012209;
eval(['save d:\blissf\r4c3b010.dat' -ascii -double])
%eval(['save d:\blissf\rcn4f',int2str(i),'.dat m -ascii -double'])
end
```

4. This is a program that will import the February 1996 rig 3 data and ignore the header information, transpose the files and correct the data using the calibration coefficients.

```
for i= 461:469
fid=fopen(['e:\rig3.feb\r',int2str(i),'un3f.txt']);

dp=0;
while 1==1,
 m=fscanf(fid,'%s ',[1 1]);
 mot=sscanf(m,'%s');
 l=length(mot);
 for j=1:l
  let=mot(j);
  if let==':', dp=dp+1; end
 end
 if dp==2 & mot(l)~=':', break, end
end

m=fscanf(fid,'%e',[10 inf]);
fclose(fid);
m=m';
m(:,2)=m(:,2)*0.008758+(-10.228);
%m(:,3)=m(:,3)*0.0019194+(13.336);
%m(:,4)=m(:,4)*0.0019194+(13.336);
m(:,5)=(m(:,5)*0.2225)+(-1.0754);
m(:,6)=(m(:,6)*0.2395)+(-10.219);
m(:,7)=(m(:,7)-(64))*0.0012209;
m(:,8)=(m(:,8)-(216))*0.0012209;
m(:,9)=(m(:,9)-(37))*0.0012209;
m(:,10)=(m(:,10)-(101))*0.0012209;

eval(['save e:\rig3.feb\rcn3f',int2str(i),'.dat m -ascii -double'])
end
```

5. This is a program that will import the February 1996 rig 2 data and ignore the header information, transpose the files and correct the data using the calibration coefficients.

```
for i=332:355
fid=fopen(['d:\r296feb\r',int2str(i),'un2f.run']);

dp=0;
while 1==1,
 m=fscanf(fid,'%s ',[1 1]);
 mot=sscanf(m,'%s');
 l=length(mot);
 for j=1:l
  let=mot(j);
  if let==':', dp=dp+1; end
 end
 if dp==2 & mot(l)~=':', break, end
end

m=fscanf(fid,'%e',[10 inf]);
fclose(fid);
m=m';
m(:,2)=m(:,2)*0.008758+(-10.228);
m(:,3)=m(:,3)*0.002494+(13.298);
m(:,4)=m(:,4)*0.0002826+(-0.011173);
m(:,5)=(m(:,5)*0.33376)+(-14.683);
m(:,6)=(m(:,6)*0.23378)+(1.1172);
m(:,7)=(m(:,7)-(15))*0.0012209;
m(:,8)=(m(:,8)-(23))*0.0012209;
m(:,9)=(m(:,9)-(0))*0.0012209;
m(:,10)=(m(:,10)-(35))*0.0012209;

eval(['save d:\r296cal\rcn2f',int2str(i),'.dat m -ascii -double'])
end
```

6. This is a program to calculate salinity from temperature and conductivity ratio using the practical salinity scale UNESCO -78. Program to calibrate rig 2 July inner 1995 and February outer 1996.

```
for i=4:355
eval(['load d:\r296cal\rcn2f',int2str(i),'.dat']);
rcn2f=eval(['rcn2f', int2str(i)]);
t=rcn2f(:,3);
r=rcn2f(:,4);
eval(['clear rcn2f', int2str(i)]);
a=[0.0080 -0.1692 25.3851 14.0941 -7.0261 2.7081];
b=[0.0005 -0.0056 -0.0066 -0.0375 0.0636 -0.0144];
c=[0.6766097 0.0200564 0.0001104259 0.00000069698 0.0000000010031];
delt=t-15;
k=0.0162;
cr=0;
```

```
for n=1:5;
tempr=(c(n)*(t.^(n-1)));
cr=cr+tempr;
end;
Rt=r./cr;
sal=zeros(size(t));
for n=1:6
tempr=(a(n)+delt./(1+k*delt)*b(n)).*Rt.^((n-1)/2);
sal=sal+tempr;
end
eval(['save c:\feb\outer\salinity\salin', int2str(i),'.dat sal -ascii']);
end
```

7a. This program changes mean conductivity ratio values into salinity for February inner station using temperature values of February outer BLISS station. 0.3 degrees has been taken off the February outer station temperature data to represent February inner conditions. 0.3 difference based on the CTD profiles taken during 10 hour station.

```
load c:\bliss\feb\inner\cond\tcrsalfi.txt
t=tcrsalfi(:,1);
r=tcrsalfi(:,3);
a=[0.0080 -0.1692 25.3851 14.0941 -7.0261 2.7081];
b=[0.0005 -0.0056 -0.0066 -0.0375 0.0636 -0.0144];
c=[0.6766097 0.0200564 0.0001104259 0.00000069698 0.0000000010031];
delt=t-15;
k=0.0162;
cr=0;
for n=1:5;
tempr=(c(n)*(t.^(n-1)));
cr=cr+tempr;
end;
Rt=r./cr;
sal=zeros(size(t));
for n=1:6
tempr=(a(n)+delt./(1+k*delt)*b(n)).*Rt.^((n-1)/2);
sal=sal+tempr;
end
```

7b. This program takes the conductivity data from February inner d:\blissf\rcn4f data set and calibrates it to conductivity ratio using the pre bliss 4 calibration coefficients.

```
for i=124:356

eval(['load d:\blissf\rcn4f',int2str(i), '.dat']);
t=eval(['rcn4f', int2str(i)]);
cond=t(:,4);
cr=cond.*0.0002783+(-0.0899603);
file=['c:\bliss\feb\inner\cond\ficr', int2str(i), '.dat'];
eval(['save ',file, ' cr -ascii']);
```

```
eval(['clear rcn4f',int2str(i)])
end
```

8. Program to remove outliers from the data. It is a continous program so that I can leave it running. The data was depeaked before data analysis.

```
for i=1:51
eval(['load c:\bliss\feb\middle\rcn3f',int2str(i),'.dat'])
eval(['M=depeakf(rcn3f',int2str(i),');'])
eval(['save c:\bliss\feb\middle\rcn3f',int2str(i),'.dat M -ascii -double'])
clear
end
```

9. Progam to calculate tidal ellipse parameters from M_2 components using Pugh's estimation, (1987)

```
U=input('amplitude of u-velocity')
gu=input('phase of u-velocity  ')
V=input('amplitude of v-velocity  ')
gv=input('phase of v-velocity  ')
delta=0.5*(atan((V^2*sin(2*(gu-gv))))/(U^2+V^2*cos(2*(gu-gv))))
alpha=(U^4+V^4+2*U^2*V^2*cos(2*(gu-gv)))^0.25
qmax=sqrt((U^2+V^2+alpha^2)/2)
qmin=sqrt((U^2+V^2-alpha^2)/2)
thetamax=atan((V*cos(gu-gv-delta))/(U*cos(delta)))
gdiff=gu-gv
wt=28.9841*pi/180
qsqd=0.5*((U^2+V^2-alpha^2+alpha^2)*(cos(wt-gu+delta))^2)
sense=((wt*U*V/qsqd)*sin(gv-gu))
```

B.2 Programmes used in Data Analysis

10. This is a program to calculate the means and standard deviations of each file and place the results in a matrix. I have detrended the data before calculating the standard deviation. The file name was changed each time to match deployment.

```
format short
M=[]; S=[];
for i=187:340
 eval(['load d:\novdata\r2cn',int2str(i),'.dat'])
 eval(['a=r2cn',int2str(i),';'])
 a(:,1)=[];
 a(1:10,:)=[];
 m=mean(a); s=std(detrend(a));
 M=[M;m]; S=[S;s];
 eval(['clear r2cn',int2str(i)])
end
```

11. This program calculates Reynolds stress and shear velocity for February outer station. The file name was changed each time to match deployment.

```
TOTALRS=[]; SHEARVEL=[]; TRS=[]; FRICVEL=[]; UWM=[]; VWM=[];
for i=1:355
eval(['load d:\rstress\feb\outer\fuvwp', int2str(i),'.dat']);
t=eval(['fuvwp', int2str(i)]);
uprime=t(:,1);
vprime=t(:,2);
wprime=t(:,3);
uw=uprime.*wprime;
vw=vprime.*wprime;
uwm=mean(uw);
vwm=mean(vw);
trs=uwm+vwm*(-1025);
fricvel=(sqrt(trs/1025));
uwsq=uwm.*uwm;
vwsq=vwm.*vwm;
total=(sqrt(uwsq+vwsq));
totalrs=total*(-1025);
shearvel=(sqrt(totalrs/1025));
eval(['clear fuvwp', int2str(i)])
TOTALRS=[TOTALRS,totalrs]; SHEARVEL=[SHEARVEL,shearvel]; TRS=[TRS,trs];
FRICVEL=[FRICVEL,fricvel]; UWM=[UWM,uwm]; VWM=[VWM,vwm];
end
```

12. This program calculates the Inertial Dissipation Method devised by Huntley (1988, Stapleton and Huntley, 1995) using the vertical spectrum. The program is altered each time depending on which deployment, and the size of the file.

```
TAU=[]; USTAR=[];
for i=224:356
eval(['load c:\stresses\rstress\feb\inner\fiuvw',int2str(i),'.dat']);
t=eval(['fiuvw', int2str(i)]);
%program to calculate a value for ustar using the Intertial Dissipation method.
%calculate mean speed
cross=t(:,1);
long=t(:,2);
vertical=t(:,4);
height=0.41;
a=mean(cross);
b=mean(long);
c=mean(vertical);
magvel=(a^2+b^2)^0.5;
d=detrend(vertical);
s=std(d);
var=s*s;
urms=std(cross);
%calculate predicted limits on the inertial subrange
f1=magvel/height;
f2=2.3*magvel/(2*pi*0.055);
if f1<0.3
```

```
f1=0.3;
end
if f2>2
f2=2;
end
%calculate spectrum of vertical time series
[p,f]=spectrum(vertical,256,128,256,5);
g=128;
pt=p(:,1);
ps=pt/2.5;
o=sum(ps);
test=o*5/256;
ef1=(ceil(f1*51.2))+1;
ef2=(floor(f2*51.2))+1;
if ef2>g
 ef2=g;
end

meanfreq=mean(log10(f(ef1:ef2)));
meanphi=mean(log10(ps(ef1:ef2)));
logconst=(meanphi)+5/3*(meanfreq);
uhat=(10^(logconst)*(2*pi/magvel)^(2/3)/0.69)^0.5*(0.4*height)^(1/3);
ustar=((1-0.16*((urms/magvel)^2))^0.5)*uhat;
eval(['clear fiuvw',int2str(i)])
tau=1025*ustar^2;
TAU=[TAU,tau]; USTAR=[USTAR,ustar];
end
```

13. This is a program to calculate turbulent kinetic energy shear stress for February inner station. There is a difference in size of files so use different size for computing spectrum.

```
STRESS=[];
for i=3
eval(['load d:\rstress\feb\inner\fiuvw', int2str(i),'.dat']);
t=eval(['fiuvw', int2str(i)]);
u=t(:,1);
v=t(:,2);
w1y=t(:,3);
w2y=t(:,4);
%calculate the cross shore velocity spectrum
[p,f]=spectrum(u,256,128,256,5);
loglog(f,p(:,1))
hold on
%choose the in incident wave band and click on the limits.
[x1,y1]=ginput(2);
%plot the line separating turbulence and wave fluctuations.
loglog(x1,y1)
x2=floor(x1*51.6);
%Calculate the turbulent kinetic energy method using the trapezium rule.
energy=0.019*(0.5*(p(1,1)+p(x2(1)-1,1)));
energy=energy+0.5*(f(x2(2))-f(x2(1)))*(p(x2(1),1)+p(x2(2),1));
```

```
energy=energy+0.019*(0.5*(p(x2(2),1)+p(129,1))+sum(p(x2(2)+2:128,1)));
hold off
%Calculate the alongshore velocity spectrum.
[p,f]=spectrum(v,256,128,256,5);
energy=0.019*(0.5*(p(1,1)+p(x2(1)-1,1)));
energy=energy+0.5*(f(x2(2))-f(x2(1)))*(p(x2(1),1)+p(x2(2),1));
energy=energy+0.019*(0.5*(p(x2(2),1)+p(129,1))+sum(p(x2(2)+2:128,1)));
%calculate the vertical velocity spectrum.
[p,f]=spectrum(w1y,256,128,256,5);
energy=0.019*(0.5*(p(1,1)+p(x2(1)-1,1)));
energy=energy+0.5*(f(x2(2))-f(x2(1)))*(p(x2(1),1)+p(x2(2),1));
energy=energy+0.019*(0.5*(p(x2(2),1)+p(129,1))+sum(p(x2(2)+2:128,1)));

stress=(0.19*0.5*energy)*1025;
eval(['clear fiuvw',int2str(i)])
STRESS=[STRESS,stress];
end
```

14. Program to calculate shear stress and rms turbulent intenstiy using the turbulent kinetic energy method devised by Soulsby using the Trapezium Method. The program was altered depending on what deployment.

```
%load the data.
TESTRESS=[]; USTAR=[]; RMSTIU=[]; RMSTIV=[]; RMSTIW=[]; ENERGYW=[];
ENERGYU=[]; ENERGYV=[];
for i=15:355
eval(['load c:\rstress\feb\outer\fuvwp',int2str(i),'.dat']);
t=eval(['fuvwp', int2str(i)]);
u=t(:,4);
v=t(:,5);
w=t(:,6);
%calculate the cross shore velocity spectrum
[p,f]=spectrum(u,512,256,512,5);
loglog(f,p(:,1))
hold on
%choose the in incident wave band and click on the limits.
[x1,y1]=ginput(2);
%plot the line separating turbulence and wave fluctuations.
loglog(x1,y1)
x2=floor(x1*102.8);
%Calculate the turbulent kinetic energy method using the trapezium rule.
energy=0.0098*(0.5*(p(1,1)+p(x2(1)-1,1)));
energy=energy+0.5*(f(x2(2))-f(x2(1)))*(p(x2(1),1)+p(x2(2),1));
energyu=energy+0.0098*(0.5*(p(x2(2),1)+p(257,1))+sum(p(x2(2)+2:255,1)));
hold off
%Calculate the alongshore velocity spectrum.
[p,f]=spectrum(v,512,256,512,5);
energy=0.0098*(0.5*(p(1,1)+p(x2(1)-1,1)));
energy=energy+0.5*(f(x2(2))-f(x2(1)))*(p(x2(1),1)+p(x2(2),1));
energyv=energy+0.0098*(0.5*(p(x2(2),1)+p(257,1))+sum(p(x2(2)+2:255,1)));
%calculate the vertical velocity spectrum.
[p,f]=spectrum(w,512,256,512,5);
```

```
energy=0.0098*(0.5*(p(1,1)+p(x2(1)-1,1)));
energy=energy+0.5*(f(x2(2))-f(x2(1)))*(p(x2(1),1)+p(x2(2),1));
energyw=energy+0.0098*(0.5*(p(x2(2),1)+p(257,1))+sum(p(x2(2)+2:255,1)));
energyt=energyu+energyv+energyw;
testress=(0.19*0.5*energyt)*1025;
ustar=(sqrt(testress/1025));
rmstiu=0.5*energyu/ustar;
rmstiv=0.5*energyv/ustar;
rmstiw=0.5*energyw/ustar;
eval(['clear fuvwp',int2str(i)])
TESTRESS=[TESTRESS,testress];
USTAR=[USTAR,ustar];
RMSTIU=[RMSTIU,rmstiu];
RMSTIV=[RMSTIV,rmstiv];
RMSTIW=[RMSTIW,rmstiu];
ENERGYU=[ENERGYU,energyu];
ENERGYV=[ENERGYV,energyv];
ENERGYW=[ENERGYW,energyw];
end
```

15. This is a program to calculate significant wave height from pressure data using the spectrum and Trapezium Method. for integration under the curve in the wave band. The file name was changed each time to match deployment..

```
HSIG=[]; HSIGWB=[];

for i=1:355
eval(['load d:\r296cal\rcn2f',int2str(i),'.dat']);
t=eval(['rcn2f', int2str(i)]);
pt=t(:,2);
[p,f]=spectrum(pt,512,256,512,5);
%Computes the total variance under the spectral curve
trap=trapz(p(:,1));
vartot=trap/256;
hsig=(sqrt(vartot*4));
%Computes the variance under the specific wave band between gravity and infragravity
waves
t=find(f>=0.05 & f<0.33);
y=sum((p(t(1):t(length(t))-1,1)+p(t(2):t(length(t)),1))/2.*(f(t(2):t(length(t)))-
f(t(1):t(length(t))-1)));
hsigwb=(sqrt(y*4));
eval(['clear rcn2f',int2str(i)])
HSIG=[HSIG,hsig]; HSIGWB=[HSIGWB,hsigwb];
end
```

16. This program calculates the wave orbital velocity from the cross shore and alongshore velocity spectrums. Calculating the area under the curve by the Trapezium Method.

```
WOVEL=[]; WORBDIR=[]
for i=1:355
eval(['load d:\rstress\feb\outer\fuvwp',int2str(i),'.dat']);
t=eval(['fuvwp', int2str(i)]);
u=t(:,4);
v=t(:,5);
%calculate the cross shore velocity spectrum
[p,f]=spectrum(u,512,256,512,5);
%Computes the variance under the specific wave band between gravity and infragravity
waves
t=find(f>=0.04 & f<0.18);
y=sum((p(t(1):t(length(t))-1,1)+p(t(2):t(length(t)),1))/2.*(f(t(2):t(length(t)))-
f(t(1):t(length(t))-1)));
loglog(f,p(:,1))
hold on
%choose the in incident wave band and click on the limits.
[x1,y1]=ginput(2);

%plot the line separating turbulence and wave fluctuations.
loglog(x1,y1)
x2=floor(x1*102.8);
energy=0.5*(f(x2(2))-f(x2(1)))*(p(x2(1),1)+p(x2(2),1));
varu=y-energy;
hold off
%Calculate the alongshore velocity spectrum.
[p,f]=spectrum(v,512,256,512,5);
%Computes the variance under the specific wave band between gravity and infragravity
waves
t=find(f>=0.04 & f<0.18);
y=sum((p(t(1):t(length(t))-1,1)+p(t(2):t(length(t)),1))/2.*(f(t(2):t(length(t)))-
f(t(1):t(length(t))-1)));
energy=0.5*(f(x2(2))-f(x2(1)))*(p(x2(1),1)+p(x2(2),1));
varv=y-energy;
wovel=(sqrt(varu+varv));
worbdir=atan(sqrt(varv/varu));
eval(['clear fuvwp',int2str(i)])
WOVEL=[WOVEL,wovel]; WORBDIR=[WORBDIR,worbdir];
end
WOVEL=WOVEL';
WORBDIR';
```

17. This program calculates the co-spectrum for each run of cross shore velocity and suspended sediment concentration, plots the result.

```
for i=89
eval(['load c:\oscflux\feb\outer\ffebi',int2str(i),'.dat']);
t=eval(['ffebi', int2str(i)]);
cprime=t(:,1);
```

```
uprime=t(:,2);
vprime=t(:,3);
v=t(:,4);
u=t(:,5);
c=t(:,6);
[pxy,f]=csd(c,u,512,5,512,256);
plot(f,pxy)
axis([0 0.5 -5 50])
title('Cospectrum of SSC and Cross-shore Velocity - Feb 1996 Outer station')
xlabel('Frequency')
ylabel('Co-spectrum of SSC and U')
hold on
x=[0 0.5];
y=[0 0];
plot(x,y,'-')
```

18. This is a program to plot multiple phase plots for ch 4 description of rotations.

```
cd c:\julfebro
load jipuv.txt
load jmpuv.txt

p1=jipuv(:,1);
u1=jipuv(:,2);
v1=jipuv(:,3);
p2=jmpuv(:,1);
u2=jmpuv(:,2);
v2=jmpuv(:,3);
[pt,f]=spectrum(p1,u1,62,31,62,24);
[p,ft]=spectrum(p1,v1,62,31,62,24);
[ps,ff]=spectrum(p2,u2,62,31,62,24);
[pf,fs]=spectrum(p2,v2,62,31,62,24);
subplot(2,2,1)
plot(f,180/pi*angle(pt(:,4)),'r');
ylabel('Degrees')
title('Inner Station')
subplot(2,2,2)
plot(ft,180/pi*angle(p(:,4)),'b');
title('Inner Station')
subplot(2,2,3)
plot(ff,180/pi*angle(ps(:,4)),'r');
xlabel('Frequency')
ylabel('Degrees')
title('Middle Station')
subplot(2,2,4)
plot(fs,180/pi*angle(pf(:,4)),'b');
xlabel('Frequency')
title('Middle Station')
orient tall
```

19. This is a program which is devised to rotate current velocity to alongshore and cross-coast flow, convert FTU to mgl^{-1} and then calculate the mean flux cbar*ubar, total flux and oscillating flux. The data is to be inputted into a matrix. February outer station. The file is altered for each deployment.

```
VBAR=[]; UBAR=[]; CBARL=[]; MFVL=[]; MFUL=[]; TFLUXVL=[]; TFLUXUL=[];
TOSCFLUXUL=[]; TOSCFLUXVL=[];

for i=332:355
eval(['load d:\r296cal\rcn2f',int2str(i),'.dat']);
t=eval(['rcn2f', int2str(i)]);
x1=t(:,7);
x2=t(:,9);
concl=t(:,5);
%concu=t(:,6);
%concl=t(3800:5120,5);
%concu=t(3800:5120,6);
conclc=concl*0.7845;
%concuc=concl*0.7845;
thetac=cos(66.9995*pi/180);
thetas=sin(66.9995*pi/180);
u=x1*thetac-x2*thetas;
v=x2*thetac+x1*thetas;
cbarl=mean(conclc);
%cbaru=mean(concuc);
ubar=mean(u);
vbar=mean(v);
mfvl=cbarl*vbar; mful=cbarl*ubar;
totalvl=(conclc.*v);
%totalvu=(concuc.*v);
totalul=(conclc.*u);
%totaluu=(concuc.*u);
tfluxvl=mean(totalvl);
%tfluxvu=mean(totalvu);
tfluxul=mean(totalul);
%tfluxuu=mean(totaluu);
cprimel=detrend(conclc);
%cprimeu=detrend(concuc);
uprime=detrend(u);
vprime=detrend(v);
toscul=(cprimel.*uprime);
%toscuu=(cprimeu.*uprime);
toscvl=(cprimel.*vprime);
%toscvu=(cprimeu.*vprime);
wt=[cprimel uprime vprime v u conclc];
toscfluxul=mean(toscul);
%toscfluxuu=mean(toscuu);
toscfluxvl=mean(toscvl);
%toscfluxvu=mean(toscvu);
CBARL=[CBARL,cbarl]; UBAR=[UBAR,ubar]; VBAR=[VBAR,vbar];
MFVL=[MFVL,mfvl]; MFUL=[MFUL,mful]; TFLUXVL=[TFLUXVL,tfluxvl];
TFLUXUL=[TFLUXUL,tfluxul]; TOSCFLUXUL=[TOSCFLUXUL,toscfluxul];
TOSCFLUXVL=[TOSCFLUXVL,toscfluxvl];
```

```
file=['c:\oscflux\feb\outer\ffebi', int2str(i), '.dat'];
eval(['save ',file, ' wt -ascii']);
eval(['clear rcn2f',int2str(i)])
end
```

20. This program calculates the tidal fluxes and the tidal components. The file is altered for each deployment.

```
TIDEFVL=[]; TIDEFUL=[]; CTIDEL=[]; UTIDE=[]; VTIDE=[];

for i=100:355
eval(['load d:\oscflux\feb\outer\ffebi',int2str(i),'.dat']);
t=eval(['ffebi', int2str(i)]);
cl=t(:,6);
v=t(:,4);
u=t(:,5);
cbarl=mean(cl);
ubar=mean(u);
vbar=mean(v);
%over a deployment
meancl=53.75;
meanv=-0.0033;
meanu=-0.0435;
%calcluates tidal flux (every burst)
ctidel=cbarl-meancl;
utide=ubar-meanu;
vtide=vbar-meanv;
tidefvl=vtide*ctidel; tideful=utide*ctidel;
TIDEFVL=[TIDEFVL,tidefvl]; TIDEFUL=[TIDEFUL,tideful];
CTIDEL=[CTIDEL,ctidel]; UTIDE=[UTIDE,utide]; VTIDE=[VTIDE,vtide];
eval(['clear ffebi',int2str(i)])
end
TIDEFVL=TIDEFVL';
TIDEFUL=TIDEFUL';
CTIDEL=CTIDEL';
UTIDE=UTIDE';
VTIDE=VTIDE';
save c:\fluxes\feb\outer\tidefulb.txt TIDEFUL -ascii
save c:\fluxes\feb\outer\tidefvlb.txt TIDEFVL -ascii
save c:\fluxes\feb\outer\ctidelb.txt CTIDEL -ascii
save c:\fluxes\feb\outer\utideb.txt UTIDE -ascii
save c:\fluxes\feb\outer\vtideb.txt VTIDE -ascii
```

21. This program calculates the co-spectrum of velocity and concentration. The spectrum is then split up into infragravity and gravity wave bands. Variance of each band are then calculated by integration using the Trapezium Rule.

```
GBOSC=[]; INGOSC=[]; VARTOT=[];


for i=1:355
eval(['load c:\oscflux\feb\outer\ffebi', int2str(i),'.dat']);
t=eval(['ffebi', int2str(i)]);
 u=t(:,5);
 cl=t(:,6);
 %ct=t(:,8);
 clc=cl./1000;
 %ctc=ct./1000;
 [p,f]=spectrum(clc,u,512,256,512,5);
%Computes the total variance under the spectral curve
cp=(real(p(:,3)));
trap=trapz(cp);
vartot=trap/256;
%Computes the variance under the gravity wave band
t=find(f>=0.05 & f<0.3);
gbosc=sum((cp(t(1):t(length(t))-1,1)+cp(t(2):t(length(t)),1))/2.*(f(t(2):t(length(t)))-
f(t(1):t(length(t))-1)));
%computes the variance under the infragravity wave band
tt=find(f>=0 & f<0.05);
ingosc=sum((cp(tt(1):tt(length(tt))-1,1)+cp(tt(2):tt(length(tt)),1))/2.*(f(tt(2):tt(length(tt)))-
f(tt(1):tt(length(tt))-1)));
eval(['clear ffebi',int2str(i)])
GBOSC=[GBOSC,gbosc]; VARTOT=[VARTOT,vartot]; INGOSC=[INGOSC,ingosc];
end
GBOSC=GBOSC';
VARTOT=VARTOT';
INGOSC=INGOSC';
```

22. This is a program to fit a best line on the down slope of the spectrum for vertical spectrum using Kolmogorov function -5/3.

```
for i=55
eval(['load c:\stresses\rstress\feb\outer\fuvwp',int2str(i),'.dat']);
t=eval(['fuvwp', int2str(i)]);
%calculate mean speed
cross=t(:,4);
long=t(:,5);
vertical=t(:,6);
a=mean(cross);
b=mean(long);
c=mean(vertical);
magvel=(a^2+b^2)^0.5;
[p,f]=spectrum(vertical,512,256,512,5);
spec=p(:,1)/2;
set(gca,'TickLength',[0.01 0.025])
```

```
loglog(f,spec,'r')
set(gca,'FontName','Times New Roman')
set(gca,'FontSize',12)
xlabel('Frequency (Hz)')
set(gca,'FontName','Times New Roman')
set(gca,'FontSize',12)
ylabel('Spectral density ((m/s)^2)')
set(gca,'FontName','Times New Roman')
set(gca,'FontSize',12)
pos=ginput(2);
ech=find(f>=pos(1,1) & f<=pos(2,1));
x=log10(f(ech)); y=log10(spec(ech));
fit=polyfit(x,y,1);
val=polyval(fit,pos(:,1));
pt=(val(2)-val(1))/(pos(2,1)-pos(1,1));
ps=ginput(2);
xo=log10(ps(1,1));
yo=log10(ps(1,2));
xi=log10(ps(2,1));
yi=10^(yo+pt*(xi-xo));
hold on
plot([ps(1,1);ps(2,1)],[ps(1,2);yi],'r')
txt=round(pt*100)/100;
h=gtext('k');
h=gtext(num2str(txt));
set(h,'FontName','Times New Roman')
set(h,'FontSize',14)
height=0.41;
%f1=magvel/height;
%f2=2.3*magvel/(2*pi*0.055);
%if f1<0.3;
f1=0.3;
%end
%if f2>2;
f2=2;
%end
hold on
yl=[0.00001 0.001];
xl=[f1 f1];
plot(xl,yl,'-.r')
hold on
yll=[0.00001 0.0001];
xll=[f2 f2];
plot(xll,yll,'-.r')
%isr=gtext('Expected Limits of the inertial subrange');
%set(isr,'FontSize',[12])
%set(isr,'FontName','Times New Roman')
eval(['clear fuvwp',int2str(i)])
end
```

Appendix C

LOIS land-ocean interaction study

OCTOBER 1996 ISSUE NUMBER 10

BLISSful data acquisition in the north sea

The BLISS (Boundary Layer Intelligent Sensor System) project involved the development and proving of a complex new instrument system, to measure bed-stress and near-bed sediment flux. The overall objective was to acquire an essential data-set for LOIS RACS(C) Special Topic 351 entitled "Flux and properties of Suspended Particulate Matter (SPM) through the Holderness region".

The development was started as a collaborative undertaking by the Plymouth Marine Consortium (Plymouth Marine Laboratory, University of Plymouth, and the Royal Naval Engineering College, Plymouth). However, with RNEC's closure in September 1995, the bulk of the development, construction and commissioning became the responsibility of the PML Electronics Group. Three complete systems have been built, commissioned and deployed in the North Sea off the Holderness coast.

The instrument systems were designed to investigate the physical processes responsible for sediment movement and exchange with the bed in the nearshore zone, where both tidal flow and wave activity are important. The major operational requirements are for equipment which is (a) deployable from a small fishing vessel in depths as little as 4m, (b) causes negligible interference with the flow near the seabed, and (c) has a deployment duration of one month. The systems measure flows (mean currents, waves and turbulence), suspended sediment, salinity, temperature, and pressure within 1m of the seabed. Burst sampling, at 5 Hz for 1024 seconds every hour, is necessary to characterise the turbulence, while slow background sampling, at five minute intervals, allows tidal effects to be followed.

Each instrument system consists of a seabed tripod, carrying a suite of sensors, data logger/controller, and battery pack, connected by an umbilical cable, via an anchor clump, to a surface buoy which carries a UHF radio transceiver. This allows transfer of signal and data between the controller on the tripod and a shore-station. Because of the vulnerability of the

(continued on page 6)

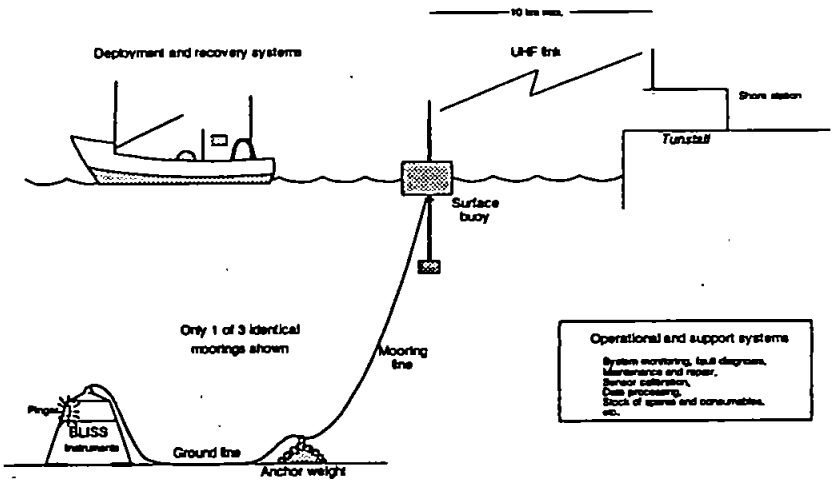

Outline of the total BLISS system, showing subsystems and major components.

Flow through the north channel of the irish sea

The North Channel measurement programme took place between July 1993 and October 1994. The main objectives of the project were to estimate the mean volume flux from the Irish Sea to the Malin Shelf, to quantify the relationship between the volume flux and the driving forces, and to test POL's 2D and 3D numerical model calculations of the flow through the North Channel. This article describes how an estimate of the mean volume flux was derived from the measurements.

The North Channel connects the Irish Sea to the Malin Shelf. At its narrowest point between Orlock Point and Portpatrick it is 31km wide and has a cross-sectional area of 3.1×10^6 m^2. Its deepest point is in Beaufort's Dyke where the water depth approaches 315m. It is in a region where the tidal currents are strong and rectilinear (maximum flow >1.5ms^{-1}).

Surface currents were measured in one km grid boxes across the North Channel for

(continued on page 4)

.. development and deployment of BLISS

(continued from page 1)

tripods to storms and fishing activity in shallow inshore waters, the telemetry link was seen from the outset as an important part of the system. It enables data to be transmitted to shore in near real-time, so that system performance can be checked and the data safely recorded. It also gives the potential to alter the logging mode of the rig from the shore, for example, by putting it into standby mode during extended periods of calm weather, to conserve battery and memory capacity.

The BLISS sensors consist of two electromagnetic current meters oriented to measure the x y z components of flow at 0.4m above the seabed; transducers for temperature, conductivity (for salinity) and Optical Back-Scatter (OBS) also at 0.4m height; a second OBS sensor at 0.9m (for the vertical gradient), with a transmissometer at the same height (for intercalibration); and a pressure transducer (for tidal level and wave activity). These are all sampled during the burst periods. During the background periods, pitch, roll and compass sensors are also sampled, along with three battery voltages (see table below). A miniature, low power, single board computer, manufactured by Triangle Digital Systems Ltd, forms the brains of BLISS. It is programmed in the high level language FORTH to control the operation of logger and communications, and to allow user-selection of logging parameters. Following a belt and braces philosophy, accumulated data are logged *in-situ* on a miniature 40 Mbyte hard disc, as well as being transmitted to shore at three hour intervals.

The overall aim of this LOIS Special Topic is to study the processes responsible for the flux of suspended sediment along and across the coastal waters adjacent to the rapidly eroding Holderness cliffs. Specific objectives include assessing the importance of sediment resuspension from the seabed, and the relative importance of storms and tidal flows to the overall net sediment flux. Collaboration with Dr Colin Jago at University of Wales, Bangor involves the application of a number of *in-situ* and laboratory techniques to determine the size characteristics of suspended sediment as well as concentrations, so that reliable estimates of flux can be obtained. We are also collaborating with modellers at the University of Plymouth and Plymouth Marine Laboratory to help in data interpretation and to assist in the development of predictive models.

The three BLISS rigs have been deployed off the Holderness Coast (see above) at three sites in the nearshore zone from a small chartered trawler (the MFV "Janet M") working out of Bridlington. The four deployment periods during 1995/96 have spanned both fair weather and stormy conditions, although not all the BLISS systems have been used each time, due to teething problems with the prototype equipment and to faults in the commercial electromagnetic current meters used on the rigs. In July and November 1995 there was data overlap (figure, bottom page 7) with Challenger cruise 119 and deployments of Proudman Oceanographic Laboratory Monitoring Packages (PMP's) along the northern line off the

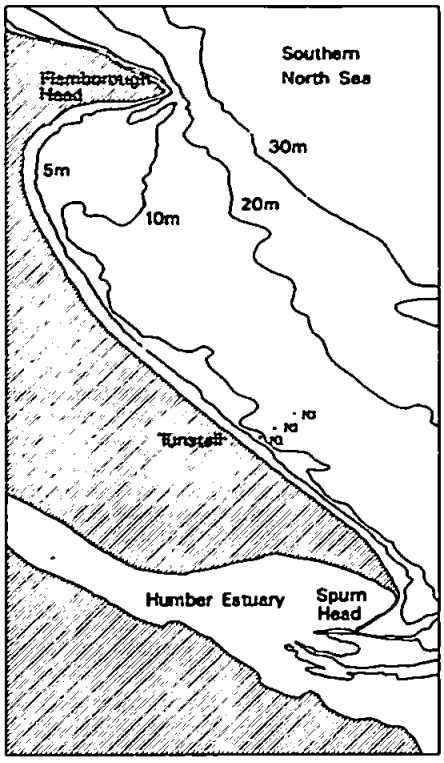

BLISS moorings off the Holderness Coast

Holderness coast. A series of CASI overflights were also completed at these times. In the February 1996 BLISS deployment, aerial photographs of the region were also taken. Two 13 hour stations were conducted during July 1995 and February 1996 concentrating on taking water samples close to each BLISS station to aid in the calibration of the Optical Back-scatter (OBS) sensors, using a cut-down version of the bottom-landing *in-situ* water sampling system designed by Plymouth

Data Channel	Sensor	Manufacturer	Max input range of channel	Height above seabed (m)	Sampling rate (Hz)
1	Pressure	Druck Ltd	0 - 4 bar abs	0.70	5
2	Temperature	Lab. Facility Ltd	4 - 22°C	0.48	5
3	Conductivity	Anderraa Instruments	0 - 55 mScm^{-1}	0.48	5
4	OBS 1	D & A Instrument Co.	0 - 900 FTU	0.41	5
5	OBS 2	D & A Instrument Co.	0 - 900 FTU	0.90	5
6	EMCM 1X	Valeport Ltd	± 5 ms^{-1}	0.39	5
7	EMCM 1Z	Valeport Ltd	± 5 ms^{-1}	0.39	5
8	EMCM 2Y	Valeport Ltd	± 5 ms^{-1}	0.41	5
9	EMCM 2Z	Valeport Ltd	± 5 ms^{-1}	0.41	5
10	Compass	K.V.H. Industries Inc.	0 - 360°	NA	0.2
11	Tilt (pitch)	Spectron Systems Technology Inc.	± 45°	NA	0.2
12	Tilt (roll)	SpectronSystems Technology Inc.	± 45°	NA	0.2
na	Transmissometer	UoW Bangor	0 to 100%	0.93	4

Marine Laboratory, coupled with water column profiles of CTD and suspended solids from transmissometers and OBS. These results are currently being analysed. Post-deployment calibrations have been completed for the first three deployment periods and are currently in progress for those in February 1996. With our data collection phase only just completed, it is at present possible to give a limited overview of the success of BLISS, but the results do demonstrate the overall quality of the data.

Preliminary analysis of the data sets has been concentrated on calculating the burst means and variances for all the working sensors in each BLISS deployment. Current velocity data show, as expected, that the tidal flow is rectilinear, running almost parallel with the coastline in a northwest-southeast direction. The average two-week time series for longshore velocity, pressure variance and suspended sediment concentration (SSC) in July 1995 (see above) shows that sediment suspension is more active during spring tides than neaps. Oscillations at the M2 tidal frequency give peaks in SSC at low water slack only. This suggests that suspended fine-sediment concentration increases towards the southeast and is advected alongshore by the tidal flow. The tidal excursion over the BLISS tripods is estimated to be between 6.4 and 4.1 km, from spring to neap tides. On springs, the greater amplitude of the tidal excursion is seen in an increase in the amplitude of M2 optical backscatter signal, but there is also evidence that the tidally-averaged concentration also increases towards springs. Superimposed on this is the action of waves, which also appears both to increase the tidally-averaged concentration and to increase the concentration gradient towards the southeast, though separating the effects of the spring/neap cycle from the storm sequence is proving difficult due to the limited record length. Wave activity was negligible during neap tides and background levels of fine sediment are lower. Double peaks in suspension every tidal cycle suggests that local resuspension of a coarse material is occurring in the vicinity of the tripod on both ebb and flood stages of the tide. As there were no waves, the energy required for this process, must be generated by the tides. Local resuspension is also likely to be occurring during springs, but its signature is

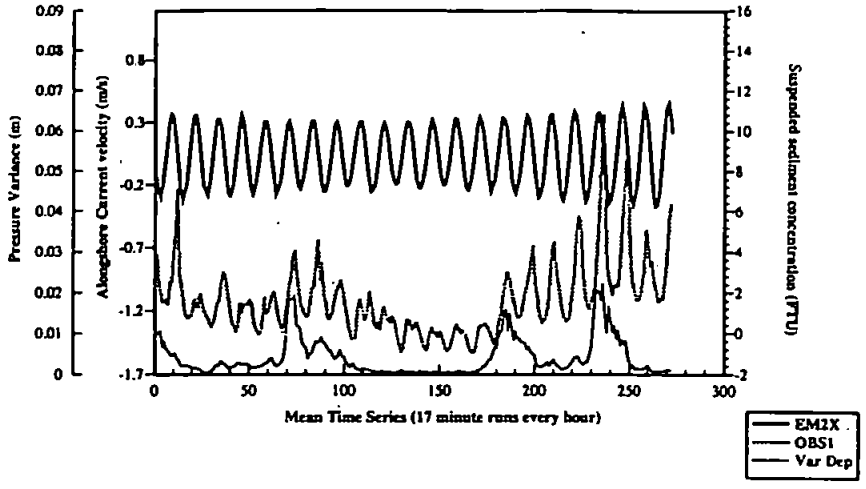

Time series of longshore current velocity, suspended sediment concentration and pressure variance for July at the BLISS Inner Station (N1).

being swamped by the stronger advective signal of the finer sediments. We are presently analysing turbulence within the bursts for July 1995 and February 1996, to determine the relationship between the resulting seabed stresses and the suspended sediment signals. Ultimately, we aim to qualify and quantify the role of storm activity in moving the cliff material away from the coastline.

Acknowledgements

We would like to thank Colin Jago and Ray Wilton of University of Wales, Bangor, for providing transmissometers, and the skipper and crew of the MFV Janet "M" whose help and skilled seamanship made the difficult deployment and recovery operations possible.

Professor D A Huntley, Miss Joanna Blewett, P P Ganderton, University of Plymouth, and Dr R H Bruce, C D Barrett, N J Bloomer, Plymouth Marine Laboratory.

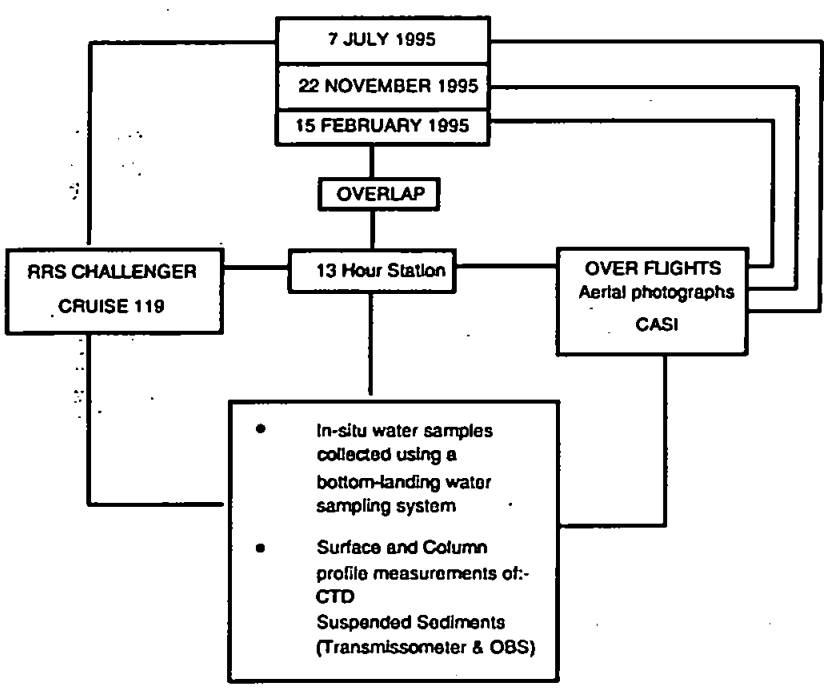

Summary of contemporaneous data acquisition during BLISS deployments on the Holderness coast.